



**Politecnico
di Torino**

ScuDo

Scuola di Dottorato ~ Doctoral School

WHAT YOU ARE, TAKES YOU FAR

Doctoral Dissertation
Doctoral Program in Electrical, Electronics and Communications Engineering
(37th Cycle)

Materials and processing for power electronics packaging and green technologies

Giulia Mossotti

* * * * *

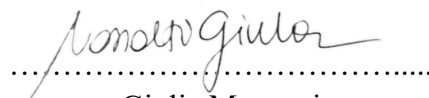
Supervisors

Prof. F. Pirri, Supervisor
Prof. L. Scaltrito, Co-Supervisor
Prof. S. Ferrero, Co-Supervisor

Politecnico di Torino
February 2025

This thesis is licensed under a Creative Commons License, Attribution - Noncommercial - NoDerivative Works 4.0 International: see www.creativecommons.org. The text may be reproduced for non-commercial purposes, provided that credit is given to the original author.

I hereby declare that, the contents and organization of this dissertation constitute my own original work and does not compromise in any way the rights of third parties, including those relating to the security of personal data.

A handwritten signature in black ink, appearing to read 'Giulia Mossotti', written over a horizontal dotted line.

Giulia Mossotti

Turin, February, 2025

Summary

This thesis focused on **developing customize sensors and sensor platforms for the *in-situ* monitoring of heavy metals** in environmental and industrial settings.

Traditional laboratory analysis suffers significant delays in data response due to sample collection, transportation, and processing. This lag can hinder effective remediation efforts, potentially allowing pollution to spread and cause further harm. The monitoring platform addresses this critical gap by providing real-time, on-site analysis of heavy metal concentrations. This capability enables a much faster response to contamination events, allowing competent authorities to take immediate action to contain the pollution and mitigate its impact on human health and the environment. By providing continuous data and eliminating the delays inherent in traditional methods, this *in-situ* monitoring system represents a significant advancement in the field of environmental monitoring and pollution control.

This research utilized chemical methodologies to prototype sensors capable of detecting these metals at concentrations as low as ppb (parts per billion) to ensure the safety of drinking water. In particular, the developed sensors employed colorimetric methodology with UV-Vis spectrophotometry technologies and stripping voltammetry.

Specifically, arsenic and hexavalent chromium were targeted due to their severe toxicity, even at trace levels. The sensors were designed to detect these contaminants in drinking water within the parts per billion (ppb) range, ensuring compliance with stringent safety standards. Recognizing the importance of monitoring industrial wastewater, where heavy metal concentrations can reach significantly higher levels (g/L), the study also focused on broader applications. A prototype sensor for trivalent chromium detection was developed, and the

research was further expanded to encompass the detection of copper and nickel, common pollutants in galvanic wastewater.

Exploiting on a **multidisciplinary approach**, it was possible integrating knowledge and techniques from chemistry, mechanics, and electronics to create versatile tools for heavy metal monitoring. This synergistic strategy was crucial for addressing the complex challenges of sensor development, enabling the creation of devices capable of accurate and reliable detection. The realization of these sensors involved a comprehensive exploration of design, fabrication, and integration of sub-systems, with a keen focus on optimizing key performance parameters such as sensitivity, selectivity, stability.

This research has the potential to significantly improve heavy metal monitoring by providing a rapid and accurate method for detecting these pollutants, ultimately contributing to the protection of human health and the environment.

Acknowledgment

I would like to express my sincere gratitude to Professor Luciano Scaltrito and Professor Sergio Ferrero for their invaluable guidance and support throughout my doctoral research project. Their kind mentorship has been instrumental in my development as a researcher, providing me with the opportunity to grow both professionally and scientifically. I also wish to acknowledge the contributions of the research group in the Department of Applied Sciences and Technology, with special thanks to Professor Fabrizio Pirri.

I would also like to deeply thank all my colleagues at ChiLab, with a special mention to Valentina Bertana, Matilde Aronne and Giulio Galfré who supported and encouraged me during the research activities and endured me during coffee breaks. I deeply appreciate their patience and the wealth of knowledge they have shared with me, which has been crucial to the successful completion of my research.

I would also like to express my gratefulness to the entire team of Microla Optoelectronics, with particular thanks to Andrea Piscitelli. Their generous sharing of technical expertise and precious knowledge was essential to the successful completion of this project and in my personal scientific assets.

Finally, I would like to extend my heartfelt thanks to my family. Their unwavering love, support, and encouragement have been constant throughout all my studies careers. They have celebrated my successes, offered comfort during setbacks, and always believed in my ability to achieve my goals. I am truthfully

grateful for their understanding and for providing the foundation that made all of this possible.

Contents

1. Introduction.....	1
1.1 Water pollution	3
1.1.1 Different types of water	4
1.1.2 Source of water pollution.....	5
1.1.3 Pollutants	6
1.1.4 Heavy metals (HMs).....	7
1.1.5 Health effects of HMs.....	8
1.1.6 Directives and Legislations.....	9
1.1.7 HMs limits of detection	11
1.1.8 Type of Monitoring.....	12
1.2 Analytical techniques.....	13
1.2.1 Undissolved pollutants.....	14
1.2.2 Dissolved pollutants.....	15
Spectroscopic techniques	16
Electrochemical techniques	19
1.3 Transition from the Laboratory to Field	20
1.4 Water <i>In-Situ</i> Sensors	22
1.4.1 Importance of Continuous Real-Time Monitoring.....	22
1.4.2 Design parameters.....	23
1.4.3 Sensors for HMs detection.....	24
1.5 Scope and outline of the work	30
2. Methodologies.....	32
2.1 Optical Methods.....	32
2.1.1 Electromagnetic radiation	32
2.1.2 Absorption of Electromagnetic Radiation by Species	36

2.1.3	Absorbance vs Transmittance	38
2.2	Absorption Methods: Lambert-Beer Law	39
2.2.1	Deviation of Lambert-Beer Law:	40
2.3	Colorimetric detection	42
2.4	Instrumentation of UV-Visible spectroscopy	42
2.4.1	Light Source.....	43
2.4.2	Monochromator	44
2.4.3	Sample Holder	44
2.4.4	Detector.....	45
2.4.5	Configuration: single vs double beam spectrophotometer.....	46
2.5	Electrochemical methods	47
2.5.1	Classification	47
2.5.2	Principle	48
2.5.3	Electrochemical cells	49
2.6	Voltammetry	49
2.6.1	Stripping Techniques	51
2.6.2	Three electrode electrolytic cell.....	53
2.6.3	Electrolyte solution	56
2.6.4	Mass transport in solution and Diffusion Layer	57
2.6.5	Voltammogram	58
2.7	Selection of methodologies:.....	60
3.	Optical Detection.....	62
3.1	UV-Vis colorimetric evaluation.....	63
	Design of optical sensors	64
3.2	Arsenic Detection	65
3.3	Copper Detection	67
	Colorimetric range of investigations.....	67
	Evaluation of pH, aging test and dilutions.....	69
	Colorimetric evaluation by Zincon TM	71
3.4	Nickel Detection	72
	Colorimetric range of investigations.....	73
	Evaluation of pH, aging test and dilutions.....	75

3.5	Chromium (III) Detection.....	77
	Colorimetric range of investigation	77
	Aging test and dilutions	81
3.6	Chromium (VI) Detection.....	82
	Colorimetric range of investigation	82
	Colorimetric evaluation by 1,5-Diphenylcarbazide (DFC)	84
	DFC aging test	86
	DFC solvent optimization	88
	DFC dilution 50:1	89
	Tests on field “Real sample analysis from ACDA”	90
4.	Electrochemical Detection.....	92
4.1	Different types of commercial sensors	93
	Flow-through cell electrode (Istran)	94
	ScTrace Gold (Metrohm).....	94
	Screen-Printed Electrode (Metrohm).....	96
4.2	Arsenic Detection	96
4.2.1	Chronoamperometry	97
	Calibration and optimization	97
	Tests on field “Real sample analysis”	98
4.2.2	Voltammetry - SWV	99
	Calibration	100
	Aging tests	100
	Solid Electrodes and Square Wave Voltammetry: Advantages in Electroanalysis.....	101
4.3	Cadmium Detection.....	102
	Calibration	102
5.	Developed Sensor Platforms	104
1.1	Definition and parameters of monitoring system	105
1.1.1	Parameters to monitor.....	105
1.1.2	System specifications.....	107
1.2	Development of sensing platform.....	108
1.2.1	Mechanical design	108
	Drinking water hydraulic system.....	108

Industrial galvanic water hydraulic system.....	109
Wiring and Calibration of micro-dispensers and pumps	111
Mechanics components material and chemical compatibility	113
1.3 Filtering system.....	114
Design and fabrication	114
FEM Simulation.....	116
Characterization	117
1.4 Optical section	118
Design and fabrication	118
FEM Simulation.....	120
Optoelectronic calibration.....	122
1.5 Voltammetric section.....	126
Design of a measurement flow	126
Design and fabrication	126
Calibration	128
1.6 Electronic section.....	129
Control and Interface Electronics Design	129
Electromechanical Components and Interface	129
Firmware Development	131
Energy storage	133
1.7 Water monitoring sensing platform	134
1.7.1 Platform for industrial water monitoring.....	134
1.7.2 Platform for drinking water monitoring.....	135
Sub-systems integration and assembly, and offline testing	138
Multiparameter probe	139
<i>In-situ</i> installations.....	140
Maintenance.....	140
1.8 Testing on real samples provided by ACDA	141
6. Conclusion and Future Perspective.....	143
6.1 Reached Results.....	143
6.2 Key Achievement	144
6.3 Significance and Implications	145

Monitoring vs Alarm system.....	145
6.4 Challenges and Limitations	146
6.5 Future Perspectives.....	147
Multi optical lengths cuvette.....	147
Cadmium cell detection	148
7. References.....	150

List of Tables

Table 1: Key Parameters driven the Water Demand and the correlated effects.	1
Table 2: Common pollutants contaminating freshwater resources and their primary origins.....	7
Table 3: Comparison of Drinking Water and Wastewater Concentration Limits Across Various Regulations [29].	11
Table 4: Monitoring sample frequency volumes.....	12
Table 5: Generalized guidelines for developing new sensors.....	24
Table 6: Regions of the electromagnetic spectrum and types of transition involved.	34
Table 7: Colors of Different Wavelength Regions.....	42
Table 8: Comparative table outlining the key characteristics and applications of Tungsten-Halogen, Deuterium, Xenon lamps, and Laser.	44
Table 9: Comparative table outlining the key characteristics and differences between photomultipliers and photodiodes.	46
Table 10: Concentration Limits for Heavy Metals in Drinking Water Set by the WHO.....	63
Table 11: Concentration Limits for Heavy Metals in Drinking Water Set by the WHO.....	92
Table 12: Correlation between deposition time and limit of detection and linear working range.	95
Table 13: Definition and classification of parameters to monitor.....	106
Table 14: Heavy Metal Monitoring Parameters and Regulatory Limits, Historical Data, and Monitoring Requirements.	106
Table 15: Drinking Water Quality Standards parameters and Monitoring Targets.	106
Table 16: Selected components for building water analysis system.....	111

Table 17: Calibration of peristaltic pumps for different volume of water. ...	113
Table 18: Evaluation of commercial wavelengths of System linearity for chromium (III) detection.....	123
Table 19: (a) Laboratory solution with nominal concentration namely 10 and 20ppb and (b) real sample solution provided by the plant refers to three different moments of sampling evaluated with different power levels of diode.	125
Table 20: Desired technical features for monitoring drinking water platform.	136
Table 21: Results of the measurements carried out on the sample from Pietraporzio.....	142
Table 22: Results of the measurements carried out on the sample from Sampeyre.	142
Table 23: Comparison for arsenic and chromium(VI) results between prototype system and laboratory instrumentation.....	142

List of Figures

Figure 1: Water connecting across the SDGs.....	3
Figure 2: Global Distribution of the main Water Resource.	4
Figure 3: Environmental and human health risks associated with polluted water [15]......	9
Figure 4: Map of areas of high or extremely high-water vulnerability [25]. ..	10
Figure 5: Timeline of analytical technique for detection of pollutants in water.	14
Figure 6: Detection of particulates suspended pollutants in water by analytic methodologies.....	15
Figure 7: Schematic representation of instrumental techniques for determining HM concentrations.....	16
Figure 8: Diagram of key challenges that need to be addressed in the development and implementation of portable analytical instruments.	22
Figure 9: Identified number of publications in the last 24 years with Scopus search keywords: “water quality sensors”. (October 2024).....	23
Figure 10: Illustration of typical operating principles of contemporary sensors employed for monitoring heavy metals in water.	25
Figure 11: Schematic representation of a fully integrated water quality monitoring system (FIWQMS) with fabricated sensor for HMs detection [66]....	26
Figure 12: (a) The HMs final prototype; (b) The schematic internal disposition for the principle of pipetting sample into the instrument and how to detect the target heavy metal ions by electrochemical sensor; (c) Details the design and a visual representation of the chip containing six electrodes [63]......	27
Figure 13: On-line Environment Analyzer Applitrace (a) front view and (b) integrated into a comprehensive system.	27
Figure 14: a Implementation of filtration system and HM microfluidic detection device on the autonomous surface vehicle; b autonomous surface	

vehicle, equipped with HM microfluidic detection device, filtration system, and sampler, deployed in a field experiment; c schematic representation of components of the HM microfluidic detection device; d schematic representation of one SPE; e example of the voltammogram [68].	28
Figure 15: Diagram illustrates a portable, smartphone-based colorimetric water testing system [69].	29
Figure 16: (a) Optical detection prototyping. Magnification shows the microfluidic system; (b) 3D printing flow cell of detection; (c) Detailed dimensions of internal flow cell; (d) The complete setup with the flow cell, LED light source, and micro-spectrometer; (e) LED emission spectrum [70].	30
Figure 17: The electric and magnetic fields of electromagnetic radiation.	33
Figure 18: Wavelength (λ) and amplitude (A) associated with electromagnetic radiation.	34
Figure 19: Representation of electromagnetic spectrum. (https://www.xrayconsult.it/nota-rx.html)	34
Figure 20: (a) The energy of a molecule is quantized: there are only discrete energy levels, corresponding to different states of the molecule. (b) Possible electronic transitions that are involved in absorbance. (c) The spectrum resulting from the sum of all the energy contributions. Image modified by [73], [74].	36
Figure 21: Types of electronic transitions for organic species.	37
Figure 22: d-d transition for inorganic species.	38
Figure 24: The plot of Absorbance (A) or Transmittance (T) vs. wavelength (λ).	38
Figure 25: Transmission of light through a sample solution in a cuvette. Image modified by [77].	39
Figure 26: Deviations from Lambert-Beer law. Image modified by [72].	41
Figure 27: A simplified schematic representation of the main components in a UV-Vis single-beam monochromatic spectrophotometer. Image modified by [79].	43
Figure 28: Diagram classification of electroanalytical techniques.	47
Figure 29: Comparison between different Electrochemical Cell Configurations. (a) In Voltaic/Galvanic Cell electrons flow spontaneously from one compartment to another (black line) but cannot reverse direction (red line). A salt bridge (dotted line) or porous barrier (dashed line) is required to maintain electrical neutrality. (b) In electrolytic cell the reaction from anode to cathode is non-spontaneous (red line). An external source of energy is necessary to drive the reaction (black line). Image modified by [81].	49
Figure 30: Diagram classification for Voltammetric techniques.	51

Figure 31: Anodic stripping voltammetry: the potential-time waveform with the resulting voltammogram.	52
Figure 32: General configuration of laboratory set-up three electrode cell [86].	53
Figure 33: Timeline comparison chart of the evolution of the most used metallic materials, including their advantages and disadvantages.	54
Figure 34: (a) Mechanisms of mass transfer at a planar electrode. Adapted from (Wang 2000). (b) Diffusion layer established between a working electrode surface and the solution.	58
Figure 35: (a) Voltammogram of the discharge of M^{2+} during linear scanning potential with the peak potential and current height position and the identification of the four characteristic regions describing what happening at the working electrode surface. (b) The most three voltammetry techniques used are named as cyclic voltammetry (CV), differential pulse voltammetry (DPV) and square-wave voltammetry (SWV) with their typical form of excitation signal and the consequently current response on the voltammogram. Image modified by [89]...	59
Figure 36: Diagram showing the choice of an analytical method involves a thoughtful consideration of multiple factors, including the nature of the analyte, the desired outcomes, the reliability and comparability of results, sample integrity, and the practicality of the method itself.....	61
Figure 36: Proposed reaction mechanism for Rhodamine B shows pink color solution, but it becomes colorless when reacts with iodine produced by potassium iodide (KI) and As(III) in an acidic environment. Image modified by [90].	66
Figure 37: (a) UV-Vis spectra of Rhodamine solutions with different Arsenic concentrations in [ppm] range and (b) Calibration curve ($\lambda = 553$ nm) for Rhodamine B method.	66
Figure 38: Copper sulphate solutions with increasing metal concentration, from left to right.....	67
Figure 39: UV-Vis spectra recorded at RT with 10mm optical length (a) UV-Vis spectra of Cu solutions at high concentrations from 1 to 22 g/L. The magnification reveals the initial increase in noise, which is likely associated with signal saturation. (b) Calibration curve associated at the high range of copper solutions ($\lambda_{MAX} = 805$ nm). (c) UV-Vis spectra of Cu solutions at low concentrations from 0.05 to 1 g/L. (d) Calibration curve associated at low range copper solutions ($\lambda_{MAX} = 805$ nm).	68
Figure 40: UV-Vis spectra recorded at RT with 20mm optical length (a) UV-Vis spectra of Cu solutions at low concentrations from 0.012 to 0.1 g/L (12-	

100ppm). (b) Colourless copper solutions. (c) Calibration curve associated at low range copper solutions ($\lambda_{MAX} = 805 \text{ nm}$).	69
Figure 41: (a) Influence of pH on 1 g/L Cu solutions. (b) UV-Vis spectra recorded at room temperature for solutions containing increasing concentrations of copper in an acidic medium using a 10 mm optical path length. The magnification reveals a comparison of the absorbance increase relative to neutral pH conditions. (c) and (d) Calibration curves based on the two selected wavenumbers corresponding to the maximum absorbance peaks.	70
Figure 42: UV-Vis spectra depict (a) Sample 1:5 dilution for Cu solution exceeding 20 g/L; (b) and (c) Increase of salt dissolution due to 24h resting time.	71
Figure 43: Proposed complexation mechanism for Zincon in combination with a heavy metal ion such as copper and zinc in water solution.	72
Figure 44: (a) Experimental solutions demonstrating the color change from the Zincon solution alone (orange) to the solution containing copper (blue) confirm the complexation between the metal and the ligand. (b) UV-Vis spectra recorded at room temperature and neutral pH demonstrate the presence of two distinct peaks: one at 450 nm corresponding to free Zincon, and the other at 600 nm representing the M-L complex (c) (left) Calibration curve for Cu concentration 10-100 ppb, Zincon solution as reference. (right) Calibration curves for Cu concentration 0.25-2 ppm.	72
Figure 45: (a) Nickel nitrate solutions with increasing color and metal concentration from 20 to 1g/L (right to left). (b) UV-vis spectra of Ni solutions with increasing metal concentrations recorded at RT, neutral pH and 10mm optical length. The magnification shows the detection limit for direct colorimetry at 25g/L. (c) Calibration curve ($\lambda_{MAX} = 396 \text{ nm}$).	74
Figure 46: (a) UV-vis spectra of Ni solutions with increasing metal concentrations from 0.1 to 0.003 g/L recorded at RT, neutral pH and 20mm optical length. (b) Nickel nitrate solutions show barley color intensity with a metal concentration from 0.1 to 0.012 g/L (right to left). (c) Calibration curve ($\lambda_{MAX} = 396 \text{ nm}$).	74
Figure 47: (a) Influence of pH on 10 g/L Ni solutions. (b) UV-Vis spectra recorded at room temperature for solutions containing increasing concentrations of copper in an acidic medium using a 10 mm optical path length. (b1) The magnification reveals a comparison between acidic and neutral media with respect to the same concentration and experimental procedure. (c) Calibration curve ($\lambda_{MAX} = 396 \text{ nm}$).	75

Figure 48: (a) Influence of acidic media on absorbance on UV-Vis spectra of Ni solutions range from 1 to $1,8 \cdot 10^{-3}$ g/L; the magnification shows the improvement in absorbance with respect the same range of concentration (b) Loss of color for solutions with low Ni concentration (c) Calibration curve ($\lambda_{MAX} = 396$ nm).....76

Figure 49: (a) UV-Vis spectra of Ni solutions from 1 to 20 g/L, freshly prepared (solid lines) and 24h aged (dashed lines); (b) Calibration curve for aged solutions ($\lambda_{MAX} = 396$ nm). (c) Sample dilution 1:5; (left) Spectra of the diluted solutions overlapping the analogous fresh one; (right) Effect of 24 hours aging..77

Figure 50: (a) (top) Visual comparison of the color of solutions came from electroplating plants pilot; (bottom) UV-Vis spectra of the two real sample solutions with different concentrations of supplied chromium (III). (b) Visual comparison of laboratory standard solution from higher to lower concentration, left to right; (bottom) UV-Vis spectra of chromium (III) chloride hexahydrate standard solutions with similar concentration of real samples, 10mm optical length, RT and neutral pH.....79

Figure 51: (a) Calibration curve for laboratory standard solution from 0.6 to 10 g/L ($\lambda_{MAX} = 423$ nm) and compared table of important parameters with difference in maximum detectable concentration and wavelength. (b) UV-Vis spectra comparison of the same concentration of chromium trivalent solution from laboratory (red line) and from real plant (blue line).79

Figure 52: Series of analysis using a stock solution of trivalent chromium with a concentration of 0.73 g/L (top) and 7.3 g/L (bottom) (a) Visual comparison of the color of the solutions, (b) UV-Vis spectra for the selected dilution set from 0.73 to 0.09 g/L (top) and from 7 to 0.5 g/L (bottom), recorded at room temperature, neutral pH, and with a 10 mm optical path length, (c) Calibration curves ($\lambda_{MAX} = 423$ nm).....80

Figure 53: (a) UV-vis spectra of Cr (II) solutions with increasing metal concentrations from 0.011 to 0.73 g/L recorded at RT, neutral pH and 20mm optical length. (b) Chromium trivalent solutions show barley color intensity within the same metal concentrations. (c) Calibration curve ($\lambda_{MAX} = 423$ nm). ..81

Figure 54: (a) Comparison of UV-Vis spectra of Cr (III) real sample solutions at 0.73 g/L (blue line) respect to 7.3 g/L diluted 1:10 (red line). (b) UV-Vis spectra before and after two months for two samples of Cr (III) solution one at 0.73 g/L and the 7.3 g/L diluted 1:10.82

Figure 55: UV-Vis spectra for Chromium (VI) ions recorded with 10mm optical length, RT and pH =7 for two different range of concentrations (a) from 100 to 25 ppm, showing the intense color of the solution along with the

corresponding calibration curve ($\lambda_{MAX} = 349 \text{ nm}$), and (b) from 10 to 0.5 ppm, where the solution loses its color, accompanied by the related calibration curve ($\lambda_{MAX} = 349 \text{ nm}$).84

Figure 56: (a) UV-vis spectra of Cr (VI) solutions with increasing metal concentrations from 0.1 to 0.5 ppm recorded at RT, neutral pH and 20mm optical length. The magnification shows that at a concentration of 0.5 ppm, there is an improvement in absorbance following an increase in the optical length. (b) Calibration curve ($\lambda_{MAX} = 349 \text{ nm}$).84

Figure 57: The proposed reaction mechanism for the DFC solution is transparent, but it takes on a violet color when complexed with Cr (VI) in acidic media.....85

Figure 58: UV-Vis spectra for Chromium (VI) and DFC recorded with 10mm optical length, RT and pH =4 for two different range of concentrations (a) from 1 to 0,25 ppm, showing the intense color of the solution when combining with Cr(VI) along with the corresponding calibration curve ($\lambda_{MAX} = 520 \text{ nm}$), and (b) from 200 to 25ppb, where the solution starting loses the characteristic color, accompanied by the related calibration curve ($\lambda_{MAX} = 520 \text{ nm}$).86

Figure 59: (a) UV-Vis spectra of DFC in methanol recorded at different times to evaluate aging of the solution. (b) Table of comparison of the different absorbance values with respect to the maximum (540nm) and the evaluate peak (520nm).....87

Figure 60: UV-Vis spectra for Chromium (VI) and DFC aged solution recorded with 10mm optical length, RT and pH =4 for two different range of concentrations (a) from 1 to 0,25 ppm with 7 days aged DFC along with the corresponding calibration curve ($\lambda_{MAX} = 520 \text{ nm}$), and (b) from 1 to 0.25ppm with 28 day age DFC, supplemented by the related calibration curve ($\lambda_{MAX} = 520 \text{ nm}$).87

Figure 61: (a) UV-Vis spectra for Chromium (VI) and DFC in acetone recorded with 10mm optical length, RT and pH =4 from 200 to 25 ppb. (b) Corresponding calibration curve ($\lambda_{MAX} = 520 \text{ nm}$).88

Figure 62: (a) Visual comparison of the DFC solution in acetone and methanol showing different colors after 7 days. (b) UV-Vis spectra of DFC in acetone recorded at different time to evaluate aging of the solution. Dashed line indicated the deviation trend in linearity of the solution.89

Figure 63: UV-Vis spectra recorded at RT and 10mm optical length for (a) DFC in methanol diluted 50:1 and recording its aging from 7 to 28 days, (b) (a) DFC in acetone diluted 50:1 and recording its aging from 7 to 28 days. (c) UV-

Vis spectra for comparison between DFC solutions in methanol and acetone diluted with distilled water, and FC in methanol diluted with tap water.....	90
Figure 64: UV-Vis spectra for real sample solution contaminated with unknow level of chromium (VI).	91
Figure 65: Configuration of Istran electrode flow-through cell.....	94
Figure 66: Configuration of ScTrace Gold (Metrohm).....	95
Figure 67: Configuration of SPE (a) with the position of WE, RE and CE (b) for the immersion and drop configuration.	96
Figure 68: Evaluation of TAU values necessary before the calibration.	98
Figure 69: Calibration curve for confirming Arsenic concentration between values of nominal concentration and Istran electrode response (a) with one drop and (b) two drops of KMnO_4	98
Figure 70: (a) Chronopotentiometry curves for samples with increasing As concentration from 0 to 40 ppb and Real sample solution. (b) and (c) Chronopotentiometry calibration curves for samples within the same range.....	99
Figure 71: (a) Voltammograms curves for samples with increasing As(III) concentration from 0 to 20 ppb. (b) Calibration curves calculated with the maximum peak value in the considered range.....	100
Figure 72: (a) Comparison of voltammograms for 20ppb solution of arsenic containing freshly and aged solution of electrolyte solution. (b)Recorded voltammograms from 20,10 and 5 ppb of arsenic. (c) Calibration curve calculated with peak value for the associated range.	101
Figure 73: Metrohm SPEs before and after the activation.	102
Figure 74: Displacement during the analysis of the analyte and electrolyte solution droplet on the working electrode.	102
Figure 75: (a) Square wave voltammogram of 5 to 30ppb of Cadmium nominal concentrations with (b) associated calibration curve.....	103
Figure 76: Key parameters in sensing monitoring system developing.	105
Figure 77: Block diagram of the monitoring system.....	108
Figure 78: Fluidic diagram of the drinking water monitoring system divided by functional areas.	109
Figure 79: Fluidic diagram of the industrial water monitoring system.....	110
Figure 80: (a-g) Series of graphs and tables to illustrate the performance and calibration of micro-dosing pumps used for dispensing various solutions for HMs detection in a sensor platform.	112
Figure 81: CAD model of the PDMS device, with related measures of its features: (a) and (b) represent the section view and the top view, respectively, of	

the top layer; (c) and d) represent the section view and the top view, respectively, of the bottom layer. All the measures were in mm.	116
Figure 82: CAD model of the two filters and a zoom on the frame for filters positioning, with the related measures. All measures were in mm.....	116
Figure 83: Right: Pressure on filtering system walls. Note that the SI units are used instead of mL/min, so the flow rates are (a) 1 mL/min, (b) 2.5 mL/min, (c) 4 mL/min, (d) 8 mL/min, (e) 10 mL/min, (f) 13 mL/min, (g) 17 mL/min, (h) 20 mL/min. Left: Streamline and fluid velocity plots for (1) 1 mL/min, (2) 10 mL/min and (3) 20 mL/min flow rates.	117
Figure 84: Left: displacement plot reported in SI unit for 10 mL/min with a visual magnification of 20000 for what concerns movement in geometrical domains and colour scale unchanged. Right: displacement as a function of flow rate.	117
Figure 85: Right: Microscope images of top and bottom layers, with related features measurements. Left: Microscope images of printed filter, with relative features measurements. All measures are in mm. The scale bar is 1mm.	118
Figure 86: Measuring chamber for chromium with dual optical path and different inlets.	119
Figure 87: Chromium (VI) optical cell optic disposition.	120
Figure 88: (a) Realization of the prototype measuring chamber with laser holder and holder. (b) Implementation of the realized camera in the platform with magnification on the window dedicated to the measurement chamber control...	120
Figure 89: Left: pressure on analyte cell wall for the 10 mL/min flow rate case. Right: pressure drop between inlet and outlet.....	121
Figure 90: Streamline plots. Note that the SI units are used instead of mL/min so the flow rates are (a) 1 mL/min, (b) 2.5 mL/min, (c) 4 mL/min, (d) 8 mL/min, (e) 10 mL/min, (f) 13 mL/min, (g) 17 mL/min, (h) 20 mL/min.	122
Figure 91: Customize calibration curve for chromium (III) detection whit 450nm commercial wavelength.	124
Figure 92: Calibration curve for nominal concentration of chromium (VI) with different power of diode for 520nm wavelength.	125
Figure 93: Customize the calibration curve for chromium (VI) detection while 520nm commercial wavelength.	126
Figure 94: CAD representation of Arsenic detection chamber considering: (a) top view (b) insertion of the electrode into the measuring chamber, (c) and (d) the maximum volume of the sample with respect to the electrode.....	127

Figure 95: Prototyping of the Arsenic monitoring system. (a) solution containing analyte, (b) electronics dedicated to the control of the analysis and (c) monitoring chamber with voltammetry electrode.....	128
Figure 96: Calibration curve for Arsenic detection.....	129
Figure 97: (a) Preliminary design of the full-custom electronics that will control the system and communicate with the infrastructure developed by Informatica System; (b) Motherboard schematic for controlling the prototype components; (c) Control board for the As.	130
Figure 98: Relay board for controlling hydraulic components.	131
Figure 99: Automated Cr(III) Monitoring System Process Flow.	134
Figure 100: Top: Table of define parameters. Bottom: Stream flow (a) of initial design concept and (b) the final constructed prototype of an automated chromium (III) monitoring system.	135
Figure 101: Rendering of the measuring-constrain device with its components.	137
Figure 102: Stream working flow of the final monitoring platform system divided in three phases: (a) Design, (b) Implementation of the system with laboratory test and sub-system integration and (c) Prototyping platform with a removable front and a detail with the inlet of treated or untreated water (Inlet), the clean drain of the purge of the multiparametric probe (Out), the discharges of the complexed solutions (Waste Cr (VI) and Waste As) and the communication port with the interface system with the water treatment system.	137
Figure 103: Detail of the monitoring subsystems (a) System of hydraulic components: pumps, micro-dosers and solenoid valves; (b) Chromium (VI) and Arsenic measuring chambers; (c) multi-parameter probe testing, with sensors installed.....	138
Figure 104: Multiparameter probe sensor disposition.....	139
Figure 105: Installation in field of the sensing platform for drinking water HMs detection in Piedmont mountains.....	140
Figure 106: Top view detail of the water monitoring platform render showing the tank reload are.....	140
Figure 107: Maintenance process carried out in the field in the replacement of the electrode for the detection of arsenic.	141
Figure 108: Summary diagram of the heavy metals detected with evidence of the analytical technique used and the detection range achieved in the thesis work.	144
Figure 109: Possible multi-optical lengths cell design to be included in the prototyping of new sensor platforms.	148

Chapter 1

Introduction

Water is the very foundation of life on Earth, playing a crucial role in its structure, function, and evolution for all biological processes. The protection and preservation of water as a finite and essential resource are crucial for achieving long-term environmental sustainability and human well-being. Historically, planet Earth has earned the moniker "blue planet" due to the vast expanse of water that covers approximately 71% of its surface. However, this seemingly uniform expanse belies a remarkable diversity in water types. Far from a singular entity, Earth's water can be broadly classified into four main categories, namely freshwater, saltwater, brackish water, and groundwater each with distinct physical and chemical properties. These diverse water types play necessary and central functions in shaping the planet ecology, biogeochemical cycles, and the grounds of life itself. While the amount of water suitable for human use is finite, global water demand has surged dramatically over the last century, showing a 600% increase with an annual growth of 1.8% [1]. The alarming increase in water demand underscores the urgent need for conservation and optimized water use. This demand is projected to rise significantly in the coming decades, driven by several key considerations [2]:

Table 1: Key Parameters driven the Water Demand and the correlated effects.

Factor	Effect
Population Growth	As the global population continues to grow and by 2050 will reach between 9.4 to 10.2 billion people; so, there will be a natural increase in the overall demand for water for domestic purposes like drinking, sanitation, and hygiene.
Economic Development	Rising living standards in developing countries often lead to increased water consumption habits, such as larger homes with appliances requiring water, and dietary shifts towards more water-intensive meat production.

Intensive agriculture and industry	Industrial will grow faster than agricultural demand but demand for agriculture will remain the largest.
Climate Change	Changes in precipitation patterns and rising temperatures due to climate change can exacerbate water scarcity in some regions, while also potentially increasing water demand for irrigation in others, to compensate for reduced rainfall.
Inefficient Infrastructure	Leaky pipes and outdated irrigation systems can waste significant amounts of water, further straining supplies.

In Europe the **2030 Agenda for Sustainable Development** outlines a set of 17 Sustainable Development Goals (SDGs) that aim to create a more just, equitable, and sustainable future for all. These goals encompass a wide range of interconnected issues, from eradicating poverty and hunger to ensuring access to clean water and sanitation, promoting quality education and gender equality, tackling climate change, and protecting ecosystems.

In this frame **six of the SDGs prioritizes ensuring universal access to safe water, sustainable management of water resources, and adequate sanitation for all**. This multifaceted goal is comprised of eight distinct targets, each accompanied by eleven indicators for monitoring progress. Specific targets address access to drinking water (6.1) and sanitation and hygiene (6.2). Additionally, the goal encompasses measures for improving water quality (6.3), promoting sustainable water use and management (6.4, 6.5), and protecting water-related ecosystems (6.6). Notably, two means of implementation indicators (6.a, 6.b) specifically focus on water and sanitation-related activities at the local level.[3] Furthermore, it is important to emphasize that while SDG 6 is specifically dedicated to ensuring access to water and sanitation for all, sustainable water resource management is fundamental for progress towards achieving all SDGs. In fact, as example, water is strongly essential for human health (SDG 3) and also deeply affects the management of ecosystems (SDGs 14 and 15) and climate change mitigation (SDG 13), water is related to food production (SDG 2) and the availability of renewable energy (SDG 7), ultimately water is also indirectly related to the creation of decent jobs (SDG 8) and to the quality of the education (SDG 4) [4], [5].



Figure 1: Water connecting across the SDGs.

This focus stems from the critical function of water plays in human health and development. In fact, nowadays, the very survival of almost 8 billion people hinges on this limited quantity of accessible water. In this perspective, according to UN-UNESCO report (2021), unsafe sanitation and water stress, the latter defined as the limited availability or accessibility of usable water resources, pose significant global challenges. The report estimates that over 45% of the global population struggles to access safely managed sanitation facilities, and more than 25% inhabit areas experiencing water stress [5]. In 2024 UNESCO, on behalf of UN-Water publish a report from UN 2023 Water Conference where it is estimated that 26% of the population, corresponding at 2 billion people, is currently do not have access to safe drinking water. An estimated 2-3 billion people globally experience water scarcity for at least a month annually, posing significant threats to livelihoods, particularly regarding food security and access to electricity [6]. A stark warning from UNICEF and UNESCO highlights the impending crisis of water scarcity leading in possible conflict over water resources also the lack of clean water and basic sanitation facilities poses a significant health risk, particularly for vulnerable populations.

1.1 Water pollution

The European Environmental Agency (EEA) defines **water pollution** as the presence of **harmful substances in water, originating from sources like sewage, industrial waste, and rainwater runoff**. These substances contaminate the water to such an extent that it becomes unsuitable for its intended use. However, the threshold for contamination that renders a water body impaired varies significantly. Factors such as the type of water body (e.g., river, lake, groundwater), its geographical location, and the specific ways in which it is used (e.g., drinking water, recreation, irrigation) all play a role in determining the acceptable level of pollution [7]. To accurately evaluate chemical pollution in natural water sources, five key factors have been to consider [8]:

1. **Identification of the pollutants:** Pinpoint the specific chemicals and their sources.
2. **Measure the contamination:** Utilize reliable analytical techniques to track the changing levels of pollutants across both time and location.
3. **Understand pollutant behavior:** Grasp how these chemicals move, transform, and ultimately break down within the water system.
4. **Predict future impacts:** Employ sophisticated models to design effective monitoring strategies and forecast how the pollution scenario might evolve.
5. **Assess the risks:** Determine the potential harm these chemicals pose to both aquatic ecosystems and human health.

1.1.1 Different types of water

The distribution and the coverage of water among Earth is not uniform. Figure 2 presents a pie chart depicting the diminishing availability of usable freshwater for human consumption; oceans comprise a vast expanse, encompassing roughly 97% of total water, this saltwater is unusable for most biological processes and human consumption. Conversely, freshwater, essential for all life forms, constitutes a mere 2.5-3% of the total water volume. Even within this limited freshwater pool, significant disparity exists. Glaciers, mainly in the Antarctic areas, hold the majority (69%), followed by groundwater (30%), leaving a tiny fraction (<1%) readily available in lakes, rivers, and swamps [9].

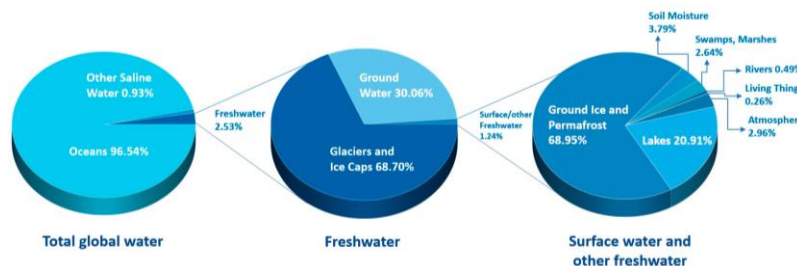


Figure 2: Global Distribution of the main Water Resource.

Drinking water resources are commonly categorized as **surface water or groundwater**. **Surface water** encompasses various open water bodies like lakes, rivers, and streams, all influenced by the surrounding land and atmosphere. In contrast, groundwater resides within underground rock formations, sometimes connected to surface water and sometimes isolated. These two water types of encounter pollutants through different routes and mechanisms. While both can serve as sources of drinking water, water intended for human consumption undergoes rigorous treatment and must meet stringent regulatory standards [7]. Additionally, it is also possible to identify another sub-category that refers to fresh water source which is **industrial water** and refers to the water used for various purposes in industrial facilities, including manufacturing, processing, cooling, washing, and diluting. Over a third of the Earth accessible renewable freshwater is used in agriculture and industry; although it may seem like water intended for a less noble purpose than others, it is still important to monitor the water used in these types of processes to optimize the process and use as little as possible

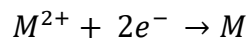
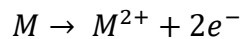
without wasting it, since it came from freshwater and generating an enormous amount of wastewaters with different chemicals [8], [10]. It is important also mention **ocean water** (97% of Earth water) is crucial for understanding the health of marine ecosystems and ensuring the safety of water for various purposes including preserving the living form that at end finish in the food chain system. Additionally, because almost 40% of the world population lives in coastal regions it is important to protect them from public health problem [11]. Also, marine plant life plays a critical role in maintaining the Earth atmosphere. It absorbs roughly 30% of human-produced CO² emissions and is responsible for producing 50-80% of the Earth oxygen [12]. Impurities in the water, both organic and inorganic, often exist as suspended particles or colloids, affecting the physical properties of water, such as temperature, color, turbidity, and odor. These impurities also influence the chemical and biological characteristics of the water [13].

1.1.2 Source of water pollution

Water pollution arises from a **complex interplay of natural and anthropogenic factors**. While attention is often focused on human-induced pollution, it is important to acknowledge that natural processes also contribute. The Earth geological composition isn't uniform, and certain areas naturally contain higher concentrations of elements like heavy metals. These can leach into water systems through weathering and erosion exacerbated by climate change, impacting water quality. Moreover, geological events, such as landslides and volcanic eruptions, can introduce a range of pollutants into water bodies, often in unpredictable and difficult-to-monitor ways. These natural sources of contamination can pose significant challenges for water quality management.

However, **human activities remain the primary drivers of water pollution**. Industrial processes release a mixture of pollutants, including heavy metals, organic chemicals, and microplastics, into waterways. Agricultural practices contribute to pollution through the runoff of fertilizers, pesticides, and animal waste. Urban areas generate significant wastewater containing sewage, detergents, and other contaminants. These anthropogenic pollutants have far-reaching consequences for both human and ecosystem health, impacting drinking water supplies, recreational water quality, and the delicate balance of aquatic ecosystems. As an example, the galvanizing process is of the main source of freshwater contamination by high concentration of HMs. It begins with substrate preparation, which involves cleaning the base material, whether metal or polymeric, to remove any contaminants that may hinder the coating adhesion. Following this, a flux solution is applied to enhance the bonding between the substrate and the metal coating. Then the substrate is immersed in an electrolytic bath, an aqueous solution containing various additives and high concentrations of dissolved heavy metals. The specific chemical reactions that occur during galvanization depend on the type of heavy metal present in the electrolytic bath. However, regardless of the metal, the overall process involves the reduction of

metals ions at the cathode (the substrate) and the oxidation of the anode material (often steel or iron) in the electrolytic bath.



This electrochemical reaction results in the transfer of metals ions to the substrate surface, where they are reduced and deposited as a metallic coating. After the galvanizing process, the coated metal is rapidly cooled (quenched) to solidify the coating. This is typically achieved by immersing the metal in water or allowing it to cool in air. The cooling process occurs repeatedly, and it is crucial to monitor and control the concentration of residual elements in the cooling bath to ensure consistent quality. The last step of the process is passivation that enhance corrosion resistance and provide a more aesthetic finish.

Water pollution sources from human activities are generally categorized into two main types: point sources and nonpoint sources [7]. **Point source pollution** originates from a single, easily identifiable location, such as a discharge pipe from a factory releasing industrial waste. This type of pollution is relatively straightforward to monitor and regulate, often through permits and specific control measures. In contrast, **nonpoint source pollution** stems from numerous diffuse sources, making it challenging to trace back to a specific origin. An example is runoff from agricultural fields, which can carry fertilizers and pesticides into streams and rivers. Addressing nonpoint source pollution requires broader, landscape-level strategies to manage land use practices and mitigate the collective impact of multiple sources [14]. Addressing these pollution sources requires a multifaceted approach involving stricter regulations, improved wastewater treatment, and sustainable practices in industry and agriculture.

1.1.3 Pollutants

Water pollutants can be broadly categorized into two main groups based on their chemical composition and properties as organic and inorganic pollutants [15].

Organic pollutants primarily originate from living organisms or their byproducts. They are carbon-based compounds, often containing hydrogen, oxygen, nitrogen, and other elements [16]. Examples include pesticides used in agriculture, pharmaceuticals that enter water through wastewater, volatile organic compounds (VOCs) which evaporate easily, petroleum products from oil spills, and microplastics resulting from the breakdown of larger plastics. **Inorganic pollutants** typically come from non-living sources like minerals and industrial processes. They generally lack carbon-hydrogen bonds and include metals, salts, and other inorganic compounds. Examples of inorganic pollutants are heavy metals like mercury, lead, and arsenic, often originating from industrial discharge or mining; nutrients like nitrates and phosphates, primarily from fertilizers and

sewage; salts from road de-icing and industrial brines; and acids and bases from industrial discharges and acid rain. In terms of danger the main difference is that organic pollutants can sometimes be broken down by microorganisms in the environment, while inorganic pollutants are often persistent and can accumulate over time.

Table 2 provides a summary of frequently encountered water pollutants originating from both anthropogenic and natural sources [17]. This table is not intended to be comprehensive, as the precise composition of pollutants in each water body is influenced by local conditions and activities. Also, some pollutants may have both natural and human-made sources. For example, nutrients like nitrogen and phosphorus can occur naturally in water bodies, but their levels can be significantly increased by human activities such as agriculture and wastewater discharge.

Table 2: Common pollutants contaminating freshwater resources and their primary origins.

	Pollutants	Natural Source	Human Activities
Inorganic	Heavy Metals	Rock weathering Volcanic eruptions	Mining Industrial discharges Vehicle emissions
	Nutrients (nitrogen, phosphorus)	Rock weathering Decomposition of organic matter Nitrogen fixation	Agricultures activities (Fertilizers and Animal manure) Sewage treatment plants Urban runoff
	Salts	Weathering of rocks and minerals Volcanic eruptions Saltwater intrusion	Road salt Agricultures activities (Irrigation and Fertilizers) Oil and gas extraction
	Acids	Volcanic activity (gases like SO ₂ and H ₂ S) Acid mine drainage	Industrial and laboratory discharges Agricultural runoff
	Microplastics*	-	Industrial activities Urban wastewater from washing machines
Organic	Pesticides, Fertilizer and Herbicides	Naturally occurred plants	Agricultural and urban runoff
	Pharmaceuticals	-	Industrial and urban discharges
	Surfactants	-	Industrial discharges Wastewater
	PFAS	-	Manufacturing of PFAS-containing products Industrial discharges (Manufacturing, Firefighting foams)
	BTEX	Volcanic eruptions Forest fire	Industrial discharges (Petroleum refining and Chemical manufacturing)

* Since plastics are made from carbon-containing polymers, they are technically organic in the chemical sense. But their origin, properties, and environmental behavior make them more appropriately classified as inorganic pollutants.

1.1.4 Heavy metals (HMs)

Heavy metals are defined in various ways, leading sometimes to ambiguity about their classification. However, the most appropriate definition often depends

on the context of the discussion. Some define them based on their chemical properties, often focusing on transition metals from group 3 to 12 of the periodic table. Others rely on density, classifying them as metals with a high density compared to water, typically greater than 5 g/cm³. Another approach defines them based on their toxicity to living organisms [18]. When **evaluating the environmental** risks of heavy metals like chromium, nickel, copper, zinc, cadmium, lead, mercury, uranium, and plutonium, and metalloids like selenium and arsenic, the primary hurdle lies in their tendency to **behave differently depending** on the surrounding environment chemical condition that influences their **redox state**. The second problem is linked to the tendency of this element to **not be subject to degradation** like many of the organic pollutants [8]. The third issue is linked to **how quickly heavy metals can bioaccumulated** in plants, animals, and humans. Bioaccumulation is defined as the process by which the rate of pollutant uptake exceeds the rate of elimination, resulting in an increase in pollutant concentration within an organism over time. While some metals like cobalt, iron, copper, and zinc are essential nutrients in small amounts and naturally occur in environment and food, constant exposure can lead to toxic levels in our bodies. Even though living organisms need these metals in trace amounts for good health, they become dangerous at higher concentrations, harming both human health and the ecosystem [19].

1.1.5 Health effects of HMs

Heavy metals pose a significant danger to human health through both direct and indirect exposure. **Direct exposure** occurs when heavy metals bypass the body primary detoxification systems, like the liver, and enter directly into the bloodstream. This can happen through inhalation of contaminated air (dust, fumes, or vapors), ingestion of contaminated soil or water, or skin contact with heavy metals or substances containing them, often in industrial settings [20]. Regardless of the pathway, direct exposure to heavy metals can have serious health consequences. **Indirect exposure** happens when HMs come into contact through a secondary source by contaminated food or water. This is often more subtle and gradual but can still have significant health consequences.

While both organic and inorganic pollutants can be harmful to life and humans, their effects differ significantly. Focusing on heavy metals, their toxicity levels in humans can be ranked from least to most toxic as follows: Cobalt, Aluminum, Chromium, Lead, Nickel, Zinc, Copper, Cadmium, and Mercury [21]. These metals can be dangerous in various ways. Some are known to cause mutations, cancer, birth defects, allergies, or hormone disruption. They can also damage the liver and kidneys, harm the immune system, and lead to heart, neurological, and behavioral problems, especially in children. Additionally, heavy metal exposure can damage bone marrow, the central nervous system, and even cause osteoporosis [22]. Statistics show that a staggering 1 billion people suffer from illnesses and various health issues each year due to exposure to HMs

contaminated water. This highlights the urgent need to address water pollution and ensure access to clean and safe water for all.

Figure 3 depicts the range of health problems that can arise from exposure to human health of inorganic pollutants in water. These problems range from minor inconveniences to severe, life-altering conditions. On the less serious end, people might experience reversible issues like skin rashes, nausea, coughing, sore throats, headaches, and dizziness. However, as contamination becomes more severe, the effects on health can be much more serious and long-lasting. These can include damage to vital organs like the kidneys and liver, the development of cancer, harm to the nervous system, and even birth defects. Additionally, conditions like asthma, chronic bronchitis, and miscarriages are also associated with exposure to these pollutants. It's important to remember that the specific health risks depend on the exact type of inorganic pollutant, the amount a person is exposed to, and individual factors like age and overall health.

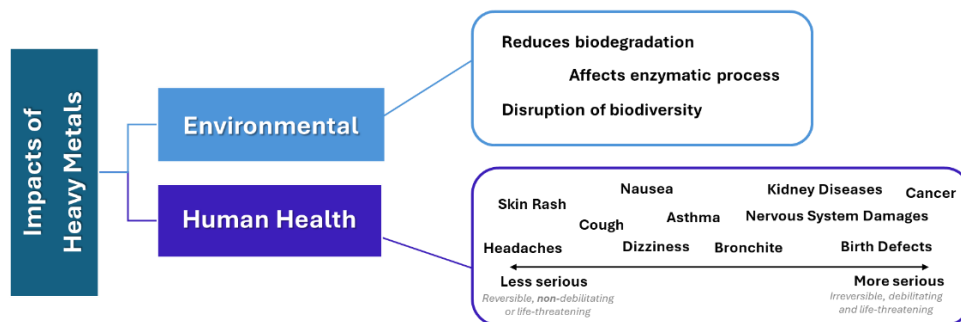


Figure 3: Environmental and human health risks associated with polluted water [15].

1.1.6 Directives and Legislations

Several studies conducted in recent years show that water resources will be scarce for over 8 billion people in the next decade. Furthermore, the pollution of surface water makes water availability even more critical, especially in arid areas. Figure 4 depicts a maps analysis of overlaying regions with physical water scarcity onto areas characterized by limited or nonexistent water service infrastructure. The reported data identifies populations lacking improved water access, leading to reliance on untreated surface water, unimproved sources, or collection times exceeding 30 minutes. The analysis revealed that 1.42 billion people live in such areas of high or extremely high-water vulnerability [23]. Moreover, by 2025, it is estimated that two-thirds of the global population will face water shortages [24]. The consequences for ecosystems worldwide would be even more severe, with all systems likely to suffer significantly.

The quality and therefore the availability of water directly influences and is influenced by the socio-economic life of human beings, therefore a rigorous assessment and monitoring of the water ecosystem is essential, accompanied by increasingly stringent regulation by public authorities.

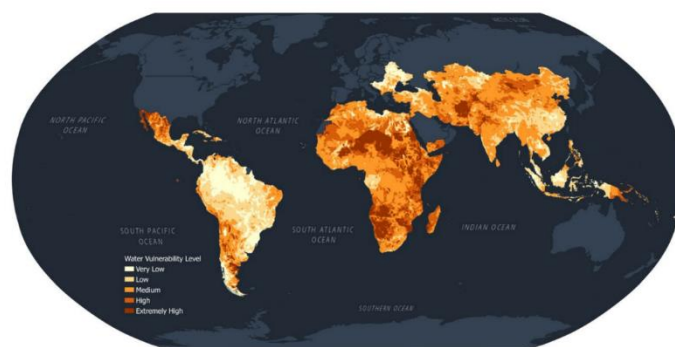


Figure 4: Map of areas of high or extremely high-water vulnerability [25].

Europe has established a robust framework for controlling water pollution and its vulnerability through a series of interconnected directives. The **Water Framework Directive (WFD) (2000/60/EC)** acts as the cornerstone, aiming to achieve good ecological status for all water bodies by addressing pollution from all sources and promoting sustainable water use. Additionally, to ensure safe drinking water for all, the EU has implemented the **Drinking Water Directive (98/83/EC)**. This directive establishes quality standards by setting minimum requirements for various microbiological, chemical, and indicator parameters. It also mandates monitoring, reporting, and public information provisions to maintain transparency and accountability. After two decades in effect, the EU Drinking Water Directive is undergoing significant revision to better protect public health. This update aims to tackle emerging pollutants like endocrine disruptors and PFAS by reducing existing limits for various contaminants and introducing new parameters. Notably, stricter limits for lead and chromium will be phased in over a 10-year period. These changes, coupled with increased monitoring and public information provisions, will further enhance the safety and accessibility of drinking water for European citizens [26].

To mitigate pollution from urban areas, the EU employs the **Urban Wastewater Treatment Directive (91/271/EEC)**. This directive mandates the collection and treatment of wastewater from urban sources before it is discharged, ensuring that it meets specific quality standards to protect both human and environmental health. This regulation plays a crucial role in safeguarding Europe's water resources from the impacts of urbanization.

Furthermore, directives like the **Nitrates Directive (91/676/EEC)** and the **Industrial Emissions Directive (2010/75/EU)** focus on controlling pollution from agricultural and industrial activities, respectively. This comprehensive legislative approach reflects the European Union's commitment to protecting and enhancing the quality of its water resources for both human health and ecosystem well-being. Other relevant EU legislation are **Groundwater Directive (2006/118/EC)** which focuses on the protection of groundwater from pollution and deterioration and **Environmental Quality Standards Directive (2008/105/EC)** which sets environmental quality standards (EQS) for priority substances in surface waters.

Italy approach to water protection integrates European Union directives with national and regional legislation. At the national level, **Legislative Decree**

152/2006 provides a comprehensive framework for safeguarding water resources, encompassing water quality standards, pollution prevention measures, and overall water resource management. Further strengthening this framework, **Legislative Decree 31/2001** specifically addresses the protection of groundwater from contamination [27]. Moreover **Resolution 917/2017/R/idr** is a key regulation issued by the Italian Regulatory Authority for Energy, Networks and Environment (ARERA) concerning the quality of water services in Italy. ARERA has defined a discipline background of the technical quality of the integrated water service from drinking water to wastewater treatment by adopting an innovative asymmetric approach to encourage water service providers to adopt efficient and innovative practices to improve service quality and reduce costs. The regulations are established based on the starting level of quality and therefore it is the same National Authority that requires the application of innovative technologies in order to *"be able to achieve significant objectives of service level and in particular the quality of the water distributed quickly"*. ARERA monitors the performance of water service providers against the defined standards and acts if necessary to ensure compliance [28]. Other important key regulation bodies in Italy are first Ministry of the Environment and Energy Security (MASE) is responsible for national water policy and for coordinating the implementation of EU water directives and Italian Institute for Environmental Protection and Research (ISPRA) institute that provides technical and scientific support for water management and monitoring setting the concentrations limits for different pollutants.

1.1.7 HMs limits of detection

By combining the different aspects mentioned above, such as the source of the contaminants, the type of water, and the European regulations, it is possible to extract Table 3 which shows the detection limits of the most dangerous metal ions. It should be emphasized that for water intended for drinking use, the detection limits are identified in micrograms per liter (ppb), while for industrial and wastewater the limits are higher in the order of milligrams per liter (ppm) or grams per liter (g/L). As for marine water, since it has a direct impact on biodiversity and on products that enter directly into the human food chain, they can fall under the regulations of the first category.

Table 3: Comparison of Drinking Water and Wastewater Concentration Limits Across Various Regulations [29].

	HMs	ITA*	EPA**	EU Directive	Units
Drinking Water	As	10	10	10	μg/l (ppb)
	Cd	5	5	5	
	Cr***	25	100	25	
	Cu		1300	2000	
	Hg	1	2	1	
	Pb	5	10	5	

Waste Water	Cd			0.05	mg/l (ppm)
	Cr**			0.5	
	Cu			0.5	
	Pb			0.2	
	Hg			0.03	
	Tl			0.05	
	Zn			1.5	

* Regulations available on the website of Ministero della Salute.

** Environmental Protect Agency (USA).

*** Total inorganic Cr encompass the total amount of both trivalent and hexavalent oxidation states.

1.1.8 Type of Monitoring

The WF Directive sets out specific types of monitoring for different aims [26], [30]:

- **Surveillance monitoring:** Provides a comprehensive overview of the current health of a water body and identifies long-term trends by considering both natural conditions and human impacts. This involves assessing a wide range of parameters, including those indicative of biological quality (e.g., fish and invertebrate communities), hydro-morphological quality (e.g., river flow and structure), and general physic-chemical quality (e.g., temperature, pH, nutrients). It also includes monitoring priority pollutants, such as heavy metals and pesticides, as well as other pollutants that may pose a risk to water quality.
- **Operational monitoring:** Assesses detailed information on the condition of water bodies that are under pressure from pollution or other human activities (e.g., industrial discharges, agricultural runoff) and it helps to track the impact of measures taken to improve water quality safety.
- **Investigative monitoring:** Used to pinpoint the specific causes of pollution or degradation in a water body. This type of monitoring is particularly important for assessing the extent and impact of accidental pollution events, allowing for targeted interventions and remediation efforts.

In Italy, the **monitoring frequency** for water quality is established by Legislative Decree 31/2001 [27], which links the number of checks to the volumes of water supplied throughout the year. The regulation sets a minimum frequency for checks, in relation to the volume of water distributed. Table 4 describes the minimum frequencies for the various types of checks in relation to the volume of water distributed. Minimum sampling and analysis frequency for water intended for human consumption supplied by a distribution network, from tanks or used in food businesses.

Table 4: Monitoring sample frequency volumes.

Water Volume (m ³)	Routine Monitoring (samples per year)	Verification Check (samples per year)
≤ 100	-	-
> 100 ≤ 1000	4	1
> 1000 ≤ 10000	4	1 + 1 for every 3300 m ³ /day

> 10000 ≤ 100000	4 + 3 for every 1000 m ³ /day	3 + 1 for every 10000 m ³ /day or 10000 fractions
> 100000	4 + 3 for every 1000 m ³ /day and 1000 fractions	10 + 1 for every 25000 m ³ /day and 10000 fractions

1.2 Analytical techniques

Water pollutant detection relies on a diverse array of **laboratory analytical techniques**. Figure 5 depicts a non-exhaust timeline showcasing the progression and milestones of analytical techniques used to identify pollutants in water, illustrating also a clear trend towards increased sensitivity, specificity, and efficiency.

Initially, water quality analysis depended on basic chemical tests and less sophisticated methods. **Capillary electrophoresis (CE)** is a versatile analytical technique that offers several particularly effective ways for separating and analyzing charged species, including inorganic ions, small organic molecules, and even larger biomolecules [31], [32]. **Field-flow fractionation (FFF)** is a chromatography-like technique, and it enabled the separation and characterization of complex mixtures, including nanoparticles and microparticles [33]. The introduction of **Mass-Spectroscopy (MS)** marked a first significant advancement. Coupling it with **Gas or Liquid Chromatography (GC-MS, LC-MS)** allowed for the separation and identification of complex mixtures of pollutants, increasing the range and accuracy of analysis and providing both qualitative and quantitative results. **Ion chromatography (IC)**, as well is a key technique for analyzing ions in water. It separates ions based on their interactions with a stationary phase, allowing them to be identified and quantified using a conductivity detector. IC is highly sensitive, capable of detecting trace contaminants, and versatile enough to analyze various ions, including common inorganic anions and cations [34]. As technology advanced, **electrochemistry** offered sensitive and selective detection of specific pollutants, particularly heavy metals. This branch encompasses various techniques (e.g., differential pulse anodic stripping voltammetry (DP-ASV), square wave voltammetry (SWV) that offer sensitive and selective detection of specific pollutants, particularly for those pollutants that came in form of ions. However, a major turning point arrived in the early 90s with the introduction of **spectroscopic techniques** for water quality analysis. **UV-Vis spectroscopy** provided a straightforward and efficient way to detect a broad range of pollutants that absorb ultraviolet or visible light. Fluorimetry and colorimetry offer both qualitative and quantitative analysis of water pollutants by measuring fluorescence at specific wavelengths and absorbance of specific species, respectively. Later, **inductively coupled plasma-atomic emission spectrometry (ICP-AES)** revolutionized the field by providing highly sensitive detection of trace metals, crucial indicators of water contamination.

The year 2000 marked a significant shift in the approach to water quality monitoring. Instead of solely relying on laboratory analysis, the scientific

community began to emphasize the importance of strategic **sensor placement approach** directly in the field. This change in perspective highlighted the growing need to optimize data collection by strategically positioning sensors in the most effective locations. Microfluidic sensors allowed for on-site, real-time analysis, making monitoring more efficient. The timeline points towards a future where sophisticated techniques like remote sensing, wireless sensor networks, and integrated within classic analytic technique where sensor systems provide a more holistic understanding of water quality.

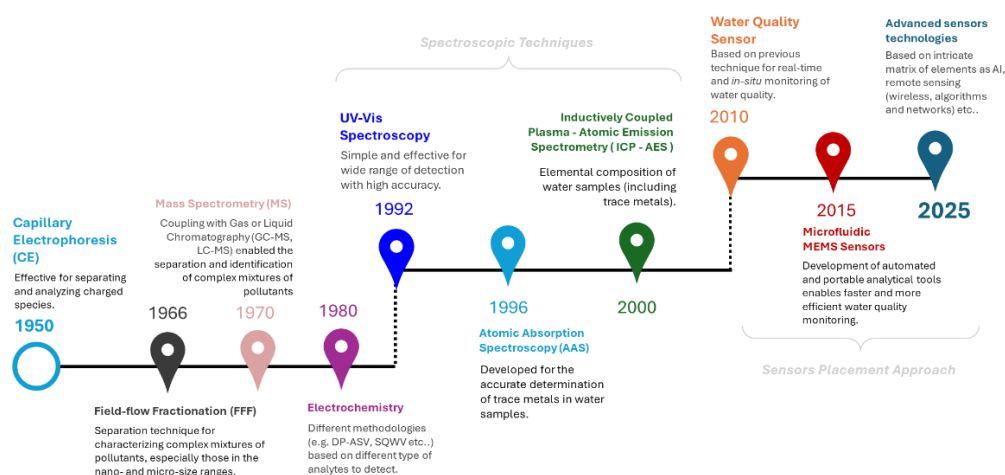


Figure 5: Timeline of analytical technique for detection of pollutants in water.

Considering laboratory techniques for water quality analysis, it is firstly crucial to differentiate based on the **physical state of the analyte**. Broadly, analytes can be categorized as either **dissolved or undissolved**, and this distinction significantly influences the choice of appropriate analytical techniques and methodologies [35].

Sample preparation: Detecting contaminants in water depend on sample preparation. This often involves steps like clean-up or pre-concentration, which are vital for ensuring the success of later analytical procedures. These preparatory measures help to remove interfering substances and increase the concentration of target pollutants, ultimately improving the sensitivity and reliability of the chosen analytical method. Without proper sample preparation, even the most sophisticated analytical techniques may yield inaccurate or misleading results [35].

1.2.1 Undissolved pollutants

The presence of undissolved substances significantly influences water quality. These substances, encompassing diverse materials and forms like sediments, organic matter, microplastics, and other pollutants, exist as suspended particles and colloids. Analyzing these particles is crucial for evaluating the overall health of water resources. Monitoring these substances aids in the development of effective management strategies to prevent issues such as clogging and maintain water quality [36]. **Quantification** of particle size and shape analysis employs

both optical and electron microscopy. **Optical microscopy** enables visualization and counting of particles exceeding 1 μm in size. For higher resolution imaging of nanoparticles, **electron microscopy (SEM/TEM)** is utilized, providing detailed information on morphology and elemental composition. Additionally, gravimetric analysis, a well-established technique for quantifying suspended particulate matter, involves filtration and subsequent weighing of collected particulates from water samples. **Turbidity meters** provide a qualitative assessment of suspended particulate matter by measuring water clarity. Quantitative analysis of particle concentration and size distribution can be achieved using particle counters [36].

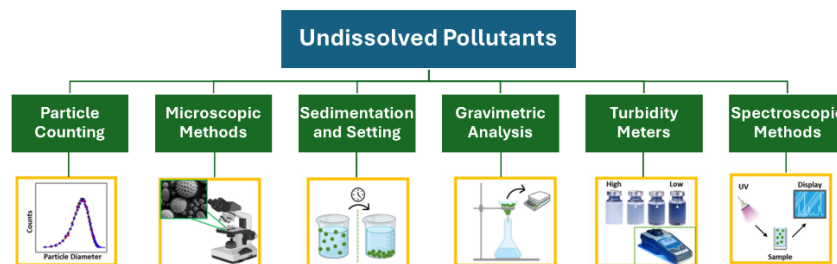


Figure 6: Detection of particulates suspended pollutants in water by analytic methodologies.

1.2.2 Dissolved pollutants

When pollutants are dissolved in water, three key aspects must be considered with a multifaceted approach to achieve the legally required limits of detection. **The nature of the water matrix** includes factors such as pH, dissolved organic matter, and the presence of other ions, all of which can influence the behavior and detectability of pollutants. Additionally, **the chemical nature of the pollutant** encompasses the specific form of the pollutant (e.g., free ion, complexed), its oxidation state, and its potential to undergo transformations in the water. Finally, **the analytical technique employed** varying sensitivities and selectivities for different pollutants. The chosen technique must be capable of achieving the required detection limits.

This diagram in Figure 7 categorizes instrumental laboratory techniques for heavy metal determination into **spectroscopic techniques**, which utilize the interaction between electromagnetic radiation and heavy metal atoms, and **electrochemical techniques**, which exploit the electrical properties of these metals for detection and quantification [37].

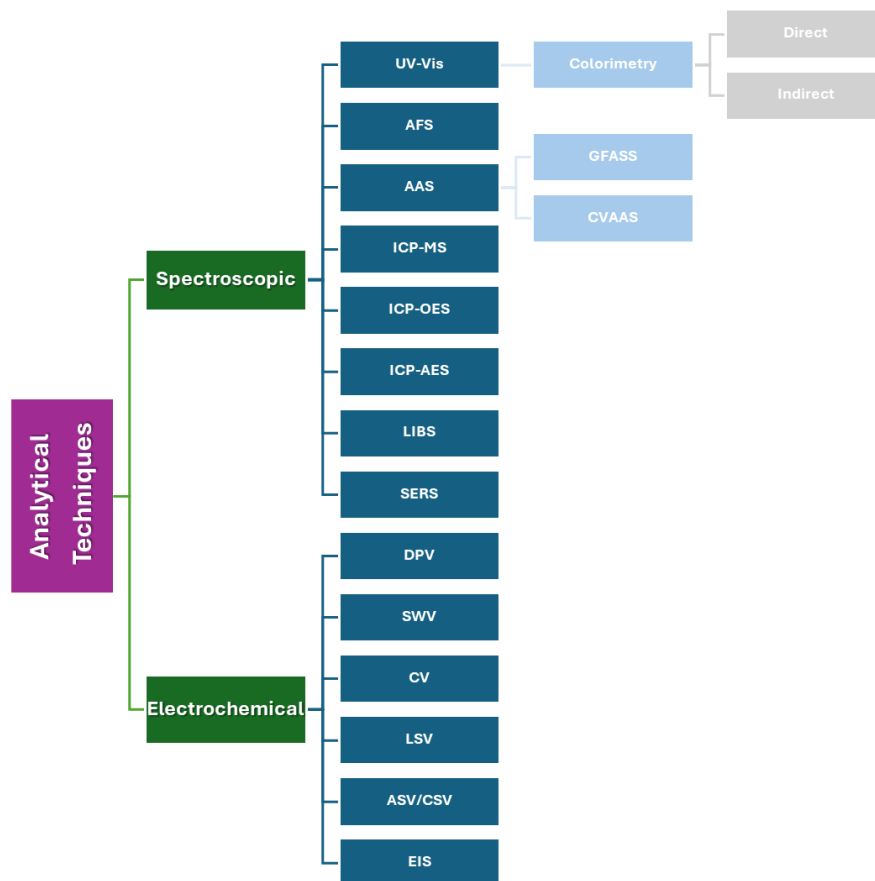


Figure 7: Schematic representation of instrumental techniques for determining HM concentrations.

Spectroscopic techniques

Atomic Absorption Spectroscopy (AAS) is a well-established and widely used technique for elemental analysis. It works by measuring the absorption of light by atoms in the gaseous state. Despite its rapid detection, accuracy, easily operated and cheap in terms of cost per analysis AAS is subject to several limitations. These include memory effects, which can arise from the carryover of analyte between measurements, and chemical interferences, encompassing analyte loss due to volatile salt formation, carbide formation, condensation, and recombination reactions. Furthermore, background absorption from particulate matter generated during atomization, often referred to as "smoke," and physical interferences arising from variations in sample viscosity, surface tension, and density can also compromise the accuracy of AAS measurements [38]. AAS has been further developed into more specialized techniques, including **Graphite Furnace Atomic Absorption Spectroscopy (GFAAS)** which offers increased sensitivity by using a graphite furnace to atomize the sample. Analysis can be time-consuming, requiring method optimization for different sample matrices. Additionally, the technique suffers from a limited dynamic range and is inherently destructive [39]. GFAAS is often employed for the analysis of heavy metals in wastewater due to its ability to handle complex matrices and various forms of contamination [40]. However, for other water sources such as river water, irrigation water, surface water, well water, and drinking water, the traditional

AAS technique remains widely preferred [41]. **Cold vapor atomic absorption spectrometry (CVAAS)** is a specialized technique used primarily for measuring mercury levels. It involves adding a component to the system to efficiently convert mercury ions (Hg(II)) into elemental mercury (Hg(0)) before detection. CVAAS is a fast and highly sensitive technique for measuring very low concentrations of mercury. Its sensitivity can be further improved by combining it with other analytical techniques such as ICP-AES. This combined approach can achieve limits of quantification and detection that are at least 5 and 10 times lower than the maximum allowable limits, highlighting the effectiveness of CVAAS for mercury analysis [42]. **Atomic Fluorescence Spectroscopy (AFS)** offers an alternative approach to elemental analysis. In AFS, the sample is first atomized into the gaseous phase. The atoms are then excited by absorbing light, and subsequently emit photons at specific wavelengths as they return to a stable state. This emitted fluorescence is measured and used to quantify the elemental composition. A key distinction between AFS and AAS lies in the arrangement of the instrumental components. In AFS, the light source is positioned perpendicular to the detector, minimizing interference from the excitation source and enhancing the sensitivity of fluorescence detection. Despite this configurational difference, the fundamental principles underlying AFS and AAS share significant similarities [43]. **UV-Vis spectroscopy** is among the simplest yet most powerful techniques for detecting dissolved metals in water. Thanks to Lambert-Beer law, a quantitative analysis of the metal is possible. The absorbance can be correlated to the concentration of the metal in solution. Additionally, the unique position of the peak in the spectrum, associated with the species under analysis, allows for qualitative analysis. The most established methodology in this type of analysis is colorimetry. Colorimetry can be direct, in cases where the solution already shows an identifying color (usually correlated to high concentrations), while it can also be indirect when it is necessary to add a chromophore to give the solution a color. In fact, employing synthesized Ag-doped ZnO nanoparticles, researcher investigation successfully demonstrated the detection of several heavy metal ions, including Ni²⁺, Cu²⁺, Cr³⁺, Cr⁶⁺, Fe²⁺, and Fe³⁺, at concentrations as low as 100 μM [44]. A potential limitation of this technique is light scattering caused by suspended particles within the sample solution. Therefore, ensuring complete clarity of the solution is essential for accurate measurements [45]. **Inductively Coupled Plasma Mass Spectrometry (ICP-MS)** is a widely used analytical technique for determining the elemental composition of a sample. This multi-elemental technique utilizes an inductively coupled plasma to generate ions, enabling the detection of both major and trace elements. The ions are then passed through a quadrupole mass spectrometer, which rapidly and continuously measures their mass-to-charge ratio, facilitating the identification and quantification of various elements. This method, with its high sensitivity and ability to analyze over seventy elements, has become an indispensable tool in various HMs identification. ICP-MS has proven effective in determining heavy metal concentrations in various matrices. For example, studies have successfully utilized ICP-MS to quantify copper, chromium, and nickel in environmental

samples. Furthermore, closed-vessel microwave digestion coupled with ICP-MS has enabled the determination of chromium, manganese, cobalt, copper, zinc, and selenium in freshwater fish [46], [47]. This technique provides exceptional sensitivity for detecting a wide array of heavy metals at trace levels, achieving detection limits in the ppb to ppm range. It offers the advantages of high sensitivity, excellent precision, and rapid analysis. However, it is susceptible to spectral and chemical interferences, which may require careful matrix matching or interference correction strategies [38]. **Inductively Coupled Plasma Atomic Emission Spectrometry (ICP-AES)** is another robust technique for detecting and quantifying heavy metals. ICP-AES employs an inductively coupled plasma to excite atoms within a sample, causing them to emit light at characteristic wavelengths. The intensity of this emitted light is directly proportional to the concentration of the corresponding element, enabling quantitative analysis with a wide linear dynamic range. This allows for the simultaneous measurement of numerous heavy metals, including trace elements, within a single analysis [37]. **Inductively coupled plasma atomic emission spectroscopy (ICP-OES)** quantify HMs in various samples by measuring the light emitted from excited ions generated in a high-temperature plasma. The process involves sample preparation, atomization in the plasma, excitation of atoms, and analysis of the emitted photons to determine elemental concentrations. It is a versatile and cost-effective technique for rapid multi-elemental analysis and offers a wide linear dynamic range and high tolerance to matrix effects due to minimal ionization and chemical interferences [37]. However, for elements with stringent regulatory limits in drinking water, such as Pb and As, ICP-MS may be a more suitable choice due to its superior sensitivity [48]. Wastewater contamination in industrial effluents and agricultural runoffs introduce various metallic micropollutants into water systems. **Laser-induced breakdown spectroscopy (LIBS)** offers a promising approach for rapid and non-destructive elemental analysis of complex matrices with metallic micropollutants like wastewater contamination in industrial effluents and agricultural runoffs. LIBS is an atomic emission spectroscopic technique that uses a high-powered laser to ablate a small amount of material from a sample. This ablation creates plasma, and as the plasma cools, the excited atoms within it emit light at specific wavelengths characteristic of the elements present. By collecting and analyzing this emitted light, LIBS can identify and quantify the elemental composition of the sample. The technique is highly versatile and can be used for both qualitative and quantitative analysis of various materials. While LIBS is applicable to various sample states (solid, liquid, and gas), analysis of liquid samples presents unique challenges that necessitate careful consideration and optimization of experimental parameters [41]. **Surface-Enhanced Raman Spectroscopy (SERS)** is a promising technique for detecting heavy metals in water. It works by amplifying the Raman signals of molecules attached to nanostructured metal surfaces, like gold, silver, or copper. When heavy metal ions interact with these surfaces, their Raman signals become significantly stronger, allowing for detection even at very low concentrations. In a recent study, a nanoporous chromium thin film was created on an aluminum substrate for SERS

analysis. This film, covered in rough nanoporous chromium particles and ultrafine chromium nanoparticles, acted as a highly effective SERS substrate. These surface features created "hot-spots" areas of intense electromagnetic fields that noticeably enhance the Raman signals of heavy metal ions, leading to improved detection sensitivity [49], [50].

Electrochemical techniques

Electrochemical (EC) techniques have emerged as attractive methods for heavy metal ion detection due to their speed, simplicity, cost-effectiveness, and suitability for field applications. Various electrochemical approaches, including voltammetric techniques (e.g., DPV, SWV, CV, ASV), potentiometry, amperometry, and EIS, offer diverse capabilities for the detection and quantification of heavy metal ions [37], [51]. Generally, for EC technique an electrochemical cell, comprising a working electrode, a counter electrode, and a reference electrode immersed in an electrolyte solution, is connected to a potentiostat. This setup facilitates the measurement of current flowing through the cell as a function of the applied potential. Growing concerns about pollution have prompted researchers to explore and utilize various EC methods for the detection and quantification of environmental pollutants such as HMs. **Linear sweep voltammetry (LSV)** is the simplest EC technique used to detect HMs in water samples. It involves applying a linearly increasing voltage to an electrode immersed in the sample and measuring the resulting current. When the voltage reaches a level where a specific metal is oxidized or reduced, a peak in the current signal is observed. By analyzing the position and size of these peaks, the presence and concentration of different heavy metals can be determined. LSV is particularly useful for detecting metals like lead, cadmium, and copper [52]. **Differential Pulse Voltammetry (DPV)** to develop a highly sensitive and selective electrode for Cr (VI) detection in water. Fabricated using a drop-casting method and optimized for key parameters like electrolyte strength, pH, and concentration, the electrode demonstrated a remarkable detection limit of 0.0885 $\mu\text{mol L}^{-1}$ and excellent linearity ($R^2 = 0.999$) [53]. DPV offers excellent sensitivity and linearity, enabling detection at very low concentrations with a lower signal-to-noise ratio, it is disadvantaged by a long analysis time compared to other techniques and it is not able to identify the oxidation state of the metallic ions [37]. **Square wave voltammetry (SWV)** is another highly effective technique for trace metal analysis, offering excellent sensitivity and selectivity, reaching nano- to picomolar range. SWV has proven effective in detecting heavy metal ions such as Pb(II), Cd(II), and Hg(II) within complex sample matrices, achieving accuracy comparable to ICP-MS [54]. As advantages SWV offers excellent portability, precision, and selectivity for analytical measurements. However, it generates complex data that can be challenging to interpret compared to simpler tec[37]. **Anodic stripping voltammetry (ASV)** and **cathodic stripping voltammetry (CSV)** are highly sensitive electrochemical techniques employed to detect trace heavy metals (ppm-ppb range). ASV preconcentrates

metal ions on the electrode surface before stripping them via anodic scan, while CSV forms an insoluble compound on the electrode, subsequently stripped via cathodic scan. Stripping voltammetry, while capable of simultaneous multi-element analysis even at trace levels, offers relatively fast analysis times. However, the duration is influenced by factors affecting metal deposition rate, including concentration, electrode area, and solution diffusion parameters. This technique is also highly cost-effective [37][55]. This method allows for rapid determination of trace Cd and Pb in wastewater, achieving high accuracy (>88%) compared to standard methods. Its applicability extends even to complex matrices like blood serum, where it demonstrates impressive sensitivity with low limits of detection (LODs) for Cd, Cu, Hg, and Pb (0.00114 ppb, 0.00261 ppb, 0.00232 ppb, and 0.00154 ppb, respectively) [56], [57]. **Differential pulse anodic stripping voltammetry (DPASV)** builds upon the foundation of ASV by incorporating a differential pulse waveform during the stripping step. This enhancement improves sensitivity and resolution, enabling more precise measurements of heavy metal concentrations. The concentration of Cu, Pb, Cd, and Zn in wine samples was, for example, determined using this method. Accuracy yielded recovery percentages ranging from 82.5% to 105.9%, demonstrating the method reliability for analyzing HMs in liquid samples [58]. **Cyclic voltammetry (CV)** is widely used for detecting and quantifying metallic species due to its user-friendly nature and its versatile. It measures the reduction and oxidation processes of various molecular species, providing also insights into the kinetics of electron transfer. CV exhibits sensitivity to residual currents, impacting analysis accuracy. Additionally, controlling background noise proves challenging, hindering trace analyte detection. CV also suffers from comparatively lower resolution [37]. Finally, **Electrochemical Impedance Spectroscopy (EIS)** offers a robust and sensitive approach to heavy metal detection in water samples, achieving high recovery rates (96.4% - 101.6%) in water and even in complex matrices like honey [59]. This technique analyzes the impedance response of an electrochemical system to a small AC voltage, providing insights into the electrode-solution interface and the mechanisms of heavy metal detection. While EIS offers real-time analysis capabilities and high sensitivity to interfacial and bulk parameters, it necessitates a Faraday cage to minimize environmental noise and requires tailored data analysis approaches for different situations [37].

1.3 Transition from the Laboratory to Field

The transition from laboratory to field monitoring methods presents several challenges (Figure 8). Field environments can be more complex and variable than laboratory conditions, with factors like temperature, humidity, and the presence of interfering substances affecting measurements. Understanding all the parameters that can affect the measurement helps minimize interferences, especially in non-inert environments. When approaching a systematic transition from laboratory methods to field monitoring methods for pollutants, it is crucial to have a

thorough understanding of all components and parameters that can influence the measurement. In the first case, an in-depth knowledge of the laboratory setup allows for the individual optimization of each component, enabling its implementation in a prototype that minimizes unnecessary elements for the customized analysis.

Figure 8 presents a diagram summarizing the key challenges in transitioning from laboratory to field-based sensors employing analytical techniques. Instrument design and performance are closely tied to two critical factors: portability and size, which require the device to be compact and lightweight for easy transport and use in various field environments. Additionally, power supply and battery life are essential, as the instrument must have a reliable and efficient power source to operate for extended periods without the need for frequent recharging or external power connections. Effective sample handling and analysis in the field requires the development of reliable methods for collecting, storing, and preparing samples, often in environments with limited resources and infrastructure. Simplifying these processes is critical, to achieve an automatic system. Automating procedures minimize manual handling, reducing the risk of errors and variability in the analysis, ultimately improving efficiency and accuracy. The most critical factor in field-based techniques is ensuring data quality and reliability. This begins with maintaining precise calibration of the instrument to guarantee that it can accurately detect and quantify analytes at the necessary sensitivity levels. Simplicity is key—since field operators may not be highly trained specialists, the equipment and procedures must be straightforward and easy to use. A major advantage of the mentioned above techniques is their ability to deliver high data quality, even under non-laboratory conditions, achieving detection limits at the parts-per-billion (ppb) level. This combination of simplicity and sensitivity makes these techniques exceptionally valuable for field applications. Nonetheless, data quality is essential to enable authorities to take immediate action in case of anomalies that may be harmful to the environment and human health. The acquired data can be instantly transmitted via the cloud for close monitoring of a contaminated or suspected site, or it can be stored within the instrument for later analysis following large-scale sampling. The use of chemical reagents necessary for monitoring the chosen pollutant, depending on the analytical technique employed, involves specific reagents (chromophores for UV-Vis and electrolyte solutions for voltammetry), which require manual maintenance and cannot be automated. Unlike typical laboratory practices, where reagents are prepared and used immediately, these reagents must be tested and guaranteed for long-term reliability when used in field conditions. Finally, two important practical considerations should be emphasized. First, laboratory instrumentation tends to be significantly more expensive than portable field devices. This higher cost is due to the advanced capabilities, precision, and complexity of lab-based equipment. Second, laboratory instruments offer the advantage of producing data that is certified according to established standards, ensuring the highest levels of accuracy, reliability, and reproducibility. These certifications are crucial in regulatory environments where data quality must meet strict compliance

requirements, which are often not guaranteed with more affordable field instruments.

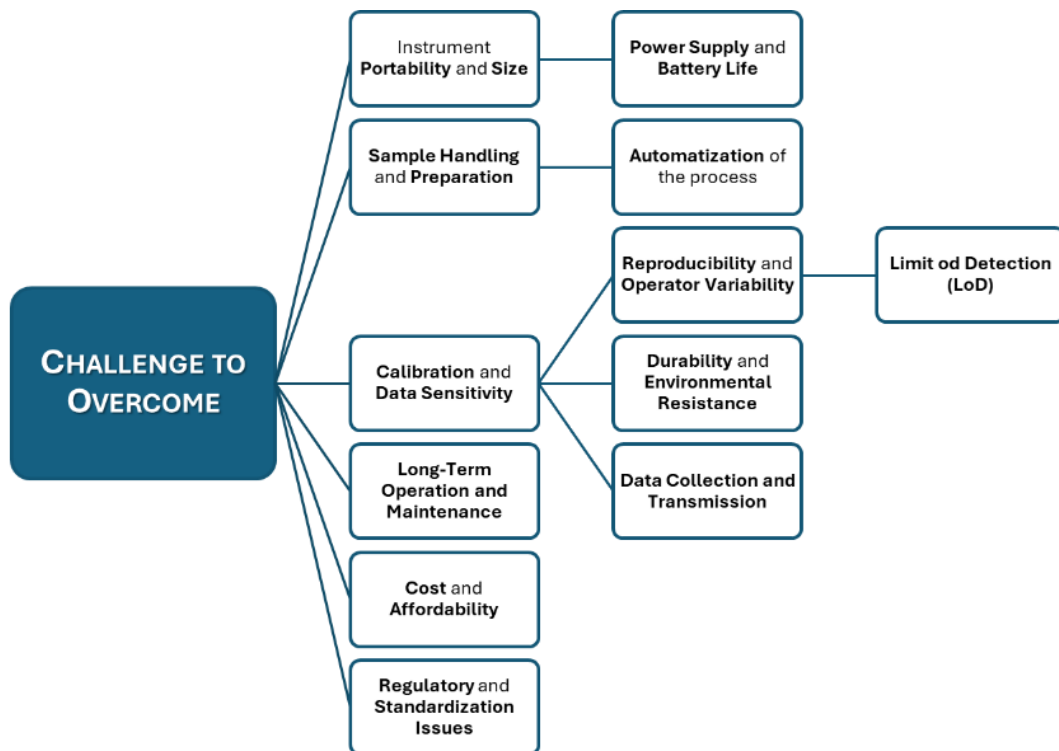


Figure 8: Diagram of key challenges that need to be addressed in the development and implementation of portable analytical instruments.

1.4 Water *In-Situ* Sensors

1.4.1 Importance of Continuous Real-Time Monitoring

Human settlements, pollution, and climate change have long generated problems that can directly affect the quality of water supply sources. Increasing levels of contamination are being detected in bodies of water due to fertilizers, heavy metals, pesticides, etc. Environmental monitoring of water is an important key to controlling and taking care of human life and the health of the environment. The quality of water influences river and marine fauna, but also the surrounding environment. **Protecting public health** relies heavily on clean water. It is necessary that water monitoring tools become available to local authorities and control units, to increase the amount of data available on water pollution and facilitate sharing.

The Figure 9 clearly shows an intense rise in scientific publications related to keywords water and sensors over the past 24 years. Starting from around 1,000 publications in 2000, the number soared to approximately 10,000 in 2023. This surge is likely driven by a combination of factors, including rapid advancements in sensor technology, increased awareness of water-related challenges, and the growing need for accurate water quality monitoring. This trend is the results of the 115,866 results found on Scopus for "water sensor," highlighting the extensive research conducted in this field. The increasing importance of water sensor

technology in tackling critical issues such as water scarcity, pollution, and efficient resource management is evident. The cited documents have a territorial distribution with publications originating predominantly from China, followed by the United States, India, and Germany. Italy ranks seventh in this classification for the number of publications.

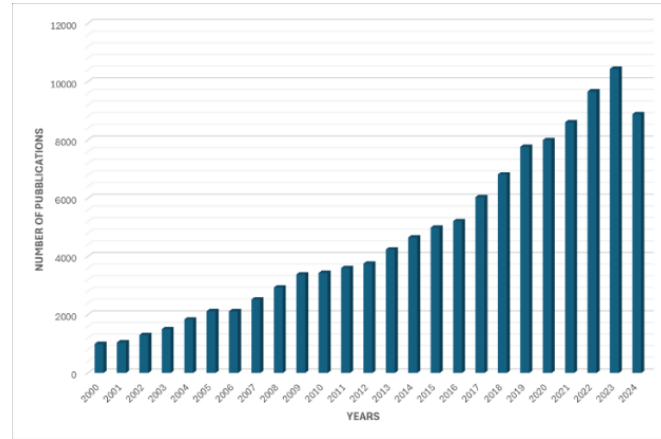


Figure 9: Identified number of publications in the last 24 years with Scopus search keywords: “water quality sensors”. (October 2024).

1.4.2 Design parameters

In this context **water quality monitoring *in-situ*** acts as a safeguard in several crucial ways. Despite the growing need for effective heavy metal detection, the development of sensing platforms that truly integrate practical considerations remains limited. A realistic approach to sensor design must encompass not only **analytical performance**, but also crucial factors such as **adherence to regulatory requirements**, **user-friendliness**, and **cost-effectiveness**. Currently, there is a notable gap in the development of sensing platforms that successfully balance these multifaceted demands [51], [60].

Sensor incorporation and optimization necessitates careful consideration of several factors. The sensor usually is integrated into a flow cell with high adaptability and mechanical stability, ensuring the sensing area is strategically positioned for efficient analysis of HMIs. Flow cell geometry must be optimized to eliminate dead volume, and a reliable sealing method is essential to prevent leakage between the sensor and flow cell assembly. Furthermore, the sensor's response and recovery time must be evaluated and minimized to ensure rapid and accurate measurements [61]. Table 5 provides a general overview of the typical requirements for environmental monitoring sensors [62]. These requirements encompass key aspects such as cost-effectiveness, portability, ease of use, and analytical performance. Ultimately, choosing and deploying environmental monitoring sensors requires a careful assessment of the specific context, ensuring the technology aligns with the unique needs and characteristics of the monitoring environment. The unique characteristics of each field monitoring scenario, such as

the target analyte, the environmental matrix, and the desired level of accuracy, will dictate additional, more specific requirements.

Table 5: Generalized guidelines for developing new sensors.

Feature	Target Specification
Cost per analysis	€1 - € 20
Portability	Lightweight and operable by one person. No external power source required or autonomous to be able to perform one to three analyses.
Analysis time	1 - 60 minutes
Training required	Minimal training (1-2 hours)
Measurement type	Capable of continuous, <i>in-situ</i> measurements with reversible sensors.
Sample compatibility	Minimal sample preparation needed for groundwater and soil extracts.
Sensitivity	mg/L to µg/L
Dynamic range	At least two orders of magnitude

1.4.3 Sensors for HMs detection

This project focuses on developing a sensor platform with the goal of transitioning it from research into a commercially viable product for real-world applications. To achieve this, it's crucial to understand the competitive landscape and the milestone achieved in the field. To assess the commercial viability of this sensor platform, it is mandatory to first analyze the existing market for similar technologies and achieve milestone in this sector. The rise of portable sensor devices has been fueled by technological advancements, particularly **the miniaturization of electronics** and the **ubiquity of smartphones and digital cameras**. These devices leverage LEDs, CMOS, and CCD technology to process optical or electrochemical signals, offering a cost-effective and efficient alternative to traditional, bulky laboratory equipment. This strategy opens new possibilities for portable, rapid, and quantitative detection in various applications [63].

Commercially available sensor devices often **integrate electrochemical or optical detection methods with microfluidic circuits**. This combination allows for a wide range of configurations, enabling the integration of multiple chemical reaction mechanisms and electrochemical analysis techniques within a compact chip. This approach leads to the creation of microelectromechanical systems (MEMS), also known as lab-on-a-chip devices. These devices shrink down the complex functionalities of a laboratory onto a single chip, offering a portable and efficient platform for water analysis. Microfluidic sensors offer several advantages. They minimize the need for large sample volumes and reduce reagent consumption, leading to cost-effective and environmentally friendly analysis. Moreover, these compact, "notebook-sized" devices provide rapid results, making them ideal for on-site water quality monitoring. While this technology offers a promising bridge between laboratory and field analysis, deploying MEMS sensors in real-world scenarios presents unique challenges. The interaction of these

miniaturized devices with aqueous solutions, like drinking water, introduces complexities that must be carefully addressed. Factors such as the added mass of the liquid affecting the sensor movement, increased damping hindering its response, surface tension influencing fluid behavior within the microchannels, the potential for electrolysis altering the chemical environment, and changes in thermal conductivity impacting sensor performance all need to be considered and mitigated for accurate and reliable results [61]. Despite some challenges in implementation, MEMS sensors have emerged as a popular solution for water quality monitoring, particularly for detecting HMs. Their integration with microfluidics has led to the development of compact and efficient water sensors that utilize a variety of analytical methods, with two main approaches being particularly prominent reported in Figure 10:

Chemical-based: These methods use chelating ligands that bind to heavy metal ions. This interaction causes a change in the spectroscopic properties of the sensor, such as absorption or fluorescence, which can be measured to quantify the concentration of heavy metals.

Electrochemical based: These methods measure changes in current, voltage, or potential caused by the presence of heavy metal ions. This can be done using techniques like voltammetry or amperometry.

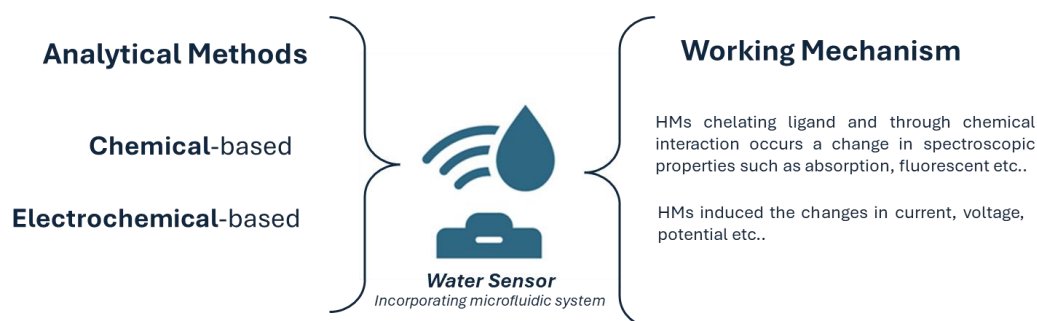


Figure 10: Illustration of typical and most common operating principles of contemporary sensors employed for monitoring heavy metals in water.

Starting with commercial devices based on electrochemistry techniques such screen-printed electrodes (SPEs), the literature offers numerous solutions based on innovative microfluidic designs or modifications of the working electrode that customize the final sensor to the specific analytical target. Electrode surface enhancement can be achieved by incorporating various **nanomaterials**, such as metal nanoparticles, metal oxide nanoparticles, or carbon-based nanomaterials. These nanoparticles increase the electrode surface area due to their small size. Metallic nanoparticles enhance mass transport and electron transfer rates, ultimately improving the sensitivity of the electrodes [64]. Highly sensitive method for detecting trace amounts of lead (Pb) in seawater using disposable screen-printed electrodes modified with nanomaterials: single-walled carbon nanotubes, electro-reduced graphene oxide, and gold nanoparticles. The WE was enriching with gold nanoparticles around 100 nm achieving a remarkable detection limit of 3.21×10^{-10} M for Pb^{2+} in seawater without requiring pH adjustment [65]. The most advanced applications attempt to achieve the

development of a fully integrated electrochemical sensor array capable of simultaneously monitoring multiple parameters, including pH, free chlorine, and temperature. This advanced system provides highly sensitive and targeted on-demand detection capabilities. It can identify and quantify minute traces of pharmaceuticals at concentrations below 10 nM and heavy metals at concentrations below 10 ppb. A custom-designed readout circuit, potentiostat, and Android app provide control and user interface. Its modular design allows for easy modification and integration of additional sensors, making it adaptable for monitoring a wide range of water quality parameters. Figure 9 illustrates the integrated system for monitoring water quality in various sources like tap water, swimming pools, and lakes. This system boasts high sensitivity, rapid response time, and user-friendly operation, all at a low cost of approximately \$336 CAD [66]. The whole design successfully integrates the entire signal chain for electrochemical sensors, seamlessly connecting signal transduction, conditioning, processing, and low-power wireless transmission. This approach overcomes the challenges typically encountered in integrating these individual components.

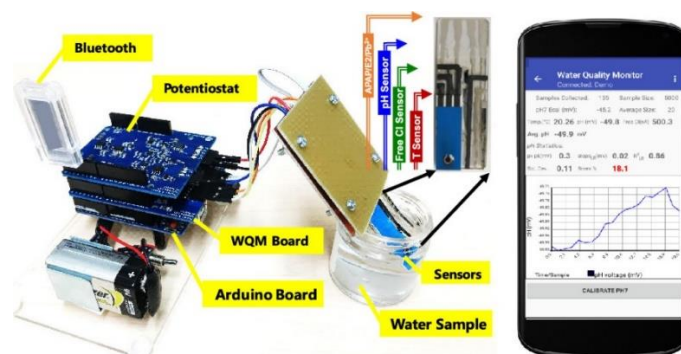


Figure 11: Schematic representation of a fully integrated water quality monitoring system (FIWQMS) with fabricated sensor for HMs detection [66].

Another possible design and configuration for portable and affordable (US\$160) device for on-site detection of heavy metal pollutants in water is depicted in Figure 10. This user-friendly device utilizes a disposable plastic pipette with a six-electrode configuration (two sets of counters, reference, and working electrodes) and a pump valve to prevent cross-contamination between samples. To operate, the user activates the pump valve, drawing the liquid sample into the pipette and onto the electrochemical sensor. This system achieved impressive detection limits for various heavy metals: zinc (Zn) [10 ng/mL], mercury (Hg) [2.5 ng/mL], copper (Cu) [5.5 ng/mL] and lead (Pb) [2.2 ng/mL]. The device was successfully tested with industrial wastewater and rainwater samples, demonstrating its practical applicability. Its portability, minimal sample requirement (30 μ L), user-friendly design, and cost-effectiveness make it a promising tool for point-of-care testing of heavy metal contamination [67].

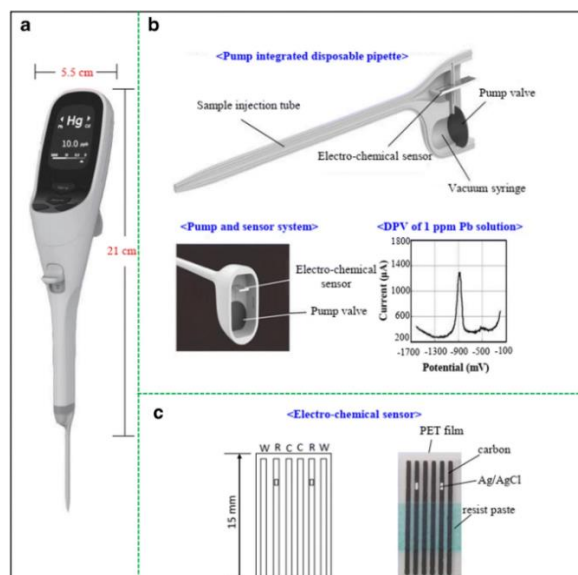


Figure 12: (a) The HMs final prototype; (b) The schematic internal disposition for the principle of pipetting sample into the instrument and how to detect the target heavy metal ions by electrochemical sensor; (c) Details the design and a visual representation of the chip containing six electrodes [63].

AppliTrace is a commercially available platform for comprehensive water quality analysis. It utilizes anodic stripping voltammetry to provide online monitoring of heavy metals such as cadmium, lead, copper, arsenic, zinc, and iron in both clean and contaminated water sources. To ensure accurate and sensitive detection (limit of detection = 1 $\mu\text{g/L}$), AppliTrace incorporates hot acid digestion to break down organic matter and minimize interference. Additionally, pre-concentration methods are employed to enhance the detection of trace levels of these heavy metals [64].

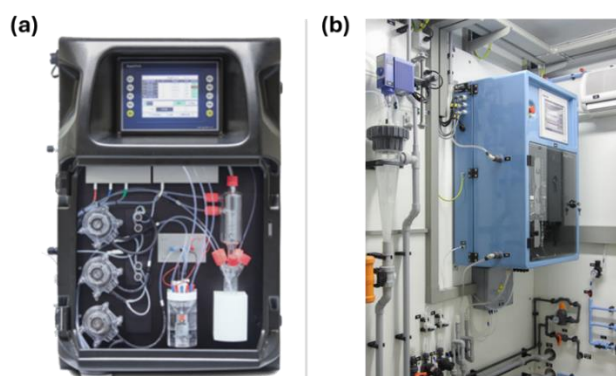


Figure 13: On-line Environment Analyzer AppliTrace (a) front view and (b) integrated into a comprehensive system.

Another level of complexity is introduced with an original approach to water quality monitoring by combining a semi-autonomous surface vehicle with a microfluidic device for on-site heavy metal detection using square wave anodic stripping voltammetry with carbon-based screen-printed electrodes to detect lead (Pb) and copper (Cu) pollution in surface water. Laboratory experiments simulating real-world scenarios validated the system effectiveness in identifying heavy metal. The system performance was rigorously evaluated according to ISO

15839 standards. It demonstrated a measurement bias of 75% for lead (Pb) and 65% for copper (Cu). Reproducibility was assessed by relative standard deviation, ranging from 11-18% for Pb and 6-10% for Cu. The system achieved a limit of detection of 4 $\mu\text{g/L}$ for Pb and 7 $\mu\text{g/L}$ for Cu, with a lowest detectable change (LDC) of 4-5 $\mu\text{g/L}$ for Pb and 6-7 $\mu\text{g/L}$ for Cu. Furthermore, the screen-printed electrodes exhibited a lifespan of approximately 39 measurements per day, ensuring sufficient durability for typical monitoring campaigns[68].

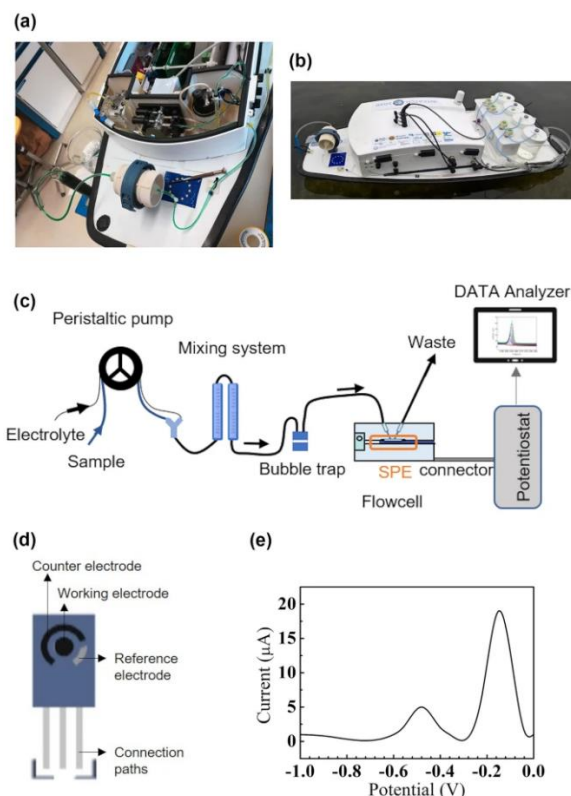


Figure 14: a Implementation of filtration system and HM microfluidic detection device on the autonomous surface vehicle; b autonomous surface vehicle, equipped with HM microfluidic detection device, filtration system, and sampler, deployed in a field experiment; c schematic representation of components of the HM microfluidic detection device; d schematic representation of one SPE; e example of the voltammogram [68].

Portable colorimetric sensors are increasingly being utilized with smartphones for quick and cost-effective water analysis. For example, a 2016 system detected mercury (Hg^{2+}) in just 20 minutes using a smartphone and a nano-adaptor colorimetric sensor. This system achieved a remarkable detection limit of 0.28 ng/mL . Building on this, researchers developed a 3D-printed smartphone-based device for rapid colorimetric detection of heavy metals like lead (Pb^{2+}), mercury (Hg^{2+}), cadmium (Cd^{2+}), and zinc (Zn^{2+}). LED lamp emits light that is filtered and then analyzed by a smartphone built-in optical sensors and light meter apps. This setup achieves impressive detection limits, measured in micrograms per milliliter ($\mu\text{g/mL}$), for various metals. A key advantage of this system is its ability to provide reliable results even with complex real-world water samples. This is because the reagents used are designed to resist interference from other substances, ensuring accurate measurements of the target metals [69].

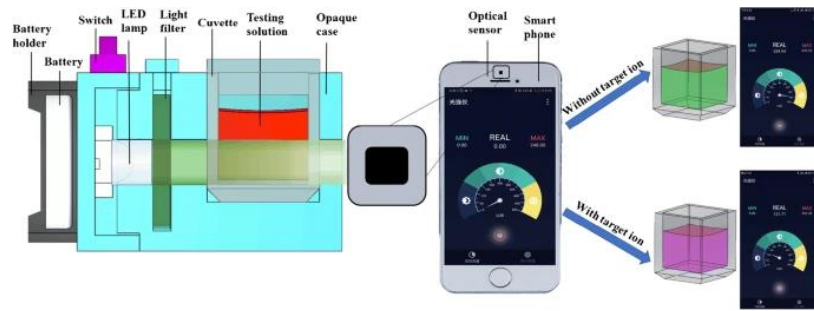


Figure 15: Diagram illustrates a portable, smartphone-based colorimetric water testing system [69].

For optical absorbance detection combine with microfluidics often are utilizes Light Emitting Diodes (LEDs) as light source are the preferred one. These LEDs, paired with fiber optics, offer several advantages since they emit a narrow band of wavelengths, eliminating the need for complex optical components like couplers or monochromators. LEDs are durable and can operate reliably even in challenging environments with high humidity and vibrations, making them well-suited for microfluidic *in-situ* applications for a new portable optofluidic system for on-site water quality analysis. The optical detection module consists of a flow cell, LED light source, and a micro-spectrometer. This optofluidic device analyzes water samples using chromogenic reactions. It features a micromixer made of PDMS with rugged microchannels on a glass slide. Water samples, deionized water, and reagents are introduced through three inlets. Mixing and reactions occur in the microchannels, and the resulting solution flows to an optical detection module. This module includes a 3D-printed flow cell, LED light source, and micro-spectrometer for analysis. The device can automatically adjust the concentration of water samples by varying the flow rate ratio between the sample and deionized water. This allows for on-chip calibration and the creation of a standard curve for accurate measurement of target substances. It features automatic calibration for measuring pollutants like hexavalent chromium, orthophosphate, and ammonia nitrogen. The system uses a modified algorithm to generate standard curves and achieves a detection limit of 0.05 mg/L for chromium (VI) with a relative error of about 6% compared to standard methods. By simply changing the reagents, this adaptable instrument can monitor various pollutants in surface water [70].

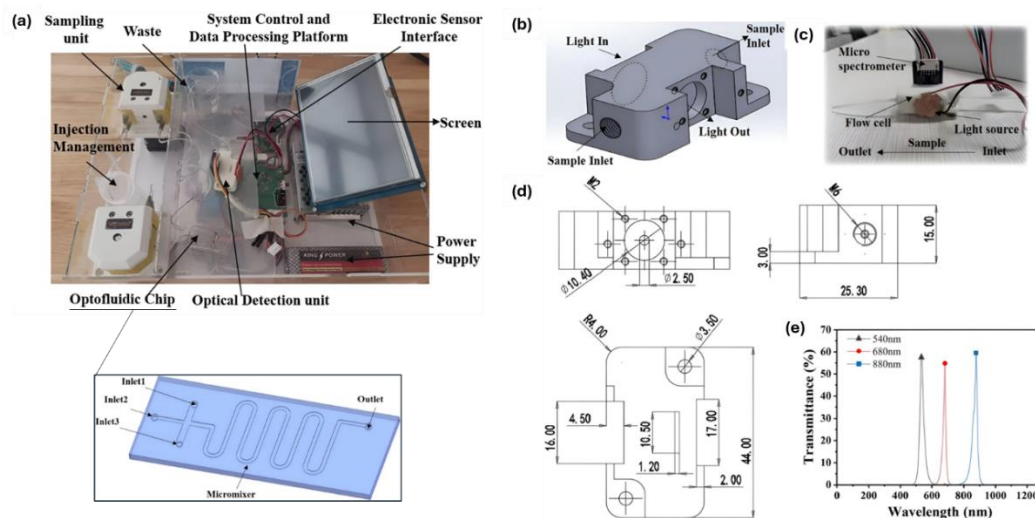


Figure 16: (a) Optical detection prototyping. Magnification shows the microfluidic system; (b) 3D printing flow cell of detection; (c) Detailed dimensions of internal flow cell; (d) The complete setup with the flow cell, LED light source, and micro-spectrometer; (e) LED emission spectrum [70].

1.5 Scope and outline of the work

This thesis aimed to develop a sophisticated and innovative sensor platform and MEMS devices for the environmental monitoring of heavy metal contamination in both drinking and industrial water sources. This objective was pursued through three distinct projects, TrAcqua, IntelWATT and Agritech, developed within the research group at Polito Materials and Processes for Micro and Nano Technologies (MP4MNT) at Chilab Laboratory.

The **TrAcqua project** seeks to address groundwater safety and quality through a dual approach. Firstly, it introduces a novel treatment module comprised of two distinct electrochemical systems. One system is specifically designed to neutralize bacterial contamination, ensuring the water is safe from harmful microorganisms. The second system targets and removes metallic pollutants, further enhancing the purity of the water. To further enhance the efficacy of the process, a sophisticated monitoring system that was integrated into the system provides a comprehensive analysis of water samples taken from the reservoir both before and after treatment, with a specific focus on detecting and quantifying heavy metal concentrations. This system leverages cutting-edge technologies, including Lab-on-Chip (LoC) miniaturized devices and the Internet of Things (IoT). This allows for real-time data collection and analysis, providing continuous insights into the water's condition and the effectiveness of the treatment process.

The **Intelwatt project** was conceived with the aim of developed in-line MEMS sensors for monitoring industrial process and wastewater, particularly those originating from the electroplating industry. This has a twofold purpose: ensuring the quality of the final product by monitoring the concentration of heavy

metals within the galvanic bath and guaranteeing the correct management of wastewater.

The **Agritech project** aims to shape future agricultural and rural systems to create an operational space that ensures nutritious, healthy, and sustainable food for all, while achieving full circularity of food and agricultural systems. Within the project's framework of nine research areas, this work concentrated on developing technology to monitor heavy metal contamination, specifically cadmium, in rural water systems.

In collaboration with Microla Optoelectronics, the purpose of this thesis was to develop a system prototype specifically designed for water monitoring. This involved the development of MEMS sensors utilizing established chemical techniques, namely UV-Vis spectrophotometry with colorimetric methods and stripping voltammetry. A comprehensive review of these techniques, encompassing the state-of-the-art and fundamental laboratory principles, methodologies, and instrumentation, is presented in Chapters 1 and 2.

Following the selection of appropriate techniques and methodologies, rigorous laboratory validation and optimization were conducted. Chapter 3 details the development and optimization of the UV-Vis spectroscopy method, while Chapter 4 focuses on the electrochemical technique.

Through a collaborative effort integrating chemical, mechanical, and electronic engineering expertise, supported by Microla Optoelectronics, a prototype sensor platform was realized. This platform incorporates dedicated MEMS sensors for the detection of arsenic and chromium (VI) and (III), alongside multi-parameter probes capable of measuring essential physicochemical parameters. The intricate integration and prototyping process, culminating in the *in-situ* installation of the realized prototype, are meticulously documented in Chapter 5.

Finally, Chapter 6 offers concluding remarks and future perspectives. It emphasizes the potential of achieving significant sensitivity and accuracy in heavy metal detection through the application of relatively straightforward yet powerful techniques. The chapter also includes a brief discussion of future work in the Agritech field and underscores the significance of this research in contributing to the advancement of sustainable water monitoring systems and the preservation of water resources.

Chapter 2

Methodologies

Among the techniques suitable for the quantification of heavy metals (HM) in water, the most widely used are inductively coupled plasma mass spectrometry (ICP-MS), atomic absorption spectroscopy (AAS), and atomic emission spectroscopy (AES). These methods are renowned for their reliability and sensitivity in detecting trace amounts of metals. However, despite their effectiveness, they come with notable limitations especially for *in-situ* sensors. The cost of acquiring and maintaining the necessary instruments is high, making them an expensive option for many laboratories. Additionally, the procedures involved are often time-consuming, particularly regarding sample preparation, which can be a complex and labor-intensive process. Furthermore, these sophisticated instruments and the expertise required to operate them are not always readily available, especially in smaller or less well-funded facilities.

2.1 Optical Methods

The word **spectroscopy is used to characterize optical methods** where, in general, the study is made of the emission, absorption or scattering of electromagnetic radiation involving energy changes in nuclei, atoms or molecules. The electromagnetic radiation interaction with matter provides a versatile platform for investigating the intrinsic properties and characteristics of a sample. Through these interactions, a diverse array of analytical techniques can be developed to extract both qualitative and quantitative information. Optical methodologies can explore the composition, structure, and physical properties of materials on a molecular and macroscopic level. The range of electromagnetic radiation may vary from X-rays, through visible to radio waves [71].

2.1.1 Electromagnetic radiation

Electromagnetic radiation (EMR) encompasses a spectrum of energy propagated through space in the form of waves, characterized by oscillating

electric and magnetic fields perpendicular to each other. Electromagnetic waves propagate in matter but also in vacuum. For optical phenomenon only the electric displacement needs to be considered.

Electromagnetic radiation has indeed dual nature:

- A stream of discrete particles, called photons (or quanta).
- A type of energy that is transmitted through space with enormous velocities, called waves.

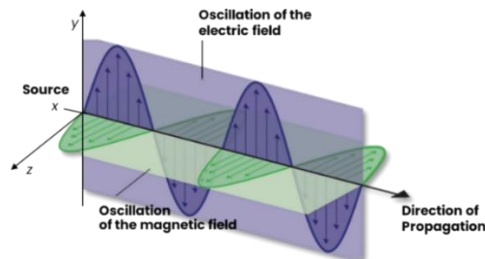


Figure 17: The electric and magnetic fields of electromagnetic radiation.

Every electromagnetic wave is characterized by the following parameters [72]:

1. **Wavelength (λ):** This is the distance between two consecutive points in the wave that are in phase with each other (e.g., two crests or two troughs). It determines the color of visible light and influences the wave ability to interact with matter. It is designated by λ (lambda), and its units depend upon the region of the spectrum. In ultraviolet and visible region Angstrom (\AA) and nanometer (nm) are widely used with the follow correlation $\text{\AA} = 10^{-10} \text{ m} = 1 \text{ nm}$.
2. **Frequency (ν):** This is the number of oscillations per second, or the number of waves passing a fixed point in one second. It is inversely proportional to the wavelength and is closely related to the energy of the wave. Unit of frequency is Hertz, $1\text{Hz} = 1 \text{ waves per sec}$. Frequency is denoted by ν (nu). Frequency is determined by the source and remains invariant regardless of the medium through which the radiation travels.
3. **Amplitude (A):** This is the maximum displacement of a point from its equilibrium position. It determines the intensity of the wave and, for light, corresponds to its brightness.
4. **Intensity (I):** This is the power per unit area carried by the wave. It is directly proportional to the square of the amplitude and represents the amount of energy the wave transfers per unit time across a unit area perpendicular to the direction of propagation.
5. **Velocity of propagation:** The velocity of an electromagnetic wave is the rate at which the wave front moves through a medium. The velocity of all electromagnetic waves in vacuum is the same (equal to $2.998 \times 10^8 \text{ m/s}$ (meter per second) and is denoted by c . However, velocity is dependent upon both the

composition of the medium and the frequency. But in vacuum the velocity of radiation becomes independent of frequency and is at its maximum.

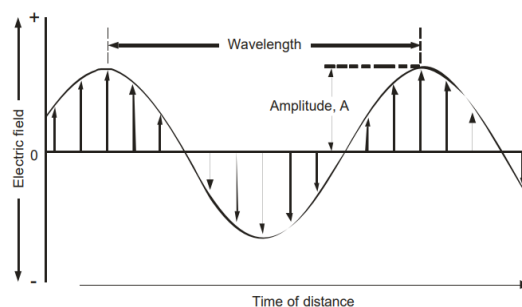


Figure 18: Wavelength (λ) and amplitude (A) associated with electromagnetic radiation.

The **electromagnetic spectrum** is broken down in different regions of wavelengths and frequencies. It includes, from longest wavelength to shortest, radio waves, microwaves, infrared radiation, visible light, ultraviolet radiation, X-rays, and gamma rays. Each region of the spectrum has distinct characteristics and applications: radio waves are used for communication, microwaves for radar, infrared for thermal imaging, visible light for human vision, ultraviolet for sterilization, X-rays for medical imaging, and gamma rays for cancer treatment. The energy of electromagnetic radiation increases with frequency, meaning that gamma rays have the highest energy, while radio waves have the lowest.

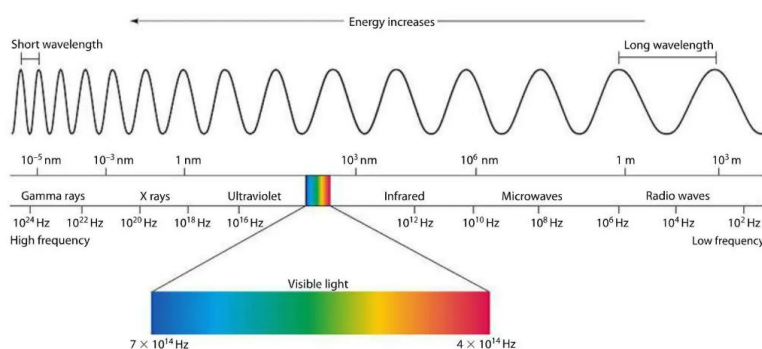


Figure 19: Representation of electromagnetic spectrum.
(<https://www.xrayconsult.it/nota-rx.html>)

When light is absorbed, the energy of the radiation increases the internal energy of the atom or molecule, leading to various phenomena. These effects, detailed in Table 6, depend on the wavelength of the light and are associated with specific types of spectroscopies.

Table 6: Regions of the electromagnetic spectrum and types of transition involved.

Electromagnetic Radiation	Wavelength Range	Type of Transition
γ - Rays (Moss Bauer spectroscopy)	0.005 – 1.4 Å	Nuclear transition (change of nuclear configuration)

X-rays (Diffraction, Absorption, Emission, Fluorescence)	0.1 – 100 Å	Inner electron transition (change of electron distribution)
Vacuum UV (Absorption)	10 – 180 nm	Bonding electrons transition (change of electron distribution)
Ultraviolet- Visible (Absorption, Emission, Fluorescence)	180 – 780 nm	Bonding electrons transition (change of electron distribution)
Infrared (Absorption) and Raman (Scattering)	0.78 – 300 μm	Vibration/Rotation of molecules (change of configuration)
Microwaves (Absorption)	0.75 – 3.75 nm	Rotation of molecules (change of orientation)
Electron Spin Resonance (ESR)	3 cm	Spin of electrons in a magnetic field (change of electron spin)
Nuclear Magnetic Resonance (NMR)	0.6 – 10 m	Spin of nuclei in a magnetic field (change of nuclear spin)

The **internal energy of molecules** refers to the total energy contained within a molecule due to its various forms of motion and interactions. This includes **vibrational energy**, which arises from the oscillation of atoms within the molecule. The energy required to alter this state is associated with microwaves, and the technique used to study such transitions is called microwave spectroscopy. The **rotational energy**, resulting from the molecule rotation about its center of mass. **Translational energy**, associated with molecule movement through space. Additionally, **internal energy encompasses electronic energy**, related to the arrangement and excitation of electrons within the molecule. These forms of internal energy contribute to the overall molecule state and influence its behavior in chemical reactions and physical processes. The energy levels are quantized, and the radiation capable of causing electronic transitions falls within the visible and ultraviolet (UV) regions. The technique used to study these transitions is called UV-Visible spectroscopy [73].

Within a molecule, electronic energy levels are further subdivided into vibrational levels. Transitions between these vibrational levels can be probed using infrared (IR) spectroscopy. Furthermore, each vibrational level is further quantized into rotational levels. Transitions between these rotational levels occur at lower energies and can be investigated using microwave (MW) spectroscopy.

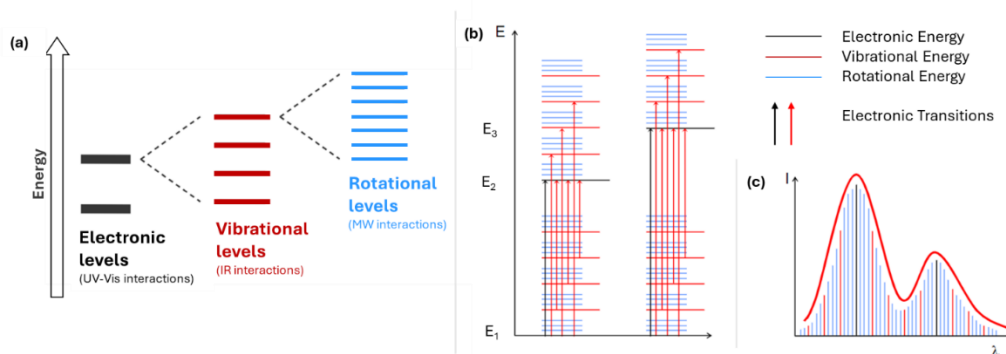


Figure 20: (a) The energy of a molecule is quantized: there are only discrete energy levels, corresponding to different states of the molecule. (b) Possible electronic transitions that are involved in absorbance. (c) The spectrum resulting from the sum of all the energy contributions. Image modified by [73], [74].

According to quantum mechanics, electromagnetic radiation can be considered as a flux of photons, which are massless particles possessing a specific energy. The system may absorb energy and go from the lower energy state (ground state), E_1 , to higher energy state (excited state), E_2 . This transfer of energy is quantized and energy difference, ΔE , between these two states is defined by the following equation:

$$\Delta E = E_2 - E_1 = h\nu$$

where E is energy (J), h is Planck constant (6.62×10^{-34} J s) and ν in frequency (sec).

In fact, a beam of light is more or less intense depending on whether it carries more or fewer photons per unit of time, but the energy of each photon (the quantum of energy) is always the same for a given frequency of the radiation.

Because **radiation acts as a wave**, it can be classified in terms of either **wavelength or frequency**, which are related by the following equations:

$$\nu = \frac{c}{\lambda}$$

$$\Delta E = hc/\lambda$$

where c is the speed of light (3×10^8 ms⁻¹) [72], [73].

2.1.2 Absorption of Electromagnetic Radiation by Species

When EMR interacts with matter, many phenomena can occur isolated or simultaneously, such as **light absorption**, reflection, dispersion, refraction, and others. In case of light absorption two important events happen: the transfer of energy from the radiation to the matter (**absorption**), followed by the complete return of energy in different forms (**emission**). Absorption occurs in an extremely

short time frame ($\sim 10^{-15}$ s): upon absorbing radiation of adequate energy, the atom or molecule transitions from the ground state with minimal energy to a higher energy state known as the excited state. The excited state is unstable and has a very short lifespan because the atom or molecule tends to return to the ground state by losing the acquired energy in the form of heat, radiation, or both. **Organic and inorganic species can both absorb electromagnetic radiation**, which allows them to be studied using spectroscopic techniques.

Organic compounds, such as dyes and pigments, often absorb radiation in the visible and ultraviolet (UV-Vis) regions, leading to color changes that can be analyzed, according to molecular orbital theory. The three kinds of electrons responsible for electronic transitions are:

- Sigma (σ) electrons in saturated molecules
- Pi (π) electrons in unsaturated molecules
- Nonbonding (n) electrons in nonbonded elements

These electrons absorb ultraviolet radiation, which causes excitation. The movement from the ground state to a higher energy state is categorized into four types of electronic transitions depicted in Figure 21 [75].

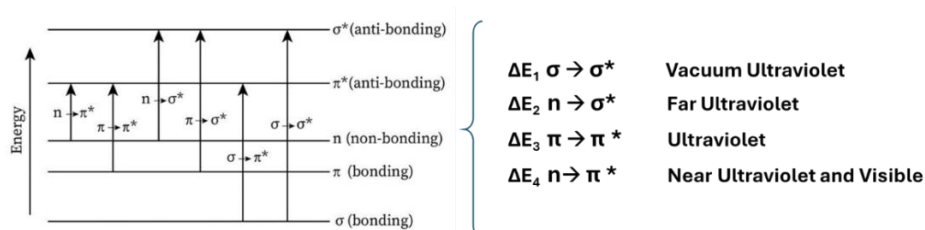


Figure 21: Types of electronic transitions for organic species.

Absorption by **inorganic compounds** in UV-Vis region usually can be ascribed to one or more of the following transitions [71]:

- Excitation of the metal ion
- Excitation of the ligand
- Charge transfer transition.

The interaction of light with their electronic structures in inorganic compounds involves, especially those containing transition metals in coordination compounds, often exhibit electronic transitions where electrons are excited from lower energy d-orbitals to higher energy d-orbitals according to crystal field splitting energy (Figure 22). The electrons present in the ground state absorb light in visible range and jump into a higher energy level and the complementary colours appear. These transitions are typically observed in the visible and ultraviolet (UV-Vis) regions of the electromagnetic spectrum [76].

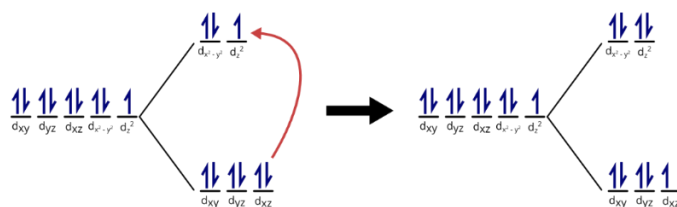


Figure 22: d-d transition for inorganic species.

2.1.3 Absorbance vs Transmittance

Spectroscopy analysis methods involve examining the spectrum of substances, which can be classified as either emission or absorption spectra. An absorption spectrum is obtained by plotting absorbance or transmittance against wavelength. Figure 23 illustrates two maxima peaks occurring at points (i) and (ii), indicating intense absorption at the corresponding wavelengths [72]. These maxima values remain constant regardless of the type of parameters represented on the y-axis. **Absorption Methods** in general, **using ultraviolet-visible regions**, are probably the most frequently used analytical technique for the quantitative estimation of substances in traces.

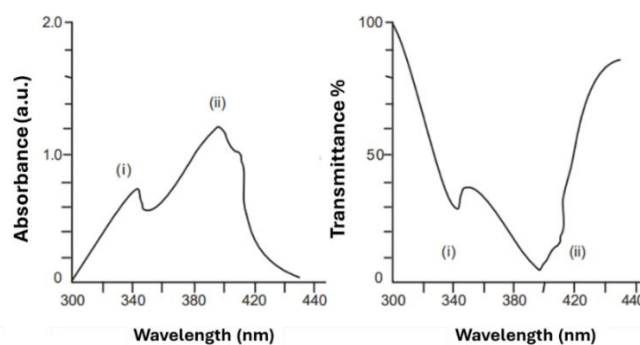


Figure 23: The plot of Absorbance (A) or Transmittance (T) vs. wavelength (λ).

When examining an absorption spectrum, several important parameters must be considered to accurately interpret the data. The **wavelength of the absorption peaks** is crucial, as it indicates the specific energies at which a substance absorbs light, reflecting its electronic transitions and molecular structure. The **intensity of these peaks**, often measured as absorbance or transmittance, provides information about the concentration of the absorbing species according to Beer-Lambert's law. Additionally, **the bandwidth of the peaks** can reveal details about the environment around the absorbing molecules, such as temperature and solvent effects. The **baseline of the spectrum** must be evaluated to correct for any background absorption or instrument noise. Finally, the **shape of the peaks** can offer insights into interactions between molecules, including broadening effects due to molecular collisions or binding events. Together, these parameters help in identifying substances, determining their concentrations, and understanding their interactions and environments.

2.2 Absorption Methods: Lambert-Beer Law

The Lambert-Beer Law is a fundamental principle in spectroscopy that relates the absorption of light to the properties of the material through which the light is traveling.

To perform **quantitative spectrophotometric analyses**, sources emitting radiation are used, which pass through the sample, absorbing part of this radiation before reaching a detector capable of detecting the non-absorbed radiation. Specifically, Figure 24 schematically represents the intensities of the incident radiation (I_0) on the sample and the intensity of the transmitted radiation (I).

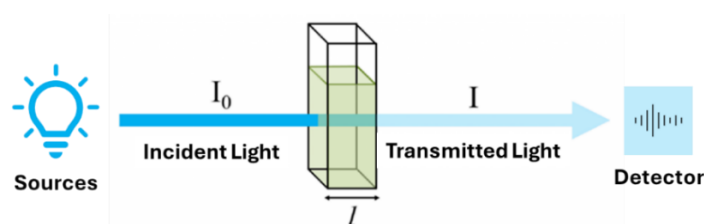


Figure 24: Transmission of light through a sample solution in a cuvette. Image modified by [77].

From the measurement of I_0 and I , the technique directly provides the values of transmittance and absorbance, which represent the characteristic quantities of absorption spectroscopy.

Transmittance (T) is the fraction of incident light that passes through a sample. It is a measure of how much light is transmitted through the substance. Transmittance is defined as the ratio of the intensity of the transmitted light (I) to the intensity of the incident light (I_0) and takes values between 0 and 1:

$$T = \frac{I}{I_0}$$

Transmittance is often expressed as a percentage:

$$T\% = T \times 100$$

Where $T\% = 100$ means that the beam has not undergone any attenuation, i.e., there has been no absorption by the substance; $T\% = 0$ means that the beam has been completely absorbed.

Absorbance (A), also known as optical density, measures how much light is absorbed by a sample. It is related to transmittance but is logarithmic in nature. Absorbance is defined as:

$$A = -\log T$$

Absorbance itself is unitless, but it is common to see absorbance values followed by AU, which stands for either arbitrary units or absorbance units.

Absorbance is linearly related to the concentration of the absorbing species in the sample, as described by Lambert-Beer Law. This law quantitatively expresses that the absorbance of light passing through a substance is directly proportional to both the concentration of the absorbing species and the path length of the light through the material. The molar absorptivity, or extinction coefficient, is a constant that indicates how strongly the substance absorbs light at a specific wavelength. The relationship is given by the following equation:

$$A = \epsilon cl$$

where:

ϵ is the molar absorptivity (or molar extinction coefficient) in L/(mol·cm),

c is the concentration of the absorbing species in mol/L,

l is the optical path length of the sample cell in cm.

This law is essential for analytical chemistry as it enables the determination of the concentration of an unknown sample by measuring its absorbance at a specific wavelength and comparing it to a standard curve. Several key aspects make the Lambert-Beer Law particularly important. First, the linear relationship between absorbance and concentration allows for the straightforward calculation of unknown concentrations, provided that the system adheres to the conditions of the law. Secondly, the molar absorptivity (ϵ), is unique for each substance and wavelength, providing a specific fingerprint that can be used for identification purposes. Thirdly, the law assumes that the absorbing species does not change their nature over the range of concentrations used, that the light is monochromatic, and that the system follows ideal behavior without deviations due to interactions between absorbing molecules or scattering of light.

2.2.1 Deviation of Lambert-Beer Law:

Deviations from Lambert-Beer Law can arise from various factors that caused a variation in absorptivity. When analyzing a calibration curve, which is a plot of absorbance versus concentration, it is expected to yield a straight line passing through the origin (see Figure 25b). However, if the plot shows a curve instead of a straight line, this indicates deviations. An upward curvature, as seen in curve (a), represents a positive deviation, while a downward curvature, as shown in curve (c), represents a negative deviation. In real case scenarios, the calibration curve often displays a slope that resembles either curve (a) or (c). Even if the relationship between absorbance (A) and concentration (c) remains linear, deviations in the slope can still occur, though these deviations are generally small and gradual. Typically, the path length of the cell remains constant and does not contribute to deviations in this linear relationship.

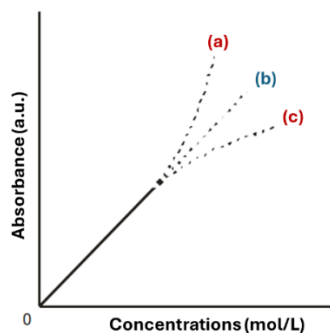


Figure 25: Deviations from Lambert-Beer law. Image modified by [72].

Variations in absorptivity are generally classified into two main classes. The first category includes factors such as non-monochromatic radiation, dissociation, association, complex formation, polymerization, solvolysis, the stability of the absorbing species, pH, photochemical reactions, reaction time, and temperature. Deviations from Lambert-Beer Law due to these factors are referred to as **apparent deviations**, as they arise from experimental conditions rather than from limitations inherent to the law itself. Usually, these limitations are easily overcome, as they disappear when the appropriate conditions are applied. The two conditions that require the most attention is reported:

1. **Temperature:** The temperature-induced shift in ionic equilibrium can lead to deviations from expected absorbance values. This is because the concentration of absorbing species changes with temperature, and the absorptivity may also vary. Thus, careful control of temperature is important to ensure accurate spectrophotometric measurements.
2. **Non-monochromatic Radiation:** Lambert-Beer's Law assumes that accurate measurements require monochromatic radiation at a single wavelength where the substance's absorptivity is well-defined. Typically, spectrophotometers use narrow-band filters to approximate this condition. However, if the radiation is not perfectly monochromatic, the relationship between absorbance and concentration may become non-linear.

The other category is **real limitations**. These deviations are considered genuine rather than apparent and may happen due to the following factors:

3. **Concentration:** At high concentrations, the law may no longer applicable due to significant intermolecular interactions, such as aggregation or complex formation, which affect absorbance. On the other hand, at low concentrations, the absorbance might be too low to measure accurately due to limitations in detector sensitivity and noise. Generally, Lambert-Beer law is applicable to dilute solutions only (that is for concentration lower than 0.01M).
4. **Refractive Index:** Absorptivity is dependent on wavelength and can vary with the medium used during the analysis. Changes in the refractive index (μ) of the medium affect absorptivity, making it contingent on the solution's

refractive index. However, this effect is typically minor and usually falls within the experimental error range of spectrophotometric measurements.

5. **Non-Homogeneous Solutions:** Beer's Law assumes a homogeneous solution. Deviations occur if the sample is not uniformly mixed or disperse.

2.3 Colorimetric detection

Color in chemistry is a very important and exploited aspect since it is a perceptual quality that arises from how our eyes and brain interpret different wavelengths of light. Colorimetry, particularly through techniques like UV-Vis spectroscopy, measures the intensity of color in a solution [78]. By analyzing how light is absorbed and transmitted, colorimetry allows to determine the concentration of solutes, characterize chemical compounds, and track the progress of chemical reactions.

When light interacts with an object, it can be absorbed or reflected. The color we perceive is based on the wavelengths of light that are reflected to our eyes. For instance, if a substance has a λ_{\max} in the blue region of the spectrum, it means it absorbs blue light most strongly. Consequently, the wavelengths that are not absorbed (which are on the opposite end of the spectrum, such as orange or yellow) are reflected. This reflection determines the color we see. Thus, the color perceived is often complementary to the color absorbed. If blue light is absorbed (where λ_{\max} is in the blue region), the object will appear more towards the complementary colors, such as orange or yellow, which are reflected [71].

Table 7: Colors of Different Wavelength Regions.

Wavelength Absorbed (nm)	Absorbed Color	Transmitted Color (Complement)
380–450	Violet	Yellow-green
450–495	Blue	Yellow
495–570	Green	Violet
570–590	Yellow	Blue
590–620	Orange	Green-blue
620–750	Red	Blue-green

Colorimetric detection using UV-vis spectroscopy can be applied in two primary scenarios. In the first case, the sample itself exhibits an **intense color that can be directly exploited** for analysis. Aqueous samples typically exhibit an intense color when they contain a high concentration of pollutants. In the second scenario, the substance to be analyzed, colorless or weakly colored, reacts with a colorimetric reagent (chromophore) to form a stable-colored complex. The former is referred to as direct colorimetry, while the latter is **indirect colorimetry**, as it requires the addition of a second component to impart color to the solution.

2.4 Instrumentation of UV-Visible spectroscopy

The basic instrumentation of the UV-Vis spectrometer comprises four essential elements [79]:

- **Light source**
- **Monochromator:** Collimator, diffraction grating or prism and slit
- **Sample holder (cuvette)**
- **Detector**

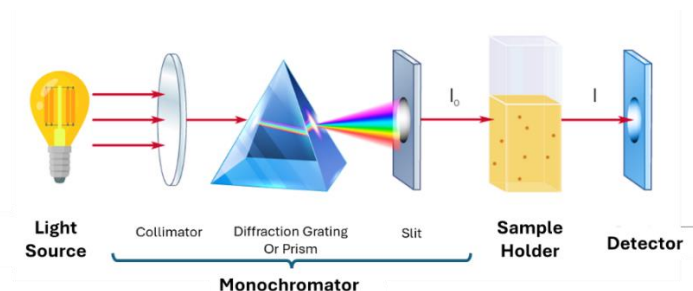


Figure 26: A simplified schematic representation of the main components in a UV-Vis single-beam monochromatic spectrophotometer. Image modified by [79].

2.4.1 Light Source

This component provides the initial EMR that will interact with the sample. Common sources include:

- **Tungsten or Halogen lamps** for visible light (350 nm to 2500 nm).
- **Deuterium lamps** for ultraviolet light (160 nm to 375 nm).
- **Xenon lamps** for a broad spectrum of UV-Visible light (190 nm to 1100 nm).
- **Lasers** for high-intensity and specific wavelength light.

In spectrophotometry, the **Tungsten or Halogen/Deuterium lamp** are commonly used together to cover a broad range of the electromagnetic spectrum. To ensure accurate measurements across both UV and visible regions, instruments need to switch between the deuterium and tungsten/halogen lamps during a scan. This switch typically occurs in the overlap region, where both lamps emit light with similar intensities, usually between 300 nm and 350 nm. The switchover is carefully calibrated so that at the transition point, the emission intensities from both lamps are comparable. This careful calibration ensures a smooth transition between light sources, preventing significant discrepancies in the measurement. Usually, the instrument software controls this switchover to ensure it happens seamlessly, maintaining consistent light intensity and minimizing any potential disruption in the data. In advanced spectrophotometers, a single **Xenon lamp** is frequently employed as a high-intensity light source capable of covering both the UV and Visible ranges. **Lasers** provide highly monochromatic, coherent, and intense light sources. Available on various specific wavelengths, depending on the type of laser (e.g., HeNe, Nd, diode lasers). Table 8 presents a comparative analysis of various lamp types to aid in the selection process.

Table 8: Comparative table outlining the key characteristics and applications of Tungsten-Halogen, Deuterium, Xenon lamps, and Laser.

Feature	Tungsten-Halogen	Deuterium	Xenon	Laser
Wavelength Range (nm)	~ 350 to 2500	~160 to 375	~200 to 1000	Very narrow and specific wavelengths
Spectral Continuity	Continuous spectrum	Continuous spectrum	Continuous spectrum	Discrete, narrow spectral lines
Intensity	High intensity in visible and NIR regions	High intensity in UV region	Very high intensity across a broad range	Very high intensity at specific wavelengths
Common Applications	Visible light measurements, colorimetry, photometry	UV-visible spectroscopy, analytical chemistry	UV-visible spectroscopy, fluorescence, and imaging	High-precision measurements, spectroscopy, research
Lifetime	Relatively long, may require periodic replacement	Moderate; relatively stable	Shorter compared to Tungsten and Deuterium	Long, stable for extended use
Cost	Moderate	Moderate to high	High	High
Maintenance	Low; easy to replace	Moderate; requires handling care	Moderate; high intensity requires cooling	Low; requires alignment and calibration
Suitability for UV Measurements	Limited; better for visible and near-infrared	Excellent; specifically designed for UV	Good; covers a broad range including UV	Limited; specific wavelengths only

2.4.2 Monochromator

A monochromator is an optical instrument used to isolate a specific wavelength from a broad spectrum of light. It operates by first using a **collimating lens or mirror** to transform incoming light into a parallel beam. This parallel light is then dispersed into its component wavelengths by a **diffraction grating or prism**. Finally, an **adjustable slit** allows only the selected wavelength to pass through, blocking all others.

2.4.3 Sample Holder

The sample holder, commonly known as a cuvette, is an essential component that holds the sample in the path of the light beam. Cuvettes are typically made from **materials such as quartz, glass, or plastic, each suitable for different wavelength ranges**. In general, cuvettes must be constructed of a material that does not absorb radiation in the region of interest. Quartz cuvettes are preferred for UV measurements as they are transparent in both UV and visible regions (200-700nm range), whereas glass cuvettes are suitable for visible light measurements but not for UV as they absorb UV radiation. Plastic cuvettes, usually made of PMMA, are cost-effective and disposable, suitable for visible and near-UV ranges. However, they are not used for organic solvents because the solvents can

degrade or dissolve plastic material. This can lead to contamination of the sample, inaccurate measurements, and potential damage to the cuvette, reducing its lifespan and reliability. Cuvettes come in **various shapes and sizes**, with standard rectangular cuvettes having a 1 cm path length being the most common. Micro cuvettes are used for small sample volumes, and flow cuvettes are designed for continuous sample flow applications. The **optical length** is typically 1 cm to ensure consistency in absorbance calculations according to Lambert-Beer Law, though variable path lengths are also available from 0.1-10 cm. Standard cuvettes have a **volume** of sample from 3 to 4 mL, while micro cuvettes are used for smaller volumes. **Optical quality** is crucial, with polished surfaces minimizing scattering and maximizing light transmission, and matched cuvettes ensuring identical optical properties for comparative measurements. Proper maintenance and handling, such as ensuring cleanliness and avoiding contamination, are essential for accurate measurements. Cuvettes provide a controlled environment for samples, ensuring accurate and reliable measurements in UV-Vis spectroscopy.

2.4.4 Detector

Several types of detectors are used to measure the intensity of transmitted or absorbed light and convert it into an electrical signal. Like the light source, it should give a **linear response** over a wide wavelength range, with **low noise and high sensitivity**. Common detectors are **photodetectors** that operate based on the photoelectric effect. This phenomenon occurs when light radiation strikes a material, causing it to emit electrons. The number of emitted electrons, which can be measured electrically, is directly proportional to the intensity of the incoming light. This proportional relationship enables photodetectors to precisely measure light intensity. Among these detectors are **photomultiplier tubes (PMTs)**, which are exceptionally sensitive and well-suited for detecting low light levels. PMTs amplify the number of electrons generated by the incident light, allowing for the detection of very weak signals. This makes them invaluable in applications requiring high sensitivity and precise light measurement in UV-Vis spectroscopy. Other types of photodetectors that are less commonly used in laboratory instrumentation include **photodiodes**. These devices are typically constructed from silicon or other semiconductor materials that are responsive to light. When exposed to light, a photodiode generates a small electrical voltage proportional to the light intensity, which can be used for measurement. Photodiodes are compact and can be easily integrated into a wide range of electronic systems. They offer a fast response time, making them capable of detecting rapid changes in light intensity. While they are suitable for applications requiring large quantities of detectors and are versatile in their use, photodiodes generally have lower sensitivity compared to more specialized detectors like photomultiplier tubes (PMTs).

Table 9: Comparative table outlining the key characteristics and differences between photomultipliers and photodiodes.

Feature	Photomultiplier Tube (PMT)	Photodiode
Operating Principle	Photoelectric effect followed by electron multiplication	Photoelectric effect generating an electrical current
Sensitivity	High sensitivity; capable of detecting very low light levels	Lower sensitivity compared to PMTs
Response Time	Fast, but generally slower than photodiodes	Very fast; ideal for detecting rapid light changes
Light Range	Effective over a broad range of wavelengths (UV to visible)	Effective primarily in the UV-visible range
Signal Amplification	Internal amplification of the signal through electron multiplication	No internal amplification; relies on direct current generation
Size	Larger and more fragile	Smaller and more robust
Cost	Generally higher due to complexity and sensitivity	Generally lower; more cost-effective
Application Areas	High-precision measurements, low-light detection, research	General light detection, imaging systems, communication
Noise Level	Low noise; high signal-to-noise ratio	May have higher noise levels compared to PMTs
Maintenance	Requires careful handling and calibration	Low maintenance; robust and durable
Power Requirements	Requires higher power and specialized circuitry	Requires less power and simpler circuitry

2.4.5 Configuration: single vs double beam spectrophotometer

There are different types of spectrophotometers, depending on how their various components are arranged.

- Single-beam spectrophotometers
- Double-beam spectrophotometers
- Diode array spectrophotometers (UV-visible only)
- Fourier-transform instruments (IR only)

Single-beam and double-beam spectrophotometers are two fundamental configurations of instruments used in laboratory for measuring the absorbance or transmittance of light by a sample in UV-Vis range. **A single-beam spectrophotometer measures the intensity of light passing through the sample and compares it to a reference measurement taken sequentially.** This method requires frequent calibration and baseline corrections to ensure accurate results, as any fluctuations in the light source or instrument can affect the measurements. In contrast, **a double-beam spectrophotometer uses two separate beams of light—one passing through the sample and the other through a reference or blank solution.** This simultaneous measurement approach compensates for any variations in the light source intensity and optical path, providing more stable and accurate results. The double-beam design reduces errors due to light source

instability and allows for continuous monitoring of absorbance, making it especially useful in applications requiring high precision and reliability.

2.5 Electrochemical methods

Electrochemistry is the study of the relationship between electrical energy and chemical reactions. It investigates how chemical reactions can produce electricity, as seen in batteries, and how electrical energy can be used to induce chemical changes, such as in electrolysis.

2.5.1 Classification

Though the primary measurements in electrochemical analysis are **potential, current, and charge**, a wide range of experimental approaches can be employed. These methods are generally categorized into two types:

1. **Bulk methods** which assess the properties of the entire solution.
2. **Interfacial methods** where the signal is determined by phenomena occurring at the interface between an electrode and the solution it contacts.

Figure 27 outlines various interfacial electrochemical methodologies. These methods can be broadly categorized into **static** and **dynamic** approaches. In static methods, there is no current flow between the electrodes, and the concentrations of species within the electrochemical cell remain constant. Potentiometry is a prime example of a static method, where the potential of an electrochemical cell is measured under conditions of no current flow. Dynamic methods, defined by the flow of current and concentration changes due to redox reactions, are primarily categorized based on whether the current or potential is controlled. The first category, called amperometry, involves measuring the current in an electrochemical cell while holding the potential constant. The second, known as coulometry, involves measuring the total charge passed during the electrochemical reaction [80].

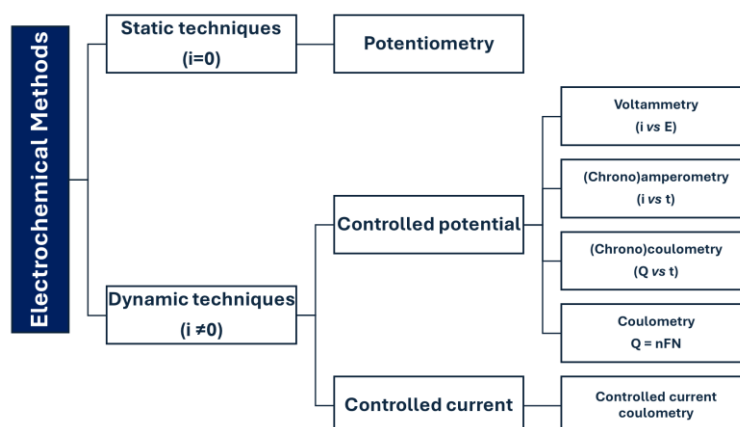
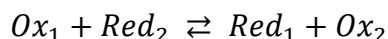


Figure 27: Diagram classification of electroanalytical techniques.

2.5.2 Principle

At its core, electrochemistry focuses on the movement of electrons during **oxidation-reduction (redox) reactions**.



Following the previous equation Ox_1 is reduced to Red_1 , and Red_2 is oxidized to Ox_2 . The oxidizing or reducing tendencies of substances can be assessed by studying electrochemical cells and electrode potentials. This involves analyzing how easily a substance can gain or lose electrons, which is reflected in its electrode potential within an electrochemical cell. By measuring these potentials, one can determine the strength of a substance as an oxidizing agent (which gains electrons) or a reducing agent (which loses electrons).

The potential (E) of a redox reaction is determined by the **Nernst Equation**, a fundamental principle in electrochemistry. This equation relates the equilibrium potential of the reaction to the concentrations of the reactants and products. In the equation, the activities of the oxidized and reduced species are represented as a_{Ox} and a_{Red} respectively. Other parameters in the equation include the universal gas constant (R), the temperature (T), the Faraday constant (F), the standard electrode potential of the reaction (E^0), and the number of electrons transferred per molecule (z).

$$E = E^0 + \frac{RT}{zF} \ln \frac{a_{Ox}}{a_{Red}}$$

Faraday Law is the other fundamental principles that govern the quantitative relationship between the amount of electrical charge passed through an electrolyte and the amount of substance transformed at the electrode during electrolysis. The Faraday Law describes the relationship between the electric charge (Q) passing through a cell and the amount of substance (n) transformed at the electrodes. Here, (F) represents the Faraday constant, and (z) denotes the number of electrons required for each conversion.

$$Q = n \cdot z \cdot F$$

Nernst Equation provides insight into how electrode potential varies with concentration, while Faraday's Laws quantify the relationship between charge and the amount of substance transformed. Together, they provide a comprehensive understanding of electrochemical processes, linking the potential of electrochemical cells with the quantitative aspects of electrolysis.

2.5.3 Electrochemical cells

Electrochemical cells can be categorized into two primary configurations: voltaic/galvanic cells and electrolytic cells. In both cell types, the anode is the electrode where oxidation occurs, while the cathode is the electrode where reduction takes place.

Voltaic/galvanic cells harness the energy released from a spontaneous chemical reaction to generate electrical energy. In this configuration two half-cells are set up in different containers, connected through the salt bridge or porous barrier, to maintain electrical neutrality, and allows ions to flow between the compartments. The bridge or barrier typically contains a gel containing KCl since K^+ and Cl^- move at equal speeds. As current flows, Cl^- comes into the anode compartment and K^+ comes into the cathode compartment to maintain charge balance. The potential difference between the electrodes (voltage) drives electrons from the reductant to the oxidant through the external circuit, producing an electric current. Here the anode is negative, and the cathode is the positive electrode. The reaction at the anode is oxidation and that at the cathode is reduction. Conversely, electrolytic cells utilize external electrical energy to drive non-spontaneous chemical reactions. In this configuration, for most of the possible applications, the electrodes are immersed within a single container containing molten electrolyte. The anode is positive, and the cathode is the negative electrode. The reaction at the anode is oxidation and that at the cathode is reduction.

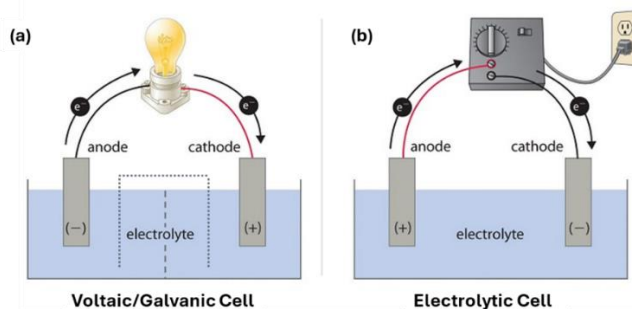


Figure 28: Comparison between different Electrochemical Cell Configurations. (a) In Voltaic/Galvanic Cell electrons flow spontaneously from one compartment to another (black line) but cannot reverse direction (red line). A salt bridge (dotted line) or porous barrier (dashed line) is required to maintain electrical neutrality. (b) In electrolytic cell the reaction from anode to cathode is non-spontaneous (red line). An external source of energy is necessary to drive the reaction (black line). Image modified by [81].

2.6 Voltammetry

Voltammetry is an electrochemical technique in which the current flowing through an electrochemical cell is measured as the applied potential is varied systematically. This method is used to investigate the electrochemical properties of analytes, providing insights into redox potentials, reaction kinetics, and concentration of the species involved in oxidation-reduction reactions.

Voltammetry is roughly divided into two categories based on the electrode movement which could be **hydrodynamic**, where a continuous flow of solution is maintained past the electrode, or **stationary**, where the electrode remains fixed in position while the potential is scanned (Figure 29)[82].

In **hydrodynamic voltammetry (HV)** the flow helps to enhance mass transfer, which is the movement of the analyte from the bulk solution to the electrode surface. By increasing mass transfer, hydrodynamic voltammetry can improve the sensitivity and reproducibility of electrochemical measurements since the flow reduces the diffusion layer thickness, allowing for faster transport of the analyte and helping to minimize the effects of impurities or interfering species. The HV can be divided into three different subcategories set-up namely stirred solution, flow system and rotating electrode. In the first configuration the solution is continuously stirred, typically using a magnetic stirrer or other mechanical agitators, to enhance mixing and promote uniformity. Stirring creates convective flow, which increases the rate of mass transport to the electrode surface. In a flow system, the solution is pumped through an electrochemical cell where the electrode is positioned. The flow rate of the solution can be precisely controlled. The continuous flow of the solution past the electrode surface provides a steady-state condition and enhances mass transport, like but more controlled than stirring. This system is ideal for maintaining a constant analyte supply. In rotating electrode set-up, the electrode is rotated at a controlled speed within the solution. The rotation creates a well-defined and reproducible hydrodynamic environment around the electrode.

In **stationary voltammetry (SV)** the electrode does not move during the measurement and the solution is typically unstirred or stirred at a low rate. The transport of the analyte to the electrode is primarily governed by diffusion. The **linear potential scan voltammetry** is divided into two sub-categories. The first is **Linear Sweep Voltammetry (LSV)** where the potential is applied continuously and linearly, increasing or decreasing at a constant rate while the current is measured throughout the potential scan. LSV suffers from charging currents due to the rapid change in potential. When the potential is scanned linearly at a relatively high rate, the double layer capacitance of the electrode-solution interface cannot respond instantaneously. This mismatch between the applied potential and the interfacial charge causes a current to flow, known as the charging current. The second is **Cyclic Voltammetry (CV)** where linear scan followed by a reversal to the initial potential. This cyclic potential sweep allows for the study of both oxidation and reduction processes in a single experiment. The current flowing through the cell is measured as a function of potential.

In **pulse voltammetry**, a series of potential pulses are applied to the working electrode, with the ability to vary both the amplitude and duration of these pulses. The current is measured at the end of each pulse, after the transient charging current has decayed, allowing for more accurate analysis of the faradaic current associated with the redox reactions. Pulse voltammetry is further categorized into different techniques based on the nature of the applied pulses. Normal Pulse Voltammetry (NPV) is a sequence of discrete potential pulses which are applied

to the electrode. Each pulse is incrementally stepped up from the previous one, and the current is measured at the end of each pulse. Differential Pulse Voltammetry (DPV) is a technique that involves applying a series of pulses, each with a progressively increasing amplitude. The current is measured before and at the end of each pulse, and the difference between these two measurements is recorded. This approach improves sensitivity and resolution. Finally, in Square Wave Voltammetry (SWV) a series of square-wave pulses is applied, where each pulse alternates between two potential levels. The current is sampled at the end of each half-cycle, allowing for rapid and sensitive detection of analytes with high resolution. Each of these pulse voltammetry techniques is designed to minimize background noise and enhance the detection of specific redox processes, making them powerful tools in analytical electrochemistry.

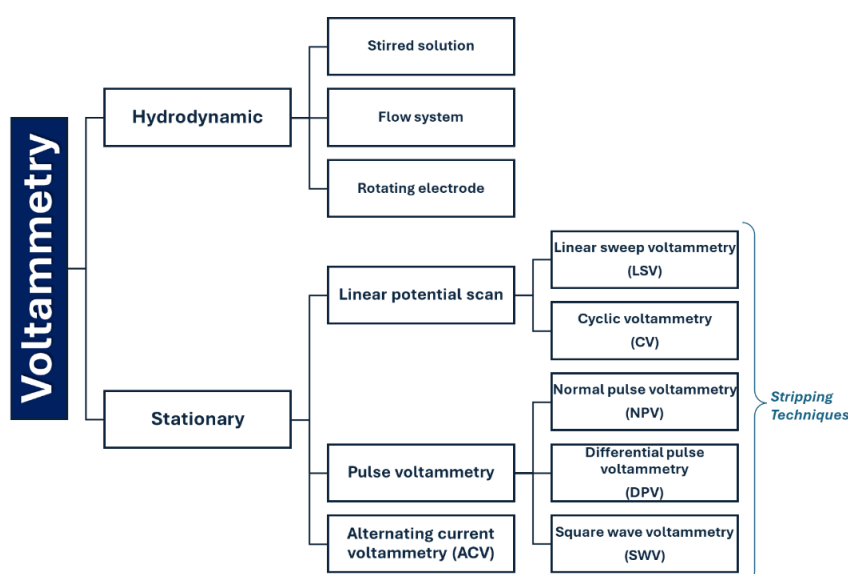


Figure 29: Diagram classification for Voltammetric techniques.

2.6.1 Stripping Techniques

Voltammetric techniques are **stripping techniques**, and they are often used to determine the concentration of trace analytes in a solution.

These procedures typically consist of two main steps:

1. **Pre-concentration:** In this initial step, the analyte is concentrated onto the surface of the working electrode. This is achieved by applying a potential that induces the reduction or oxidation of the analyte, causing it to deposit onto the electrode surface. This step increases the local concentration of the analyte, enhancing the sensitivity of the measurement.
2. **Stripping:** Following pre-concentration, the analyte is removed from the electrode surface by reversing the potential. This reversal re-oxidizes or re-reduces the analyte, leading to its release from the electrode. The resulting current is recorded and is directly proportional to the concentration of the analyte in the original solution.

This approach allows for highly sensitive detection of trace amounts of analytes because it effectively amplifies the signal associated with the analyte by concentrating it on the electrode surface before measurement. During pre-concentration, the analyte is accumulated on the electrode surface over a period, significantly increasing its local concentration compared to the bulk solution. This process converts a dilute analyte solution into a more concentrated form at the electrode, making even trace levels detectable. The stripping step, where the analyte is released from the electrode, results in a measurable current that is directly proportional to the amount of analyte that was pre-concentrated. Since the pre-concentration step boosts the analyte local concentration, the resulting current during stripping is much larger than it would be without pre-concentration, thereby amplifying the signal. The combination of pre-concentration and signal amplification leads to a lower detection limit, meaning that even very small amounts of analyte can produce a detectable signal. This makes stripping voltammetry particularly effective for analyzing trace amounts of substances that would otherwise be undetectable using conventional methods. It is possible then to divide the stripping voltammetry as follows[83], [84]:

- **Anodic Stripping Voltammetry (ASV):** Involves preconcentration of analyte (typically metal ions) on the electrode surface, followed by an oxidation (stripping) step that generates a measurable current. The sensitivity of the technique is extremely high, and the detection limits reach nano- and sub-nano-molar levels. As the main disadvantages, the electrode surface fouling can reduce accuracy, and experimental condition should be carefully controlled [85].

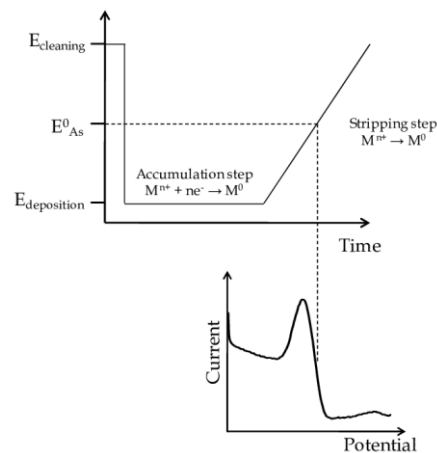


Figure 30: Anodic stripping voltammetry: the potential-time waveform with the resulting voltammogram.

- **Cathodic Stripping Voltammetry (CSV):** Like ASV but involves the preconcentration of the analyte by reduction (rather than oxidation) on the electrode, followed by a stripping step. Allowing detection of trace species which are highly selective for reducible analytes. However, electrode stability and reproducibility can be challenging.

- **Adsorptive Stripping Voltammetry (AdSV):** The adsorption of the analyte occurs on the electrode surface (without electrochemical reduction or oxidation), followed by an electrochemical stripping process. Suitable for detecting organic molecules, complex metal ions, and compounds that adsorb strongly to the electrode surface (e.g., pharmaceuticals, pesticides) and for non-electroactive species. Adsorption process can be influenced by surface contamination.

2.6.2 Three electrode electrolytic cell

The cells used in voltammetry technique usually employ a setup having three electrodes, working electrode (WE), count electrode (CE) and reference electrode (RE) depicts in Figure 31. The three electrodes are immersed in an electrolyte solution that contains the ions necessary for the electrochemical reaction. A potentiostat is used to control the potential between the working and reference electrodes and measure the resulting current. This allows for precise control and measurement of electrochemical processes.

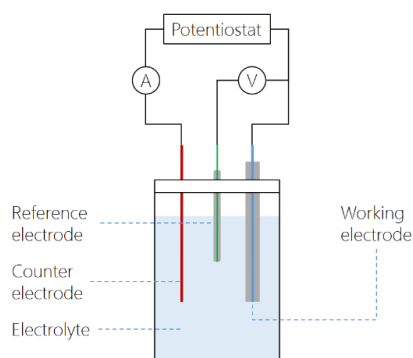


Figure 31: General configuration of laboratory set-up three electrode cell [86].

The working electrode (WE):

The working electrode is the cornerstone of a three-electrode cell. The choice of material for the working electrode (WE) plays a pivotal role in determining the type of electrochemical reactions that can occur. **Different materials** influence factors such as the electrode's potential range, conductivity, and compatibility with specific analytes. The most used working electrode materials can be categorized into three main groups: metals, carbon-based materials, and semiconductors.

Metals:

Metals are frequently employed as working electrode materials, especially in redox reactions involving metal ions. They offer excellent conductivity and are often chosen based on their specific electrochemical properties. The type of metal used directly affects redox potential and determines the range of ions or molecules that can be involved in the electrochemical process. For example, **gold** and **platinum** are commonly used for detecting heavy metals, while **silver** electrodes

are ideal for halide reactions. The stability, durability, and wide potential window of metals make them suitable for a range of both oxidation and reduction reactions. Historically, among the metals used as WE **mercury** is a well-established material for working electrodes in electrochemical techniques, particularly in anodic and cathodic stripping voltammetry. Its unique electrochemical properties make it ideal for specific applications, especially those involving trace metal detection. Mercury electrodes are typically used in various forms, such as dropping mercury electrodes (DME), hanging mercury drop electrodes (HMDE), and mercury film electrodes (MFE). Mercury electrodes, though highly effective in electrochemical applications like trace metal detection, are being increasingly phased out due to their toxicity. Despite this, their distinct features—such as the ability to form amalgams with metal ions, a broad cathodic potential range, and high reproducibility—have made them historically important and still useful in specialized contexts. In response to the health and environmental concerns surrounding mercury, **bismuth and antimony** electrodes have emerged as safer alternatives. These materials provide similar electrochemical capabilities, particularly in detecting trace metal ions, while eliminating the health risks and regulatory issues associated with mercury. Below is a comparison of the characteristics and applications of bismuth and antimony electrodes as viable replacements for mercury.[87]

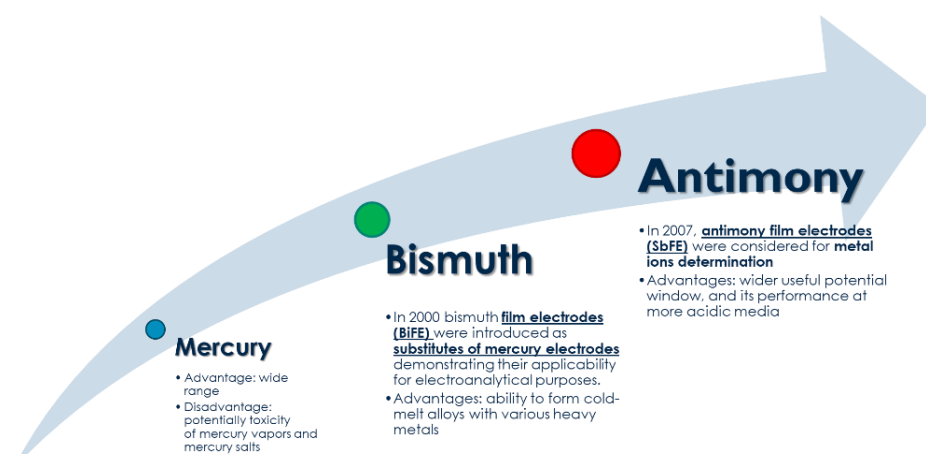


Figure 32: Timeline comparison chart of the evolution of the most used metallic materials, including their advantages and disadvantages.

Carbon-based materials (Graphite and Glassy Carbon): Carbon-based electrodes, such as graphite and glassy carbon, are highly versatile and widely used in electrochemical applications. These materials can accommodate a broad range of reactions, including organic electrochemistry and biosensing. Their inert nature, wide potential window (especially for oxidative processes), and low cost make them ideal for detecting both organic and inorganic species. Additionally, the surface of carbon electrodes can be easily modified with functional groups, enhancing selectivity and enabling the detection of specific analytes, including biomolecules and pharmaceuticals.

Semiconductors:

Semiconductors represent another category of working electrode materials,

typically employed in specialized reactions involving semiconductor-electrolyte interfaces. These materials are especially useful in **photoelectrochemical processes**, where the interaction between light and the electrode surface generates a current. Semiconductors such as **silicon** or **titanium dioxide (TiO₂)** are widely used in applications like solar cells, water splitting, and other light-driven reactions. Their ability to harness light energy makes them essential for studies in renewable energy and environmental monitoring.

Another important factor to consider is the **surface characteristics of the WE**, which play a significant role in determining the efficiency and dynamics of electrochemical reactions. The key surface properties that affect electrode performance include **a large surface area** to enhance the rate of electrochemical reactions by offering more active sites for the process to take place. This larger area allows for greater interaction between the electrode and the analyte, which can lead to higher current densities and improved sensitivity. In addition, electrodes with **a rough or textured surface** often exhibit enhanced reaction rates. The increased roughness introduces additional active sites and creates microenvironments that can trap reactants, facilitating more efficient electron transfer and improving overall reaction kinetics. This is linked to the possibility of **tailoring the electrode surface** by incorporating functional groups, coatings, or specific materials that can dramatically affect its performance. These modifications can enhance the selectivity towards analytes, improve its sensitivity, and increase stability under various experimental conditions. Such modifications allow for fine-tuning the electrode to meet specific analytical or catalytic requirements. Finally, the WE performance can be significantly **influenced by the properties of the electrolyte solution**. An unsuitable electrolyte can result in the formation of passivating layers, corrosion, or other forms of electrode degradation, ultimately compromising the accuracy and reliability of measurements.

The counter electrode (CE):

The counter electrode, also known as the auxiliary electrode, maintains the overall electrical neutrality of the electrochemical cell. Its primary function is to provide a pathway for the current to flow, balancing the current that passes through the working electrode. While the working electrode undergoes the desired electrochemical reaction, the counter electrode typically experiences a complementary redox reaction. This reaction is often a simple, reversible process that does not interfere with the primary reaction. By providing a pathway for current flow, the counter electrode helps to prevent polarization at the working electrode, which can lead to distorted or inaccurate measurements. The choice of material for the counter electrode depends on the specific requirements of the experiment. Common materials including platinum, gold, and silver are often used due to their inertness and wide electrochemical window. Graphite or glassy

carbon can be used for certain applications, especially when a large surface area is needed. In some cases, more specialized materials may be required, such as when studying reactions involving specific ions or when working in non-aqueous solvents. **The placement** of the CE is also important. It should be positioned in a way that minimizes its influence on the primary reaction at the working electrode. This can often be achieved by placing the counter electrode at a distance from the working electrode or by using a compartmentalized cell to separate the two electrodes.

The reference electrode (RE):

The reference electrode is a critical component of a three-electrode cell, serving as a stable reference point for measuring the potential of the working electrode. Its primary function is to maintain constant, known potential, independent of the current flowing through the cell. Common Types of RE include **Standard Hydrogen Electrode (SHE)**, it consists of a platinum electrode immersed in a 1 M hydrogen gas solution at 1 atm pressure and serves as the universal reference point for measuring electrode potentials, **Silver/Silver Chloride (Ag/AgCl)**, commonly used reference electrode that consists of a silver wire coated with silver chloride immersed in a potassium chloride solution, **Calomel Electrode**, uses a mercury/mercurous chloride paste (calomel) in contact with a potassium chloride solution, and Glass Electrode, consists of a glass membrane that is sensitive to hydrogen ions useful to measured pH. Reference electrodes require more maintenance than other electrodes. They must be stored in a suitable solution, such as saturated potassium chloride, to prevent drying out and maintain stability. Additionally, regular calibration against a known standard is essential for accurate measurements.

2.6.3 Electrolyte solution

The selection of the appropriate electrolyte solution is critical for the success of electrochemical measurements. The quality, accuracy, and efficiency of these measurements depend on the chosen electrolyte composition and its compatibility with the analyte of interest. In fact, the electrolytic solution acts as the medium in which the electrochemical reactions occur for this reason the nature of the electrolyte can influence the reactivity of the species involved, the stability of the electrode, and the overall efficiency of the reaction. The primary function of the electrolyte solution is to facilitate the flow of ions between the working and reference electrodes. Containing ions, atoms, or molecules that have lost or gained electrons, the electrolyte solution ensures electrical conductivity within the electrochemical cell. Conductivity is essential for the flow of electric current during the measurement. Without sufficient conductivity, the measured current could be weak or inaccurate. Since many electrochemical reactions are pH-dependent, the electrolytic solution often includes buffers or acids/bases to maintain a stable pH and ionic strength which affect the activity coefficients of the reactants and products. This can impact the current response and the shape of

the voltammogram. The composition of the electrolytic solution can enhance or suppress the electrochemical response of the analyte and can help in minimizing interference from other substances present in the sample. By carefully selecting the electrolyte, one can reduce background currents and improve the signal-to-noise ratio, leading to more accurate results.

2.6.4 Mass transport in solution and Diffusion Layer

Mass transfer through a planar electrode in solution occurs through three primary mechanisms, as illustrated in Figure 33.

Convection is the bulk movement of the solution itself, driven by external forces such as stirring, mixing, or temperature gradients. This process involves the physical displacement of the entire liquid, which carries dissolved substances along with it. Convection is particularly important in situations where rapid mixing or uniform distribution of substances is needed. **Migration** refers to the movement of charged particles (ions) in response to an electric field. This process is governed by electrostatic forces that drive ions towards electrodes of opposite charge. Migration is essential in electrochemical processes such as electrolysis, electrophoresis, and ion-selective measurements. It allows for the separation and analysis of ionic species based on their charge and mobility. **Diffusion** is the process by which particles move from an area of higher concentration to an area of lower concentration due to random thermal motion. This movement continues until the concentration of the substance is uniform throughout the solution. Diffusion is critical in many natural and industrial processes, including the mixing of reagents, the transport of nutrients and waste products in biological systems, and the operation of sensors and separation techniques. When electroactive species approach the working electrode, they create a region near the electrode where their concentration is significantly different from the concentration in the bulk solution. This region is known as the **diffusion layer** and arises from electrochemical reactions at the electrode and its formation is due to the diffusion process. The diffusion layer is a critical region in voltammetry, affecting mass transport, peak current, and reaction kinetics. The movement of material to and from the electrode surface is a complex interplay of all three modes of mass transport. In the limiting case where diffusion is the sole significant form of mass transport, the current in a voltammetric cell is described by the following equation:

$$i = \frac{nFAD (C_{bulk} - C_{x=0})}{\delta}$$

where n is the number of electrons in the redox reaction, F is Faraday's constant, A is the area of the electrode, D is the diffusion coefficient for the species reacting at the electrode, C_{bulk} and $C_{x=0}$ are its concentrations in bulk solution and at the electrode surface, and δ is the thickness of the diffusion layer. Migration can be eliminated by adding a high concentration of an inert supporting electrolyte since ions of similar charge equally are attracted to or repelled from the surface of the

electrode, each has an equal probability of undergoing migration. A large excess of an inert electrolyte ensures that few reactants or products experience migration. Although it is easy to eliminate convection by not stirring the solution.

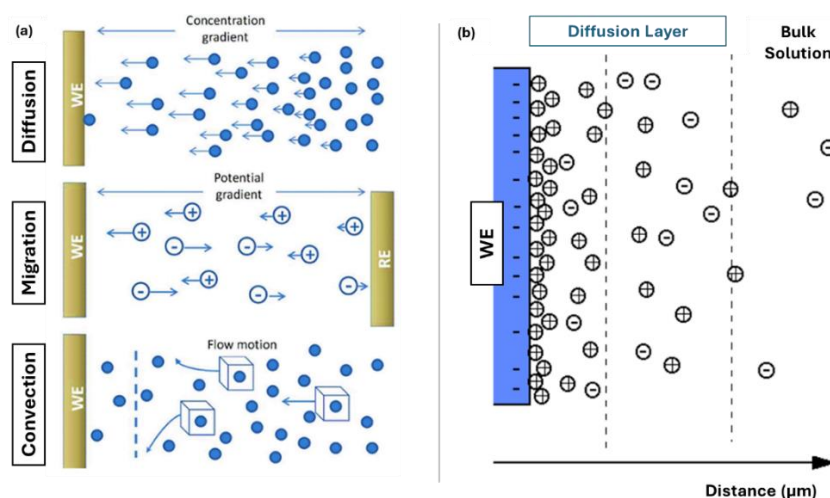


Figure 33: (a) Mechanisms of mass transfer at a planar electrode. (b) Diffusion layer established between a working electrode surface and the solution.

2.6.5 Voltammogram

A voltammogram is a graphical representation of the current response of an electrochemical cell as a function of the applied potential to the working electrode. As depicted in Figure 34a there are two most important parameters to consider in the interpretation of a voltammogram: **peak potential (E_p)** and **peak current height (i_p)**.

Peak potential helps identify the specific redox processes occurring in the system. Each electroactive species has its own characteristic peak potential, making it a valuable tool for qualitative analysis and analyte identification. By examining peak potentials, researchers can also extract information about the reaction mechanism and the nature of the electrochemical process. For instance, in cyclic voltammetry, the difference between anodic and cathodic peak potentials can reveal information about reaction reversibility and kinetic factors. Moreover, significant shifts in peak potential may indicate changes in the chemical environment, interactions with other species, or alterations in experimental conditions, potentially leading to data inaccuracies. While the **peak current height** is directly correlated with the concentration of the electroactive species in the solution. Higher peak currents typically indicate higher analyte concentrations, making them a crucial parameter for quantitative analysis. Additionally, analyzing peak heights provides insights into the kinetics of the electrochemical reaction. For instance, in cyclic voltammetry, peak currents can reveal information about reaction rates and the speed of species reduction or oxidation. The peak's shape, whether symmetrical or distorted, can offer further clues about the reaction's kinetics and diffusion characteristics.

Together the shape, position, and height of the peak provide valuable information about the processes occurring at the working electrode surface and it is possible to identify four distinct regions within the voltammograms [88]:

1. **Starting background current:** the initial portion of the voltammogram is primarily influenced by background recorded noise as the applied potential in this region is insufficient to induce the discharge of M^{2+} ions.
2. **Ascending part of the peak:** near the discharge potential, the curve rises sharply as the M^{2+} ions are rapidly reduced at the electrode. In this moment the diffusion layer becomes increasingly depleted ions, establishing a spontaneous flow of additional metal ions from the bulk solution towards the electrode. The rate at which M^{2+} ions move towards the diffusion layer is proportional to their concentration in the bulk solution.
3. **Descending part of the peak:** the current decrease because the potential scanning velocity is so high that the electro active compound is not able to reach early the electrode.
4. **Signal acquisition termination:** current trends than to diminish.

Figure 34b illustrates that in voltammetry, the excitation signal is the applied potential that drives electrochemical reactions at the working electrode. By varying this signal in different patterns, we can explore the electrochemical behavior of the system. The waveform of the excitation signal, such as linear, triangular, or other shapes, determines the specific voltammetric technique employed and the congruent form of voltammogram.

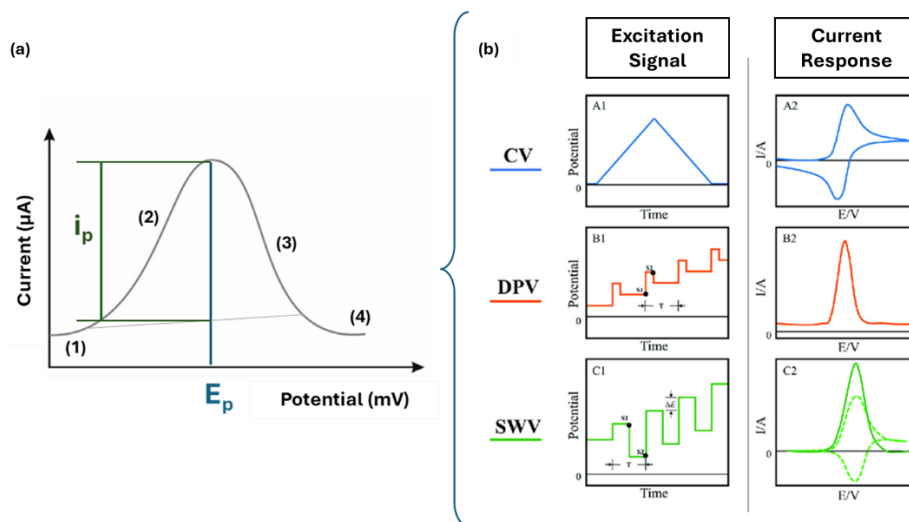


Figure 34: (a) Voltammogram of the discharge of M^{2+} during linear scanning potential with the peak potential and current height position and the identification of the four characteristic regions describing what happening at the working electrode surface. (b) The most three voltammetry techniques used are named as cyclic voltammetry (CV), differential pulse voltammetry (DPV) and square-wave voltammetry (SWV) with their typical form of excitation signal and the consequently current response on the voltammogram. Image modified by [89].

2.7 Selection of methodologies:

The selection of a chemical method for analysis is influenced by several critical factors that must be carefully considered to ensure the most effective approach. Among these factors, the primary considerations are **the type of information** desired and **the specific analyte** to be detected. An appropriate analytical method combines these elements while addressing additional essential factors, which are illustrated in the accompanying diagram in Figure 35.

Firstly, the range of the analyte significantly impacts the sensitivity and specificity of the chosen method. For instance, if the analyte is present at low concentrations, the technique must be highly sensitive to detect it accurately. This relationship highlights the importance of understanding both the concentration levels of the analyte and the inherent capabilities of the analytical technique. Moreover, the reliability of the results is paramount; they should yield values that are not only trustworthy but also comparable to those generated by standard laboratory instrumentation. This comparability is crucial in validating the accuracy of the method, especially when cross-referencing with existing data or regulatory standards.

Another important issue is the potential degradation of the sample between the point of sampling and the actual analysis. If a sample is prone to degradation, it may skew the results or lead to erroneous conclusions. Therefore, it is advisable to choose methods that are straightforward and require minimal preparation. This simplicity helps maintain the integrity of the sample throughout the analytical process, ensuring that the results accurately reflect the sample's original state. Lastly, the stability of the chosen method and the availability of the necessary analytical instrumentation must also be considered. A stable method will provide consistent results over time, which is vital for longitudinal studies or repeated measurements. Furthermore, having access to appropriate analytical tools is essential for implementing the selected method effectively.

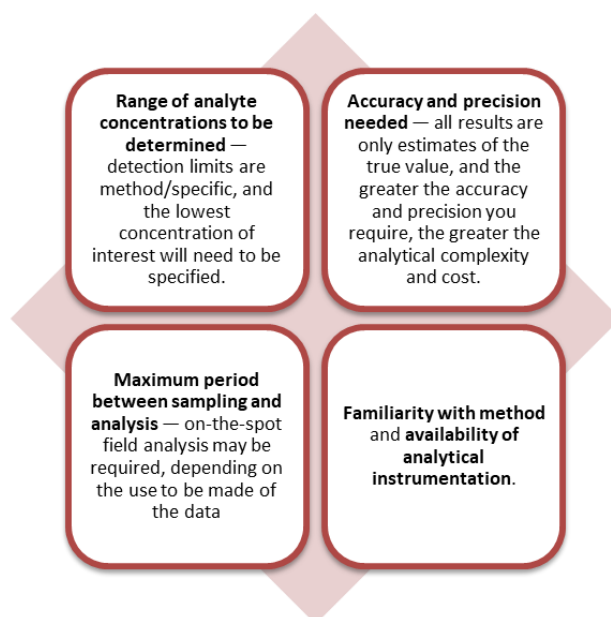


Figure 35: Diagram showing the choice of an analytical method involves a thoughtful consideration of multiple factors, including the nature of the analyte, the desired outcomes, the reliability and comparability of results, sample integrity, and the practicality of the method itself.

Despite the vast array of techniques available in the literature, the decision to prioritize UV-Vis spectrophotometry and voltammetry in this thesis work was likely influenced by several factors.

1. **Versatility:** both techniques are versatile and can be applied to a wide range of analytes, especially heavy metals.
2. **Sensitivity:** these techniques are capable of detecting and quantifying analytes at low concentrations, which is often necessary for environmental monitoring.
3. **Portability:** while UV-vis spectrophotometers and voltammetric instruments can be bulky, portable versions are increasingly available, making them suitable for field applications.
4. **Simplicity of the technique:** to automate a system process, it should be designed to be as straightforward as possible, minimizing the need for human intervention during analysis
5. **Ex-laboratory possible configurations:** the laboratory instrumentation has a well-established configuration and technologies to allow miniaturization of the system.

Chapter 3

Optical Detection

This chapter focuses on the **optical detection of heavy metals**, specifically Chromium in both oxidation states (Cr (III) and Cr (VI)), Copper (Cu), and Nickel (Ni).

Monitoring these metals potentially has a dual purpose and application in both environmental and industrial fields. In fact, in a big picture view, environmental monitoring can focus on both natural water contamination and industrial wastewater control. Natural contamination stems from geological events and erosion, while the galvanizing industry is an example of main source of industrial wastewater pollution. The aim is to address two critical monitoring objectives:

1. Wastewater Management:

In industrial process, as galvanizing, large quantities of heavy metals are used, which necessitates stringent monitoring of their levels in wastewater. Given that these metals are used in concentrations as high as grams per liter, continuous monitoring is crucial to ensure that the levels remain within legal limits and do not pose environmental or regulatory risks.

2. Quality Control and Efficiency:

For maintaining high-quality final products and minimizing reagent waste, it is essential to monitor the concentrations of these metals within the galvanic solutions. Consistent and homogeneous metal concentrations are required throughout the galvanizing process to ensure optimal results and high process yields. Additionally, it is important for the plant to confirm that post-process water treatments effectively remove all metals ions before the treated water is discharged. To mitigate any possible risks, regulatory bodies like the Environmental Protection Agency (EPA) and World Health Organization (WHO) have established strict limits on the concentration of HMs in drinking water and the same limits should be followed by industry when it comes to discharge water with potential pollutants. Table 10 summarizes the guideline values for the metals considered and analyzed in this works.

Table 10: Concentration Limits for Heavy Metals in Drinking Water Set by the WHO.

Metal	WHO Guideline Value ($\mu\text{g/L}$)
Arsenic (As)	10 $\mu\text{g/L}$
Copper (Cu)	2 mg/L
Nickel (Ni)	70 $\mu\text{g/L}$
Chromium (VI)	20 $\mu\text{g/L}$
Chromium (III)	<i>*No specific guideline value set, but considering the fast bioaccumulation the concentration should be in the order of ppm and ppb.</i>

TrAcqua and IntelWATT, focused on developing innovative sensors for monitoring heavy metal contamination in water. These projects, which have enabled the application of the methodologies described in the following chapters for the development of multi-sensor platforms, explore diverse water metrics to provide a comprehensive understanding of pollution levels.

The analysis of HMs in high-range concentrations was conducted by **IntelWATT project**. The project seeks to optimize process conditions in real-time using tailored sensors and automated decision-making mechanisms. Specifically, the goal is to detect primary chromium (III) and (VI), then copper and nickel in galvanic bath within high concentrations range. **The TrAcqua project** provides the opportunity to study and detect Arsenic and Chromium (VI), at trace concentration levels, as it focuses on monitoring drinking water quality and addresses natural contamination along riverbanks in the Piedmont mountains. This is particularly important because the presence of Chromium (VI) in such environments poses potential risks to both water quality and public health, making accurate monitoring and assessment crucial for ensuring safe drinking water and understanding the extent of contamination in these natural water systems.

3.1 UV-Vis colorimetric evaluation

The samples used were prepared from laboratory standards with increasing concentrations, to reach the simulation of the composition of an electrolytic bath. Direct colorimetric data were obtained in the **range between 100 ppm and 100 g/L**. In addition, for the more hazardous metals, indirect colorimetric tests were also conducted to add the possibility of monitor trace amounts. Samples with high concentrations were subjected to simple pretreatment steps, including magnetic stirring, heating, and resting. These pretreatment steps were necessary only for the laboratory experiments. Real-world samples from the plants could be analyzed directly, even at high concentrations, as the complete dissolution of salt was ensured by the process parameters. Metals solutions were analyzed by UV-Vis spectroscopy (LAMBDATM 35, PerkinElmer) to assess the detection limits, in terms of HMs concentration, and the linearity of the calibration curve. The quality of spectra and the absorbance peak were also investigated.

The **experimental conditions** under which the tests were conducted involved room temperature and distilled water as a blank reference. Distilled water was used as a solvent and compared to the same analyte dissolved in both basic and acidic buffers. The physical experimental conditions included the use of PMMA or quartz cuvettes, depending on the matrix of the solution in which the analyte was diluted, with a path length of 10 mm for higher concentration ranges and 20 mm for lower concentration ranges.

To study the **influence of pH on the solubility and spectroscopic characteristics of salts**, solutions were prepared at controlled pH levels using commercial buffers. Acidic, basic, and neutral conditions were specifically examined. The results obtained enable the prediction of data patterns and the detection of possible interferences that may affect the shape or intensity of spectral peaks, thereby optimizing experimental parameters. Finally, **aging tests** were also performed, which are essential for ensuring the quality and reliability of experimental results and the time response validity for the calibration of the final sensor. By evaluating the stability of the solution over time and maintaining its physicochemical properties, it is possible to prevent degradation due to exposure to light or oxygen, avoid the formation of precipitates, estimate potential solvent volatilization, which can modify the solute concentration within the solution, and monitor possible oxidation that can lead to the formation of new compounds that interfere with analyses. Noteworthy, in analytical chemistry, a specific starting 24-hour waiting period for an aging test is used to allow all the possible chemical reactions, equilibria, or sample stabilization processes to fully occur before measurement. As a result of this set of experimental tests, instrument calibration can be performed without delay, since the solution reaches its equilibrium state right after preparation, ensuring accurate and reliable measurements from the outset. Performing **dilutions** of the initial sample, especially in this context, is essential for analytical chemistry analysis because the techniques detectability may not be sufficient for the required level of analysis. By diluting the samples, their concentration is reduced to a range where the analytical technique can provide accurate and reliable measurements, thus ensuring that the analysis meets the necessary sensitivity and precision. The purpose of performing dilutions is to enhance calibration accuracy and the possibility of using less reagents. **Calibration curves** are created using a series of known concentrations. By diluting samples to fall within this range, it is possible to achieve precise calibration and effectively compare the results against established standards. Furthermore, dilutions help ensure that samples are analyzed under consistent conditions, which improves the accuracy of comparisons between them. This process of standardization is essential for obtaining reliable and comparable results across different samples.

Design of optical sensors

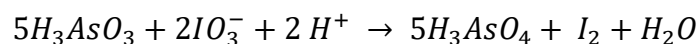
Laboratory testing is a critical stage in the process of transferring technology from research to practical application. These tests serve several essential purposes

starting from verifying the functionality of the technology, identifying its operational limits, optimizing the production process, and minimizing the risks involved in its practical application. Investing significantly in comprehensive testing is crucial for ensuring the successful implementation of new technology. Once the method is fully understood and validated in the laboratory, it can be applied to the creation of field sensors. To effectively monitor water quality for heavy metal contamination, a cost-effective, adaptable optical sensor is imperative. This sensor should possess several key characteristics such as high sensitivity, selectivity, speed, reliability, portability, robustness, and ease of use. A promising approach to meeting these requirements is to **combine colorimetric detection with lab-on-a-chip technology in a (micro)fluidic device**. This synergy offers a practical and efficient way to conduct routine water monitoring for heavy metal concentrations across a wide detection range.

3.2 Arsenic Detection

Arsenic, a metalloid and the 33rd element on the periodic table, exists in both organic and inorganic forms within the environment. Inorganic arsenic, including its trivalent and pentavalent states, poses a significantly greater health risk compared to its organic counterparts. In its pure form, arsenic doesn't dissolve in water. However, the solubility of arsenic salts varies depending on the surrounding environment's properties, such as its pH level.

Colorimetric detection using a chromophore, specifically Rhodamine B, has been employed to detect traces of arsenic in samples contaminated by natural spillages, especially when considering methods that do not require arsine development which is toxic. There are several reagents capable of inducing color changes upon contact with arsenic compounds under specific conditions. Rhodamine B is a synthetic dye commonly used in various applications, including as a fluorescent tracer and in analytical chemistry, particularly for detecting metal ions. When it comes to arsenic detection, Rhodamine B can be employed in a specific analytical method that relies on its chemical reactivity with arsenic compounds, particularly arsenic trioxide (As (III)). The detection method using Rhodamine B involves the reduction of arsenic species, particularly As (III), in the presence of iodide ions (typically provided by potassium iodide, KI). Under acidic conditions, As(III) reacts with KI to produce iodine (I₂).



The iodine generated in this reaction can lead to a discoloration of the Rhodamine B solution. This occurs because iodine can affect the electronic structure of the Rhodamine B dye, resulting in a change in color or fluorescence [90].

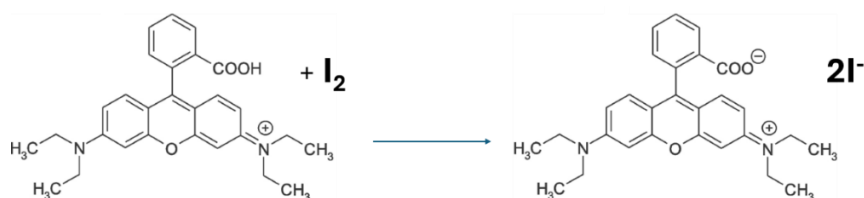


Figure 36: Proposed reaction mechanism for Rhodamine B shows pink color solution, but it becomes colorless when reacts with iodine produced by potassium iodide (KI) and As(III) in an acidic environment. Image modified by [90].

The procedure is relatively straightforward, and while Rhodamine B is typically resistant to many interferences, certain substances can still impact the accuracy of the results. Therefore, meticulous sample preparation and careful control of conditions are essential. Calibration solutions with arsenic concentration between 0 and 1ppm were prepared by proper dilution of the standard of high-purity quality As standard for ICP-MS 1ppm (Sigma Aldrich).

Calibration samples were prepared by adding 1 mL of 0.4 M hydrochloric acid and 2 mL of a 2% (w/v) potassium iodide aqueous solution to each sample. After thorough mixing and a brief waiting period for the characteristic purple color to develop, the samples were transferred to 10 mm optical path length glass cuvettes. Absorbance measurements were then performed at a wavelength of 553 nm using distilled water as a reference. The measurements were conducted under ambient conditions and at a neutral pH. The resulting solutions exhibited stability for 24 hours and reproducibility for up to 7 days, with a standard deviation of 1.76%.

Despite its limited robustness in a laboratory environment, the method's R^2 value, approaching unity, suggests that alternative analytical techniques could be investigated to quantify the metal. While the current testing conditions allow for the detection of arsenic concentrations up to approximately 250 ppb, it may be possible to lower this detection limit by using more dilute Rhodamine B solutions or reducing the optical path length. However, achieving the ultra-low arsenic concentrations necessary for effective water monitoring remains challenging.

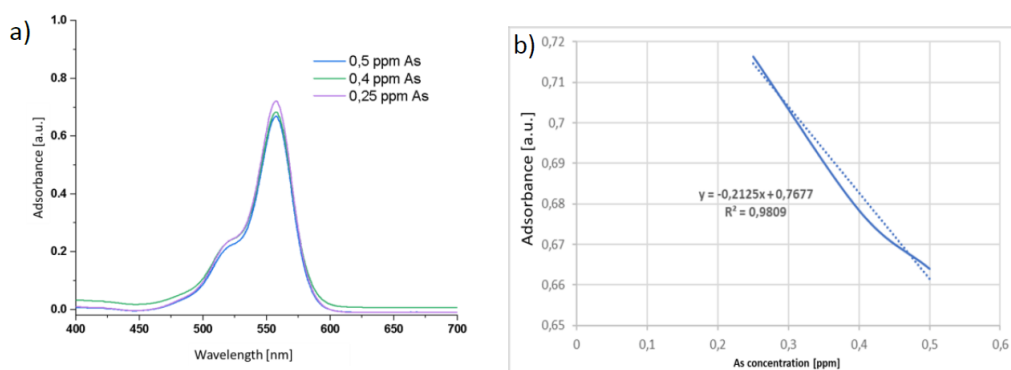


Figure 37: (a) UV-Vis spectra of Rhodamine solutions with different Arsenic concentrations in [ppm] range and (b) Calibration curve ($\lambda = 553$ nm) for Rhodamine B method.

3.3 Copper Detection

Copper is a chemical element with the symbol Cu (from Latin cuprum) and atomic number 29. Copper, renowned for its high electrical conductivity, malleability, and corrosion resistance, is a popular choice for electroplating applications. In this process, a metal or polymeric substrate is immersed in an electrolytic bath containing copper salts, such as copper sulfate (CuSO_4) or copper chloride (CuCl_2). By applying an electric current, copper ions from the solution are deposited onto the substrate surface, forming a thin, conductive, and aesthetically pleasing copper coating. The electrolytic bath for copper plating typically consists of a high concentration of different additives and copper salts (up to 100 g/L) dissolved in water. These salts dissociate into copper ions (Cu^{2+}) and if release in large quantities into water and soil can have detrimental long-term consequences for the environment, organisms, and ecosystem health [91].

Colorimetric range of investigations

A high-purity copper sulphate pentahydrate powder (Sigma-Aldrich) was used to prepare 50 mL aqueous solutions with varying copper concentrations ranging from 1 to 75 g/L. All solutions exhibited a distinct blue color, demonstrating a linear relationship between intensity and concentration. For copper concentrations exceeding 50 g/L, vigorous magnetic stirring and heating at 100°C for approximately 10 minutes were necessary to ensure complete salt dissolution.

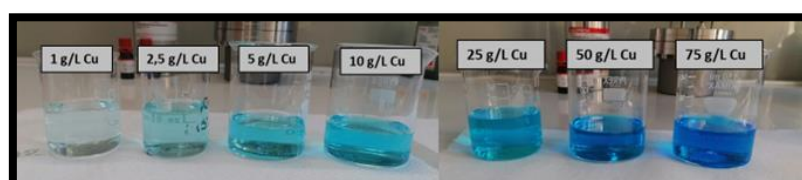


Figure 38: Copper sulphate solutions with increasing metal concentration, from left to right.

Figure 39a presents the spectra for Cu solutions within the concentration range of 1–22 g/L, highlighting the maximum absorbance observed at a clearly defined wavelength of 805 nm, with distilled water serving as the reference. The magnified section reveals increasing noise in the absorbance peaks at higher Cu concentrations, introducing uncertainty to the measured values. Consequently, 22 g/L is identified as the upper limit of detectable concentration for the system without dilution. Additional tests were conducted using higher concentration solutions; however, these resulted in saturated spectra. This saturation occurs when the absorbance reaches a level beyond the detection capability of the instrument, preventing accurate measurements. As a result, the system could not effectively distinguish further increases in concentration under these conditions. In Figure 39b the calibration curve obtained by absorbance values at 805 nm is reported; the high linearity toward metal concentrations from 1 to 22 g/L is

confirmed by the R^2 value, close to 1 ($R^2=0,9983$). Within the industrial context, the minimum detectable concentration was assessed over a range of 0.05 to 1 g/L. Although the starting loss of color, UV-Vis spectroscopy revealed distinct differences. The spectra closely resembled previous patterns, exhibiting a consistent peak at the same wavelength (Figure 39c). The corresponding calibration curve in Figure 39d demonstrated excellent linearity ($R^2=0.9872$). However, the absorbance peak became undetectable for copper concentrations below 0.1 g/L, indicating the detection limit of this method.

For environmental purpose copper solutions with concentrations ranging from 0.05 to 0.12 g/L were tested. Since the lower concentration was necessary increasing the optical path length of the cuvette from 10 mm to 20 mm. As shown in Figure 40b, the solutions lose their visible color appears transparent to the naked eye. However, Figure 40a and c demonstrate that even at such low concentrations, thanks to the extended optical path allows for the detection of the absorbance peak, and the calibration curve maintains excellent linearity ($R^2 = 0.9986$). This result indicates that detectable concentration can effectively lower the detectable concentration threshold.

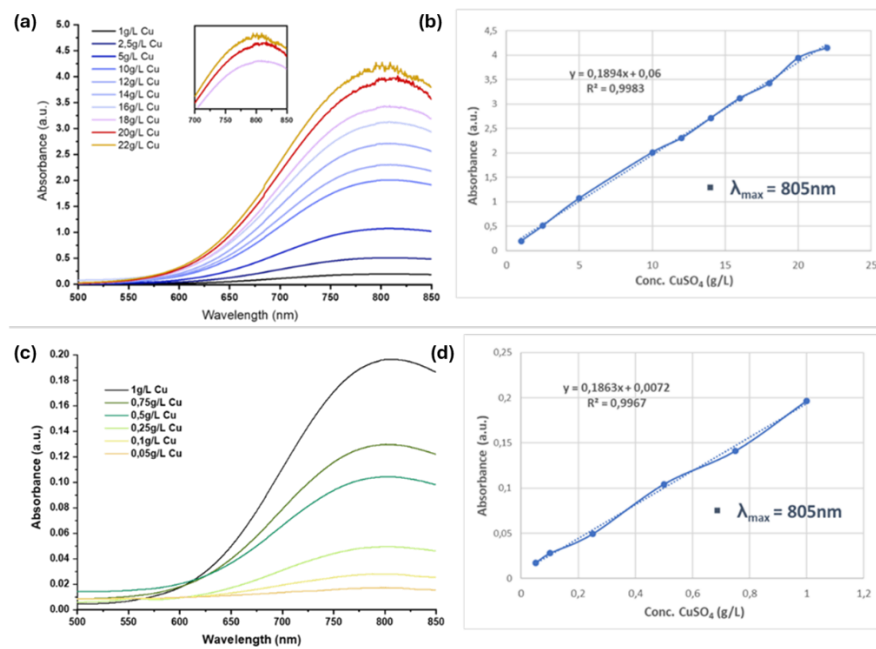


Figure 39: UV-Vis spectra recorded at RT with 10mm optical length (a) UV-Vis spectra of Cu solutions at high concentrations from 1 to 22 g/L. The magnification reveals the initial increase in noise, which is likely associated with signal saturation. (b) Calibration curve associated at the high range of copper solutions ($\lambda_{MAX} = 805\text{ nm}$). (c) UV-Vis spectra of Cu solutions at low concentrations from 0.05 to 1 g/L. (d) Calibration curve associated at low range copper solutions ($\lambda_{MAX} = 805\text{ nm}$).

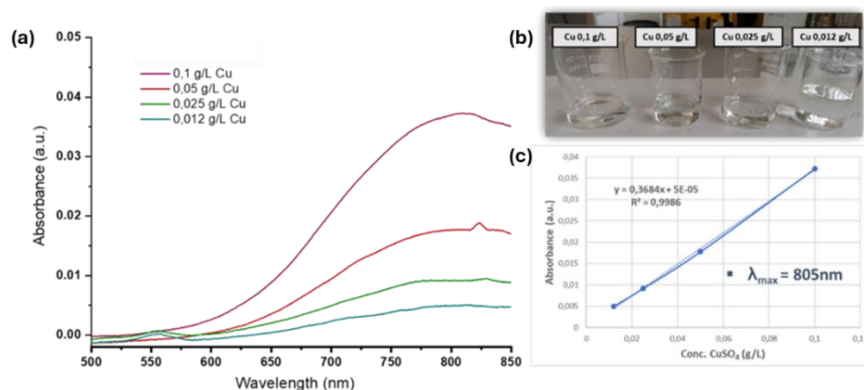


Figure 40: UV-Vis spectra recorded at RT with 20mm optical length (a) UV-Vis spectra of Cu solutions at low concentrations from 0.012 to 0.1 g/L (12-100ppm). (b) Colourless copper solutions. (c) Calibration curve associated at low range copper solutions ($\lambda_{MAX} = 805$ nm).

Variation in the optical path length was necessary to measure a broad range of copper concentrations, however, the wavelength remained constant at 805 nm for all analyses. This finding suggests that a single monochromatic LED can be integrated into the device to cover a wide concentration range from g/L to ppm, making it versatile and attractive for various applications. In the prototype design, only the parameters along the x-axis, which vary the optical path length of the laser, will be modified.

Evaluation of pH, aging test and dilutions

To assess the response of the solution under different conditions, the influence of pH was evaluated using a 1 g/L copper solution in both acidic and basic buffers. As shown in Figure 41, the salt dissolves completely and more rapidly, if not better, in an acidic solution compared to pure water. This indicates that, for a given concentration, comparing neutral and acidic solutions suggests that a slightly acidic condition is ideal for complete and homogeneous dissolution of the salt. Conversely, under basic conditions, the salt does not dissolve and the analyte precipitates. The UV-Vis spectra were recorded at room temperature using 10mm optical length. A first significant comparison emerges from the analysis of the spectrum shown in magnification of Figure 41b. The higher absorbance observed in the acidic solution, compared to the neutral one, unequivocally suggests a greater dissolution of the salt under acidic conditions. The reported spectra of copper solutions in an acidic environment (1-10 g/L) depicts the overall peak shape resembles that observed in neutral conditions, a distinct variation in maximum absorbance is apparent. Considering the absorbance in the range 760-780 nm, where the absorbance peak occurs, the calibration curves show good linearity, with a value of R^2 almost close to 1 regardless of the wavelength considered. This suggests that the working environment must be extremely controlled and well known, as it is essential to determine the exact wavelength to be used to select the most appropriate LED for the chosen working environment.

To assess the stability of the solutions and overcome the maximum detectable concentration aging tests and dilutions were conducted. While complete salt dissolution at high concentrations (≥ 20 g/L) proved challenging, various methods were investigated to enhance solubility. Magnetic stirring, heating, and resting periods were explored, with a 24-hour resting period yielding the most favorable results. Figure 42a shows that a 1:5 dilution of the higher concentration solutions (75 g/L and 50 g/L), which are closer to the concentrations found in the electrolytic bath, results in measurements below the 3% threshold, identified at 20-22 g/L. Although salt dissolution can be an issue, it is not critical for the application, in fact, to enable direct measurement of the metal concentration in the electrolytic bath, a dilution system must be integrated. Aging tests were performed 24 hours after solution preparation to evaluate potential degradation or color changes due to metal deposition.

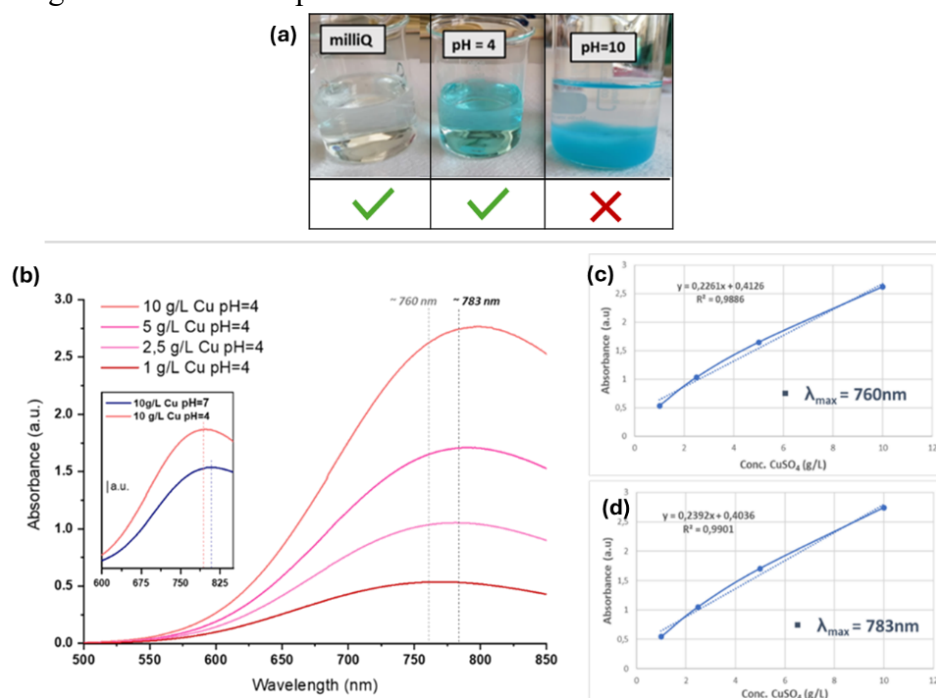


Figure 41: (a) Influence of pH on 1 g/L Cu solutions. (b) UV-Vis spectra recorded at room temperature for solutions containing increasing concentrations of copper in an acidic medium using a 10 mm optical path length. The magnification reveals a comparison of the absorbance increase relative to neutral pH conditions. (c) and (d) Calibration curves based on the two selected wavenumbers corresponding to the maximum absorbance peaks.

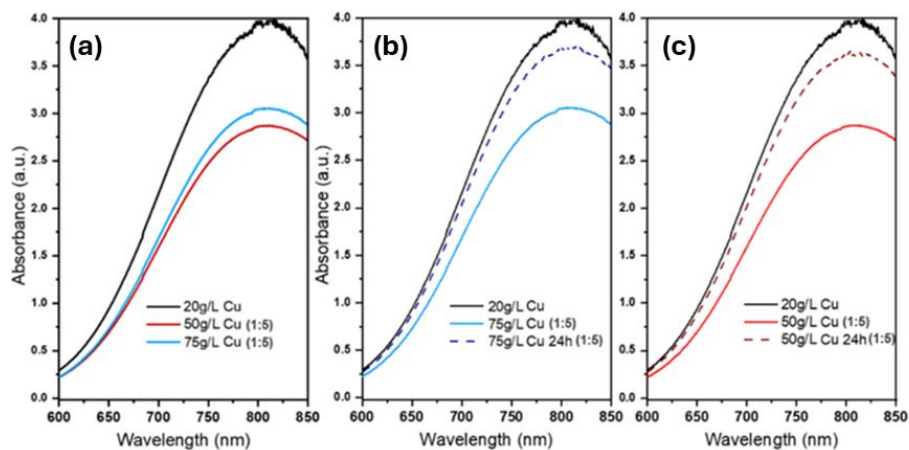


Figure 42: UV-Vis spectra depict (a) Sample 1:5 dilution for Cu solution exceeding 20 g/L; (b) and (c) Increase of salt dissolution due to 24h resting time.

Colorimetric evaluation by ZinconTM

Zincon (2-carboxy-2'-hydroxy-5'-sulfoformazylbenzene) is a chemical compound that acts as a chromophore for the detection of HMs ions in solution. Figure 43 shows the structure and the proposed reaction mechanism of Zincon [92], [93]. The proposed reaction mechanism for Zincon in combination with a heavy metal involves a complexation process. In its free form, Zincon has an intense orange color due to its specific chemical structure, which absorbs light at certain wavelengths. When it binds to a heavy metal, such as copper (Cu^{2+}), the interaction between Zincon and the metal causes an electronic reorganization within the complex (Figure 44a). The Zincon method was employed to detect trace levels of copper (less than 5 ppm). To cover a broad range in this preliminary analysis two concentrations, ranges were investigated: 250-2000 ppb and 10-100 ppb. In this concentration range, the copper solutions became colorless, rendering spectrophotometric analysis impossible without the presence of a ligand (L). A distinct UV-visible peak at approximately 450 nm, indicative of free Zincon, gradually decreases in intensity as a new peak appears at 600 nm (Figure 44b). This spectral change is consistent with the formation of the HM-L complex. For this specific application, either distilled water or a solution containing only the chromophore can serve as a reference, since the analyte of interest is not present either. However, when analyzing lower concentrations, the presence of un-complexed Zincon in the solution hindered accurate measurements due to the persistent orange color. This issue was solved by using the same Zincon solution as a reference for spectrophotometric analysis, effectively eliminating the orange background signal. Even within the 250 ppb to 2 ppm range, no significant differences were observed between using water or the Zincon solution as a reference. The proposed method reliability was validated by constructing and confronting calibration curves that in both cases reach R^2 close to unit. To maintain a wide analytical range and simplify the procedure, a Zincon solution was selected as a reference for both concentration ranges.

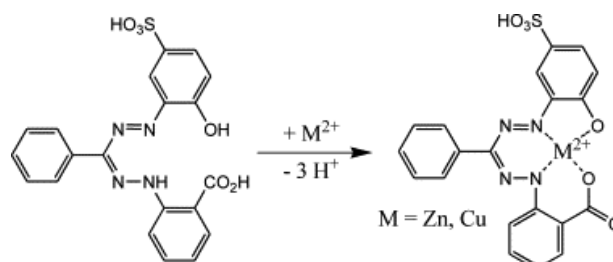


Figure 43: Proposed complexation mechanism for Zincon in combination with a heavy metal ion such as copper and zinc in water solution.

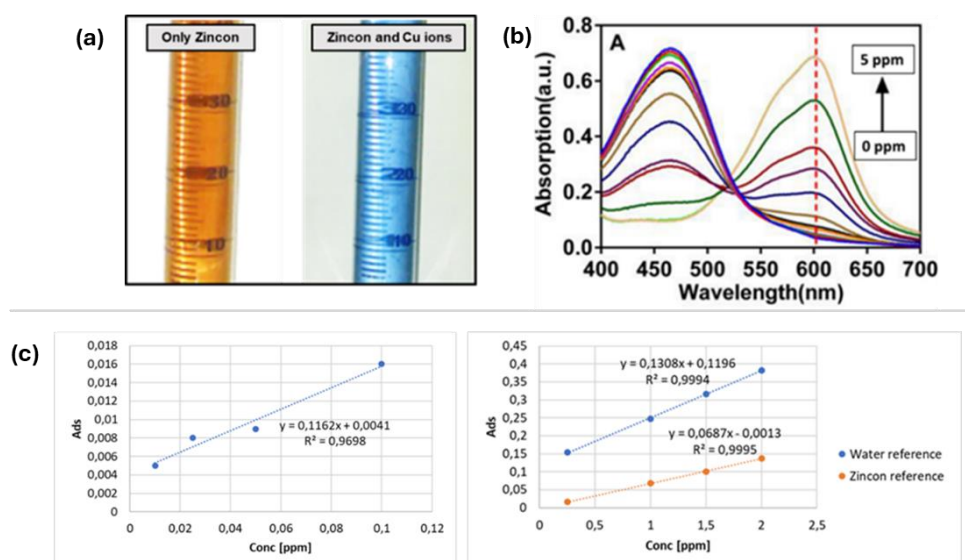


Figure 44: (a) Experimental solutions demonstrating the color change from the Zincon solution alone (orange) to the solution containing copper (blue) confirm the complexation between the metal and the ligand. (b) UV-Vis spectra recorded at room temperature and neutral pH demonstrate the presence of two distinct peaks: one at 450 nm corresponding to free Zincon, and the other at 600 nm representing the M-L complex (c) (left) Calibration curve for Cu concentration 10-100 ppb, Zincon solution as reference. (right) Calibration curves for Cu concentration 0.25-2 ppm.

3.4 Nickel Detection

Nickel is a metal member of the transition series in the periodic table with atomic number 28 and symbol Ni. Its most common oxidation state is +2, but nickel complexes have also been observed in oxidation states of 0, +1, and +3. Nickel is an abundant element in the Earth's crust, with an average concentration of about 75 parts per million (ppm). It is primarily found in minerals such as pentlandite, millerite, and garnierite. It is also an essential element for human life. It is a component of many enzymes, including urease and hydrogenase. Nickel is also a component of some proteins that help repair DNA. Despite its role in the human body, nickel is a highly toxic element, with stringent exposure limits. For prolonged exposure to low doses in mammals, Nickel has been revealed to have negative effects on the reproductive system and to prevent these effects, EFSA (European Food Safety Authority) in 2020 established a Tolerable Daily Intake (TDI) of 13 $\mu\text{g}/\text{kg}$ body weight per day.[94]

On the industry side Nickel is an indispensable material for electroplating, offering numerous advantages linked to its unique properties. Nickel plating

provides a wear-resistant and corrosion-resistant layer, extending product life, its finishes offer a variety of aesthetic appeal visual options, from high-gloss to matte accounts for approximately 80% of nickel consumption in plating and it can be applied to a wide range of substrates, including steel, copper, brass, and even plastics [95]. It is also commonly used as a base layer in multi-layer coatings, such as those preceding chrome plating, to enhance adhesion and overall durability.

Nowadays, the Watts nickel solution is the most widely used and requires a mixture of nickel chloride, nickel sulphate and boric acid with high metal concentration, as far as 100g/L. [96]

Like other electroplating processes, Nickel electroplating generates waste that must be managed carefully to prevent environmental contamination. Nickel is classified as a hazardous material, and prolonged exposure to nickel dust or fumes can have adverse health effects. As a result, industries must follow strict guidelines for waste treatment, including the proper disposal of nickel-containing solutions and by-products, to minimize their environmental impact.

Colorimetric range of investigations

Samples with increasing Ni concentrations, ranging from 1 to 25 g/L, were prepared by dissolving appropriate amounts of high-purity Nickel (II) nitrate hexahydrate ($\text{Ni}(\text{NO}_3)_2 \cdot 6\text{H}_2\text{O}$) (Sigma-Aldrich) in 50 mL of distilled water (neutral pH) at room temperature. To achieve complete dissolution of the metal, vigorous magnetic stirring was required for a few minutes, but only for the solutions with the highest analyte concentrations. As illustrated in Figure 45a, the UV-Vis direct spectrophotometric colorimetric method enables the rapid, simple, and direct detection of nickel, which exhibits a distinct green hue within the analyzed concentration range. The spectra recorded for the nickel solution (20-1 g/L), with the following conditions of RT, 10mm optical path length, neutral pH, and distilled water as reference, exhibited maximum absorbance at a precisely defined wavelength of 396 nm. At higher metal concentrations (25g/L), a deviation from the established trend was observed. This is likely attributed to the onset of signal saturation, characterized by a steadily increasing peak at 380nm in the spectrum. Despite this saturation, the system linearity remains unaffected up to a certain concentration because the peak is sufficiently distant from the maximum wavelength and it is still possible to proceed with the analysis, ensuring a good quality of the final data. However, as shown in the magnified portion of Figure 45b, the signal becomes completely saturated at a 25 g/L solution, resulting in a significantly reduced R^2 value on the calibration curve (not reported). For industrial calibration purposes, the maximum detectable nickel concentration is 20 g/L. Figure 45c presents the calibration curve constructed using the specific absorbance values. The R^2 value of 0.99 indicates a strong linear relationship between absorbance and metal concentrations up to 20g/L with $\text{SD}=1.84\%$.

Direct colorimetry has proven to be a powerful tool for analytical chemistry, as it has been possible to reach a limit of detection (LoD) of 3 ppm without the

need for external chromophores. In fact, visual analysis indicates a loss of the typical green color of the solutions. Despite the loss of visual color, UV-Vis spectrophotometry detected subtle variations in the absorption spectrum, indicating the presence of the analyte at concentrations below the limit of visual perception. To enhance sensitivity, the proposed method was evaluated using a longer optical path length, increasing from 10 to 20mm. As depicted in Figure 46a, a new series of samples within a lower concentration range, spanning 0.1 g/L to 0.003 g/L (1000-3ppm), exhibited spectra similar in shape to the previous ones, featuring the same peak at the same wavelength. The calibration curve confirms a strong linear relationship ($R^2=0.9974$ with $SD=1.7\%$). For nickel concentrations below 0.003 g/L (3ppm), the absorbance peak becomes imperceptible, suggesting this as the approximate limit of detection for this setup. However, increasing the optical path length could potentially lower this detection limit [96].

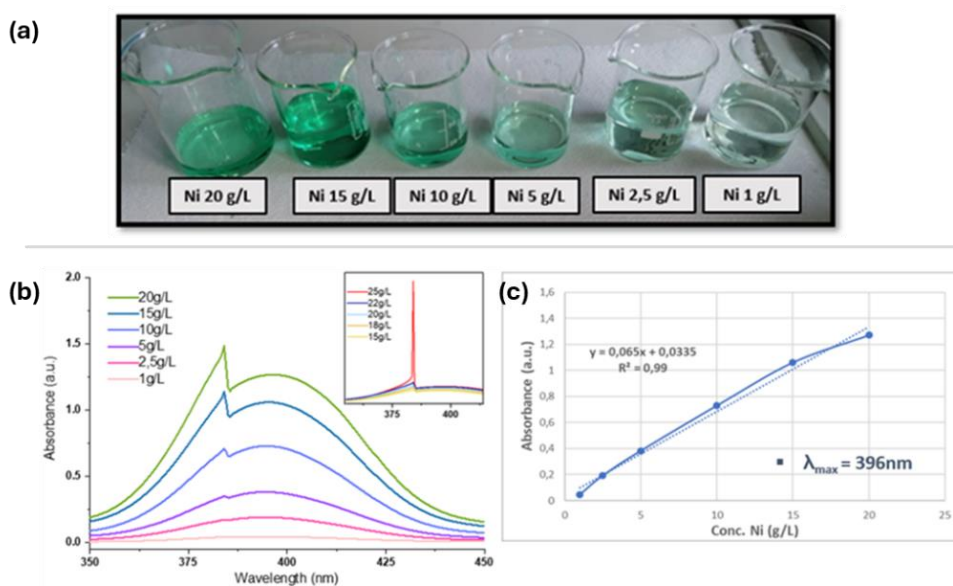


Figure 45: (a) Nickel nitrate solutions with increasing color and metal concentration from 20 to 1g/L (right to left). (b) UV-vis spectra of Ni solutions with increasing metal concentrations recorded at RT, neutral pH and 10mm optical length. The magnification shows the detection limit for direct colorimetry at 25g/L. (c) Calibration curve ($\lambda_{MAX} = 396$ nm).

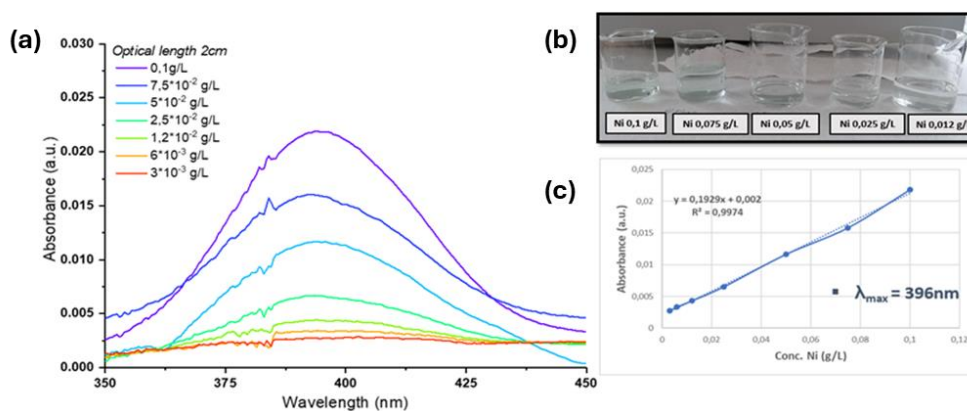


Figure 46: (a) UV-vis spectra of Ni solutions with increasing metal concentrations from 0.1 to 0.003 g/L recorded at RT, neutral pH and 20mm optical length. (b) Nickel nitrate solutions show barley color intensity with a metal concentration from 0.1 to 0.012 g/L (right to left). (c) Calibration curve ($\lambda_{MAX} = 396$ nm).

Evaluation of pH, aging test and dilutions

The effect of pH on two 10 g/L Ni solutions was examined in both acidic and basic buffer conditions. The behaviour of the nickel salt varied with pH levels. Specifically, as expected, the salt remained undissolved and produced a turbid solution under basic pH conditions. In contrast, the salt dissolved in acidic pH, producing a clear, bright green solution. This effect was ideal for the objectives of this study, making the acidic pH condition the preferred choice for evaluating the influence of pH. This is evident in the UV-Vis spectra shown in Figure 47(b₁). Compared to neutral pH, the acidification leads to higher absorbance values because the salt dissolves more effectively in acidic conditions. However, despite the increased absorbance, the position of the maximum absorbance peak remains consistent with that observed at neutral pH. Spectroscopic analyses were performed across a concentration range of 20 to 25 g/L using a 10 mm optical path length. The estimated maximum detectable concentration is 22 g/L at this pH. While the 25 g/L solution does not show evident signs of saturation in the spectrum, it does affect the linearity of the calibration curve, resulting in an R² value of less than 0.98. This suggests that the accuracy of the calibration diminishes at higher concentrations.

The impact of acidic pH on the minimum detectable concentration is considerable. Under acidic conditions, particularly at pH 4, the spectral resolution is enhanced by using the longest optical path length of 20 mm. This combination, as illustrated in the magnified section of Figure 46, results in synergistically improved absorbance compared to similar concentrations tested under less acidic conditions. In laboratory experiments, solutions ranging from 1 to 1.8×10^{-3} g/L were evaluated at acidic pH levels. These solutions displayed a noticeable loss of color, indicating that the acidic environment facilitates better dissolution of the metal. As a result, a minimum detectable concentration of approximately 2 ppm was achieved, demonstrating effective dissolution and accurate measurement.

Furthermore, the lower limit of detectable metal concentration improved to 1.8×10^{-3} g/L compared to neutral pH conditions, reflecting enhanced sensitivity and linearity in the calibration curve under acidic conditions. This improvement highlights the advantage of acidic media in increasing the accuracy and precision of metal concentration detection.

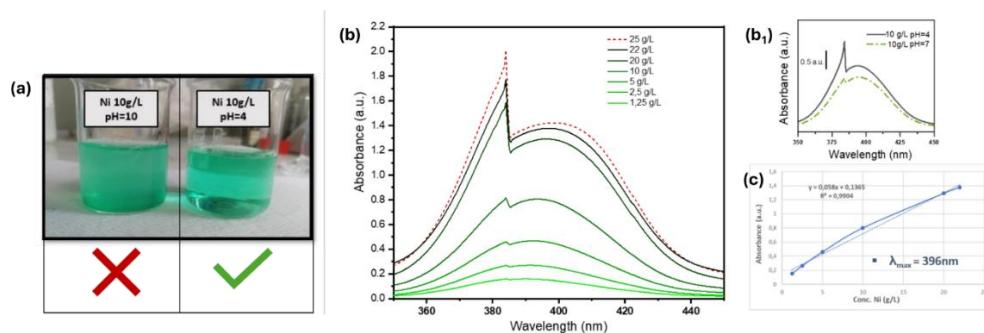


Figure 47: (a) Influence of pH on 10 g/L Ni solutions. (b) UV-Vis spectra recorded at room temperature for solutions containing increasing concentrations of copper in an acidic medium using a 10 mm optical path length. (b1) The magnification reveals a comparison

between acidic and neutral media with respect to the same concentration and experimental procedure. (c) Calibration curve ($\lambda_{\text{MAX}} = 396 \text{ nm}$).

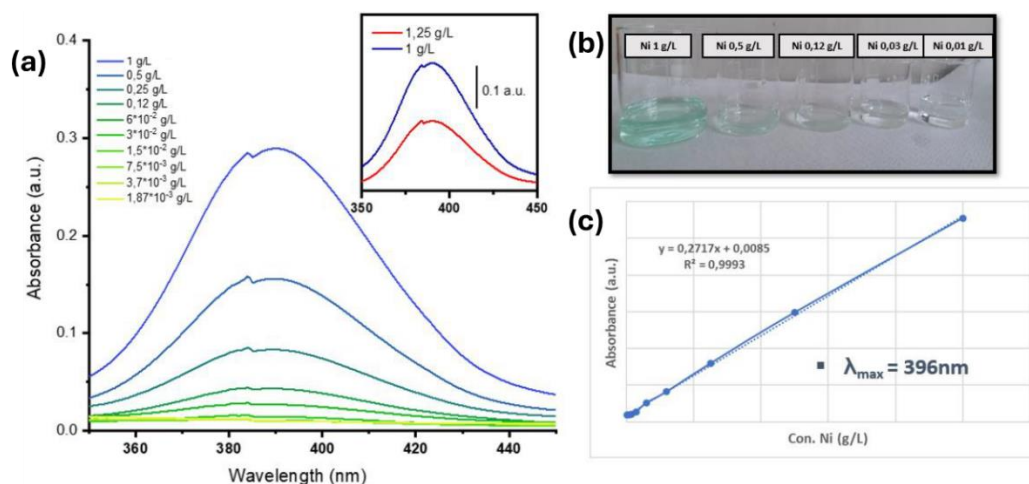


Figure 48: (a) Influence of acidic media on absorbance on UV-Vis spectra of Ni solutions range from 1 to $1,8 \cdot 10^{-3}$ g/L; the magnification shows the improvement in absorbance with respect the same range of concentration (b) Loss of color for solutions with low Ni concentration (c) Calibration curve ($\lambda_{\text{MAX}} = 396 \text{ nm}$).

The spectra reported in Figure 49a illustrates that, within the same investigation range (1 to 20 g/L) and under identical conditions, the spectra for both freshly prepared (solid lines) and aged solutions (dashed lines) show a strong similarity. This close resemblance indicates that the aging process has a minimal impact on the spectral properties within this concentration range. The consistency of the data is further validated by the R^2 value of the calibration curve for the resting solutions, which is close to unity, confirming the high correlation and reliability of the measurements across both fresh and aged samples. These findings suggest that no modifications occur in the coordination structure of the Ni^{2+} hexa-aqua complex, as evidenced by the absence of any shift in the maximum absorbance peak. This indicates that the salt dissolves completely and immediately in the freshly prepared solution. Finally, since the maximum detectable concentration was not reached, given that electroplating processes require high metal concentrations, dilutions were performed on two solutions with higher concentrations, specifically 75 and 50 g/L. Figure 49c illustrates that the spectra of the 1:5 diluted Nickel solutions match almost precisely with those of the starting prepared solutions, with no shift in the absorbance peak. Additionally, these dilutions show that the salt remains soluble in the diluted solutions even after 24 hours. Therefore, metal solutions, even at very high concentrations, can be accurately analyzed by diluting them with water to bring their concentration into a detectable range. This approach ensures precise measurements and effectively manages high concentration levels.

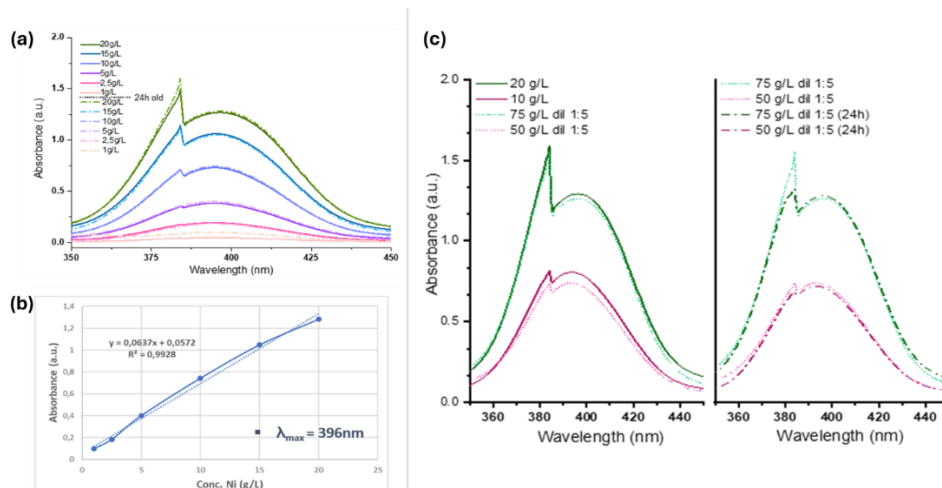


Figure 49: (a) UV-Vis spectra of Ni solutions from 1 to 20 g/L, freshly prepared (solid lines) and 24h aged (dashed lines); (b) Calibration curve for aged solutions ($\lambda_{MAX} = 396\text{ nm}$). (c) Sample dilution 1:5; (left) Spectra of the diluted solutions overlapping the analogous fresh one; (right) Effect of 24 hours aging.

3.5 Chromium (III) Detection

Chromium (III) electroplating is a highly effective technique for enhancing the appearance, durability, and functionality of metal components, offering several advantages over traditional chromium (VI) plating methods. Chromium (III) plating can be employed in a diverse range of applications, providing both aesthetic and functional benefits. It enhances the visual appeal of components while improving their wear resistance and corrosion protection. Chromium (III) is significantly less toxic than its hexavalent form, which is known for its hazardous properties. This reduced toxicity makes chromium (III) a more environmentally friendly choice, contributing to safer working conditions and minimizing environmental impact. The use of chromium in its trivalent oxidation state not only lowers health risks for workers but also reduces the overall environmental footprint.

However, there are challenges associated with chromium (III) electroplating. Ensuring proper adhesion of chromium (III) coatings can be difficult, necessitating meticulous surface preparation to achieve optimal results. Additionally, maintaining precise control over the plating parameters—such as temperature, pH, and current density—is crucial for attaining the desired coating quality and properties. Effective management of these factors is essential to ensure that the coatings meet performance and durability standards.

Colorimetric range of investigation

Initially, two real sample solutions provided by the **IntelWatt** project, sourced from a pilot rinse bath, were examined separately to determine the maximum absorbance peak, check for signal saturation, and assess the presence of any potential interferences. The first assessment that can be made is a visual one, as the two samples display distinct colors visible to the naked eye. Therefore, the

direct visible colorimetry method can be used. As shown in Figure 50a, the more concentrated solution (7.3 g/L) exhibited a darker color, and its UV-Vis spectrum immediately saturated, indicating signal overload at higher concentrations. In contrast, the less concentrated solution (0.73 g/L) presented a lighter green color and displayed a clear absorbance peak at 423 nm, providing a good resolution and no saturation. The two solutions were tested with a pH meter, which revealed a pH of approximately 7. Based on these simple but useful findings, the second step involved validating the presence of analyte and its concentrations relative to standard laboratory ranges. To ensure accuracy and reliability, a concentration range from 10 to 0.6 g/L was selected and prepared with respect to the same conditions, encompassing the concentrations from the pilot samples, allowing for direct comparison between the two. Following this comparison allowed to effectively handle varying concentration levels, ensuring accurate detection and reducing the risk of interference in subsequent analyses. The top of Figure 50b illustrates that the laboratory-prepared solutions exhibit a distinct green color, with the intensity directly proportional to the concentration of the analyte. This color variation makes it possible to utilize the sample solutions for direct colorimetry, allowing for a straightforward visual assessment of concentration levels. The visible intensity gradient enables precise calibration and analysis, confirming that the green hue can serve as a reliable indicator of the analyte concentration in the solution, supporting the use of colorimetry as a simple yet effective analytical method. The series of standards prepared with trivalent chromium provides a well-defined peak at 425 nm, allowing for the identification of a maximum concentration at 10 g/L. At around 420 nm, a distorted signal begins to appear. The first scientific evidence that can be drawn is that, given the comparable wavelength and similar peak shape, the analyte in question is indeed trivalent chromium.

The calibration curve reported in Figure 51a displays an R-squared value near 1 for the laboratory standards tested at the specified concentrations, demonstrating strong linearity and the accuracy of the system for these concentration ranges. However, a comparison reveals a minor difference in the maximum absorbance wavelengths between the samples, but this difference is negligible and does not significantly impact the analysis since the values are very close. Notably, the laboratory standards were able to detect higher concentrations more effectively than the solutions from the electrolytic plant. This discrepancy may be due to potential degradation in the plant samples, which could result from interactions with additives used in the electrolytic process or from the deposition of metal during electroplating. These factors could alter the composition or clarity of the sample, affecting the absorbance and overall performance in spectroscopic analysis. The comparison of UV-Vis spectra highlights a difference in absorbance values between the supplied samples and the laboratory-prepared ones. After recording the spectra of the two samples at the same concentration and in the same condition, the absorbance difference was measured at $\Delta = 0.18$ (a.u). This light discrepancy is in line with signal saturation occurring earlier in the real sample solutions. Saturation affects the accuracy of absorbance readings, as the

signal becomes less responsive to concentration changes at higher levels, resulting in the observed difference compared to laboratory-prepared samples [97].

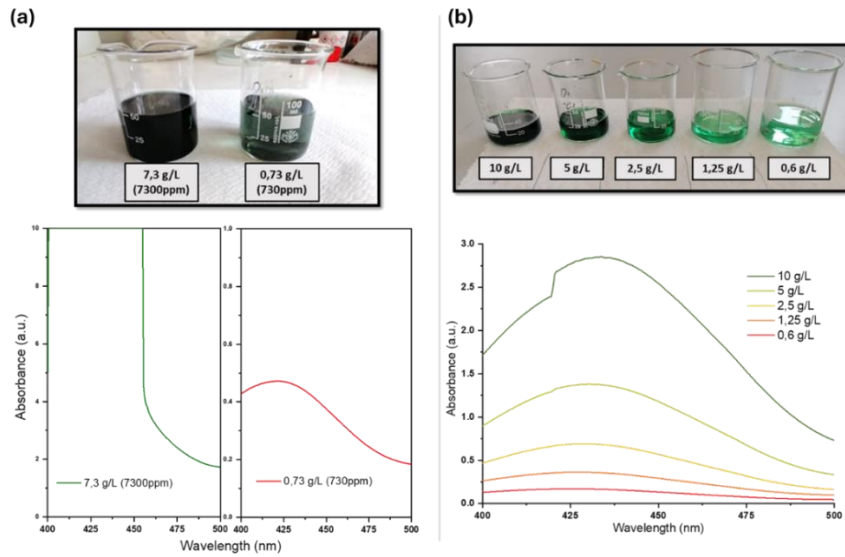


Figure 50: (a) (top) Visual comparison of the color of solutions came from electroplating plants pilot; (bottom) UV-Vis spectra of the two real sample solutions with different concentrations of supplied chromium (III). (b) Visual comparison of laboratory standard solution from higher to lower concentration, left to right; (bottom) UV-Vis spectra of chromium (III) chloride hexahydrate standard solutions with similar concentration of real samples, 10mm optical length, RT and neutral pH.

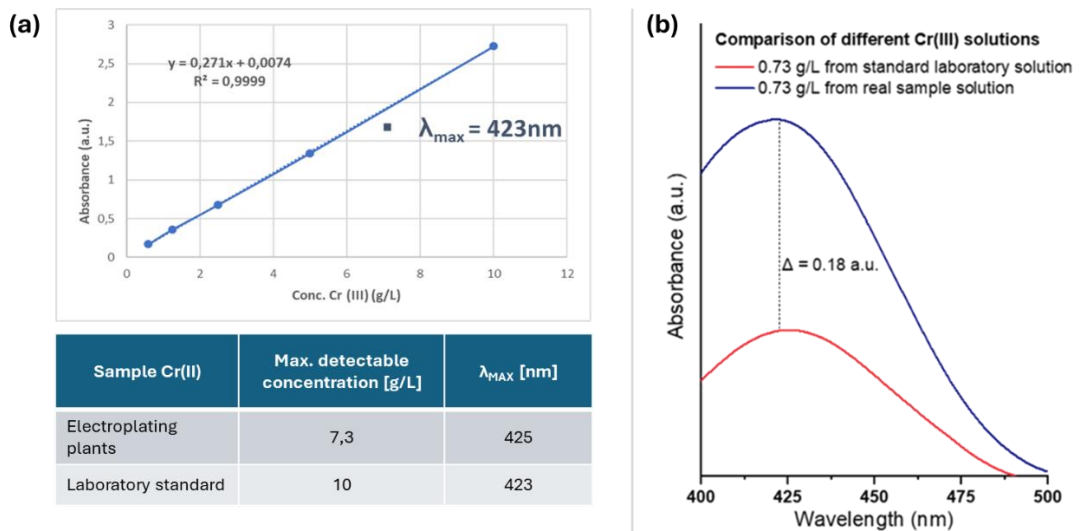


Figure 51: (a) Calibration curve for laboratory standard solution from 0.6 to 10 g/L ($\lambda_{MAX} = 423 \text{ nm}$) and compared table of important parameters with difference in maximum detectable concentration and wavelength. (b) UV-Vis spectra comparison of the same concentration of chromium trivalent solution from laboratory (red line) and from real plant (blue line).

To calibrate a custom sensor for real-world concentration scenarios, two dilution series were analyzed, starting with the provided solutions, as depicted in Figure 52. For the lower concentration range of 0.73 to 0.09 g/L, a clear,

proportional relationship between absorbance and concentration was observed, confirming a consistent correlation between the absorbance curves and concentration levels. This is reflected in an excellent calibration curve with an R^2 value close to unity. When diluting from the more concentrated solution and examining concentrations from 7 to 0.5 g/L, the maximum wavelength remained stable, while absorbance decreased proportionally with lower concentrations. However, the dotted purple line in the spectra, representing the highest concentration investigated, began to exhibit some noise, suggesting possible signal saturation. The analysis demonstrated good linearity for Cr (III) concentrations between 0.5 and 6.3 g/L, as shown in the calibration curve (Figure 52c). However, the presence of noise, indicated by small spikes, restricted the maximum detectable concentration to 6.3 g/L. This finding is essential for defining the optimal operational range for accurate measurements.

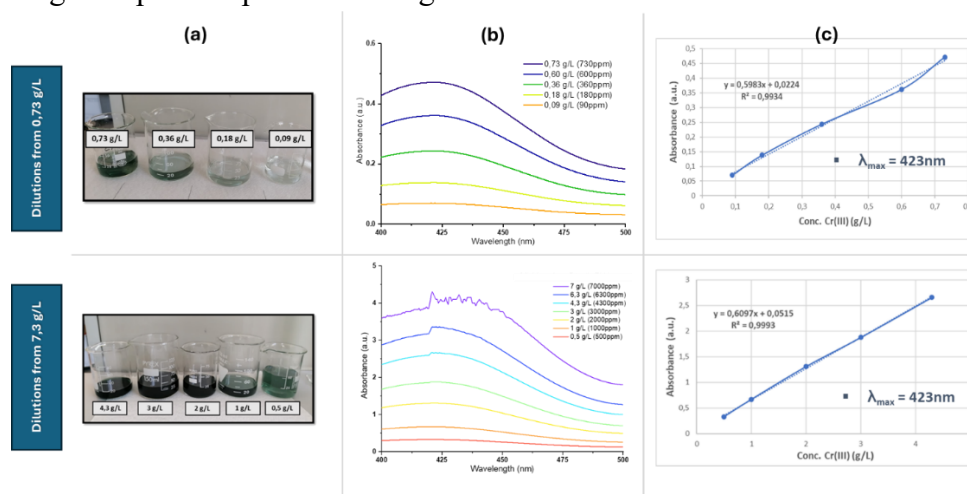


Figure 52: Series of analysis using a stock solution of trivalent chromium with a concentration of 0.73 g/L (top) and 7.3 g/L (bottom) (a) Visual comparison of the color of the solutions, (b) UV-Vis spectra for the selected dilution set from 0.73 to 0.09 g/L (top) and from 7 to 0.5 g/L (bottom), recorded at room temperature, neutral pH, and with a 10 mm optical path length, (c) Calibration curves ($\lambda_{MAX} = 423\text{ nm}$).

To extend the sensor range of detection at even lower concentrations using the UV-Vis direct method, additional analyses were conducted. As anticipated, the solutions became increasingly transparent to the naked eye as the metal concentration decreased. Significant improvements in detecting lower analyte concentrations were achieved by doubling the optical path length from 10 mm to 20 mm. As illustrated in Figure 53, this extension enabled the detection of concentrations as low as 0.011 g/L (11 ppm). Importantly, the maximum absorbance wavelength remained consistent at 423 nm across both path lengths, and the calibration curve demonstrated excellent linearity.

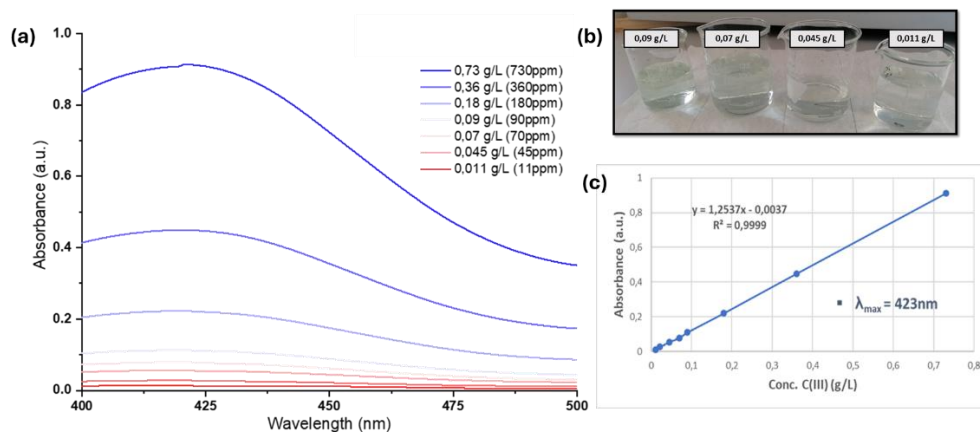


Figure 53: (a) UV-vis spectra of Cr (III) solutions with increasing metal concentrations from 0.011 to 0.73 g/L recorded at RT, neutral pH and 20mm optical length. (b) Chromium trivalent solutions show barley color intensity within the same metal concentrations. (c) Calibration curve ($\lambda_{MAX} = 423$ nm).

Aging test and dilutions

In this case, the evaluation of an environment with a different pH was not considered, as the conditions are set according to a real sample.

To overcome the limitation in the limit of detection (LoD) inherent to direct UV-Vis spectroscopy, a 1:10 dilution of the most concentrated sample was prepared. The UV-Vis spectra obtained, as depicted in Figure 54, exhibited excellent agreement in terms of the maximum wavelength ($\lambda_{max} = 423$ nm), peak shape, and absorbance. This consistency is essential for effectively diluting highly concentrated real samples and achieving a reliable calibration curve that maintains the same excellent linearity observed at lower concentrations.

Additionally, the stability of the sample solutions was assessed over a two-month period, with particular attention given to a 0.73 g/L sample and its 1:10 dilution. This analysis was crucial for validating sensor calibration. Figure 54 shows that both the undiluted and diluted samples consistently exhibited an absorbance peak at 423 nm throughout the observation period. Notably, the diluted sample had a slightly higher absorbance compared to the undiluted one. Over the two months, absorbance variations were minimal, though it is important to note that the undiluted sample showed a marginally lower absorbance. This indicates that while the diluted solution provided slightly better results, both the undiluted and diluted samples demonstrated stable and reliable performance for sensor calibration over time.

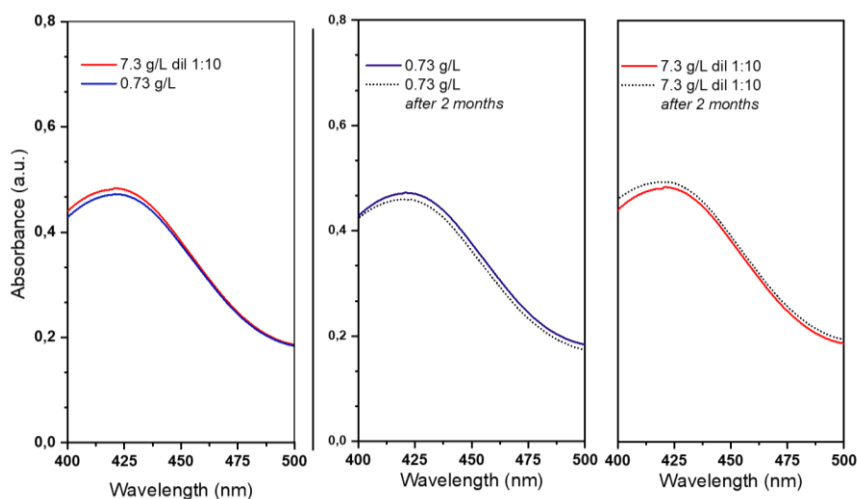


Figure 54: (a) Comparison of UV-Vis spectra of Cr (III) real sample solutions at 0.73 g/L (blue line) respect to 7.3 g/L diluted 1:10 (red line). (b) UV-Vis spectra before and after two months for two samples of Cr (III) solution one at 0.73 g/L and the 7.3 g/L diluted 1:10.

3.6 Chromium (VI) Detection

Chromium (VI), also known as hexavalent chromium, is a highly toxic and carcinogenic form of chromium. It is commonly used in various industrial processes, such as electroplating, stainless-steel production, leather tanning, and as a pigment in dyes and paints. However, due to its toxicity, exposure to chromium (VI) poses significant health risks, including lung cancer, skin irritation, and respiratory issues. It is also a potent environmental contaminant, capable of polluting soil and water from natural sources. Regulatory measures have been implemented to limit its use and minimize human and environmental exposure.

Colorimetric range of investigation

The electronic configuration of chromium (VI) allows it to absorb light within a specific range of wavelengths. In its hexavalent form, chromium absorbs light in the blue to violet region of the spectrum. Due to the absorption of these colors, the remaining light that is reflected or transmitted to the eyes appears orange. At higher concentrations, chromium (VI) exhibits a vibrant orange color, making it well-suited for direct colorimetric detection through UV-Vis spectroscopy. This distinct coloration enhances its effectiveness as an analyte in such analyses. For the specific purpose of studying this heavy metal, two distinct concentration ranges were examined: the first from 100 ppm to 25 ppm, and the second from 10 ppm to 0.5 ppm. This dual-range approach was driven by the potential applications of the final sensor, catering to both industrial and environmental monitoring needs. In both concentration ranges, the UV-Vis spectra consistently showed a maximum absorbance at 349 nm, with a clearly defined peak. This absorbance peak corresponds to the d-electron transition of chromium ions, which is characteristic of their optical behavior, providing a reliable signature for quantifying their presence. The presence of this well-defined peak across both

ranges demonstrates the sensor's potential to reliably detect chromium concentrations with precision. As illustrated in Figure 55a, the spectrum associated with the concentration of 100ppm begins to show an increase in noise around the maximum absorbance. This is reflected in the concentration curve, which, when considering this concentration, shows a decrease in the R-squared value to about 0.96. However, when examining the range from 75 to 25ppm, it can be observed that the R-squared value improves, approaching unity. Therefore, the maximum detectable concentration considered is 75ppm, as it provides a more linear system response under recording conditions of 10 mm optical path length, RT, and neutral media. Figure 55b depicts the spectra related to the concentration range from 10 to 0.5 ppm with the same recorded parameters mentioned above. As shown in the figure, the samples completely lose their characteristic color, but a visible spectrometer analysis was still able to detect differences in concentration. The peak remains well-defined at 349 nm, resulting in a calibration curve that confirms the system linearity. The trend depicted in the magnification indicates that for concentrations ranging from 1 to 0.5 ppm, there are still significant differences in absorbance. By focusing on just these three concentrations, a calibration curve can be constructed with an R-squared value approaching unity, with a minimum detectable concentration set at 0.5ppm. This demonstrates the potential to enhance sensor sensitivity for lower concentrations in order to ensure environmental safety. It is important to note that again by doubling the optical length, from 10mm to 20mm, the previously detectable limit of 0.5 ppm for chromium VI ions shows an improvement in terms of absorbance. Within the 0.5-0.1 ppm range, the calibration curve at 349 nm exhibited a linear relationship. This linearity enabled us to determine the minimum detectable concentration under consistent pH and temperature conditions by simply adjusting the optical path length to achieve a concentration of 0.1 ppm (100 ppb).

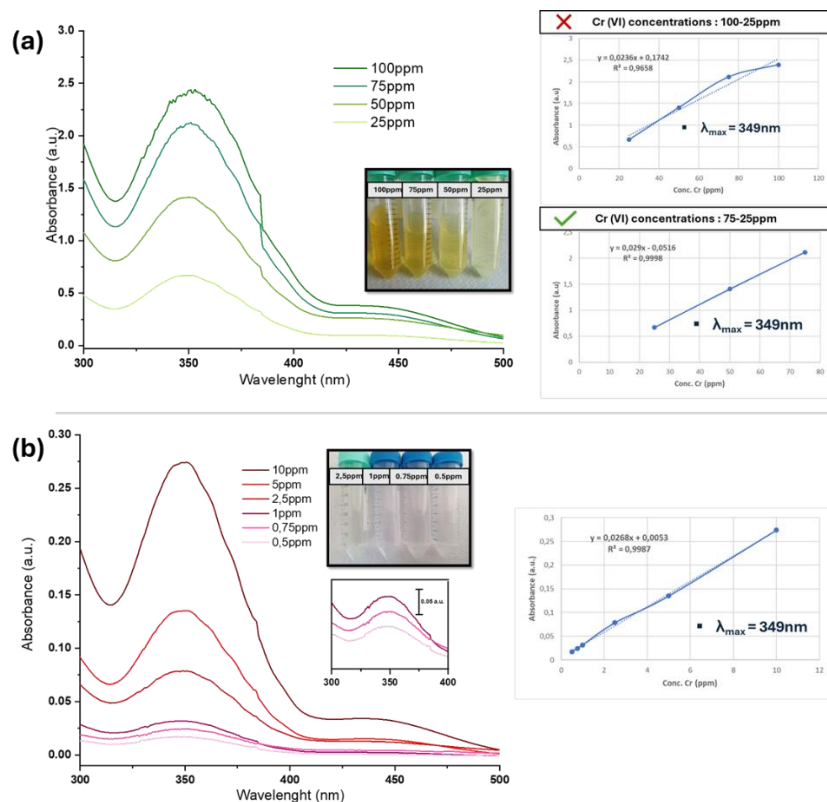


Figure 55: UV-Vis spectra for Chromium (VI) ions recorded with 10mm optical length, RT and pH =7 for two different range of concentrations (a) from 100 to 25 ppm, showing the intense color of the solution along with the corresponding calibration curve ($\lambda_{MAX} = 349\text{ nm}$), and (b) from 10 to 0.5 ppm, where the solution loses its color, accompanied by the related calibration curve ($\lambda_{MAX} = 349\text{ nm}$).

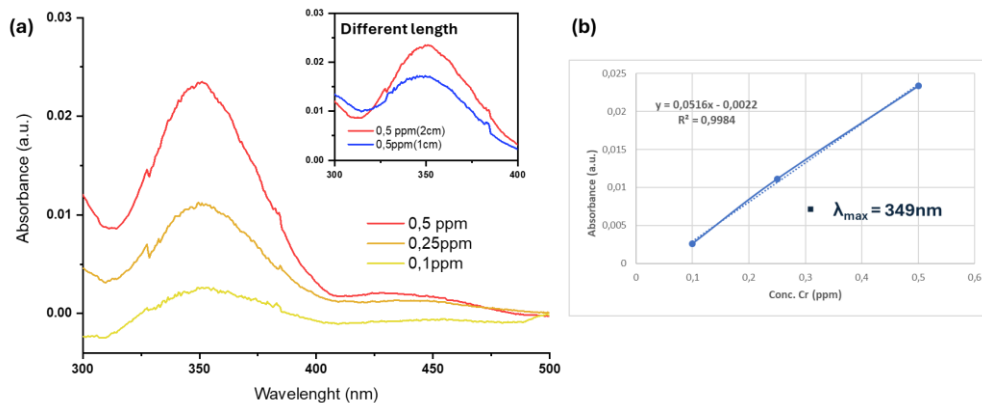


Figure 56: (a) UV-vis spectra of Cr (VI) solutions with increasing metal concentrations from 0.1 to 0.5 ppm recorded at RT, neutral pH and 20mm optical length. The magnification shows that at a concentration of 0.5 ppm, there is an improvement in absorbance following an increase in the optical length. (b) Calibration curve ($\lambda_{MAX} = 349\text{ nm}$).

Colorimetric evaluation by 1,5-Diphenylcarbazide (DFC)

The DFC (Diphenyl-carbazide) method is a widely used analytical technique for detecting hexavalent chromium (Cr (VI)) in various water sources, including drinking water, surface water, and both domestic and industrial wastewater. This method is particularly effective in the concentration range of 0.1 mg/L to 1.0 mg/L, making it suitable for regulatory compliance and environmental

monitoring. The principle behind the DFC method involves the chemical reduction of Cr (VI) to Cr (III) in a strongly acidic solution. This reduction is facilitated by the addition of 1,5-diphenylcarbazide, which acts as a reducing agent. When Cr (VI) is present, it reacts with the DFC, leading to its oxidation and the formation of 1,5-diphenylcarbazone. This newly formed compound exhibits a characteristic reddish-purple color [98].

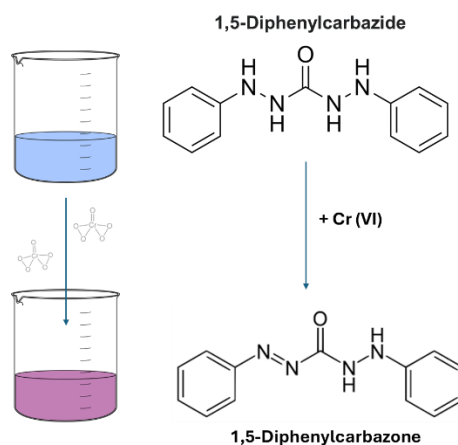


Figure 57: The proposed reaction mechanism for the DFC solution is transparent, but it takes on a violet color when complexed with Cr (VI) in acidic media.

The intensity of this color is directly related to the concentration of hexavalent chromium in the sample. The maximum absorption of this colored complex occurs at approximately 540 nm, which allows for quantification through spectrophotometric measurements. By comparing the absorbance of the sample to a standard calibration curve created with known concentrations of Cr (VI), analysts can determine the concentration of chromium in the sample. The DFC method is valued for its sensitivity and specificity, making it an essential tool in environmental analysis, particularly for ensuring that water sources meet safety standards regarding chromium contamination. Its effectiveness, combined with the straightforward nature of the procedure, makes it a preferred choice for laboratories conducting routine water quality assessments.

To validate the proposed methodology from the literature, the first experimental set was carried out using two ranges of known concentrations of chromium VI ions: the first ranging from 1 ppm to 0.25 ppm, and the second from 200 ppb to 25 ppb. DFC was dissolved in methanol as a solvent. Methanol is often used as a solvent in scientific experiments due to its ability to dissolve a wide range of compounds and its relatively low boiling point. For all subsequent experiments, samples were prepared as follows:

- 50 mL of a solution containing the analyte
- 0.5 mL of a 30:1 diluted H₂SO₄ solution
- 1 mL of DFC dissolved in the appropriate solvent

As shown in the figure, for both concentration ranges, the analyzed solutions display a pink-violet color depending on the concentration of the metal inside. Moreover, in both cases, the wavelength, as expected, is well-centered with a

broad peak at 520 nm. The calibration curves for both experiments yield good linearity values for the system.

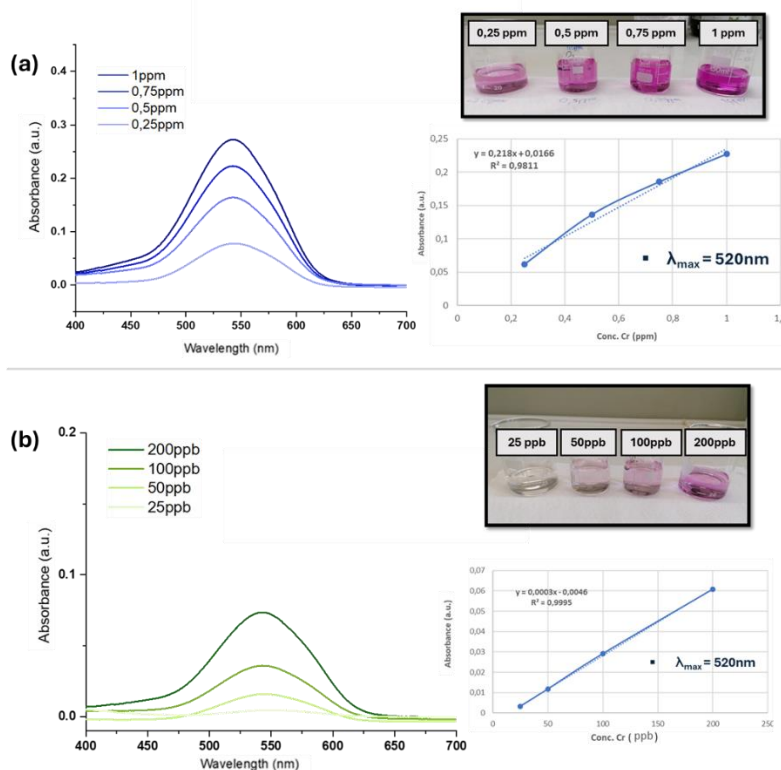


Figure 58: UV-Vis spectra for Chromium (VI) and DFC recorded with 10mm optical length, RT and pH =4 for two different range of concentrations (a) from 1 to 0,25 ppm, showing the intense color of the solution when combining with Cr(VI) along with the corresponding calibration curve ($\lambda_{MAX} = 520\text{ nm}$), and (b) from 200 to 25ppb, where the solution starting loses the characteristic color, accompanied by the related calibration curve ($\lambda_{MAX} = 520\text{ nm}$).

DFC aging test

Sample preparation was carried out with 10 mL of methanol (2 g/L) and 0.02 g of DFC. Distilled water was used as the blank, and the parameters used were 10 mm optical path length at RT. Spectrophotometric monitoring over time was carried out at various, closely spaced time intervals, as shown in Figure 59, to be compared with the freshly prepared solution. Visually, the solutions change from a light pink color (freshly prepared) to an intense orange (after 7 days). The λ_{MAX} value remains stable around 495 nm. The absorbance value increases progressively during the first 3 hours after preparation, then stabilizes within a specific range after 24 hours. Absorbance increases in units up to 24 hours, after which it begins to gradually decrease in a regular manner until 7 days after preparation. On 14 and 21 days, the absorbance value at the wavelength of 520 nm remains constant with the value measured at 7 days (around 0.7 a.u.).

Following the evaluation of the DFC stability over time, the spectrophotometric investigation of hexavalent chromium was carried out using a 7-day-old solution of DFC in methanol and 10mm optical length. As shown in Figure 60, the range from 1 ppm to 0.25 ppm was first evaluated. The maximum

value of peak was around 545 nm, slightly shifted compared to the previous one, likely due to the aging of the solution. The calibration curve, calculated at a maximum absorbance of 520 nm to be compared with previous results, was found to be perfectly aligned with that of the freshly prepared solution, considering the values at the same wavelength. A similar experiment was repeated for the range from 1 ppm to 0.25 ppm using a solution of DFC in methanol 28 days after its preparation. As shown in the calibration curve, the R^2 value deviates by far from unit, indicating that the chromophore solution performance is maintained for up to a maximum of 7 days.

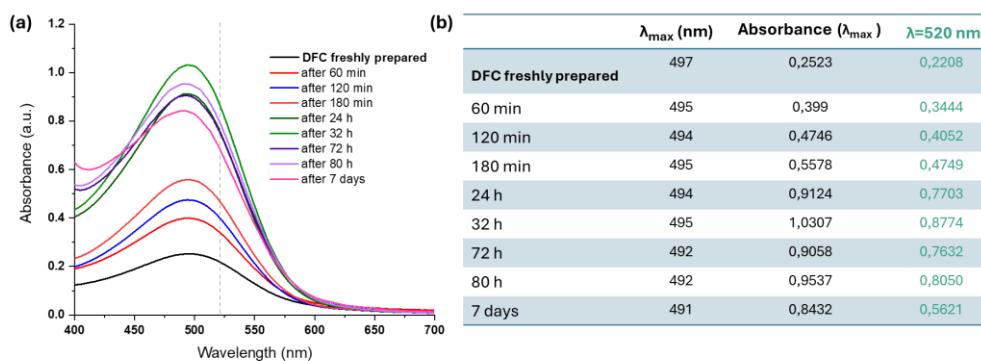


Figure 59: (a) UV-Vis spectra of DFC in methanol recorded at different times to evaluate aging of the solution. (b) Table of comparison of the different absorbance values with respect to the maximum (540nm) and the evaluate peak (520nm).

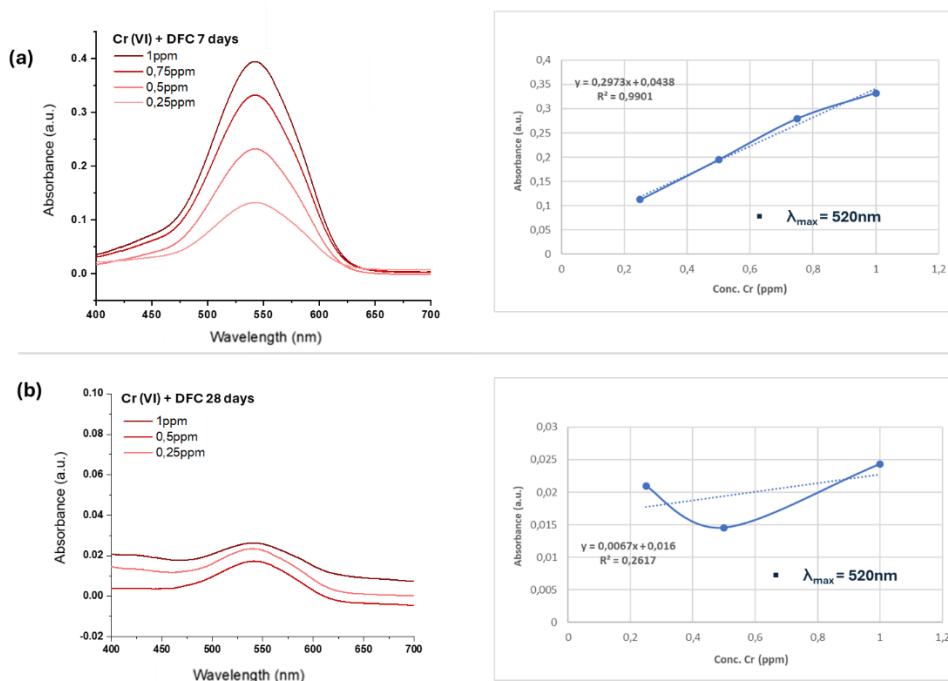


Figure 60: UV-Vis spectra for Chromium (VI) and DFC aged solution recorded with 10mm optical length, RT and pH =4 for two different range of concentrations (a) from 1 to 0,25 ppm with 7 days aged DFC along with the corresponding calibration curve ($\lambda_{MAX} = 520$ nm), and (b) from 1 to 0.25ppm with 28 day age DFC, supplemented by the related calibration curve ($\lambda_{MAX} = 520$ nm).

DFC solvent optimization

Methanol is metabolized in the body into formaldehyde and formic acid, both of which are extremely toxic. Even a small ingestion, as little as 10 mL, can lead to permanent blindness, while larger doses, ranging from 30 to 240 mL, can be lethal if not treated promptly. Symptoms of methanol poisoning include headaches, dizziness, nausea, respiratory distress, and, in severe cases, blindness or death. Beyond its toxicity, methanol is also highly flammable, with a flashpoint of approximately 11°C. It can form explosive mixtures when in contact with air, and its flames are often invisible, making methanol fires particularly hazardous and difficult to detect.

Given these significant health and safety risks, there was a clear need to explore alternative solvents that could dissolve the chromophore with similar efficiency to methanol but pose fewer dangers. While acetone is also classified as a hazardous chemical, it offers certain advantages over methanol, particularly in terms of toxicity. Although acetone can cause irritation upon inhalation or prolonged skin contact, it does not lead to the severe metabolic or systemic toxicity associated with methanol. Moreover, like methanol, acetone is highly flammable, but it tends to be somewhat safer to handle due to its more detectable symptoms of overexposure, such as eye or throat irritation, allowing for easier identification and avoidance of excessive exposure. Thus, while acetone still requires careful handling, it represents a potentially safer alternative to methanol in many applications.

The preparation procedure for the analytical procedure remains the same as described above, with identical quantities of analyte, acidic solution, and chromophore solution. The first range of samples considered went from 200 to 25 ppb, recorded at RT with an optical length of 10 mm. The maximum absorbance is observed around 540nm; however, the linearity of the system can also be appreciated at 520 nm. This confirms that the analytical system works just as well in the presence of acetone instead of methanol.

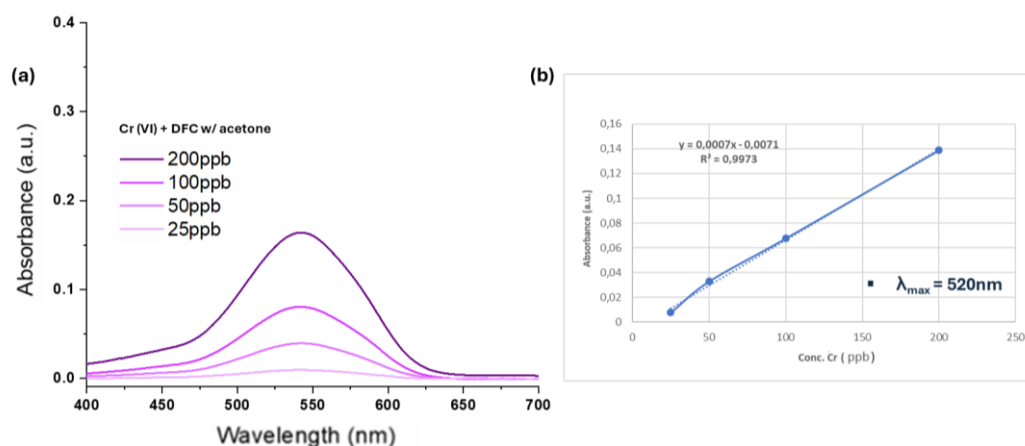


Figure 61: (a) UV-Vis spectra for Chromium (VI) and DFC in acetone recorded with 10mm optical length, RT and pH =4 from 200 to 25 ppb. (b) Corresponding calibration curve ($\lambda_{MAX} = 520\text{ nm}$).

Subsequent aging analyses were conducted on the pure solution of DFC in acetone. As shown in the figure, during the initial visual comparison, the impact of the two solvents on DFC is evident. In the presence of acetone, the solution remains colorless even after 7 days, while in the presence of methanol, the solution turns orange within the same timeframe. This can affect the choice of a specific blank used as a reference, such as water or the same-colored DFC solution. From the recorded visible spectra, it can be observed that over a period of 14 days, the solution does not deviate and shows virtually zero absorbance values. However, as illustrated in the figure by the dashed line, the first spectrum associated with a deviated behavior is recorded at 28 days, indicating that, compared to the methanol solution, the acetone solution appears to be more stable for a longer duration.

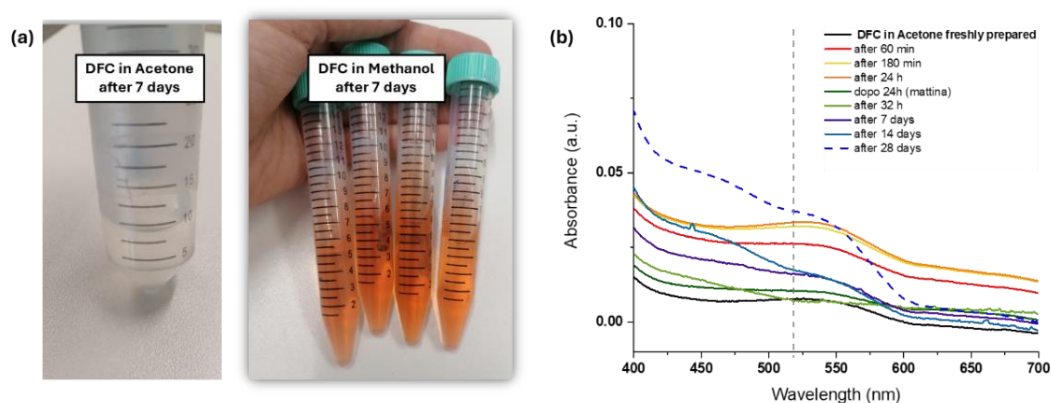


Figure 62: (a) Visual comparison of the DFC solution in acetone and methanol showing different colors after 7 days. (b) UV-Vis spectra of DFC in acetone recorded at different time to evaluate aging of the solution. Dashed line indicated the deviation trend in linearity of the solution.

DFC dilution 50:1

The DFC solution, both in methanol and acetone, was subjected to testing after being diluted 50:1 with distilled water. This approach is particularly significant within the framework of sensor miniaturization, as it addresses several key factors that enhance the practicality and sustainability of analytical methods. Diluting the DFC solution allows for a more efficient use of reagents, minimizing the amount of chemical required for analysis. This reduction is not only economically advantageous but also environmentally responsible. By using smaller quantities of chemicals, it can significantly decrease the volume of waste generated during the analytical process. This is especially relevant in contexts where waste disposal regulations are stringent, or where the environmental impact of chemical use is a major concern. Additionally, using a diluted solution helps maintain the integrity of the DFC solution, as the lower concentration may mitigate potential interactions or degradation that could occur in more concentrated solutions. This aspect further contributes to the reliability of the technique and the sensor readings, ensuring that the data obtained is both accurate and representative of the sample being analyzed. As shown in Figure 63, the absorbance of the DFC solution in both methanol and acetone remains virtually

zero or negligible over the course of several days. Figure 63c shows a comparison between the DFC solution in methanol, represented by the red line, diluted 50:1 with distilled water, and the DFC solution in acetone, represented by the blue line, also diluted 50:1 with distilled water. The comparison clearly indicates that, in both cases, there are no absorbance values that significantly affect the result of the analysis. In the same figure, the gray dashed line represents a DFC solution in methanol diluted 50:1 with tap water. For this solution, a peak is observed with a maximum absorbance at approximately 500 nm, indicating that the DFC solution has reacted with the analyte present in the tap water, albeit at negligible levels.

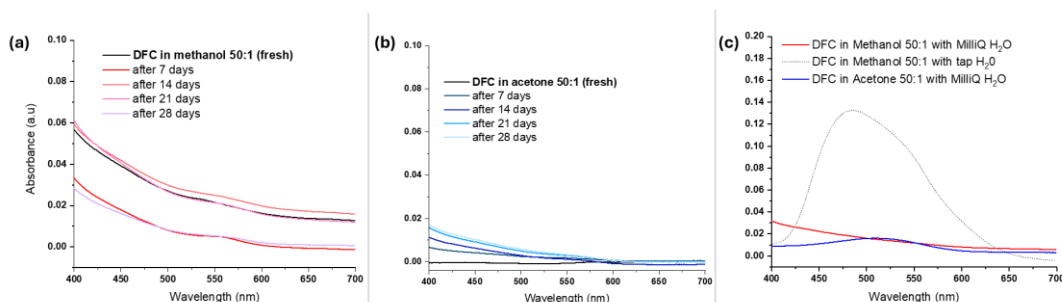


Figure 63: UV-Vis spectra recorded at RT and 10mm optical length for (a) DFC in methanol diluted 50:1 and recording its aging from 7 to 28 days, (b) (a) DFC in acetone diluted 50:1 and recording its aging from 7 to 28 days. (c) UV-Vis spectra for comparison between DFC solutions in methanol and acetone diluted with distilled water, and FC in methanol diluted with tap water.

Tests on field “Real sample analysis from ACDA”

In the laboratory experimental analyses conducted thus far, the best chromophore solution chosen was the one diluted 50:1, maintaining consistent initial conditions and acidic solution within the sample under examination. Subsequently, real samples contaminated by a natural chromium spill in the Cuneo mountains of Piedmont were sent from ACDA for testing using the proposed method. Tests were performed using both acetone and methanol. As shown in Figure 64, methanol provides a higher absorbance value; however, the absorbance value recorded with acetone, while minimal, is not negligible. By inputting these two values into the previously proposed calibration networks, **the contamination level of the sample returns an approximate result of 14 ppb (SD=0.4%).**

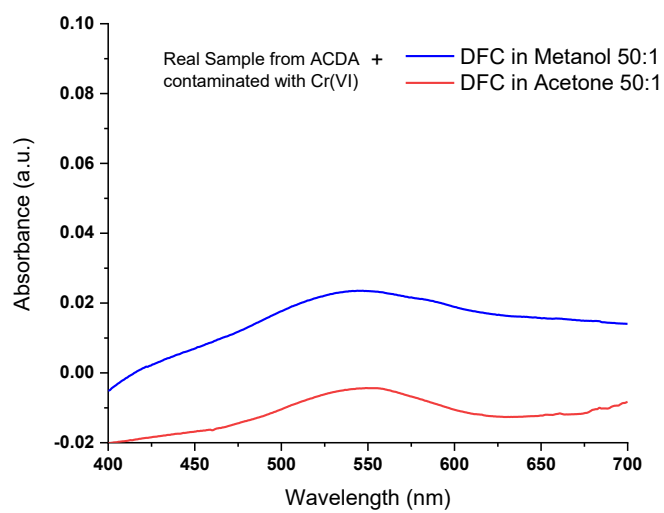


Figure 64: UV-Vis spectra for real sample solution contaminated with unknown level of chromium (VI).

Chapter 4

Electrochemical Detection

In the context of the electrochemical analyses carried out during this thesis work, a specific focus was placed on the **detection of arsenic** and preliminary studies were conducted on **monitoring of cadmium**.

Although the literature includes methods that employ spectrophotometric techniques for measuring arsenic concentrations, these approaches frequently pose challenges regarding their complexity and feasibility, particularly for *in-situ* sensors. Suitable spectrophotometric methods for this ions analysis typically necessitate extensive sample preparation and precise calibration, and they may be impacted by interfering substances present in the sample matrix. This complexity can render them less practical for routine analyses, especially in field settings or situations where quick results are required.

Given these challenges, the research efforts opted to explore the use of electrochemical techniques, specifically voltammetry, which have been shown to deliver highly accurate analytical results. Electrochemical methods are advantageous due to their sensitivity, precision, and the ability to detect arsenic at extremely low concentrations, reaching detection limits as low as parts per billion (ppb). This level of sensitivity is particularly crucial for environmental monitoring and regulatory compliance, as it enables the detection of arsenic concentrations that fall well below the established legal limits. For context, it is essential to note that the **legal limit for arsenic in drinking water is set at 10 ppb**, as outlined WHO in regulatory guidelines. This means that any effective analytical method must be capable of reliably measuring concentrations at or below this threshold.

Table 11: Concentration Limits for Heavy Metals in Drinking Water Set by the WHO.

Metal	WHO Guideline Value
Arsenic (As)	10 µg/L
Cadmium (Cd)	3 µg/L

The electrochemical techniques employed in this research work, in particular **chronopotentiometry and voltammetry**, demonstrate a clear advantage in this regard, as they provide the necessary accuracy and precision for meeting these stringent regulatory standards. Furthermore, electrochemical methods often require less elaborate sample preparation compared to spectrophotometric techniques, making them more suitable for on-site analysis or situations where time and resources are limited. The simplicity of these techniques not only enhances their practicality but also improves the overall efficiency of the analytical process.

In summary, the choice to focus on electrochemical techniques for arsenic analysis stems from the need for reliable, sensitive, and practical methods in environmental monitoring. By utilizing voltammetric approach, this research aims to provide accurate measurements of arsenic in drinking water, contributing to public health safety and environmental protection.

4.1 Different types of commercial sensors

The current state of commercial sensors also stresses the critical importance of calibration, optimization, and validation of any chosen method related to them. This is especially crucial when tailoring a method for a specific application, ensuring accurate and reliable results. A customized approach that prioritizes these steps will ultimately enhance the performance and effectiveness of sensor technology.

The calibrations and analyses were performed directly on the selected sensors that will be integrated into the customized system to maximize accuracy and minimize potential issues arising from sensor variation or environmental factors. For each graph presented for system validation, the data reported are the average of three replicates on the same sample under the same conditions. The analyses conducted on these sensors serve a threefold purpose:

Validation of the proposed method: By utilizing commercially available sensors, the efficacy and accuracy of the proposed methodology can be rigorously tested and confirmed against established benchmarks.

Optimization: Through experimentation with commercial sensors, opportunities for refinement and enhancement of the method can be identified and implemented, leading to improved performance and efficiency.

Calibration and long-term system validation: The integration of commercial sensors allows for precise calibration of the overall system. Moreover, ongoing analysis with these sensors enables monitoring of system integrity and performance over time, ensuring its continued reliability and accuracy.

The use of commercial sensors in this context is particularly crucial as it bridges the gap between laboratory established instrumentations and practical implementations. It provides a tangible well-known platform to evaluate, fine-tune, and validate the proposed method, ultimately paving the way for its successful integration into a customized system.

Flow-through cell electrode (Istran)

The analysis leverages automated flow-through coulometry and voltammetry within a robust electrochemical hydrodynamic cell. This cell integrates maintenance-free, built-in reference and auxiliary electrodes alongside a disposable working electrode for prolonged operational lifespan. As illustrated in Figure 65, the **working electrode (WE)** is available in porous or rod configurations, typically exceeding 1000 measurements before replacement; however, improper handling or installation may reduce its longevity. The electrode is secured at the input tube with a silicone O-ring and plastic screw, ensuring electrical contact via an internal cell connector. The **Ag/AgCl reference electrode (RE)** is housed in a membrane-separated compartment, filled to two-thirds capacity with saturated KCl electrolyte. Regular inspection and replenishment of this solution is vital, as is ensuring the absence of bubbles in the compartment's lower section for optimal measurement quality. The **Pt wire auxiliary electrode** is fixed within the cell body and requires no upkeep.

The flow system operates under full microprocessor control, utilizing peristaltic pumping for sample transport. Response times vary from 1 to 10 minutes, with a resolution of 0.01 ($\mu\text{g/l}$, mg/l , g/l) and a precision of 5% full scale for calibration or validation solutions.

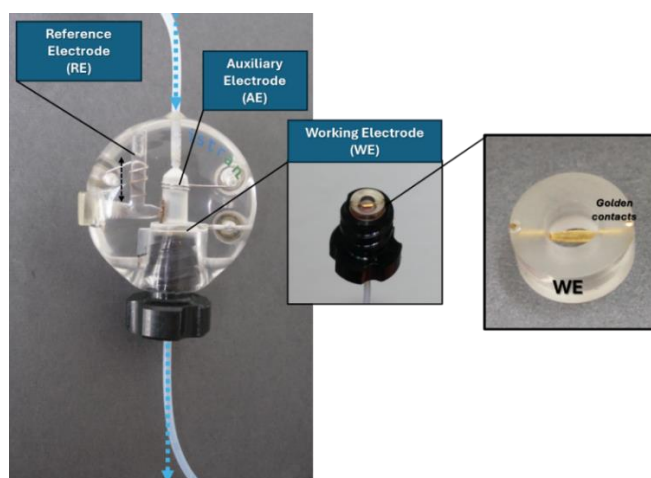


Figure 65: Configuration of Istran electrode flow-through cell.

ScTrace Gold (Metrohm)

The scTRACE Gold provides a user-friendly and high-performance solution for voltammetric trace metal analysis, specifically arsenic, across a variety of sample types. Its design combines three electrodes – a **gold micro-wire working electrode**, **Ag/AgCl reference electrode**, and **carbon auxiliary electrode** – into a single, compact unit. This eliminates the need for separate electrodes, streamlines operation, and is particularly advantageous for in-field analysis due to its virtually maintenance-free nature and lack of preconditioning requirements, allowing for immediate measurements upon setup. Furthermore, the sensor boasts

a detection limit significantly lower than the 10 µg/L regulatory threshold for different heavy metals in drinking water and enables rapid analysis with a maximum measurement time of 10 minutes per sample. A new sensor only needs to be activated and then it is possible to perform a great number of analysis (>500 repetition) with respect to the quality of the data which indicated the deterioration of the sensor itself.



Figure 66: Configuration of ScTrace Gold (Metrohm).

The **deposition time** of the analyte on the working electrode is correlated to the limit of quantification. Proportionally, the longer the deposition time, the higher the detectable limit. For this electrode, it is possible to estimate from the literature the limit of detection (LoD) and the linear working range (LWR) as follow:

Table 12: Correlation between deposition time and limit of detection and linear working range.

Deposition	LOD	LWR
30 s	0.5 µg/L	30 µg/L
60 s	0.3 µg/L	21 µg/L
90 s	0.2 µg/L	11 µg/L

In this scenario, it is mandatory to prioritize the LOD because the primary goal is to determine the presence or absence of the analyte. While the LWR is crucial for precise concentration measurements, it necessitates certified instrumentation, which may not be readily a prototype. Furthermore, the LOD, being at the lower end of the concentration range, is more suitable for detecting trace amounts of the analyte, whereas the LWR covers a broader range of concentrations and typically begins above the LOD to guarantee that quantifiable signals fall within the linear response region of the instrument.

Potential interference, typically in tap water, usually arises **from inorganic anions**, especially I⁻ and Cl⁻, which can affect the reference potential. Therefore, to maintain sensitivity when analyzing samples with higher chloride concentrations, it's necessary to adjust both the cleaning and deposition potentials. Likewise, **interference from various metal cations** is possible, but copper is the

most problematic contaminant in the sample. Excessive copper levels can result in falsely low arsenic readings or even completely obscure the arsenic peak.

Screen-Printed Electrode (Metrohm)

Screen-printed electrodes (SPEs) are fabricated by printing conductive inks (like carbon, gold, or platinum) onto a substrate (like ceramic or plastic), forming a compact design with a working, reference, and counter electrode. Commonly, ASV is utilized, where heavy metal ions are first deposited onto the working electrode by applying a negative potential. Subsequently, a positive potential scan strips the metals, generating a current signal proportional to the heavy metal concentration in the water sample. For optimal results, carbon-based working electrodes are often modified with a salt. Historically, mercury-based salts were used, but due to safety concerns, bismuth salts are now preferred. This electrode is constructed on a 3.38 cm x 1.02 cm x 0.05 cm ceramic substrate, using carbon for the auxiliary electrode, silver for both the reference electrode and contacts. SPEs can only be used for a limited number of measurements and must be replaced at regular intervals. The electrode can have two configurations depending on its use in immersion (Figure 67b):

Immersion Configuration: The WE (working electrode) is located at the top of the system body.

Drop Configuration: The WE is located at the centre, and it's preferable to use a drop (180 microliters) of solution to better protect the electrical contacts.

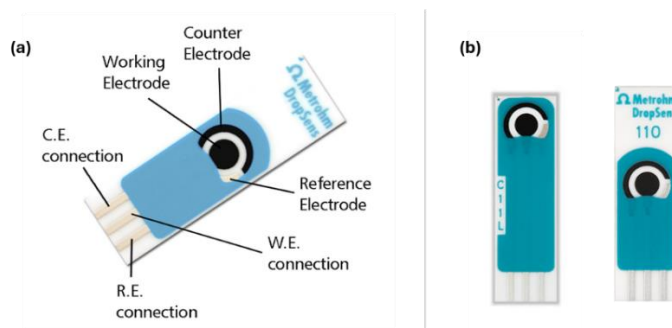


Figure 67: Configuration of SPE (a) with the position of WE, RE and CE (b) for the immersion and drop configuration.

4.2 Arsenic Detection

This thesis works investigated arsenic monitoring using two electrochemical techniques: chronoamperometry and voltammetry. Chronoamperometry involves applying a constant current and measuring the resulting potential over time. This technique is particularly useful for studying kinetics and concentration of the analyte, as the measured potential is directly related to the amount of arsenic deposited on the electrode over time. Voltammetry, on the other hand, varies the applied potential and measures the resulting current. The resulting voltammogram provides information about the identity and quantity of electroactive species

present in the sample, as well as insights into the underlying electrochemical processes.

4.2.1 Chronoamperometry

A gold sensor is used to measure arsenic in a sample. The sample is mixed with a diluted acid solution and introduced into a measuring cell. Arsenic ions in the sample are reduced onto the gold electrode. The amount of arsenic deposited is then measured by stripping it off the electrode. The time it takes to strip the arsenic is directly related to the amount present in the original sample. Calibration solutions containing varying concentrations of arsenic (0-50 ppb) were made by diluting a standard 1 ppm of arsenic solution (Sigma Aldrich).

The chemical method used was as follows:

- 40 mL volume of the as prepared samples
- 10 mL of the reagent solution: a 3% vol. HCl
- one drops (~ 0.05 mL) of potassium permanganate (KMnO_4) 0.01M solution in water

Potassium permanganate, a powerful oxidizing agent due to its ability to accept electrons and the stability of its reduced forms, is crucial for the complete oxidation of trivalent arsenic to pentavalent arsenic, allowing for the detection of all arsenic species in the sample solution. From the as prepared sample solution A minimum volume of 5 ml was pumped into the measuring cell for each analysis. Multiple measurements on the same sample can be averaged to improve the accuracy of the result.

Preliminary laboratory experiments were carried out to assess the commercial sensor capabilities, including its calibration, response to process conditions (HCl and KMnO_4), measurement consistency, precision, and detection limits.

Calibration and optimization

Linearity was assessed by analysing samples with known arsenic concentrations, generating a calibration curve. Sensor stability was evaluated through repeated measurements of each sample, followed by calculation of statistical metrics such as mean, absolute and relative errors, and standard deviation. Upon completion of calibration measurements, the system utilizes an internal parameter for assessment: the **calibration coefficient (TAU)**, which is the median of the last three recorded calibration coefficients. This value should be recorded at least every month and should be between 0.40 and 0.20 to ensure a good analysis. Typically, the initial recorded value for this two-month analysis period was excluded due to its anomalous nature, likely stemming from an internal calibration error.

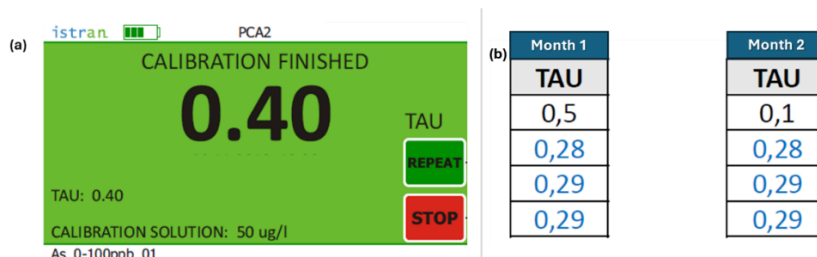


Figure 68: Evaluation of TAU values necessary before the calibration.

Then the calibration tests were performed both with and without permanganate and repeated across various samples containing arsenic concentrations from 0 to 40 ppb.

The Figure 70 demonstrates the successful electrochemical detection of arsenic using the combination of this technique/sensor. A series of voltammograms illustrating the current response (ΔI) of the sensor to varying nominal concentrations of arsenic (0, 10, 20, 25, 40 ppb). The regions bounded by the dashed line represent the charging and discharging processes at the working electrode. As the arsenic concentration increases, a well-defined and symmetrical peak correspond to the oxidation of deposited arsenic, emerges at a potential of 200 millivolts. Calibration curves were generated using both peak height and peak area detection (Figure 69 (b) and (c)). The obtained R-squared values demonstrate excellent linearity, confirming the validity of the commercial instrument calibration, within the defined concentration range, with R^2 values greater than 0.99. Furthermore, to ensure the accuracy of the instrument readings, an additional calibration curve was generated. This involved comparing the nominal values of the analyte solutions with the values returned by the sensor after three repeated measurements for each solution. The calibration curve reveals excellent linearity when a single drop of permanganate is utilized, with a slight deviation observed when two drops are employed. This suggests that the proposed methodology, utilizing one drop, yields optimal linearity and is therefore the preferred approach.

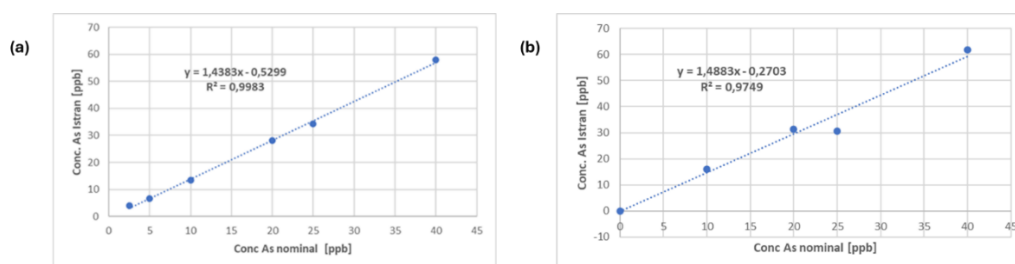


Figure 69: Calibration curve for confirming Arsenic concentration between values of nominal concentration and Istran electrode response (a) with one drop and (b) two drops of KMnO_4 .

Tests on field “Real sample analysis”

A real sample contaminated with arsenic from a natural spill was provided by ACDA (light blue line in Figure 70). The current response of the real sample most closely matched the 10ppb arsenic standard. Interpolating the

real sample data onto the calibration curves confirmed an arsenic **concentration of 10 ppb** in the unknown sample.

A final validation was conducted on a real water sample collected from an arsenic-contaminated site in Cuneo, Italy. This sample had previously been analyzed using inductively coupled plasma mass spectrometry (ICP-MS), yielding an arsenic concentration of 9ppb. Subsequent analysis using chronopotentiometry, averaged over 5 measurements, resulted in an arsenic concentration of 9.22 ppb, demonstrating excellent agreement with the ICP-MS data.

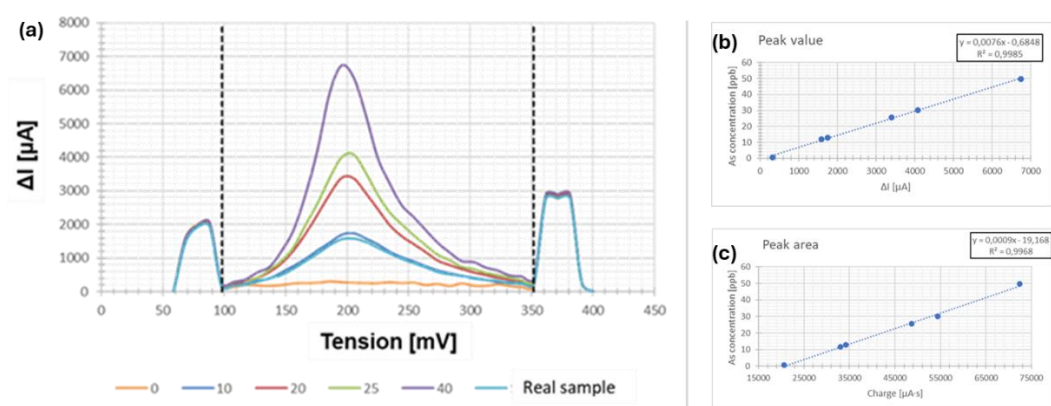


Figure 70: (a) Chronopotentiometry curves for samples with increasing As concentration from 0 to 40 ppb and Real sample solution. (b) and (c) Chronopotentiometry calibration curves for samples within the same range.

4.2.2 Voltammetry - SWV

Prior to analysis, the electrode was activated by pipetting 18 mL of the cleaning solution into the measuring vessel. The cleaning solution, which will also be used to clean the electrode in case of deposits on the gold wire, is composed as follows:

- 2.78 mL of H_2SO_4 0.5M
- 0.37g KCl in 80mL H_2O (0.05M)

The measurement technique for activation was LSV - Linear Sweep Voltammetry, with a stirring rate of the solution set at 2000 min^{-1} . For electrode cleaning, the same solution was used with a volume of 12 mL and a cyclic voltammetric stripping (CVS) technique was employed.

The determination of trivalent arsenic utilizes square wave voltammetry as the measurement mode, with a stirring rate of $2000 \text{ minutes}^{-1}$. Inside the measuring chamber were placed:

- 10 mL of the sample containing the analyte
- 2 mL of the electrolyte solution

The electrolyte solution was composed as follows:

- 9.70g of sulfamic acid

- 10.50g of citric acid
- 3.35g of KCl
- 80mL H₂O

The deposition potential (E_{dep}) is -0.5 V with a waiting time of 60 seconds and an equilibration time of 5 seconds. The deposition potential value is related to the fact that for more negative values than -0.6 volts, pentavalent arsenic is also partially reduced and deposited, potentially interfering with the analysis and being quantified in its trivalent form.

Calibration

Figure 71 presents the calibration process of the arsenic on SCTrace Gold sensor. The reported graph displays multiple voltammograms obtained during the analysis of a different nominal concentration of As(III) as indicated by the legend (0 ppb, 5 ppb, 10 ppb, 15 ppb, and 20 ppb). The peaks in the voltammograms correspond to the electrochemical reduction of As(III) at the sensor working electrode. As the As(III) concentration increases, the peak current also increases, demonstrating a relationship between concentration and the measured signal. To confirm the linearity of the system a linear regression line has been fitted to the data points and the high R^2 value indicates a strong linear correlation between the peak current and As(III) concentration. Overall, the sensor exhibits good sensitivity as it can detect low levels of As(III) (down to 5 ppb).

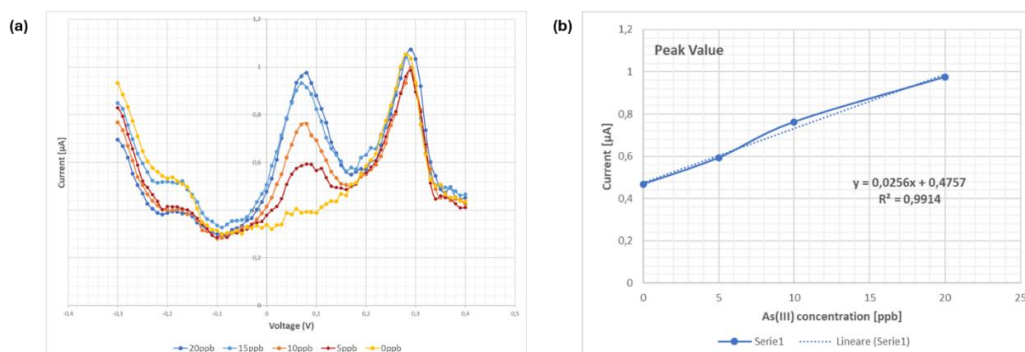


Figure 71: (a) Voltammograms curves for samples with increasing As(III) concentration from 0 to 20 ppb. (b) Calibration curves calculated with the maximum peak value in the considered range.

Aging tests

Electrolyte solution

Figure 72 illustrates the impact of aging on the electrolyte solution. Ten days after preparation, the solution was tested and compared to a freshly prepared one, both containing a 20ppb analyte concentration. Figure 72a visually demonstrates this comparison, with the yellow curve representing the fresh solution and the purple curve representing the aged solution. While the peak position remains consistent, a slightly increase of 0.19 μ A was observed in the maximum peak

current of the electrolyte solution. This phenomenon could be attributed to changes in the solution itself, given its acidic composition. Over time, some acids can slowly decompose, particularly when exposed to light or heat. This decomposition may generate new species in the solution that are more readily oxidized or reduced at the electrode, resulting in an increased current. Alternatively, the observed effect could stem from modifications to the electrode surface. Depending on the electrode material, a thin oxide layer might gradually form, especially in an acidic environment. Such an oxide layer could alter the electrode's electrochemical properties and promote certain redox reactions, also leading to a higher peak current. A calibration curve with 20, 10, and 5 ppb arsenic solutions of nominal concentration and a 10-day aged electrolyte solution results in a perfectly linear calibration curve. Therefore, it can be concluded that the electrolyte solution does not show any relevant degradation that would impact its effectiveness in the electrochemical detection of arsenic.

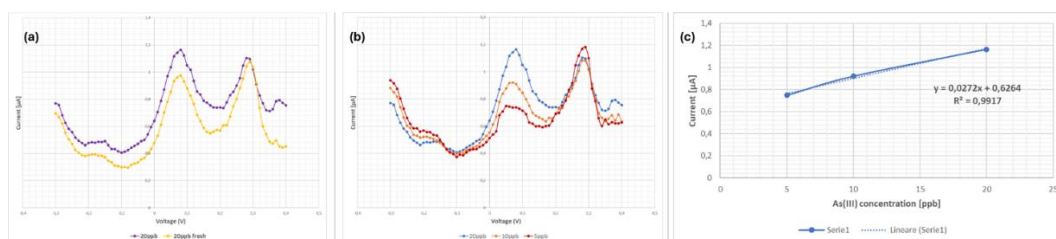


Figure 72: (a) Comparison of voltammograms for 20ppb solution of arsenic containing freshly and aged solution of electrolyte solution. (b) Recorded voltammograms from 20, 10 and 5 ppb of arsenic. (c) Calibration curve calculated with peak value for the associated range.

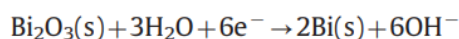
Solid Electrodes and Square Wave Voltammetry: Advantages in Electroanalysis

Solid electrodes offer numerous benefits compared to flow-through electrodes in various electrochemical applications. Their straightforward design and ease of production result in durable and budget-friendly experimental setups. In contrast to flow-through electrodes, concerns about potential clogging or fluctuations in flow rate are eliminated, simplifying data analysis and interpretation. Furthermore, solid electrodes enable meticulous control over both surface area and composition, leading to enhanced reproducibility and selectivity in electrochemical measurements. These qualities make solid electrodes especially desirable for foundational research, sensor advancements, and situations with limited sample volumes. When evaluating electrochemical techniques specifically for solid electrodes, square wave voltammetry (SWV) frequently emerges as the preferred method over chronopotentiometry. SWV excels in sensitivity and its capacity to differentiate between background currents and analyte signals, yielding distinct and readily understandable voltammograms. Its swift scan rates allow for faster analysis times compared to chronopotentiometry. Moreover, the exceptional peak resolution of SWV proves indispensable when working with intricate mixtures containing multiple analytes with overlapping redox potentials.

This unique combination of advantages positions SWV as a robust and adaptable technique for electrochemical investigations utilizing solid electrodes.

4.3 Cadmium Detection

Specifically for detecting Cd(II) ions, the SPE with Bismuth, designed for microvolume assays and environmentally friendly heavy metal detection, requires a pre-treatment step where bismuth oxide is electrochemically reduced to bismuth for optimal performance.



To achieve this reduction, a 0.1M KOH supporting electrolyte was used, applying a reduction potential of -1.2V for 600 seconds.



Figure 73: Metrohm SPEs before and after the activation.

Calibration

A drop of 180 μL was extracted from a solution containing 5 mL of analyte and 1 mL of 0.2 M acetate buffer (pH 4.5). This volume was then precisely dispensed onto the working electrode, following the removal of the previous activation droplet using a controlled N_2 stream.



Figure 74: Displacement during the analysis of the analyte and electrolyte solution droplet on the working electrode.

The analysis employed Differential Pulse Voltammetry (DPV) with the following parameters:

- Deposition potential (E_{dep}): -1.2 V
- Deposition time: 420 seconds
- Pulse amplitude (E_{pulse}): 0.1 V
- Pulse width (t_{pulse}): 0.005 seconds
- Potential step (E_{step}): 0.002 V
- Scan rate: 0.05 V/s

The peak position (around -0.6 V) is characteristic of Cadmium (II) reduction. The plot shows the relationship between the peak area (integral of Cd) and the concentration of Cd(II) in $\mu\text{g/L}$ (ppb). The decision was made to use the peak area value because the voltammogram exhibits a very broad shape, and therefore it is better to utilize the entire area under the peak. A linear trendline with a good R^2 value (0.996) suggests a strong correlation, confirming the seeks accuracy for quantification within the tested range.

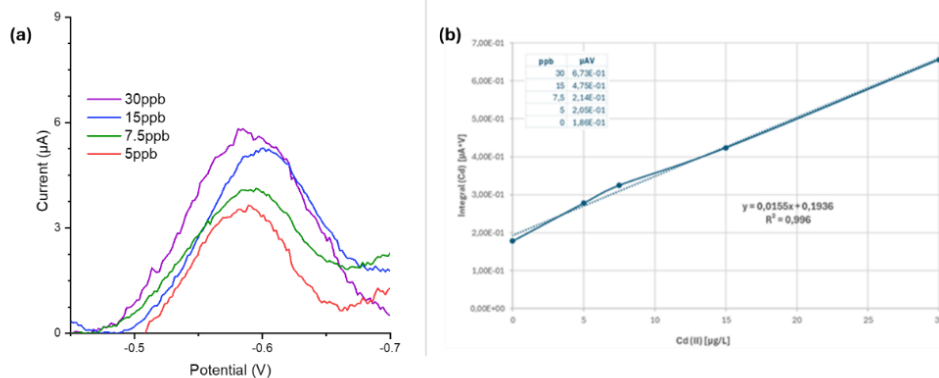


Figure 75: (a) Square wave voltammogram of 5 to 30ppb of Cadmium nominal concentrations with (b) associated calibration curve.

Chapter 5

Developed Sensor Platforms

Water quality monitoring often relies on collecting samples and transporting them to laboratories for analysis, a process that can be time-consuming, expensive, and lacking in real-time insights. This delay can hinder swift responses to contamination events, posing potential risks to human health and the environment.

To address this, there is a growing demand for portable, autonomous water monitoring systems capable of providing continuous, on-site analysis. Developing such sophisticated systems necessitates a **multidisciplinary approach**, drawing upon expertise from various fields: chemistry, mechanical and electronic. Chemistry plays a crucial role in this endeavour since it is responsible for identifying the most suitable sensing technologies for detecting specific pollutants or water quality parameters. Then mechanical approach is accountable for design the physical housing, fluidic system, and sampling mechanisms. This ensures the prototype is robust, reliable, and can withstand the environmental conditions where it will be deployed. They also focus on ease of use and maintenance. Finally electronic components are responsible for signal processing and acquisition, power management system, including energy harvesting (e.g., solar panels) and storage (e.g., batteries) to enable autonomous operation in remote locations, data communication, through IoT and system Integration in order to ensure all electronic components work together seamlessly and reliably, enabling accurate and efficient data acquisition and analysis.

By integrating these diverse disciplines, the project aims to create a practical and adaptable water monitoring solution that meets the demands of real-world applications. This collaborative approach enables the development of a prototype that is not only portable and autonomous but also accurate, reliable, and capable of providing timely insights into water quality, ultimately contributing to better water resource management and protection.

This is a complex and lengthy process in which each aspect is studied individually and then integrated into a unified system. Each step in the process

addresses a specific system requirement, as illustrated in Figure 76. Emphasizing the complexity and iterative nature of the development process highlights the importance of careful planning, rigorous testing, and a systematic approach to creating a successful water monitoring system.



Figure 76: Key parameters in sensing monitoring system developing.

1.1 Definition and parameters of monitoring system

1.1.1 Parameters to monitor

This project focuses on developing a portable, self-contained system for continuous, real-time water quality monitoring. The best way to define system key parameters is categorized into two groups: physico-chemical properties (like pH, conductivity, and temperature) and concentrations of dissolved pollutants (such as heavy metals or other chemicals).

Defining these parameters is fundamental because they provide a comprehensive picture of water quality. Physico-chemical properties influence the overall water chemistry and can affect the behavior of dissolved pollutants.

Meanwhile, monitoring dissolved pollutants helps identify specific contaminants that pose risks to human health and the environment. By analysing both categories, the system offers a more thorough and accurate assessment of water quality, enabling timely interventions and ensuring water safety. Once the pollutants and parameters for monitoring were established, it was crucial to conduct a comprehensive review of existing knowledge. This involves examining relevant scientific literature and consulting local and international regulatory frameworks to define safe concentration thresholds (Table 14 and Table 15). This comparative analysis ensures that the monitoring system aligns with established safety standards and best practices, enabling effective environmental protection and public health safeguards.

Table 13: Definition and classification of parameters to monitor.

Parameters	
Physico-chemical	Heavy Metals
Temperature	Chromium (VI)
Conductivity	
pH	Chromium (III)
Hardness	
Turbidity	Arsenic
Chloride	

Table 14: Heavy Metal Monitoring Parameters and Regulatory Limits, Historical Data, and Monitoring Requirements.

HMs parameter	U.M.	Statutory Limits (d.Lgs. 31/2001)	Required Minimum Measuring Range	Historical range of installation point	Range ACDA
Arsenic	µg/l	10	0 - 50	7 – 15	0 - 20
Chromium (VI)	µg/l	10	0 - 50	12 – 15	0 - 15

Table 15: Drinking Water Quality Standards parameters and Monitoring Targets.

Parameters	U.M.	Statutory Limits (d.Lgs. 31/2001)	Limit of Detection
Temperature	°C	/	/
Conductibility	µS/cm	2500	2000
pH		6.5 - 9.5	6 - 9
Hardness	mg/l	150 - 500	100 - 450
Turbidity	NTU	<i>Acceptable to consumers and without anomalous variations.</i>	/
Chloride	mg/l	250	200

1.1.2 System specifications

This system is designed for autonomous operation, featuring a built-in energy harvesting and storage module. This allows for flexible installation near the drinking water source, eliminating the need for external power sources. The system specifications detail the technical requirements, features, and capabilities, ensuring it can effectively monitor water quality independently.

The Figure 77 depicts a simplified block diagram outlining the key components of a system, likely designed for environmental monitoring or industrial process control. The spatial arrangement of the blocks suggests a hierarchical relationship, with the control electronics module overseeing the other components. The diagram communicates the system fundamental architecture and highlights its key functionalities.

It shows a modular design with five primary functional blocks:

- **Control Electronics:** This module, highlighted in green, likely houses the main processing unit, which governs the overall operation of the system, data acquisition, and communication with other modules.
- **Energy Harvesting and Storage:** This red block indicates the system's capacity for self-powered operation. It suggests the presence of components like solar panels, batteries, or supercapacitors to harvest and store energy, enabling deployment in locations without readily available power sources.
- **Fluidic System (Sampling/Process):** This blue block represents the components responsible for handling the fluid sample. This could include pumps, valves, filters, and any necessary pre-treatment steps to prepare the sample for analysis.
- **Measurement System:** This orange block denotes the core analytical component of the system. It likely comprises sensors and transducers that measure the target analyte's concentration or other relevant parameters within the fluid sample.
- **Data Communication System:** This purple block signifies the module responsible for transmitting the acquired data. It could involve wired or wireless communication protocols to relay the measurement results to a central monitoring station or user interface.

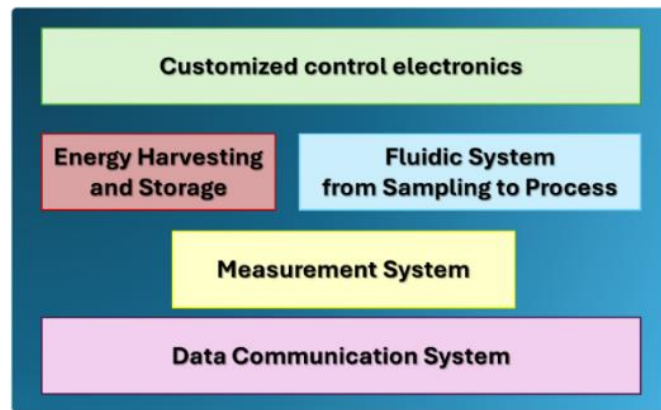


Figure 77: Block diagram of the monitoring system.

1.2 Development of sensing platform

This phase refers to the process of creating and implementing systems that track, analyze, and report on specific parameters.

1.2.1 Mechanical design

The development of these continuous water monitoring devices followed a systematic, multi-stage process. Initially, the focus was on meticulously **designing the fluidic system**, which is responsible for the precise handling and movement of water samples within the device. This involved careful consideration of factors such as:

- **Sample Acquisition:** How the water sample is drawn into the device, ensuring it is representative of the source and free from contaminants or bubbles that could affect the readings.
- **Flow Control:** Precisely regulate the flow rate of the water sample through the device to optimize sensor contact time and measurement accuracy.
- **Fluidic Channels:** Designing the network of channels and chambers within the device to ensure efficient sample delivery to the sensors and minimize dead volumes or areas where the sample could stagnate.
- **Waste Management:** Planning for the appropriate disposal or removal of the water sample after analysis, preventing contamination or buildup within the device.

Drinking water hydraulic system

The hydraulic system for water monitoring is presented in Figure 78, which illustrates the division into specific areas for monitoring the desired parameters. The system incorporates an inlet directly from the ACDA water reservoir, leading to the physico-chemical analysis section, where a commercial multi-parameter probe is employed to detect these values. Following the physico-chemical analysis, there is a sample splitting section where the water sample is divided into

two aliquots. One aliquot is directed to the hexavalent chromium analysis module, while the other is routed to the arsenic analysis module. This splitting process is necessary due to the specific reagents required for the chosen metal analysis technique. These reagents would interfere with the overall flow analysis if they were introduced into the main sample stream. Therefore, separating the sample allows for independent analysis of chromium and arsenic without cross-contamination or interference. The grey arrows in the diagram indicate the ability to refill the reagent tanks externally. For each of the two analyses (chromium and arsenic), a dedicated waste outlet is provided to manage waste separately from the continuous flow of supplied water. The chromium analysis section involves a closed circuit where the reagents, dispensed by micro-dosers, are mixed with the sample, followed by spectrophotometric analysis. The arsenic analysis section also involves a closed circuit in which the reagents, again dispensed by micro-dosers, are mixed with the sample. The measurement will be carried out using the voltammetric stripping method.

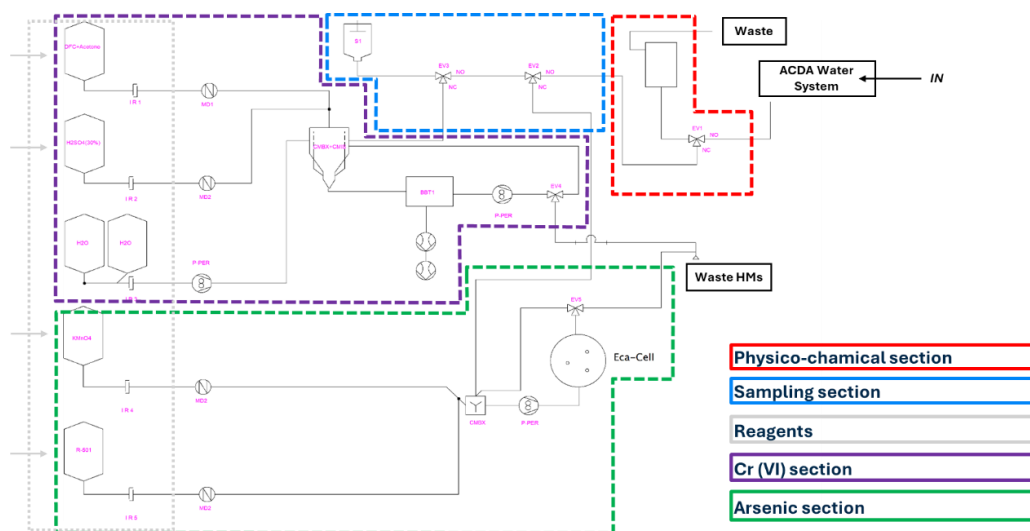


Figure 78: Fluidic diagram of the drinking water monitoring system divided by functional areas.

Industrial galvanic water hydraulic system

The fluidic system designed for the spectrophotometric analysis of Cr(III) is presented in Figure 79. The electrolytic water sample enters the system through the "IN Cr(III) sample" port (green circle). This likely connects to the main water stream from a sampling reservoir. The sample first flows into a "Tank Sample/Volume 25 ml". This tank serves as a temporary holding reservoir, potentially allowing for some initial conditioning or pre-treatment of the sample before analysis. The "EV1" component, likely an electro valve (EV), controls the flow of the sample from the tank to the next stage. This allows for precise and automated control of the sample volume entering the analysis module. If the measure is necessary, the EV1 is open, otherwise it is close, and the monitoring system is by passed. The sample then passes through "M.D.1", which appears to

be a micro-dosing dispenser. This unit ensures that a precise and consistent aliquot of the sample is dispensed for the Cr(III) analysis. The dispensed sample is then mixed with reagents from the "Tank Litres pure water/Volume 60 ml". This mixing step is crucial for preparing the sample for spectrophotometric analysis. However, since the sample is already intensely colored, no chemical reagents are required, only ultrapure water. This simplifies the process significantly and enhances the sensor longevity and autonomy. The mixture flows into the "Measure Chamber," the core of the analysis module. This chamber likely houses the optical components of the spectrophotometer, including a diode as source at the selected wavelength, which is directly related to the concentration of Cr(III) in the sample. After the measurement, the analyzed sample passes through another electro valve, "EV2," which controls the flow towards the waste outlet, represented by a black circle, serves as the exit point for the sample used. Since the sample is diluted with water, even if in small proportions, it is managed separately, ensuring proper disposal and preventing contamination of the system.

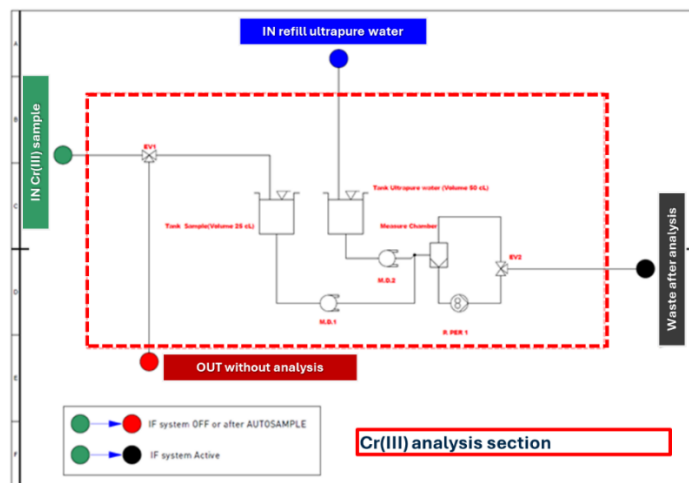


Figure 79: Fluidic diagram of the industrial water monitoring system.

Once the theoretical fluidic design was finalized, the project moved towards the **practical implementation phase**. This involved translating the design into a physical system by:

- **Component Selection:** Choosing appropriate pumps, valves, tubing, and connectors that meet the specific flow rate and pressure requirements of the system.

Table 16: Selected components for building water analysis system.

Fluidics Components	Analysis [Cr] and [As]
Electro-valves	Micro-dispensers
Micro-dispenser for reagents	
Peristaltic pump	Peristaltic pump
Analyte analysis system	Interconnections
Interconnections	

- **Fluidic Fabrication:** Potentially utilizing microfabrication techniques to create miniaturized fluidic channels and chambers, enhancing efficiency and reducing sample volume requirements.
- **Assembly and Testing:** Assembling the fluidic components into a functional system and rigorously testing their performance to ensure it meets the design specifications and operates reliably.

Wiring and Calibration of micro-dispensers and pumps

Compared to previous systems developed by the research group, the chromium and arsenic analysis sections utilize micro-dosers instead of syringe pumps. This component allows for the just right dosing of reagent quantities on the order of hundreds of microliters through a membrane adjustable by a screw. While syringe pumps are capable of dosing tens of nanoliters, they have a larger footprint, and a significantly higher cost compared to micro-dosers. The commercially available **micro-dosing pumps** were selected from a range of options based on their datasheet specifications, which indicated a suitable volume range for the sensor platform. To verify the accuracy of the dispensed volumes for each reagent and analyte, ten trials were conducted for each micro-dosing pump and its corresponding solution. The measurements were performed as follows: the solution was weighed in grams, and then multiplied by its density to obtain the volume in milliliters. The calibration results for deionized water, potassium permanganate, the DFC in acetone solution, electrolyte solution, sulfuric acid 30:1, the arsenic sample solution, and the chromium sample solution are presented below. As presented in Figure 80 the micro-dosers generally demonstrate good precision, with most standard deviations below 1%. Some solutions, like chromium and arsenic, exhibit higher variability in dispensed volume compared to others. This behavior could be attributed to variations in fluid properties such as viscosity, surface tension, and density, which may be influenced by the presence and concentration of the analyte.

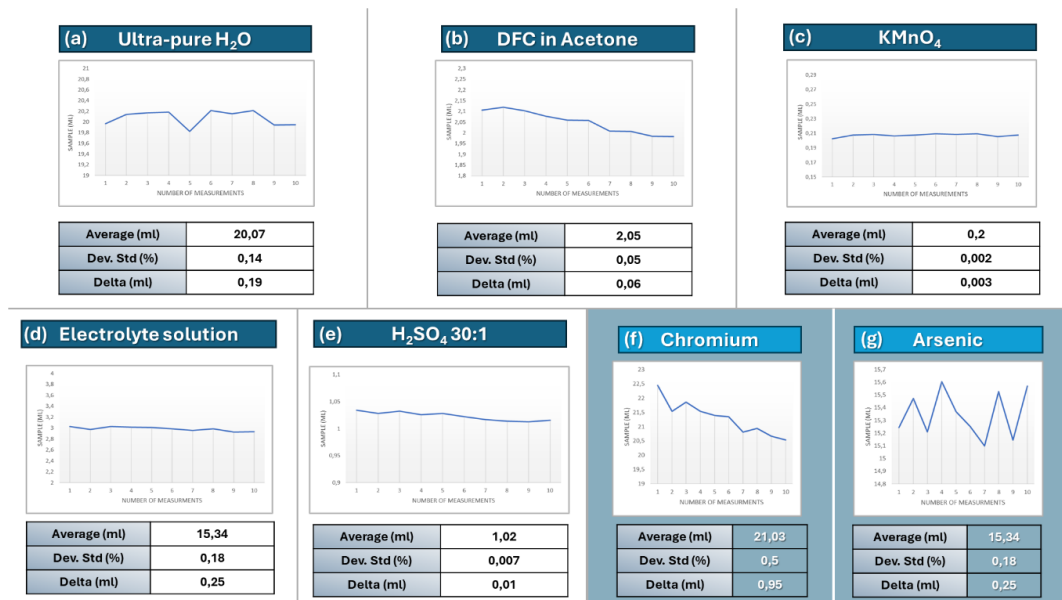


Figure 80: (a-g) Series of graphs and tables to illustrate the performance and calibration of micro-dosing pumps used for dispensing various solutions for HMs detection in a sensor platform.

The **peristaltic pumps** were also calibrated and adjusted to ensure the precise flow and delivery of the contaminated water sample within the system. The Table 17 illustrated and determined the accuracy and precision of the pump in delivering specific volumes of liquid. This is crucial in applications like chemical analysis, where precise volumes are needed for reliable results. For the pump accuracy the " Δ normalized" row shows that it varies across different target volumes. Some volumes are dispensed with higher accuracy (e.g., 0.58% error for 0.833 ml) than others (e.g., 1.60% error for 2.5 ml). The standard deviation values are relatively small, suggesting that the pump delivers consistent volumes within each test run and the dispensed volume generally increases with sampling time, as expected. However, there might be slight variations due to factors like tubing elasticity or pump pulsation.

Table 17: Calibration of peristaltic pumps for different volumes of water.

Sampling → Desired [ml]	0,417	0,833	1,250	1,667	2,500	3,333	4,167
	Sampling time[s]						
Test number ↓	1	2	3	4	6	8	10
1	0,462	0,865	1,272	1,663	2,582	3,347	4,164
2	0,446	0,861	1,270	1,689	2,507	3,354	4,110
3	0,447	0,857	1,279	1,657	2,510	3,367	4,188
4	0,452	0,859	1,270	1,694	2,523	3,352	4,186
5	0,443	0,856	1,262	1,649	2,501	3,370	4,145
6	0,440	0,865	1,284	1,688	2,533	3,347	4,175
7	0,442	0,858	1,267	1,696	2,511	3,345	4,166
8	0,452	0,856	1,266	1,666	2,510	3,338	4,175
9	0,443	0,855	1,280	1,678	2,508	3,316	4,196
10	0,444	0,864	1,268	1,683	2,515	3,358	4,165
Media [ml]	0,448	0,863	1,276	1,681	2,528	3,359	4,180
Dev.st	0,007	0,004	0,007	0,016	0,024	0,015	0,025
Δ	0,011	0,005	0,011	0,024	0,041	0,027	0,043
Δ _{normalized}	2,45%	0,58%	0,86%	1,40%	1,60%	0,80%	1,04%
Pump features [ml/min]	25						

Mechanics components material and chemical compatibility

When designing a mechanical system intended for handling chemical reagents, material compatibility is paramount. It is essential to select materials that can withstand the potentially corrosive effects of the chemicals involved, ensuring the system longevity and preventing any adverse reactions that could compromise its functionality or the integrity of the experiment.

In this specific system, aluminum was chosen for the construction of the heavy metal detection chambers due to its inherent robustness and its resistance to corrosion by the mild acid solutions used in the process. This choice ensures the chambers will maintain their structural integrity and performance over time.

Similarly, the selection of PTFE (polytetrafluoroethylene) tubing was critical due to its exceptional chemical resistance and thermal stability. PTFE is renowned for its ability to withstand a wide range of solvents and temperatures, making it ideal for transporting the chemical reagents within the system without the risk of degradation, leaching, or permeation. The fittings used between the tubing, mechanical parts, and reagents containers were chosen to be made of PTFE. To ensure the system ability to handle fluids with high purity and prevent contamination, meticulous attention was paid to the selection of pumps and micro-dosers. These components were rigorously tested and chosen specifically because they offer leak-free operation, guaranteeing precise and reliable fluid delivery over a prolonged period. A note factor in preventing contamination was the isolation of the fluid from any component other than tubing. The pumps and micro-dosers were selected within this perspective, ensuring that the fluid remains contained within the inert silicon tubing (dimensions: 1.4 x 2.8 mm; flow rate: 20

to 65 ml/min) throughout the process. This design choice effectively eliminates the risk of the fluid interacting with the pump mechanism or other materials, safeguarding it from any potential contamination and preserving its chemical composition. In fact, silicon generally exhibits good resistance to mild acid solutions. This resistance is due to the stable chemical structure of silicone, characterized by strong silicon-oxygen bonds (Si-O). These bonds are highly resistant to hydrolysis, meaning they don't readily break down in the presence of water or weak acids. Other important characteristics are that Silicone is typically non-polar and hydrophobic, ensuring the perfect flow of the sample, and it is generally inertness, doesn't react with other substance. The tanks containing the reagents were chosen to be made of HDPE (high-density polyethylene) since exhibits excellent resistance to a wide range of chemicals, including acids, bases, and solvents. In addition, HDPE is a strong and durable material that can withstand impacts and rough handling, ensuring the safe containment of the reagents, it is a relatively inexpensive material, making it a cost-effective choice for reagent storage tanks, also it is lightweight, which can be beneficial for handling and transportation of the system.

1.3 Filtering system

A **filtration system** was essential to this fluidic sensor platform for water monitoring. By removing potentially interfering particles, the filter protects sensitive components, improves measurement accuracy, and enhances overall system reliability, resulting in a more robust and effective monitoring solution. In this context, a filtration system has been designed to be installed upstream of the sensor platform. This **system can be considered an extra tool** available when measurement conditions are particularly unfavorable due to the presence of particulate matter in the solution.

Design and fabrication

This two-layer filtration system was designed to remove particles that could interfere with the water monitoring analysis for both practical applications. This filtration system effectively prevents agglomerates from reaching the detection zone, safeguarding against clogging and maintaining the integrity of the measurements.

As shown in CAD Figure 81, the top layer features an inlet hole leading to a channel and an outlet hole, while the bottom layer includes an inlet hole with a filter housing, a channel, and an outlet hole. The inlet on the top layer and the outlet on the bottom layer are sized to match the diameter of the tubing system. A key feature of this design is the **filter housing, integrated into the bottom layer inlet**. This small step securely holds the filter in place, ensuring efficient particle removal. To fabricate the device, a replica molding technique was employed using polydimethylsiloxane (PDMS). The molds themselves were produced via additive manufacturing, specifically utilizing a PolyJet 3D printer with VeroWhite™ resin.

For post-processing procedure the molds were washed with water from residual support material and overnight curing in an oven at 110°C. To ensure pristine mold surfaces, they were then subjected to a 5-minute ultrasonic bath in acetone. The PDMS prepolymer and curing agent were then combined at a 10:1 ratio, degassed to remove air bubbles, and poured into the prepared molds. Curing of the PDMS was carried out in an oven at 90°C for 1 hour. Finally, the cured PDMS devices were carefully separated from the molds using isopropanol. A custom-built stereolithography (SL) 3D printer (MicroLa Optoelectronics S.r.l.) fabricated the filter using Dental Clear resin (HARZ Labs). Figure 82 details the filter precise geometry and dimensions. The SL printer utilized a 405nm laser at 40mW power and 1500mm/s scanning speed. Post-printing, the filter underwent thorough cleaning to remove residual resin, including a 10-minute ultrasonic bath (40kHz) in resin developer (TEK 1969, KEYTECH solution) and a distilled water rinse. Finally, it was air-dried. Assembly of the device involved cleaning the PDMS replicas in an ethanol ultrasonic bath, followed by oxygen plasma treatment (1 minute gas supply, 0.7mbar pressure, 0.3 seconds exposure at 22% power). After careful positioning of the filter, the two layers were bonded together and thermally treated at 80°C for 5 minutes to enhance bond strength. The assembled device was integrated into the monitoring platform, establishing fluidic connections using PTFE tubing with varying diameters. The device was linked to the platform with 1/16" OD tubing and to the sample reservoir with 1/8" OD tubing. This choice of tubing size was deliberate, as the smaller diameter (1/16" OD) posed a potential risk of blockage due to the transport of particles within the system. This strategic selection of tubing diameters, considering the average size of floating particles (ranging from hundreds of μm upwards), effectively minimizes the risk of blockages and ensures the smooth and reliable operation of the monitoring platform. The filtration system demonstrated exceptional fluidic performance, largely attributed to the meticulous design of its inlets and outlets. These precisely engineered components ensure a secure and leak-free seal when connected to the tubing, provided they are properly aligned with the corresponding holes. This highlights the critical importance of precise system assembly in achieving optimal device operation.

The filter's design, including its geometry and material selection, was guided by both the simulated flow rate (10 ml/min) and the size of the target particles. The low flow rate allows for the use of compact filter geometries with smaller diameters, minimizing pressure drop across the filter. Additionally, the use of water as the filtration medium, without the presence of chemical reagents, broadens the range of suitable filter materials with varying pore sizes and geometries. This flexibility allows for customization based on the specific application and desired filtration efficiency for the target particle size.

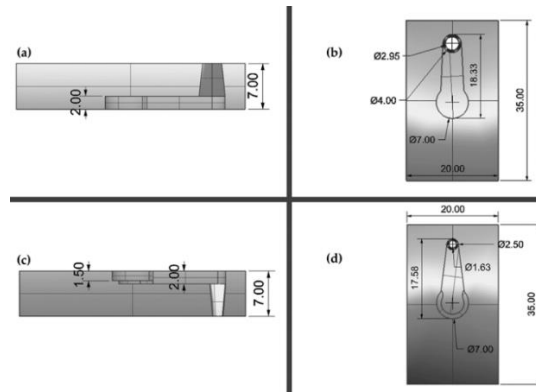


Figure 81: CAD model of the PDMS device, with related measures of its features: (a) and (b) represent the section view and the top view, respectively, of the top layer; (c) and (d) represent the section view and the top view, respectively, of the bottom layer. All the measures were in mm.

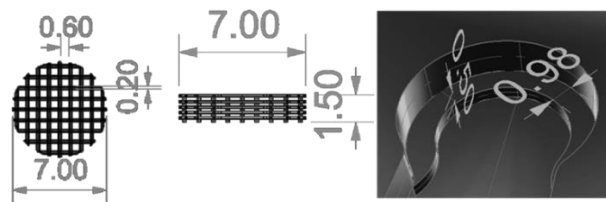


Figure 82: CAD model of the two filters and a zoom on the frame for filters positioning, with the related measures. All measures were in mm.

FEM Simulation

FEM simulations in COMSOL Multiphysics (6.1) were used to analyze pressure distribution in a 3D model of the measuring setup. Simulations, coupling Fluid Dynamics and Solid Mechanics modules, focused on the channel and filter boundary at flow rates between 1 and 20 mL/min.

negative pressure values at spurious outlet points, the average outlet pressure was positive. A maximum pressure of 28 Pa was observed at 20 mL/min. Figure 83 (1), (2) and (3) illustrate **streamlines and liquid velocity** across the filter at flow rates of 1, 10, and 20 mL/min. These visualizations confirm laminar flow and highlight how increased flow rates shift the primary filtration zone rightward from the filter center. Analysis showed that a 10 mL/min flow rate was optimal for the system, minimizing pressure fluctuations and enhancing overall design robustness. Higher flow rates risked damage to the inlet section due to increased pressure. While the detection cell could withstand higher pressures, the chosen flow rate ensured system integrity and validated the appropriate sizing of the inlet and outlet components. Figure 84 illustrates **filter system displacement**. The left plot shows deformation at 10 mL/min (20000x magnification), while the right plot shows maximum displacement versus flow rate. The analysis reveals that the area above the filter undergoes the greatest displacement, reaching approximately 8×10^{-8} m. The right plot shows the relationship between displacement and flow rate, with a maximum displacement of 2.8×10^{-7} m observed at 20 mL/min. Analysis of the PDMS filtration system showed minimal deformation localized above the filter, well within tolerance and not affecting filter position or seal. This validates the chosen filter material and design.

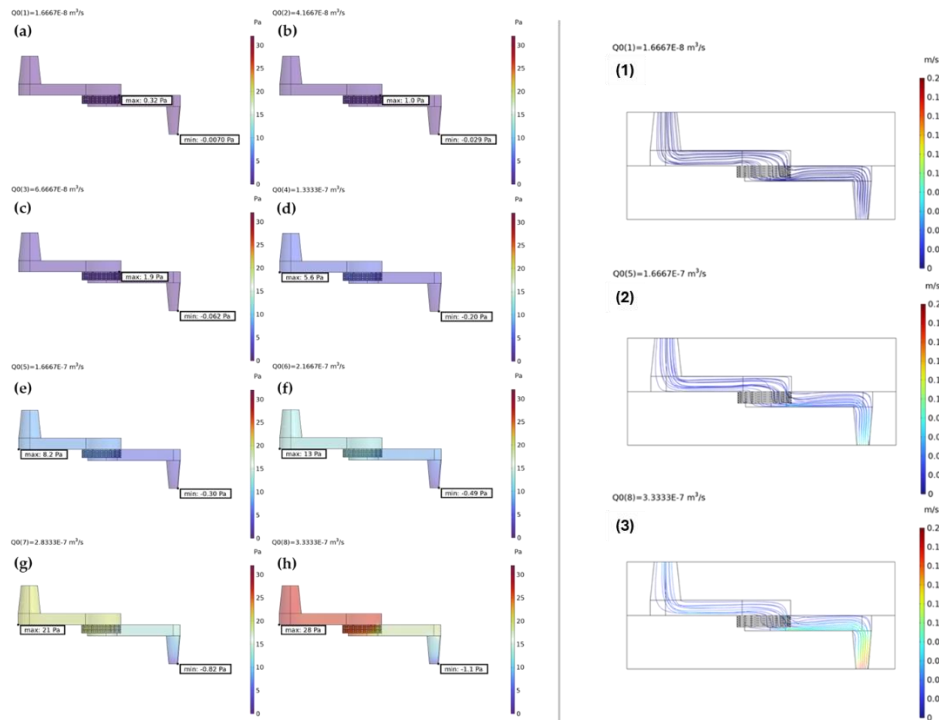


Figure 83: Right: Pressure on filtering system walls. Note that the SI units are used instead of mL/min, so the flow rates are (a) 1 mL/min, (b) 2.5 mL/min, (c) 4 mL/min, (d) 8 mL/min, (e) 10 mL/min, (f) 13 mL/min, (g) 17 mL/min, (h) 20 mL/min. Left: Streamline and fluid velocity plots for (1) 1 mL/min, (2) 10 mL/min and (3) 20 mL/min flow rates.

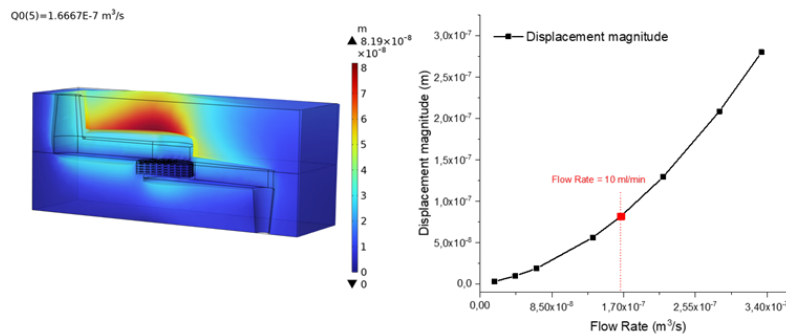


Figure 84: Left: displacement plot reported in SI unit for 10 mL/min with a visual magnification of 20000 for what concerns movement in geometrical domains and colour scale unchanged. Right: displacement as a function of flow rate.

Characterization

Characterization of the filtration system involved examination of the PDMS layers and filters using digital microscopy. The images reveal the precision achieved in fabricating the microfluidic channels and features within the PDMS layers. The inlet and outlet ports, as well as the internal channels, are clearly visible, demonstrating the accuracy of the replica molding process. The dimensional measurements provided alongside the images further confirm the precise control over the fabrication process. The microscope image of the filter shows its intricate mesh-like structure. The well-defined grid pattern with precise pore sizes is evident, highlighting the filter's ability to effectively capture particles and prevent them from entering the sensing areas.



Figure 85: Right: Microscope images of top and bottom layers, with related features measurements. Left: Microscope images of printed filter, with relative features measurements. All measures are in mm. The scale bar is 1mm.

1.4 Optical section

The optoelectronic design of a UV-Vis detection system involves careful selection and integration of key components to achieve optimal performance. The design of an innovative measuring chamber for the detection of chromium was developed in collaboration with Microla Optoelectronics. An aluminum UV-Vis monitoring sample cell was fabricated using a RAIS m450 three-axis vertical machining center.

Design and fabrication

While both the Cr(VI) and Cr(III) measuring chambers share a similar overall design, as depicted in Figure 86, there is a smaller distinction in their fluidic configurations. This difference stems from the specific requirements of the analytical procedures used to detect each oxidation state of chromium. The Cr(VI) chamber was designed to accommodate a more complex analysis. It incorporates five separate inlets to facilitate the introduction of various fluids:

- **Sample Inlet:** This inlet allows for the introduction of the sample containing Cr(VI) that needs to be analyzed.
- **Reagent Inlets (x2):** Two separate inlets are dedicated to introducing the specific reagents required for the Cr(VI) analysis.
- **Recirculation Inlet:** This inlet enables the recirculation of fluids within the chamber, potentially enhancing mixing or facilitating specific reactions.
- **Ultrapure Water Inlet:** This inlet provides a source of MilliQ water, essential for creating blank measurements or diluting the sample if needed.

In contrast, the Cr(III) chamber has a simplified design with only three inlets:

- **Sample Inlet:** This inlet, as in the Cr(VI) chamber, introduces the water sample to be analyzed for Cr(III) content.
- **Ultrapure Water Inlet:** This inlet provides ultrapure water, which may be used for dilution or blank) analysis.

The difference in the number of inlets highlights the varying complexities of the analytical procedures for Cr(VI) and Cr(III). The Cr(VI) analysis likely involves more intricate chemical reactions and requires the precise introduction of multiple reagents, necessitating a greater number of inlets. On the other hand, the Cr(III) analysis may involve a simpler procedure with fewer reagents or may rely on the inherent properties of the sample itself, reducing the need for multiple inlets.

This distinction in chamber design underscores the importance of tailoring the fluidic system to the specific requirements of the analytical method. By optimizing the number and arrangement of inlets, the system can ensure efficient and accurate analysis of both Cr(VI) and Cr(III) in water samples.

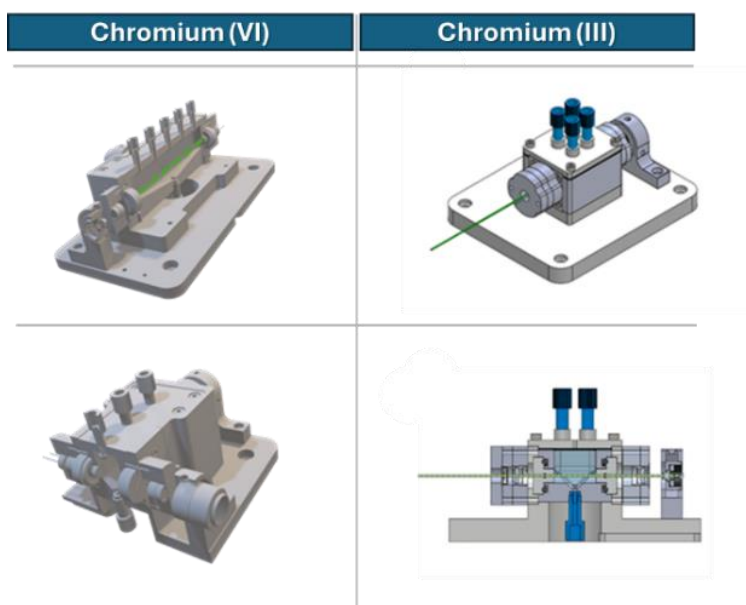


Figure 86: Measuring chamber for chromium with dual optical path and different inlets.

The chromium(VI) detection chamber has been designed to be implemented with two different optical paths: one 100mm long, used for analyte detection in the desired range, and a shorter one to potentially allow for future detection at different concentrations. Figure 87 also shows the accommodation for the chosen diode and photodiode, ensuring the laser beam is positioned precisely at the center of the chamber in order to optimize the analysis. Additionally, the chamber has been designed with a convergent shape towards the bottom to facilitate sample outflow.

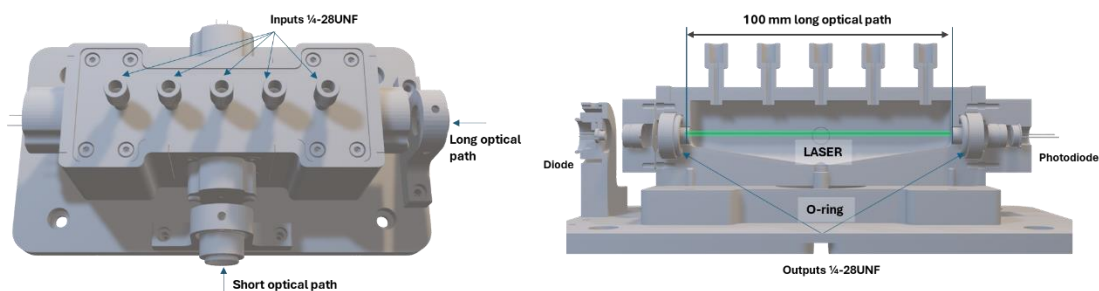


Figure 87: Chromium (VI) optical cell optic disposition.

Figure 88a shows the closed and assembly measurement chamber without inlets, designed to house the diode and photodiodes. It also illustrates (Figure 88b) how the chamber was integrated into the sensor platform, how it was connected to the reagents and samples required for analysis. The enlarged view highlights the laser in operation during analysis, visible through a dedicated inspection window. This window also allows technicians to check for contamination within the chamber during maintenance. A chamber volume of 20mL was selected, following optimization of the analysis process.

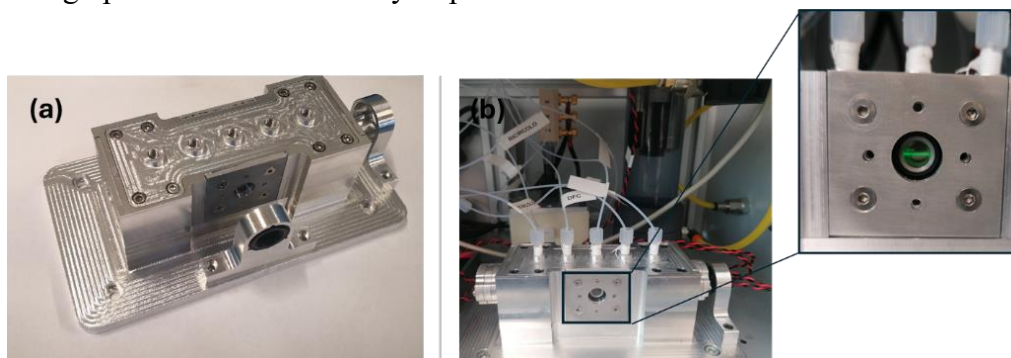


Figure 88: (a) Realization of the prototype measuring chamber with laser holder and holder. (b) Implementation of the realized camera in the platform with magnification on the window dedicated to the measurement chamber control.

FEM Simulation

To evaluate the performance and potential limitations of the optical detection cell, FEM simulations were conducted, with **pressure distribution** results shown in Figure 89. The left plot visualizes pressure on the cell walls at a 10 mL/min flow rate, highlighting a concentrated pressure drop near the outlet. This was expected as the fluid accelerates through the narrowing channel towards the outlet. The right plot shows the relationship between maximum pressure drop and flow rate showing a clear trend: as the flow rate increases, the pressure difference also increases. This is consistent with fluid dynamics principles, where higher flow rates generally lead to larger pressure drops. The red square highlights the specific data point corresponding to the pressure distribution shown in the left plot (10 mL/min flow rate).

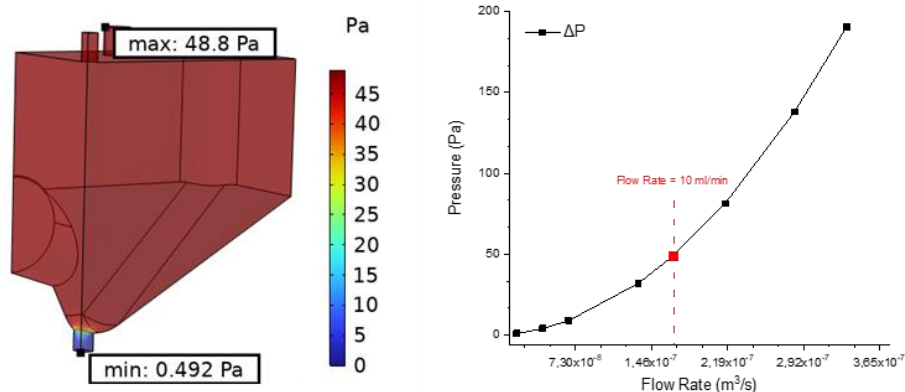


Figure 89: Left: pressure on analyte cell wall for the 10 mL/min flow rate case. Right: pressure drop between inlet and outlet.

Analysis of the **streamlines** in Figure 90 reveals a critical **flow rate threshold** of approximately 2.5 mL/min. Below this threshold, fluid flow is relatively uniform with minimal vorticity. Above this threshold, increased vortex formation enhances mixing and ensures the analyte reaches the entire detection zone. This efficient mixing, without excessive turbulence, improves analytical sensitivity and accuracy. The streamlines appear smooth and well-defined, suggesting laminar flow conditions within the chamber. This is desirable in fluidic systems as it ensures predictable and controlled fluid behaviors. The streamlines converge towards the outlet, indicating an acceleration of the fluid as it exits the chamber. The inlet also influences the flow patterns, with streamlines diverging as the fluid enters the chamber.

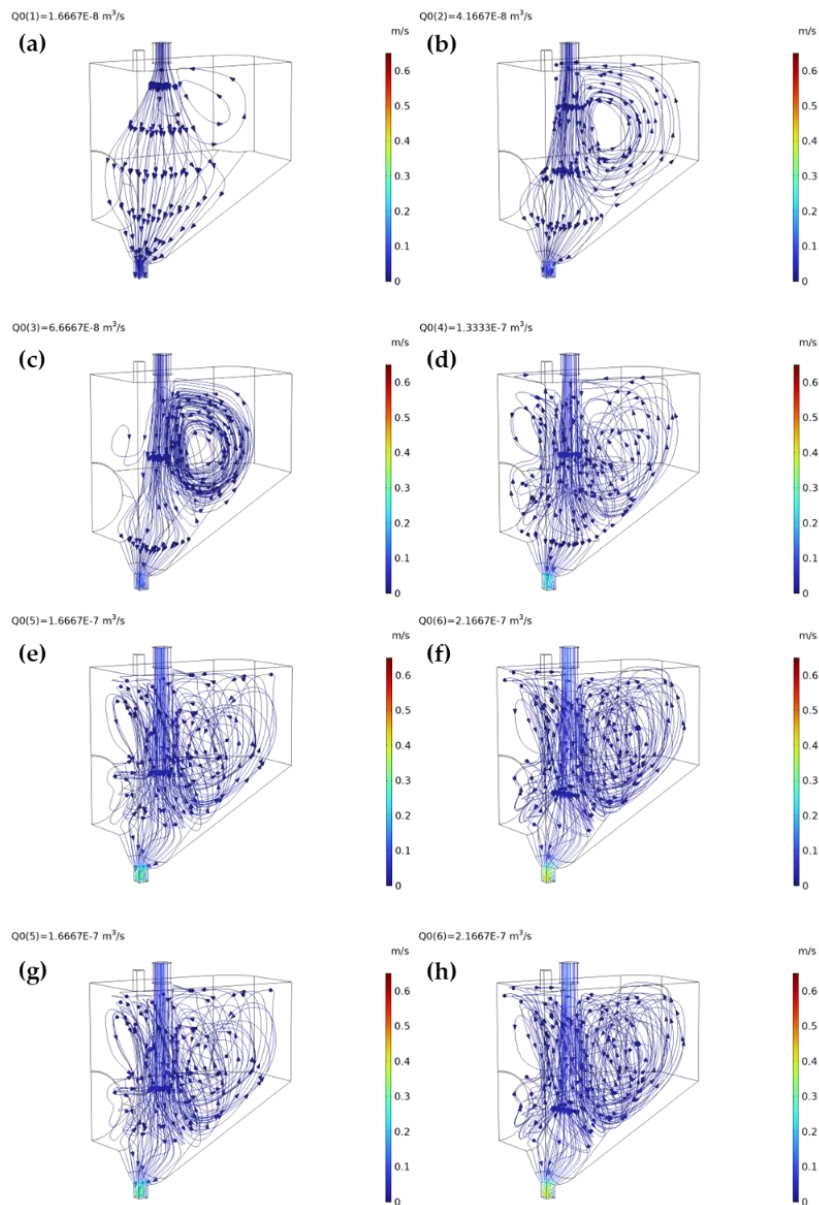


Figure 90: Streamline plots. Note that the SI units are used instead of mL/min so the flow rates are (a) 1 mL/min, (b) 2.5 mL/min, (c) 4 mL/min, (d) 8 mL/min, (e) 10 mL/min, (f) 13 mL/min, (g) 17 mL/min, (h) 20 mL/min.

Optoelectronic calibration

The subsequent reported calibrations are with respect to the internal calibration of the customize sensor for each chromium oxidation state. The selection of laser wavelengths for the analysis system was limited by the availability of commercial diode lasers. Ideally, the chosen wavelengths would perfectly match the peak absorbance values for each chromium oxidation state, as determined in laboratory experiments. However, due to market constraints, this was not feasible.

Chromium (III) sensor calibration

To detect Cr(III), five specific laser wavelengths were selected for the analysis system. These wavelengths, detailed in Table [table number], represent the closest commercially available options to the ideal wavelengths that correspond to peak Cr(III) maximum absorbance. The system linearity was then evaluated for each of these five wavelengths across two concentration ranges relevant for Cr(III) detection: a lower range from 0.09 g/L to 0.73 g/L and an upper range from 0.5 g/L to 6.3 g/L. These ranges represent the critical concentrations for accurate and reliable Cr(III) detection in the intended application. Although the Table 18 demonstrates excellent linearity across all five wavelengths, even when slightly off the peak absorbance values due to the broad absorbance signal, a 450 nm laser diode with a Ø5.6 mm package was ultimately selected for the detection cell.

Table 18: Evaluation of commercial wavelengths of System linearity for chromium (III) detection.

Commercial wavelength (nm)	R ² [0.73-0.09 g/L]	R ² [6.3-0.5 g/L]
450	0,9929	0,9875
448	0,993	0,9876
447	0,993	0,9874
445	0,9931	0,9873
405	0,9932	0,9766

After selecting the commercially available laser wavelength, a critical step in validating the functionality of the homemade *in-situ* monitoring system was to construct a calibration curve. This involved using the assembled system with the chosen commercial laser wavelength and real sample solutions to establish a relationship between the measured signal and the actual Cr(III) concentration. This real-sample calibration ensured the system reliability for practical applications. To ensure accurate measurement across a wide range of Cr(III) concentrations, a calibration curve was generated using a series of precisely prepared standards. A stock solution from the plant of 7.3 g/L Cr(III) was systematically diluted by a factor of ten to obtain five calibration standards. Absorbance measurements were taken at 450 nm for each standard, and the resulting data were used to construct the calibration curve (Figure 91). The curve exhibited excellent linearity, with a linearity factor close to unity (SD = 0.7%, calculated using Bessel's correction). This strong linear correlation between absorbance and Cr(III) concentration validates the accuracy and reliability of the monitoring system for quantifying Cr(III) across the target concentration range. This customized curve was subsequently loaded into the system's software for real-time analysis.

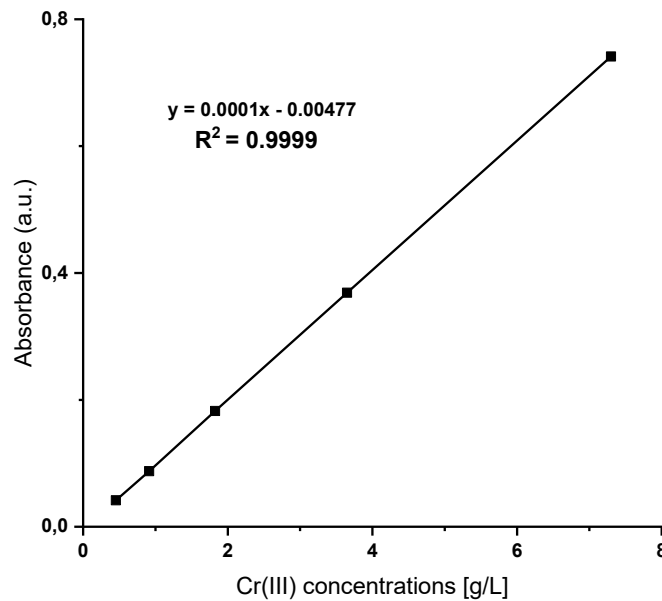


Figure 91: Customize calibration curve for chromium (III) detection whit 450nm commercial wavelength.

Chromium (VI) sensor calibration

To calibrate the optical sensor for hexavalent chromium (Cr(VI)), a 520 nm wavelength was chosen, matching a commercially available diode.

The system was calibrated using three Cr(VI) concentrations (5, 15, and 30 ppb) and three diode power levels (50%, 55%, and 60%). All three power levels demonstrated excellent linearity. The 55% power level was ultimately selected to optimize the sensor response while ensuring the longevity of the diode. The Table 19 shows the absorbance, measured Cr(VI) concentration, and relative error (E_{rel}) for different Cr(VI) concentrations (nominal 10 ppb and 20 ppb in (a), and real sample solutions A, B, C in (b)) and diode power levels (50%, 55%, and 60%). Across all tested conditions, the data suggests a good response regardless of the power level. This means the sensor output changes proportionally with Cr(VI) concentration. While all power levels show good linearity, the 55% level appears to offer slightly better consistency in terms of relative error, particularly for the real sample solutions (Sol A, B, C). This confirms that 55% might provide a more stable and predictable response across different samples.

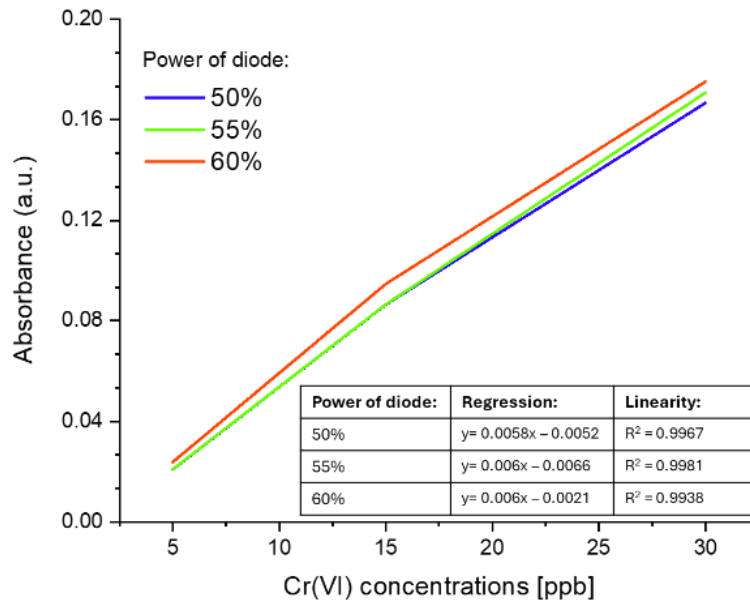


Figure 92: Calibration curve for nominal concentration of chromium (VI) with different power of diode for 520nm wavelength.

Table 19: (a) Laboratory solution with nominal concentration namely 10 and 20ppb and (b) real sample solution provided by the plant refers to three different moments of sampling evaluated with different power levels of diode.

		Cr(VI)	Absorbance (a.u.)	Concentration (ppb)	E_{rel} (%)
(a) Laboratory solutions	10ppb	50%	0.046925543	8.98	0.54
		55%	0.050215971	9.46	0.30
		60%	0.062807157	10.81	0.37
	20ppb	50%	0.117330961	21.12	0.58
		55%	0.122445619	21.04	0.12
		60%	0.133379635	22.57	0.30
(b) Real sample solutions	Cr(VI) ACDA		Absorbance (a.u.)	Concentration (ppb)	E_{rel} (%)
	Sol A	50%	0.076219379	14.03	0.56
		55%	0.079472942	14.34	0.52
		60%	0.090957796	15.50	0.29
	Sol B	50%	0.078921076	14.50	0.22
		55%	0.082524422	14.85	0.19
		60%	0.094889152	16.16	0.23
	Sol C	50%	0.074215526	13.69	0.64
		55%	0.075385439	13.66	0.48
		60%	0.085141132	14.54	0.33

A four-point calibration curve was constructed using 0.5, 15, and 30 ppb of chromium (VI). The calibration line shown in Figure 93 demonstrates that the sensor exhibits excellent linearity, achieving an R^2 value close to unity (SD = 0.14%).

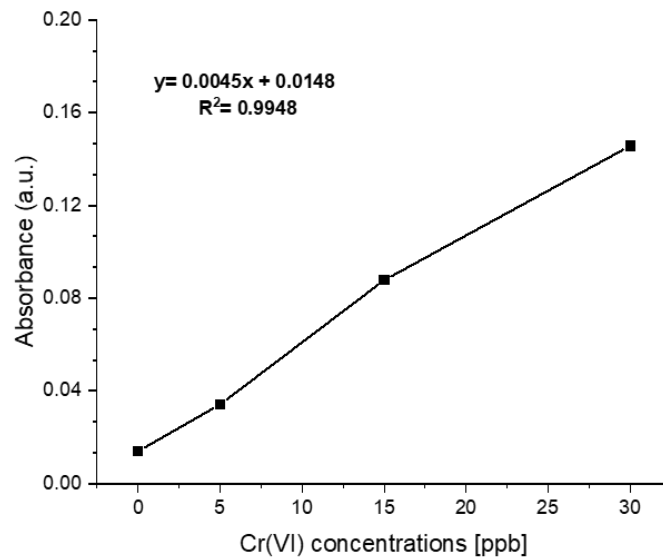


Figure 93: Customize the calibration curve for chromium (VI) detection while 520nm commercial wavelength.

1.5 Voltammetric section

Design of a measurement flow

The laboratory methodology was analyzed with the aim of converting it into a methodology suitable for implementation in a portable system. This portable system would include **electrode activation**, **arsenic determination** using appropriate chemical methods, and **electrode cleaning**.

Design and fabrication

To arsenic measurement, a dedicated measuring chamber was designed to interface with voltammetric sensors. This chamber features different separate inlets for the sample, reagent, and a recirculation line, along with a single outlet. The electrochemical sensor was integrated directly into this chamber, allowing for efficient and accurate arsenic detection.

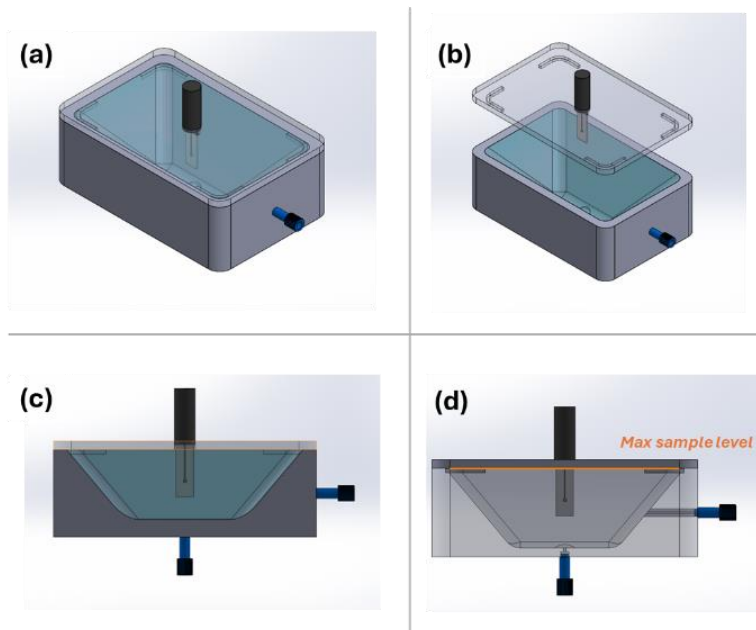


Figure 94: CAD representation of Arsenic detection chamber considering: (a) top view (b) insertion of the electrode into the measuring chamber, (c) and (d) the maximum volume of the sample with respect to the electrode.

The voltammetric sensor was placed at the centre of the analysis chamber. This placement ensures that during the filling process, the gold micro-wire serving as the working electrode was shielded as much as possible from the direct impact of the incoming sample flow.

The measurement chamber itself is 3D printed using an FFF (Fused Filament Fabrication) printer with polyethylene (PE) as the printing material. PE was chosen for its durability within the temperature range at which the system will operate and its excellent resistance to the mild acid solution used in the analysis. To maintain consistency with the previously optimized analysis protocol, a 15mL chamber volume was used. Figure 95 shows the bench prototype with which the analysis and calibration tests of the sensor dedicated to arsenic detection were carried out.

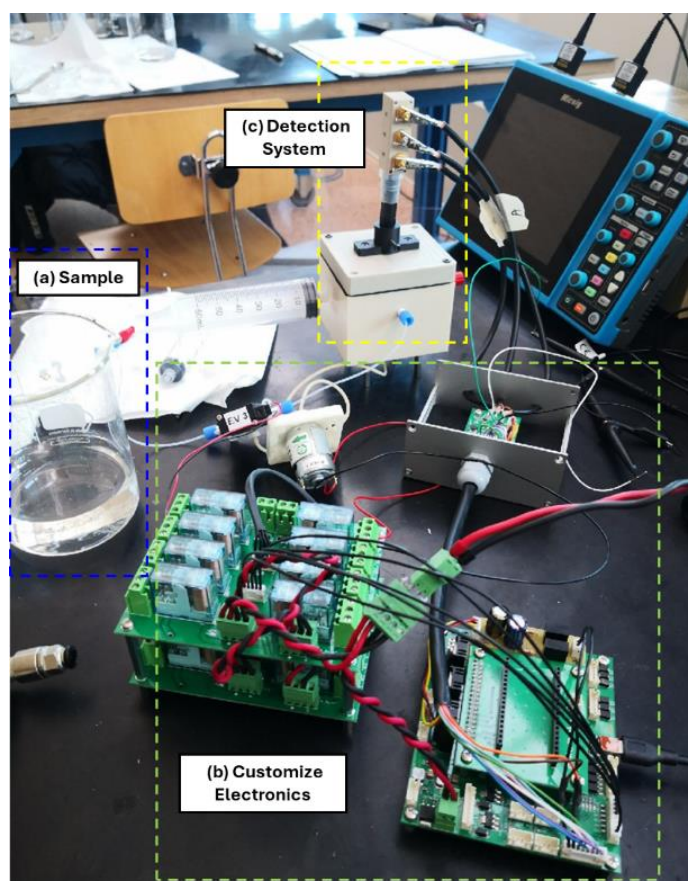


Figure 95: Prototyping of the Arsenic monitoring system. (a) solution containing analyte, (b) electronics dedicated to the control of the analysis and (c) monitoring chamber with voltammetry electrode.

Calibration

The arsenic detection system was calibrated using a five-point calibration strategy, with analyte concentrations ranging from 0 to 20 ppb. This approach allowed for a comprehensive assessment of the system's response across a relevant concentration range. Analysis of the calibration curve demonstrated excellent linearity, indicating a consistent and predictable relationship between the arsenic concentration and the measured signal as in laboratory preliminary tests. This linearity was observed both when considering the raw delta electrical current and when using the "calibration line inserted in the firmware in BITS," a digital representation of the sensor signal. The "BITS" value reported for each measurement represents an average value calculated within a specific voltage range of 0.06 to 0.1 V. This averaging process helps to improve the signal-to-noise ratio and enhance the accuracy of the measurements. The consistent linearity across both current and BITS values demonstrates the robust performance and reliability of the arsenic detection system. The conversion from BITS to current is performed using the following formula:

$$\text{BITS}/65535 * 2.048 / 100000 * 1000000$$

A strong correlation was observed between the calibration curves generated using BITS and current, indicating consistency in the system response regardless

of the specific measurement parameter. To further validate the system's performance, measurements were conducted on a real-world arsenic-contaminated water sample. The results obtained from this real-world sample analysis closely matched those predicted by the previously established calibration, with a minor discrepancy of only 1 ppb. This minimal error highlights the accuracy and reliability of the system when applied to actual environmental samples.

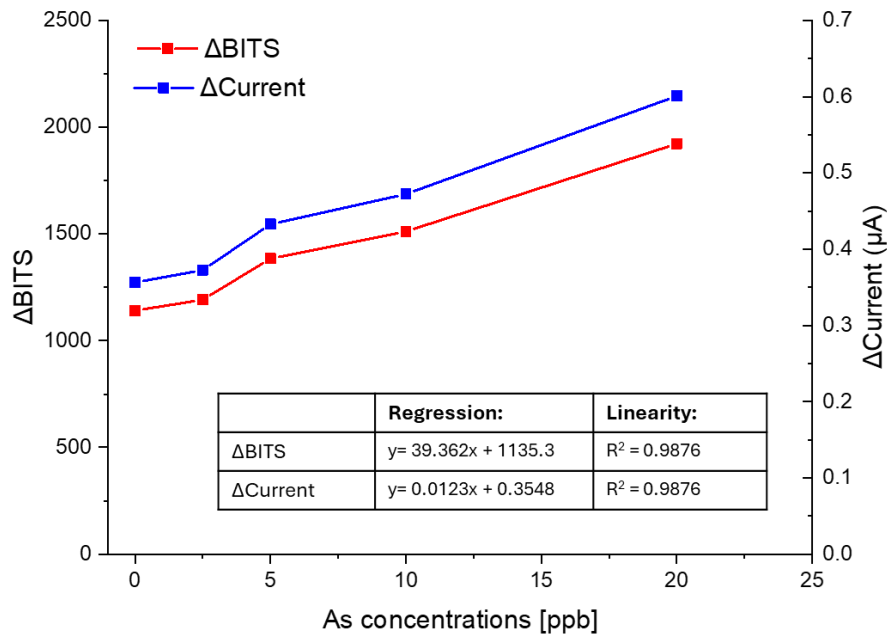


Figure 96: Calibration curve for Arsenic detection.

1.6 Electronic section

This section details the design and implementation of the firmware and software components, developed in collaboration with Microla Optoelectronics, responsible for controlling the device and managing its interfaces.

Control and Interface Electronics Design

The electronics responsible for controlling the sensors, hydraulic, and mechanical systems were designed using electronic design automation (EDA) software. This process generated schematics and PCB layouts, enabling the fabrication and testing of the electronic boards.

Electromechanical Components and Interface

The designed systems will be managed by fully customized electronics featuring microprocessors to control actuators and read system output data. These boards, totally proprietary and customized, are also interfaced with the power supply system, with the external interface module with the treatment, with commercial monitoring systems, such as the multi-parameter probe.

The system architecture comprises three distinct electronic boards:

Motherboard: This board serves as the central communication hub, facilitating communication with all other boards, providing input signals, and reading output data. It is capable of interfacing with the ESP32, supplied and programmed by Informatica System, and driving all the components and other electronic boards present in the prototype. This system can connect remotely via an external router, powered by the main module, with a 4G sim card for connection in non-wired environments. For communication with the wireless module of the ESP32, to avoid shielding the metal cabinet, an internal repeater has been integrated, wired LAN with the router, which can then be installed outside all the cabinets.

This motherboard presents:

- 24V power supply
- Hardware interface with ESP32
- Up to 4 laser control connectors, for driving the Cr(VI) measurement system and other possible expansions
- Up to 4 connectors for photodiode reading, Cr(VI) measurement
- Analog and digital I/O for interfacing with hydraulic driver boards, Arsenic sensor control board interface, multi-parameter probe interface
- MicroSD for data storage

Arsenic Control Board: This board is specifically dedicated to controlling the arsenic detection and analysis subsystem. Regarding the dissolved Arsenic detection sensor, a fully custom driver has been developed and implemented, capable of conditioning the sensor according to the curves detailed in [reference missing] and reading the current response. This response will then be interpreted by the motherboard and the value will be provided directly in concentration (ppb).

Chromium Control Board: This board manages the chromium detection and analysis subsystem.

This modular design approach allows for independent control and optimization of each subsystem, enhancing the flexibility and scalability of the overall device.

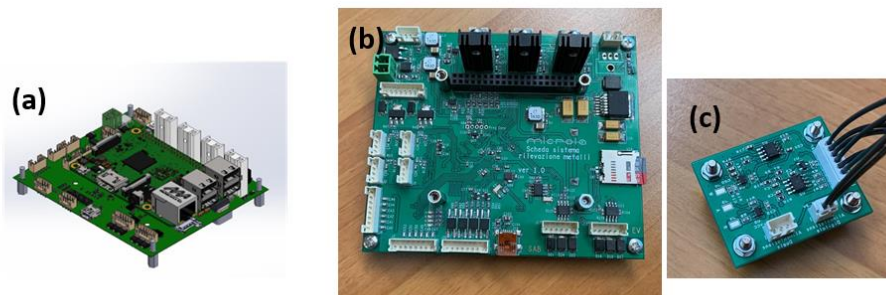


Figure 97: (a) Preliminary design of the full-custom electronics that will control the system and communicate with the infrastructure developed by Informatica System; (b) Motherboard schematic for controlling the prototype components; (c) Control board for the As.

To control the hydraulic components, a new **modular relay board** has been developed in addition to the previously discussed boards. This board, which uses electromechanical switches to control high-power circuits with a low-voltage signal, can activate either four or eight components. Specifically, it will drive the solenoid valves, recirculation pumps, and bubble traps.

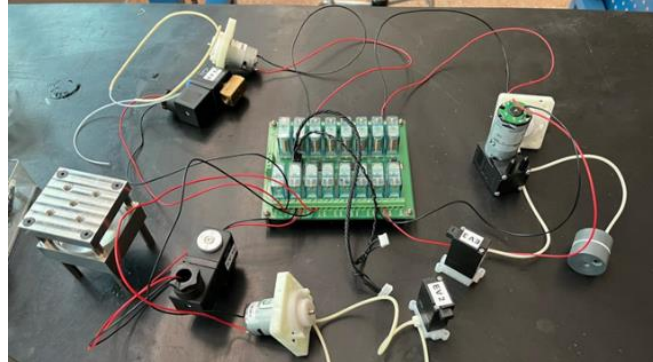


Figure 98: Relay board for controlling hydraulic components.

Firmware Development

The electronics described will be governed by firmware capable of:

- Managing the entire measurement process.
- Receiving external input signals to initiate measurements.
- Communicating measured values.
- Reporting errors, issues, and system health status.

Communication between the monitoring system and the Informatica System infrastructure has been designed and implemented. Communication parameters and commands for requesting operations from the monitoring system have been defined as follows.

Serial Properties

- Baud rate = 115200
- Data bits = 8
- Parity = none
- Stop bits = 1

Commands:

All commands and responses are encapsulated between an asterisk (*) at the beginning and a plus sign (+) at the end. Numeric values are transmitted as characters rather than numerical data types. Each successfully sent command elicits a corresponding response.

The following commands are supported:

- **Start Measurement:** Initiates a new measurement cycle.
Command length: 7 Byte
Response Length: 49 Byte

Request: *START+
Immediate response: *OK+

Response at the end of the measurement:

*[Parameter1];[Parameter2];[Parameter3];[Parameter4];
[Parameter5];[Parameter6];[Parameter7];[+/-][Parameter8];
[Parameter9];[Parameter10]+

Es: *2550;0250;013;780;184;0300;0001;-2000;0015;0002+

- Parameter1 = 4Byte of temperature to be divided by 100 and expressed in °C
 - Parameter2 = 4Byte of conductivity expressed in $\mu S / cm$
 - Parameter3 = 3Byte of hardness expressed in °F
 - Parameter4 = 3Byte of pH to be divided by 100
 - Parameter5 = 3Byte of TDS (total dissolved solid) expressed in mg/L
 - Parameter6 = 4Byte of chlorides to be divided by 100 and expressed in mg/L
 - Parameter7 = 4Byte of turbidity to be divided by 10 and expressed in FNU
 - Parameter8 = 4Byte of ORP (redox potential) to be divided by 10 and expressed in mV
 - Parameter9 = 4Bytes of chromium expressed in ppb
 - Parameter10 = 4Byte of arsenic expressed in ppb
- **Reagent Refill Complete:** Signals that the reagent reservoirs have been replenished. This command must be sent to the board to communicate that the reagents have been reloaded and resets the count of the measurements that can be taken.

Command length: 21 Byte

Response Length: 2 Byte

Request: *RICARICA;MM;dd;yyyy+ Es:
*RICARICA;05;17;2022+

- MM = Month of refill
- dd = Charging day
- yyyy = Year of the refill

Answer: *OK+

- **Status Request:** Queries the current status of the system, including operational state, error flags, and sensor readings.

Command length: 7Byte

Response Length: 17Byte

Request: *STATO+

Answer: *[Stato sistema];MM;dd;yyyy;nn+ Es: *R;05;17;2022;07+

- System Status = M if a measurement is in progress | R if the system is waiting and ready
- MM = month of recharge

- DD = Charging day
 - yyyy = year of top-up
 - nn = number of remaining measurements
- **Last Measurement Request:** Retrieves the data from the most recently completed measurement. This command is used to request the values of the last measurement taken and the response has the same format as the response you receive at the end of the measurement explained above.
Command length: 15Byte
Response Length: 49Byte

Request: *ULTIMA_MISURA+

- **Stop:** Internal command to stop the measure in progress.
Command length: 6 Byte
Response Length: 2 Byte

Request: *STOP+

Answer: *OK+

This command structure establishes a robust and reliable communication protocol between the monitoring system and the central control infrastructure. At the end of the project, the firmware instructions were tested together with Informatica System to develop command lines, and subsequently, the final software was developed. Finally, the entire device was tested with the applications developed by Informatica System to automate all procedures in preparation for the final installation.

Energy storage

To enable installation in environments without access to electricity, an energy storage system has been designed. This system utilizes stacks of Li-Po rechargeable batteries in a 24 Volt configuration per stack, as mentioned in the previous report. This system can communicate with the main system to provide information on its status and ensure balanced charging.

To guarantee an autonomy of approximately one month/30 measurements for this application, 3 stacks have been connected in parallel, each with a capacity of about 7000 mAh. This configuration will result in a total system capacity of approximately 21000 mAh.

This option was not included in the first prototype, which will have access to mains power, but it remains available for future upgrades.

1.7 Water monitoring sensing platform

1.7.1 Platform for industrial water monitoring

Figure 99 provides a visual representation of the automated monitoring system. Initiated by a single command (via software or serial command), the system executes a sequence of automated steps, illustrated by the blue line. This automated process begins with a pre-measurement cleaning of the analysis cell, followed by a baseline measurement using deionized water. As shown in the diagram, the system then drains the water, introduces the sample, and performs the measurement. After analysis, the sample is discharged into a designated waste tank. This tank is designed to accommodate multiple measurements before requiring disposal, minimizing waste generation and user intervention. Currently, the only manual operation, indicated by the black line, is manual restart of the system operation after replenishing the deionized water reservoir. The system incorporates a sensor that detects low water levels, triggering an error notification and halting the process until the reservoir is refilled. Future development aims to integrate a deionization system that utilizes filtered tap water, further enhancing automation by eliminating the manual refilling step. The entire analysis process takes approximately 15-20 minutes. Most of the time is dedicated to cleaning the analysis chamber and the measurement system. Due to the spectrophotometer sensitivity to scattering and reflection caused by external interferences, data acquisition requires pristine conditions.

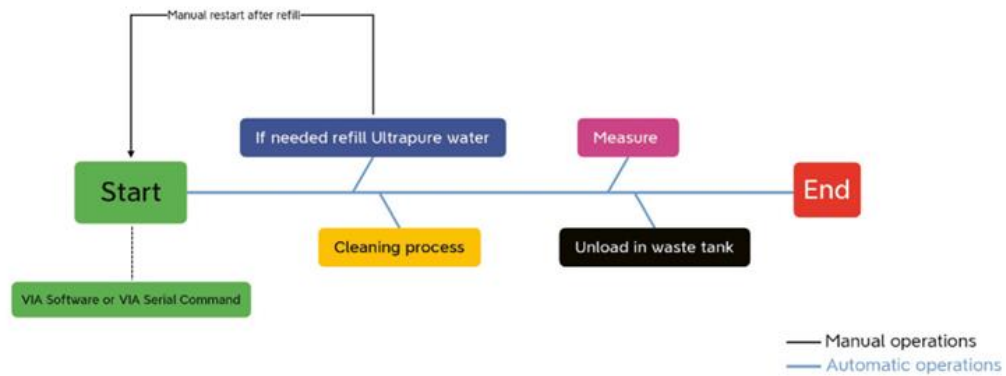


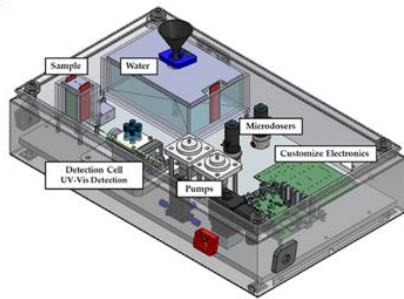
Figure 99: Automated Cr(III) Monitoring System Process Flow.

The stream flow development starts from an initial design concept and the final constructed prototype of an automated chromium (III) monitoring system. (a) showcases a 3D model of the system design. Key components are highlighted, including the sample and water reservoirs, the micro-dosing pumps responsible for fluid handling, the custom electronics controlling the system's operation, the microfluidic detection cell where the analysis occurs, and the UV-Vis spectrophotometer for optical detection. (b) displays a photograph of the fully assembled bench prototype. The physical components are arranged on a breadboard, with tubing connecting the reservoirs, pumps, and detection cell. The custom electronics and control circuitry are visible, demonstrating the translation

of the design concept into a functional prototype. The figure effectively illustrates the successful realization of the design objectives in the tangible prototype. It visually communicates the system architecture and the integration of its constituent parts.

Dimension	Length [mm]	500
	Width [mm]	300
	Height [mm]	125
Weight	Weight [kg]	7
Electrical connection	CEE 7/7	230V ~ 50Hz
Communication port type	USB Type	B
Inlet Sample	Rilsan Tube	Ø 4mm
Outlet Sample	Rilsan Tube	Ø 4mm
Waste Sample	Rilsan Tube	Ø 4mm
Inlet Ultrapure Water	Funnel	Ø 8mm

(a) Design



(b) Prototyping

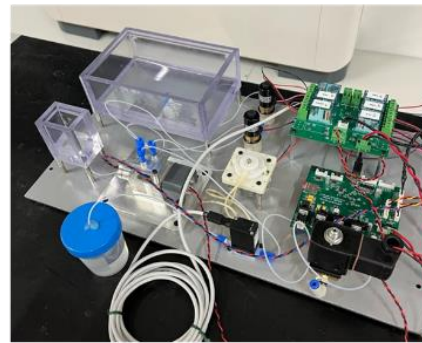


Figure 100: Top: Table of define parameters. Bottom: Stream flow (a) of initial design concept and (b) the final constructed prototype of an automated chromium (III) monitoring system.

1.7.2 Platform for drinking water monitoring

The final sensing platform was designed, built, and implemented for in situ installation, adhering to the specifications outlined in Table 20. Because this system will be integrated into a larger water monitoring network positioned both before and after water treatment, it needed to be wall-mountable and housed within a protective metal enclosure to shield it from the elements. To ensure its durability and reliability in outdoor environments, the final device was designed with an IP66 protection degree. This rating signifies that the enclosure is completely sealed against dust and other solid particles and can withstand powerful jets of water sprayed from any direction without allowing water to ingress. This robust protection ensures the system can operate effectively in harsh conditions with minimal maintenance. Furthermore, it should be possible to open it from the front to perform the necessary maintenance. It operates on a 12/24 V power supply with a battery backup and can be coupled with a photovoltaic and/or hydroelectric system for sustainable operation. The platform is designed to operate autonomously for at least one month, requiring minimal maintenance and performing at least two measurements per day. The system incorporates multiple tanks capable of suitable materials of storing all necessary reagents to ensure autonomous operation of all monitoring phases for at least one month without

operator intervention. These tanks are interfaced with measurement chambers via micro-dosing units, which dispense the precise amounts required for the chemical reactions involved in the measurements. The system allows for remote management, enabling users to adjust alarm thresholds and sampling frequency as needed. It can also interface with existing telecommunication systems for alarm notification and data exchange. Finally, the system provides continuous water quality monitoring by automatically taking measurements both upstream and downstream of the treatment process. This real-time data can be instantly transmitted to authorities as an alarm signal, enabling immediate intervention in case of water quality issues. To interface with the water treatment system, an additional satellite module was developed by Informatica System. This module connects to the main module both hydraulically and electronically, and it also interfaces with the untreated water line and the treatment system developed by Idroricerche and the Polytechnic University of Turin.

Table 20: Desired technical features for monitoring drinking water platform.

Technical Feature	Description
Installation	Wall-mounted with front opening
Dimensions	50 x 60 x 25 cm (W x H x D)
Protection degree	IP66
Power supply	12/24 V with battery and PV and/or hydroelectric system (max power 35W)
Reagent autonomy	Minimum 1 month with at least 2 daily measurements (maintenance-free)
Remote management	Adjustment of alarm thresholds and sampling frequency
TLC interfacing	Alarm reception and data exchange
Automatic measurements	Upstream and downstream of the treatment
Data communication system	Specify the system (e.g., Modbus, Ethernet, etc.)
Data platform	Specify the platform (e.g., cloud-based, local, etc.)

The initial process for this project follows the **three key phases** in the development of a new technology, taking it from a laboratory concept to a functional field device for pollutant detection (Figure 102):

(a) Design: This initial phase focuses on conceptualizing and planning the system. It likely involves creating detailed schematics and diagrams, as shown in the image, outlining the arrangement of components such as tanks, sensors, pumps, and control units. This stage is crucial for defining the system architecture, functionality, and how different parts interact follow the previously technical features. Compared to the initial specifications, the sensor platform must also take into account the constraints deriving from the size of the integrated commercial sensors.

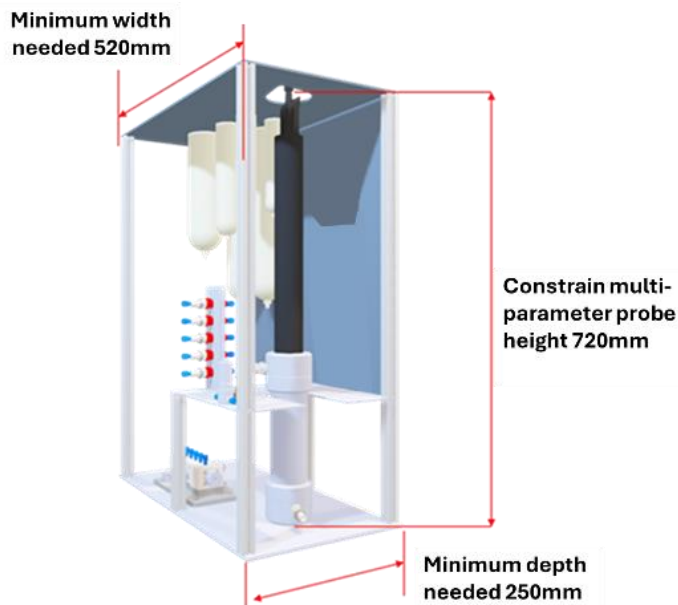


Figure 101: Rendering of the measuring-constrain device with its components.

(b) Implementation: The second phase brings the design to life. It involves the physical assembly of the system, connecting various components, and setting up the necessary electronics and control systems. The benchtop setup where individual parts were being tested and integrated representing the transition from the drawing board to a tangible prototype.

(c) Prototyping: This final phase involves building a functional prototype that closely resembles the final product. This prototype is enclosed in a protective casing making it suitable for field testing and the protection degree required. The developed prototype has been equipped with two inlets for water before and after treatment. The completed prototype underwent testing and calibration before being sent for installation. This stage allows for real-world evaluation of the system performance, identifying any necessary adjustments or improvements before full-scale deployment. In this stage also the final calibration has been set into the system.

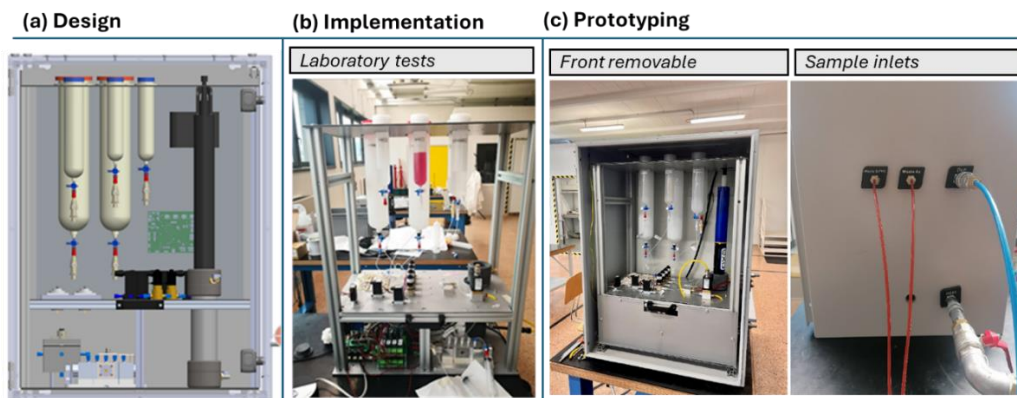


Figure 102: Stream working flow of the final monitoring platform system divided in three phases: (a) Design, (b) Implementation of the system with laboratory test and sub-system integration and (c) Prototyping platform with a removable front and a detail with the inlet of treated or untreated water (Inlet), the clean drain of the purge of the multiparametric probe (Out), the discharges of the complexed solutions (Waste Cr (VI) and Waste As) and the communication port with the interface system with the water treatment system.

Sub-systems integration and assembly, and offline testing

Subsystem integration was a critical stage in the development of a lifecycle of complex system, serving as the requirement in realizing a fully functional and optimized entity. This intricate process transcends mere assembly, demanding meticulous verification and validation of inter-component interactions to ensure cohesive operation and fulfilment of overarching system requirements. Early integration facilitates proactive identification and rectification of discrepancies, mitigating the risk of costly rework and schedule overruns. Adopting an incremental integration strategy, as opposed to a monolithic approach, further reduces risks and allows for more controlled testing and refinement. Rigorous evaluation of subsystem interdependencies during integration bolsters system robustness and stability by exposing potential points of failure. Moreover, a **modular and well-integrated architecture** promotes maintainability and facilitates future upgrades, as modifications to individual subsystems are less likely to propagate unintended consequences throughout the system. The considered and integrated sub-systems are as follows:

- **Micro-dosers:** already calibrated and tested in microliter order resolutions, with high reliability, and durability.
- **Diaphragm recirculation pumps:** mixing of the compounds for measurement, both for the colorimetric reaction for the measurement of hexavalent chromium and for the activation for electrochemical measurement, in the monitoring of dissolved arsenic.
- **Microfluidic solenoid valves:** high response times and minimization of dead volumes.
- **Multi-parameter probe beaker and sensors:** interface with hydraulic circuit, initial sample accumulation tank, and rinsing via initial purge cycle and clean discharge.
- **Dedicated measuring chambers,** both for chromium and arsenic.

The integration of the sub-systems resulted in a synergistic effect, where the overall performance exceeded the simple combination of individual components. This led to improved functionality, optimized resource use, and enhanced system reliability.

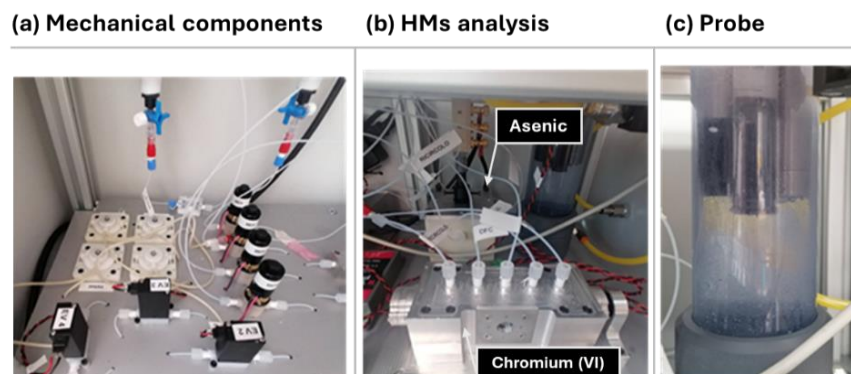


Figure 103: Detail of the monitoring subsystems (a) System of hydraulic components: pumps, micro-dosers and solenoid valves; (b) Chromium (VI) and Arsenic measuring chambers; (c) multi-parameter probe testing, with sensors installed.

Multiparameter probe

For monitoring the most important physicochemical water parameters listed previously, the most practical solution is to **integrate a multiparameter probe into the monitoring system**. Multiparameter probes are portable water analysis instruments that house various sensors, each measuring a specific parameter. This technology is well developed, and a wide variety of probes are commercially available. One of the reasons for selecting this specific probe was its ability to operate with wet-mateable sensors, allowing for the connection and disconnection of sensors even when the instrument is wet. The probe identified for monitoring within this research project is a multiparameter probe with the following features:

- 4 universal ports for interchangeable titanium sensors
- Integrated datalogger for data storage
- Calibration cup
- Internal battery power
- Included software for configuration, management, and calibration
- Battery type: 2 D-cell with an estimated 90-day lifespan
- Dimensions: Maximum length 65cm, maximum diameter 5cm
- Maximum weight: 1.5kg
- Communication types: Bluetooth wireless technology, RS-485, USB
- Output options: USB with signal output adapter
- Sample rate: Up to 4 Hz

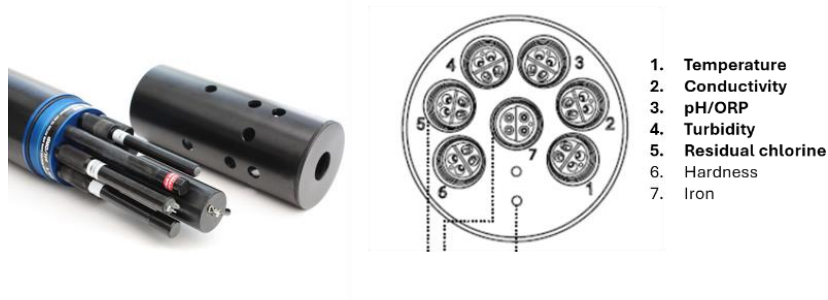


Figure 104: Multiparameter probe sensor disposition.

The tests revealed that the system requires a sample volume of 150-200 mL and the water inlet pressure supported is up to 3bar. Data acquisition and processing proved to be simple and intuitive, while measurements stabilized rapidly. It is important to note the necessity of rinsing and priming between different samples to avoid cross-contamination, a procedural aspect that can be easily integrated into the final device operation. The sensor calibration process was conducted on-site to ensure long-term accuracy and optimal performance within the actual operating environment. The conductivity sensor was calibrated directly at the Sampeyre site, along with the pH, Redox (ORP), and chloride probes. However, the turbidity sensor required calibration at a different location, the Pietraporzio site for lack of calibration reagents.

***In-situ* installations**

The monitoring system was successfully installed at the sites selected by ACDA, namely Sampeyre-Villar and Pietraporzio. The system was installed with a direct intake from the contaminated water reservoir, enabling continuous monitoring of the concentration trends and potential fluctuations over time. Then it also has a second inlet to monitor the water after the heavy metal abatement treatment. The inlet pressure was dictated by the capacity of the multi-parameter probe collector.

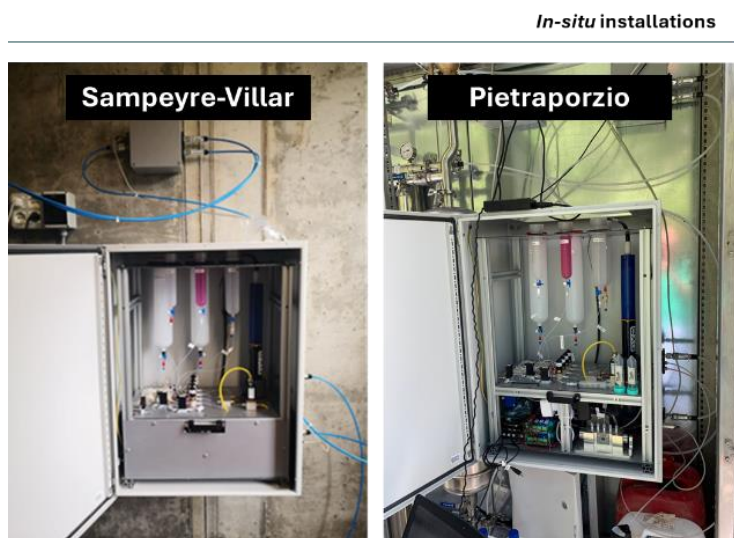


Figure 105: Installation in field of the sensing platform for drinking water HMs detection in Piedmont mountains.

Maintenance

Reagents refill

Figure 106 shows the top portion of the reagent tanks, designed for easy removal and replacement, allowing for autoclaving in a laboratory setting. The tanks featuring quick couplings with automatic shut-off valves. This design enables the operator to remove the tanks with a section of tubing while preventing any residual reagents from leaking out.



Figure 106: Top view detail of the water monitoring platform render showing the tank reload.

The system includes a multitude of tanks capable of storing all the reagents necessary to ensure **autonomy in all monitoring phases for at least one month with two measures per day**, without operator intervention. These tanks interface

with the measuring chambers via micro-dosers, which can dispense the quantities required for the chemical reactions to perform the measurements.

Sensor substitution

During field testing, the arsenic detection sensor was damaged, resulting in the loss of the working electrode and saturation of the auxiliary electrode. Consequently, the sensor had to be replaced with a new one, as documented in the images in the figure. As previously mentioned, the chosen sensor is suitable for many analyses. However, when operating in continuous flow, the working electrode, with its micrometric dimensions, loses this capacity for a large number of measurements, although it still guarantees at least one monthly analysis cycle. Thanks to the modularity of the proposed solution, this can be easily achieved. As shown in Figure 107, an in-situ activation of the sensor was performed before it was placed back into the monitoring system.

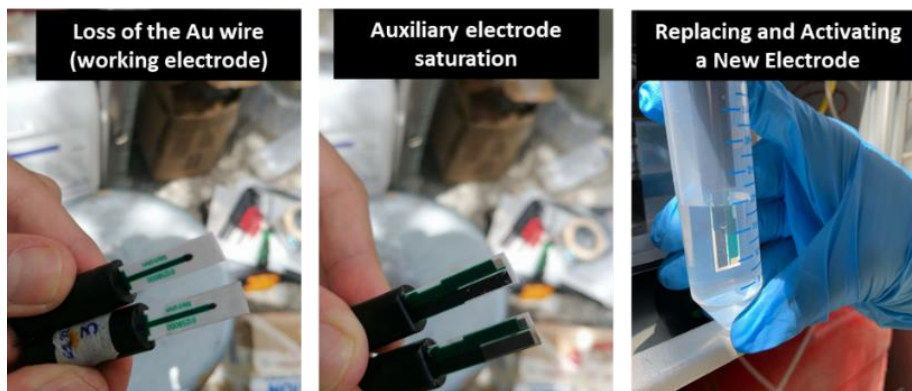


Figure 107: Maintenance process carried out in the field in the replacement of the electrode for the detection of arsenic.

The synchronization between the sensor operational lifespan and the necessary reagent replenishment presents a significant advantage in terms of maintenance efficiency. By aligning these two routine procedures, the system minimizes downtime and maximizes operational efficiency. Instead of requiring separate visits for sensor replacement and reagent refills, the operator can address both tasks concurrently. This streamlined approach not only reduces the overall maintenance burden but also minimizes any potential disruption to the monitoring process. This efficiency translates to cost savings, as it reduces the need for frequent site visits and minimizes the associated labour and travel expenses. Additionally, it ensures the system operates at peak performance, providing accurate and reliable data for effective water quality management.

1.8 Testing on real samples provided by ACDA

As previously mentioned, the tests for the multiparameter probe, the chromium (VI) monitoring system, and the arsenic monitoring system were carried out on two real solutions provided by ACDA and sampled at the contaminated sites of Pietraporzio (arsenic contamination) and Sampeyre (Cr(VI) contamination). The results obtained are reported in the following tables. Each

test requires an **operation time of 30 minutes to obtain the data reported in the tables.**

Table 21: Results of the measurements carried out on the sample from Pietraporzio.

Parameters	M.U.	Average Value	Standard Deviation
Temperature	°C	17.673	0.002
Conductivity	µs/cm	100.6	0.1
pH	upH	7.80	0.01
TDS	mg/L	76	0
Chlorides	mg/L	0.54	0
Turbidity	FNU	0	0
ORP	mV	82.9	3.2
Arsenic	µg/L	8.64	1

Table 22: Results of the measurements carried out on the sample from Sampeyre.

Parameters	M.U.	Average Value	Standard Deviation
Temperature	°C	17.691	0.001
Conductivity	µs/cm	175.2	0.1
pH	upH	8.18	0.01
TDS	mg/L	113	0
Chlorides	mg/L	1.13	0.03
Turbidity	FNU	0	0
ORP	mV	95.2	0.5
Chromium (VI)	µg/L	12.41	1

To validate the performance of the developed system, the values obtained from the afore mentioned tables were compared against laboratory analysis results. This comparison served to confirm the accuracy and reliability of the system's measurements. The prototype's performance was validated by comparing its measurements to those obtained through standard laboratory analysis. The calibration curves for arsenic and chromium (VI) exhibited excellent agreement with the laboratory results, with a measurement discrepancy of less than 5 ppb. This level of accuracy, well within the predefined tolerance limits, underscores the system's capability to reliably quantify contaminant concentrations and its suitability for water quality monitoring applications.

Table 23: Comparison for arsenic and chromium(VI) results between prototype system and laboratory instrumentation.

Sample	<i>In-situ</i> sensor prototype	Laboratory detection
Pietraporzio [As]	8,64 ppb	9,2 ppb
Sampeyre [Cr(VI)]	12,41 ppb	14 ppb

Chapter 6

Conclusion and Future Perspective

This thesis project successfully achieved the creation of a prototype for in-situ sensor water monitoring platform. This innovative platform holds immense promises for modernizing water quality monitoring due to its adaptable, modular design and its capacity for comprehensive sensing. The platform inherent modularity facilitates the seamless integration of a diverse array of sensors and tools, enabling it to be readily adapted to a wide range of monitoring requirements. This adaptability is paramount in addressing the intricate and ever-changing nature of water quality, which is influenced by a myriad of factors, starting from physicochemical parameters and including pollutants such as heavy metals and organic substances.

6.1 Reached Results

The efficacy of this sensing platform was convincingly demonstrated through its ability to effectively monitor arsenic and chromium, in both its oxidation states, and a possible broad spectrum of others heavy metal pollutants to address various field locations and aims with differing concentration ranges. Employing simple but effective analytical techniques such as UV-Vis spectroscopy and voltammetry, the sensing platform detection capabilities could be precisely modulated to target crucial heavy metals, including chromium (both trivalent and hexavalent forms), nickel, copper, arsenic, and cadmium. Importantly, the platform exhibited varying sensitivities depending on the specific metal being analyzed and the chosen detection method, underscoring the critical role of its modular design in optimizing detection strategies for specific applications and environmental conditions. This tailored approach ensures the platform can be customized to provide accurate and reliable data for a variety of water quality monitoring needs.

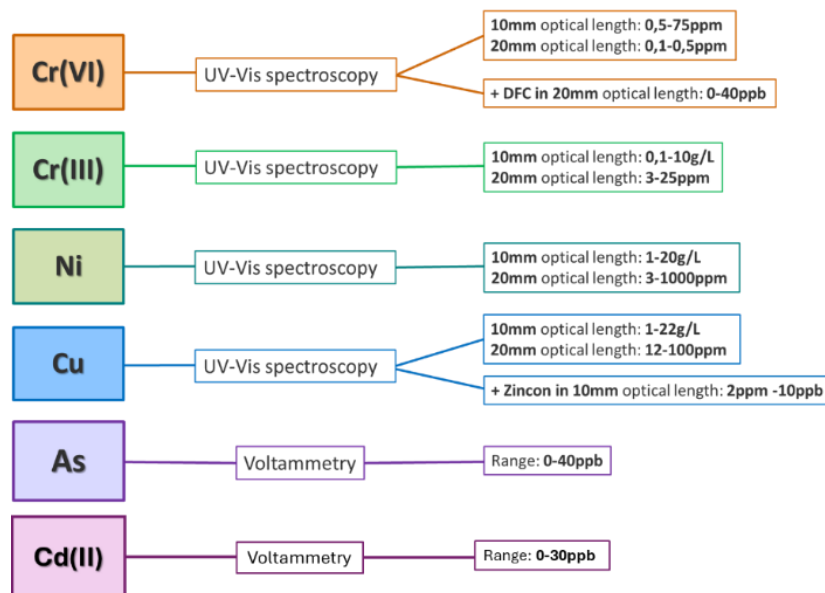


Figure 108: Summary diagram of the heavy metals detected with evidence of the analytical technique used and the detection range achieved in the thesis work.

6.2 Key Achievement

In this scientific work, **developing a prototype driven by market needs bridges the gap between innovation and real-world impact.** It ensures that research efforts are focused on addressing practical challenges and delivering solutions that are relevant, usable, and valuable to end-users. This approach not only increases the likelihood of successful technology transfer and commercialization but also fosters collaboration between researchers and industry, leading to more efficient and effective innovation. By aligning research with market demands, scientists can maximize the societal and economic benefits of their work, ensuring that their discoveries translate into tangible improvements in people lives and contribute to a more sustainable future. In the development of this water monitoring system for both drinking water and industrial use, several significant milestones have been reached, as detailed below:

- **Modularity:** The platform modular design allows for the seamless integration of different sensor types, enabling customization for specific monitoring requirements and future expansion with new sensing technologies.
- **Pollutants/Heavy Metal Detection:** The platform successfully demonstrated the detection of various heavy metals, including Cr(VI), Cr(III), and Arsenic possible tailored also for Ni, Cu and Cd(II), using UV-Vis spectroscopy and voltammetry.
- **Sensitivity and Range:** The platform exhibited varying sensitivities and detection ranges for different heavy metals, showcasing its ability to cater to diverse water quality conditions and regulatory limits.
- **In-Situ Installation:** The platform has in situ capability enables real-time, continuous monitoring, providing timely and critical data for water quality management. The system is also able to withstand extreme conditions (such as

strong variations in temperature and humidity) ensuring good quality of analysis.

- **Little maintenance required:** The reagents used in this prototype have a shelf life of one month, and the platform's modular design allows for customization of the tank size to accommodate varying testing volumes and frequency of analysis. This adaptability ensures the platform can be tailored to meet specific monitoring needs and resource availability.

6.3 Significance and Implications

This prototype represents a major leap forward in how water quality was historically laboratory monitored. Ideally it was designed like a toolbox with different sensors that can it is possible to swap in and out, allowing it to adapt to varying water conditions and monitoring needs. This flexibility is essential because water quality can change dramatically from place to place and over time. The platform is also highly sensitive, able to detect even tiny amounts of pollutants, which is crucial for catching contamination early. And unlike traditional methods that require collecting samples and analyzing them in a lab, this platform works directly in the water, providing continuous, real-time measurements – like having a constant finger on the pulse of the water health. The detection of heavy metals is of utmost importance, especially because these metals can gradually build up in geological formations like rocks and sediments. Severe weather events can then release these accumulated metals into the surrounding environment, posing significant dangers to both human health and the delicate balance of ecosystems. These customized platforms play a crucial role in providing easily accessible data on the overall wealth of water sources, including detailed information about specific pollutants such as heavy metals. By making this data readily available, it empowers various stakeholders – water resource managers, policymakers, and local communities – with the knowledge necessary to make well-informed decisions. These decisions can range from implementing effective water treatment strategies and pollution control measures to safeguarding public health and ensuring the long-term sustainability of water resources. In essence, this prototype offers a more comprehensive, adaptable, and timely approach to water quality monitoring, with the potential to significantly improve how we protect our precious water resources.

Monitoring vs Alarm system

While both real-time monitoring systems and laboratory analysis of water samples contribute significantly to the overall assessment of water quality, they fulfill distinct roles and offer unique advantages. Monitoring alarm systems provide real-time, continuous surveillance of water quality parameters. They act like vigilant guards, constantly checking for any deviations from normal conditions and triggering alarms when pre-set thresholds are exceeded. This allows for immediate response to potential contamination events, preventing further damage and protecting public health. However, the data generated by these

systems may not always be detailed enough for in-depth analysis or regulatory compliance, especially because in order to do so the precision and accuracy of the instrumentation should be as high as possible.

Laboratory data analysis, on the other hand, involves rigorous testing of water samples using sophisticated equipment and methodologies. This provides accurate and comprehensive data on a wide range of parameters, including heavy metals, organic pollutants, and microbial contaminants. The results obtained from laboratory analysis are often considered legally defensible and can be used for regulatory reporting, compliance monitoring, and in-depth investigations of water quality issues. However, this process is typically more time-consuming and may not be suitable for real-time monitoring or rapid response to contamination events.

In essence, monitoring systems with alarms offer speed and immediacy, while laboratory data analysis provides accuracy and legal validity. Ideally, both approaches should be integrated into a comprehensive water quality management strategy, with monitoring systems providing early warnings and triggering further investigation and laboratory analysis when necessary.

6.4 Challenges and Limitations

The development of in situ sensor platforms for water quality monitoring presents a complex array of challenges that must be carefully addressed to ensure successful implementation and widespread adoption. These challenges span various aspects of technology, from initial design and prototyping to data management, device durability, and user accessibility.

Cost and Accessibility: While miniaturization of sensing components has led to more cost-effective devices, the initial setup and maintenance of a comprehensive in situ monitoring platform can still pose a significant financial hurdle, particularly for small-scale applications or resource-limited settings. Exploring innovative approaches such as online continuous monitoring services, where the platform is managed and maintained remotely by specialized providers, could potentially alleviate this financial burden and enhance accessibility for a broader range of users.

Data Management and Security: The integration of multiple sensors into a single platform generates a massive influx of data, necessitating robust data management strategies. Efficient data storage, processing, and analysis are crucial for extracting meaningful insights from the collected information. Furthermore, ensuring data security is paramount, especially considering the sensitive nature of environmental monitoring data and the potential for malicious attacks or unauthorized access. Implementing strong encryption protocols and secure data transfer mechanisms are essential for safeguarding data integrity and confidentiality.

Data Delivery and User Interface: While expert technicians and researchers may be comfortable interpreting raw data and scientific visualizations, a user-friendly interface is crucial for making the platform accessible to a wider

audience, including citizen scientists, community groups, and non-governmental organizations. The platform should be able to translate complex data into easily understandable formats, such as simple summaries, color-coded alerts, or interactive dashboards. This will empower a broader range of stakeholders to engage in water quality monitoring and contribute to environmental protection efforts.

Device Durability and Environmental Protection: In situ sensor platforms are deployed in diverse and often challenging environments, exposed to fluctuating temperatures, humidity, corrosive agents, and potential physical damage. Ensuring device durability and longevity requires careful selection of robust materials and protective housing that can withstand these environmental stressors. Regular maintenance and calibration procedures are also crucial to maintain sensor accuracy and prevent premature failure.

Overcoming these challenges requires a multi-faceted approach that combines innovative engineering solutions, robust data management strategies, and user-centered design principles. By addressing these limitations, we can unlock the full potential of in situ sensor platforms and transform the way we monitor and manage our precious water resources.

6.5 Future Perspectives

Multi optical lengths cuvette

In the pursuit of developing new instruments, optimizing cost-effectiveness during the prototyping phase is paramount. Designing a spectrophotometric detection cell with adaptable optical path lengths offers a compelling solution to this challenge. By incorporating different optical paths within a single device, achieved through the use of distinct diodes for each path length, a wider range of analyte concentrations can be accurately measured. This eliminates the need for multiple instruments or costly modifications, significantly reducing development and production expenses. This approach not only streamlines the prototyping process but also enhances the versatility and potential applications of the final product, making it a more attractive and valuable tool for researchers and industries alike. The **choice of material** for a spectrophotometric detection cell is critical, as it must be highly optically transparent. From literature PDMS (polydimethylsiloxane) and PMMA (Poly(methyl methacrylate)) are strong contenders due to their excellent clarity and well-established use in optics. PDMS, a silicone-based elastomer, offers flexibility and biocompatibility, while PMMA, also known as acrylic, provides rigidity and durability. Commercially available resins specifically designed for optical applications are also being considered, as they offer high transparency and tailored properties like refractive index and UV resistance. The final decision will depend on a careful evaluation of factors such as optical transparency within the desired wavelength range, cost-effectiveness, compatibility with the chosen fabrication method (molding or 3D printing), and long-term durability and stability of the material. By carefully considering these

factors, the most suitable material can be selected to ensure optimal performance and cost-effectiveness for the spectrophotometric detection cell.

Finally, by far, two fabrication strategies are currently being considered:

- **Moulding and Casting:** A mold will be fabricated using a milling machine, and then filled with PDMS to create the desired cell structure. This technique offers precision and the ability to create complex shapes. For this solution, the support for the cell would also need to be carefully designed and potentially custom-made. This is because the PDMS material itself is not rigid once it has been cast. It would also be crucial to test the thickness at which the cell has been produced to ensure its structural integrity and performance within the device with respect to commercial cuvettes.
- **Additive Manufacturing:** Leveraging 3D printing technology, the cell will be directly constructed using an optically transparent material. This approach offers rapid prototyping and design flexibility. The cost of the printing material and the layering effect inherent in 3D printing should be considered, as this could potentially lead to scattering phenomena during spectrophotometric analysis.

Both methods have their own advantages and will be further evaluated based on factors such as cost, precision, and compatibility with the desired optical properties of the final device. Figure 109 depicts a potential geometry for prototype. It is described as a stepped section with varying optical lengths from 20 mm to 2.5 mm. This configuration would allow for the measurement of a wide range of concentrations, from grams per liter to parts per billion (ppb), for the same analyte. The laser system can be configured for the desired optical path lengths. This can be achieved by either employing multiple lasers with adjustable vertical positioning or utilizing a single laser with a mechanism to alter the optical path.

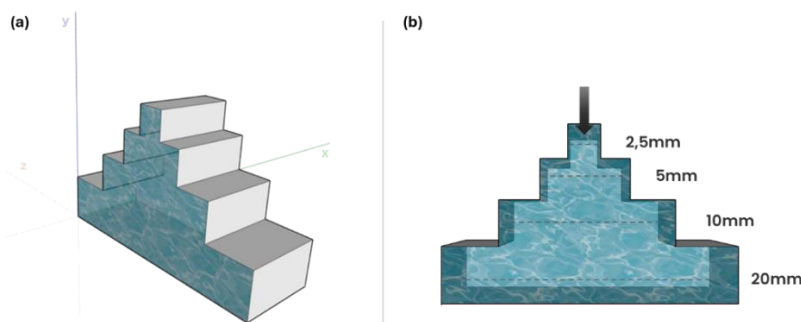


Figure 109: Possible multi-optical lengths cell design to be included in the prototyping of new sensor platforms.

Cadmium cell detection

Designing a user-friendly and safe chamber to transform into portable sensor for cadmium detection with disposable electrodes requires a holistic approach. To

ensure operator safety, the chamber should be completely enclosed to prevent the release of harmful cadmium solutions. An efficient prevention system should filter and expel any contaminants, maintaining a safe working environment. The chamber should also include a dedicated mechanism for easy and safe insertion and removal of disposable electrodes, minimizing direct contact and preventing accidental exposure to users. Integrating disposable electrodes seamlessly is key. A designated compartment for safe disposal of used electrodes is also crucial to prevent contamination and ensure responsible handling of hazardous waste. From a user perspective, the chamber design should prioritize ergonomics and intuitive operation. Clear labelling and automated features, such as electrode insertion and measurement initiation, can simplify the process and reduce errors. Visual cues like indicator lights or digital displays can provide real-time feedback on the analysis. Easy access to components and clear instructions for cleaning and maintenance will minimize downtime and ensure optimal performance.

The chamber should ensure a secure and reliable connection with the electrodes to prevent errors and maintain accuracy. The design should also minimize contamination risks between measurements, potentially through automated cleaning cycles or easily replaceable components. Cost-effectiveness should also be considered, balancing the convenience of disposable electrodes with affordability. Furthermore, if the chamber is intended for field use, portability and ruggedness are essential. Integrating data logging and transfer capabilities can streamline data management and analysis. Incorporating features that simplify calibration and quality control procedures will ensure accurate and reliable results. By addressing these considerations, the cadmium detection chamber can prioritize both user safety and convenience, while ensuring accurate and reliable measurements for a more efficient and effective approach to cadmium monitoring.

References

- [1] A. Boretti and L. Rosa, “Reassessing the projections of the World Water Development Report,” *NPJ Clean Water*, vol. 2, no. 1, Dec. 2019, doi: 10.1038/s41545-019-0039-9.
- [2] J. C. G. Sousa, A. R. Ribeiro, M. O. Barbosa, M. F. R. Pereira, and A. M. T. Silva, “A review on environmental monitoring of water organic pollutants identified by EU guidelines,” *J Hazard Mater*, vol. 344, pp. 146–162, Feb. 2018, doi: 10.1016/j.jhazmat.2017.09.058.
- [3] European Commission, “GOAL 6: CLEAN WATER AND SANITATION; Ensure availability and sustainable management of water and sanitation for all.” Accessed: Apr. 02, 2024. [Online]. Available: <https://knowsdgs.jrc.ec.europa.eu/sdg/6>
- [4] Stockholm International Water Institute, “Water and the 2030 Agenda.” Accessed: Apr. 02, 2024. [Online]. Available: <https://siwi.org/why-water/water-and-2030-agenda/>
- [5] World Water Assessment Programme (United Nations), UN-Water, and Unesco., *The United Nations world water development report 2021: Valuing Water*.
- [6] UNESCO and UN-Water, “Imminent risk of a global water crisis, warns the UN World Water Development Report 2023.” Accessed: Apr. 03, 2024. [Online]. Available: Imminent risk of a global water crisis, warns the UN World Water Development Report 2023
- [7] L. Schweitzer and J. Noblet, “Water Contamination and Pollution,” in *Green Chemistry*, Elsevier, 2018, pp. 261–290. doi: 10.1016/B978-0-12-809270-5.00011-X.
- [8] R. P. Schwarzenbach, T. Egli, T. B. Hofstetter, U. von Gunten, and B. Wehrli, “Global Water Pollution and Human Health,” *Annu Rev Environ Resour*, vol. 35, no. 1, pp. 109–136, Nov. 2010, doi: 10.1146/annurev-environ-100809-125342.
- [9] K. E. Ukhurebor *et al.*, “Applications and Contemporary Issues with Adsorption for Water Monitoring and Remediation: A Facile Review,” Jan. 01, 2024, *Springer*. doi: 10.1007/s11244-023-01817-4.
- [10] R. P. Schwarzenbach *et al.*, “The Challenge of Micropollutants in Aquatic Systems,” *Science (1979)*, vol. 313, no. 5790, pp. 1072–1077, Aug. 2006, doi: 10.1126/science.1127291.
- [11] R. Costanza, “The ecological, economic, and social importance of the oceans,” 1999. [Online]. Available: [www.elsevier.com/locate/ecocon*](http://www.elsevier.com/locate/ecocon)
- [12] J. Su *et al.*, “Chesapeake Bay acidification buffered by spatially decoupled carbonate mineral cycling,” *Nat Geosci*, vol. 13, no. 6, pp. 441–447, Jun. 2020, doi: 10.1038/s41561-020-0584-3.

- [13] F. Mohseni *et al.*, “Ocean water quality monitoring using remote sensing techniques: A review,” *Mar Environ Res*, vol. 180, p. 105701, Sep. 2022, doi: 10.1016/j.marenvres.2022.105701.
- [14] Z. KILIÇ, “Water Pollution: Causes, Negative Effects and Prevention Methods,” *İstanbul Sabahattin Zaim Üniversitesi Fen Bilimleri Enstitüsü Dergisi*, vol. 3, no. 2, pp. 129–132, Aug. 2021, doi: 10.47769/izufbed.862679.
- [15] M. Kumar, P. Borah, and P. Devi, “Priority and emerging pollutants in water,” in *Inorganic Pollutants in Water*, Elsevier, 2020, pp. 33–49. doi: 10.1016/B978-0-12-818965-8.00003-2.
- [16] J. C. G. Sousa, A. R. Ribeiro, M. O. Barbosa, M. F. R. Pereira, and A. M. T. Silva, “A review on environmental monitoring of water organic pollutants identified by EU guidelines,” *J Hazard Mater*, vol. 344, pp. 146–162, Feb. 2018, doi: 10.1016/j.jhazmat.2017.09.058.
- [17] B. Mishra, S. Varjani, G. P. Iragavarapu, H. H. Ngo, W. Guo, and B. Vishal, “Microbial Fingerprinting of Potential Biodegrading Organisms,” *Curr Pollut Rep*, vol. 5, no. 4, pp. 181–197, Dec. 2019, doi: 10.1007/s40726-019-00116-5.
- [18] U. C. Nkwunonwo, P. O. Odika, and N. I. Onyia, “A Review of the Health Implications of Heavy Metals in Food Chain in Nigeria,” *The Scientific World Journal*, vol. 2020, pp. 1–11, Apr. 2020, doi: 10.1155/2020/6594109.
- [19] N. D. Nnaji, H. Onyeaka, T. Miri, and C. Ugwa, “Bioaccumulation for heavy metal removal: a review,” *SN Appl Sci*, vol. 5, no. 5, p. 125, May 2023, doi: 10.1007/s42452-023-05351-6.
- [20] G. K. Kinuthia, V. Ngunjiri, D. Beti, R. Lugalia, A. Wangila, and L. Kamau, “Levels of heavy metals in wastewater and soil samples from open drainage channels in Nairobi, Kenya: community health implication,” *Sci Rep*, vol. 10, no. 1, p. 8434, May 2020, doi: 10.1038/s41598-020-65359-5.
- [21] G. Mansourri and M. Madani, “Examination of the Level of Heavy Metals in Wastewater of Bandar Abbas Wastewater Treatment Plant,” *Open J Ecol*, vol. 06, no. 02, pp. 55–61, 2016, doi: 10.4236/oje.2016.62006.
- [22] P. B. Tchounwou, C. G. Yedjou, A. K. Patlolla, and D. J. Sutton, “Heavy Metal Toxicity and the Environment,” 2012, pp. 133–164. doi: 10.1007/978-3-7643-8340-4_6.
- [23] UNICEF, “Reimagining WASH: Water Security for All.” Accessed: Apr. 02, 2024. [Online]. Available: <https://www.unicef.org/reports/reimagining-wash-water-security-for-all>
- [24] UNICEF for Every Child, “Billions of people will lack access to safe water, sanitation and hygiene in 2030 unless progress quadruples – warn WHO, UNICEF.” Accessed: Apr. 02, 2024. [Online]. Available: <https://www.unicef.org/press-releases/billions-people-will-lack-access-safe-water-sanitation-and-hygiene-2030-unless>
- [25] UNICEF, “WATER SECURITY FOR ALL,” Mar. 2021.

- [26] European Commission, “Water Framework Directive.” Accessed: Oct. 25, 2024. [Online]. Available: [https://environment.ec.europa.eu/topics/water/water-framework-directive_en#:~:text=The%20Water%20Framework%20Directive%20\(WF D,pollution%20and%20on%20ensuring%20that](https://environment.ec.europa.eu/topics/water/water-framework-directive_en#:~:text=The%20Water%20Framework%20Directive%20(WF D,pollution%20and%20on%20ensuring%20that)
- [27] Gazzetta Ufficiale della Repubblica Italiana, “Decreto Legislativo 2 febbraio 2001, n. 31. 2001, p. 27.”
- [28] M. Periolatto, F. Catania, M. Manachino, L. Scaltrito, F. Pirri, and S. Ferrero, “Direct online environment monitoring of water pollution,” *Chem Eng Trans*, vol. 82, pp. 193–198, 2020, doi: 10.3303/CET2082033.
- [29] A. M. Stortini, M. A. Baldo, G. Moro, F. Polo, and L. M. Moretto, “Bio- and Biomimetic Receptors for Electrochemical Sensing of Heavy Metal Ions,” *Sensors*, vol. 20, no. 23, p. 6800, Nov. 2020, doi: 10.3390/s20236800.
- [30] CNR - IRSA, “Surveillance and Investigative monitoring.” Accessed: Oct. 25, 2024. [Online]. Available: <http://www.life-inhabit.it/cnr-irsa-activities/en/cnr-irsa-activities-related-inhabit/ecological-status/surveillance-investigative-monitoring#:~:text=Investigative%20monitoring%20is%20established%20in,to%20achieve%20the%20environmental%20objectives>.
- [31] E. Poboży and M. Trojanowicz, “Application of Capillary Electrophoresis for Determination of Inorganic Analytes in Waters,” *Molecules*, vol. 26, no. 22, p. 6972, Nov. 2021, doi: 10.3390/molecules26226972.
- [32] Volpi Nicola. Maccari Francesca, *Capillary Electrophoresis of Biomolecules*, vol. 984. Totowa, NJ: Humana Press, 2013. doi: 10.1007/978-1-62703-296-4.
- [33] S. K. R. Williams, J. R. Runyon, and A. A. Ashames, “Field-Flow Fractionation: Addressing the Nano Challenge,” *Anal Chem*, vol. 83, no. 3, pp. 634–642, Feb. 2011, doi: 10.1021/ac101759z.
- [34] A. Belmonte Vega, A. Garrido Frenich, and J. L. Martínez Vidal, “Monitoring of pesticides in agricultural water and soil samples from Andalusia by liquid chromatography coupled to mass spectrometry,” *Anal Chim Acta*, vol. 538, no. 1–2, pp. 117–127, May 2005, doi: 10.1016/j.aca.2005.02.003.
- [35] D. Kadadou, L. Tizani, H. Alsafar, and S. W. Hasan, “Analytical methods for determining environmental contaminants of concern in water and wastewater,” *MethodsX*, vol. 12, p. 102582, Jun. 2024, doi: 10.1016/j.mex.2024.102582.
- [36] D. Kadadou, L. Tizani, H. Alsafar, and S. W. Hasan, “Analytical methods for determining environmental contaminants of concern in water and wastewater,” *MethodsX*, vol. 12, p. 102582, Jun. 2024, doi: 10.1016/j.mex.2024.102582.
- [37] A. Inobeme *et al.*, “Recent advances in instrumental techniques for heavy metal quantification,” *Environ Monit Assess*, vol. 195, no. 4, p. 452, Apr. 2023, doi: 10.1007/s10661-023-11058-3.

- [38] P. Punia, M. K. Bharti, R. Dhar, P. Thakur, and A. Thakur, "Recent Advances in Detection and Removal of Heavy Metals from Contaminated Water," *ChemBioEng Reviews*, vol. 9, no. 4, pp. 351–369, Aug. 2022, doi: 10.1002/cben.202100053.
- [39] S. Popović, A. Pantelić, Ž. Milovanović, J. Milinkov, and M. Vidović, "Analysis of Tea for Metals by Flame and Graphite Furnace Atomic Absorption Spectrometry with Multivariate Analysis," *Anal Lett*, vol. 50, no. 16, pp. 2619–2633, Nov. 2017, doi: 10.1080/00032719.2017.1307849.
- [40] M. A. Agoro, A. O. Adeniji, M. A. Adefisoye, and O. O. Okoh, "Heavy Metals in Wastewater and Sewage Sludge from Selected Municipal Treatment Plants in Eastern Cape Province, South Africa," *Water (Basel)*, vol. 12, no. 10, p. 2746, Oct. 2020, doi: 10.3390/w12102746.
- [41] D. Parmar, R. Srivastava, and P. K. Baruah, "Laser induced breakdown spectroscopy: A robust technique for the detection of trace metals in water," *Mater Today Proc*, vol. 77, pp. 234–239, 2023, doi: 10.1016/j.matpr.2022.11.267.
- [42] Z. H. Fernández *et al.*, "Application of Cold Vapor-Atomic Absorption (CVAAS) Spectrophotometry and Inductively Coupled Plasma-Atomic Emission Spectrometry methods for cadmium, mercury and lead analyses of fish samples. Validation of the method of CVAAS," *Food Control*, vol. 48, pp. 37–42, Feb. 2015, doi: 10.1016/j.foodcont.2014.05.056.
- [43] A. Sanz-Medel, J. M. Costa, and R. Pereiro, "Atomic Spectrometry," *Chemistry, Molecular Sciences and Chemical Engineering, Elsevier*, pp. 1–14, 2013.
- [44] A. Ahmed, A. Singh, B. Padha, A. K. Sundramoorthy, A. Tomar, and S. Arya, "UV–vis spectroscopic method for detection and removal of heavy metal ions in water using Ag doped ZnO nanoparticles," *Chemosphere*, vol. 303, p. 135208, Sep. 2022, doi: 10.1016/j.chemosphere.2022.135208.
- [45] F. Cheng, C. Yang, C. Zhou, L. Lan, H. Zhu, and Y. Li, "Simultaneous Determination of Metal Ions in Zinc Sulfate Solution Using UV–Vis Spectrometry and SPSE-XGBoost Method," *Sensors*, vol. 20, no. 17, p. 4936, Aug. 2020, doi: 10.3390/s20174936.
- [46] X. Hou *et al.*, "Synthesis of 3D porous ferromagnetic NiFe₂O₄ and using as novel adsorbent to treat wastewater," *J Colloid Interface Sci*, vol. 362, no. 2, pp. 477–485, Oct. 2011, doi: 10.1016/j.jcis.2011.06.070.
- [47] S. R. Jarapala, B. Kandlakunta, and L. Thingnganing, "Evaluation of Trace Metal Content by ICP-MS Using Closed Vessel Microwave Digestion in Fresh Water Fish," *J Environ Public Health*, vol. 2014, pp. 1–8, 2014, doi: 10.1155/2014/201506.
- [48] C. C. Kaonga, I. B. M. Kosamu, and W. R. Utembe, "A Review of Metal Levels in Urban Dust, Their Methods of Determination, and Risk Assessment," *Atmosphere (Basel)*, vol. 12, no. 7, p. 891, Jul. 2021, doi: 10.3390/atmos12070891.
- [49] P. Verma, N. Kalra, and S. Verma, "Advancement in sensory identification of heavy metal contamination in water: A review on progression from

- spectroscopic analytical techniques to handheld sensors,” *Microchemical Journal*, vol. 205, p. 111293, Oct. 2024, doi: 10.1016/j.microc.2024.111293.
- [50] A. M. Ahmed and M. Shaban, “Nanoporous chromium thin film for active detection of toxic heavy metals traces using surface-enhanced Raman spectroscopy,” *Mater Res Express*, vol. 7, no. 1, p. 015084, Jan. 2020, doi: 10.1088/2053-1591/ab6b62.
- [51] A. M. Stortini, M. A. Baldo, G. Moro, F. Polo, and L. M. Moretto, “Bio- and Biomimetic Receptors for Electrochemical Sensing of Heavy Metal Ions,” *Sensors*, vol. 20, no. 23, p. 6800, Nov. 2020, doi: 10.3390/s20236800.
- [52] D. Kadadou, L. Tizani, H. Alsafar, and S. W. Hasan, “Analytical methods for determining environmental contaminants of concern in water and wastewater,” *MethodsX*, vol. 12, p. 102582, Jun. 2024, doi: 10.1016/j.mex.2024.102582.
- [53] W. T. Dinbore, W. C. Dabbo, and A. P. Washe, “Differential pulse voltammetric determination of hexavalent chromium using nickel hexacyanoferrate modified glassy carbon electrode,” *Sustainable Environment*, vol. 7, no. 1, Jan. 2021, doi: 10.1080/27658511.2021.1978633.
- [54] N. Liu, W. Ye, G. Liu, and G. Zhao, “Improving the accuracy of stripping voltammetry detection of Cd²⁺ and Pb²⁺ in the presence of Cu²⁺ and Zn²⁺ by machine learning: Understanding and inhibiting the interactive interference among multiple heavy metals,” *Anal Chim Acta*, vol. 1213, p. 339956, Jun. 2022, doi: 10.1016/j.aca.2022.339956.
- [55] E. De Vito-Francesco *et al.*, “An innovative autonomous robotic system for on-site detection of heavy metal pollution plumes in surface water,” *Environ Monit Assess*, vol. 194, no. 2, p. 122, Feb. 2022, doi: 10.1007/s10661-021-09738-z.
- [56] L. Ma, Z. Li, S. D. Yabo, B. Li, S. Sun, and H. Qi, “Insight into the interaction between heavy metals and water-soluble organic compounds in PM_{2.5} affected by heavy haze using ultraviolet–visible and fluorescence spectra combined with two-dimensional correlation spectroscopy,” *J Clean Prod*, vol. 362, p. 132476, Aug. 2022, doi: 10.1016/j.jclepro.2022.132476.
- [57] L. Durai and S. Badhulika, “Stripping voltammetry and chemometrics assisted ultra-selective, simultaneous detection of trace amounts of heavy metal ions in aqua and blood serum samples,” *Sensors and Actuators Reports*, vol. 4, p. 100097, Nov. 2022, doi: 10.1016/j.snr.2022.100097.
- [58] J. V. Maciel, M. M. Souza, L. O. Silva, and D. Dias, “Direct Determination of Zn, Cd, Pb and Cu in Wine by Differential Pulse Anodic Stripping Voltammetry,” *Beverages*, vol. 5, no. 1, p. 6, Jan. 2019, doi: 10.3390/beverages5010006.
- [59] P. Knihnicki *et al.*, “Electrochemical Sensing of Pb²⁺ and Cd²⁺ Ions with the Use of Electrode Modified with Carbon-Covered Halloysite and Carbon

- Nanotubes,” *Molecules*, vol. 27, no. 14, p. 4608, Jul. 2022, doi: 10.3390/molecules27144608.
- [60] A. García-Miranda Ferrari, P. Carrington, S. J. Rowley-Neale, and C. E. Banks, “Recent advances in portable heavy metal electrochemical sensing platforms,” *Environ Sci (Camb)*, vol. 6, no. 10, pp. 2676–2690, 2020, doi: 10.1039/D0EW00407C.
- [61] K. M. E. Stewart, M. Al-Ghamdi, M. Khater, E. M. Abdel-Rahman, and A. Penlidis, “An overview of sensors and sensing materials for heavy metals in aqueous environments,” *Can J Chem Eng*, vol. 100, no. 4, pp. 666–679, Apr. 2022, doi: 10.1002/cjce.24139.
- [62] A. Jang, Z. Zou, K. K. Lee, C. H. Ahn, and P. L. Bishop, “State-of-the-art lab chip sensors for environmental water monitoring,” *Meas Sci Technol*, vol. 22, no. 3, p. 032001, Mar. 2011, doi: 10.1088/0957-0233/22/3/032001.
- [63] S. Mukherjee *et al.*, “Sensory development for heavy metal detection: A review on translation from conventional analysis to field-portable sensor,” *Trends Food Sci Technol*, vol. 109, pp. 674–689, Mar. 2021, doi: 10.1016/j.tifs.2021.01.062.
- [64] U. Choudhari, S. Jagtap, N. Ramgir, A. K. Debnath, and K. P. Muthe, “Screen-printed electrochemical sensors for environmental monitoring of heavy metal ion detection,” *Reviews in Chemical Engineering*, vol. 39, no. 7, pp. 1227–1268, Oct. 2023, doi: 10.1515/revce-2022-0002.
- [65] B. Molinero-Abad, D. Izquierdo, L. Pérez, I. Escudero, and M. J. Arcos-Martínez, “Comparison of backing materials of screen printed electrochemical sensors for direct determination of the sub-nanomolar concentration of lead in seawater,” *Talanta*, vol. 182, pp. 549–557, May 2018, doi: 10.1016/j.talanta.2018.02.005.
- [66] A. U. Alam, D. Clyne, H. Jin, N.-X. Hu, and M. J. Deen, “Fully Integrated, Simple, and Low-Cost Electrochemical Sensor Array for in Situ Water Quality Monitoring,” *ACS Sens*, vol. 5, no. 2, pp. 412–422, Feb. 2020, doi: 10.1021/acssensors.9b02095.
- [67] Z. Li, D. Xu, D. Zhang, and Y. Yamaguchi, “A portable instrument for on-site detection of heavy metal ions in water,” *Anal Bioanal Chem*, vol. 413, no. 13, pp. 3471–3477, May 2021, doi: 10.1007/s00216-021-03292-w.
- [68] E. De Vito-Francesco *et al.*, “An innovative autonomous robotic system for on-site detection of heavy metal pollution plumes in surface water,” *Environ Monit Assess*, vol. 194, no. 2, p. 122, Feb. 2022, doi: 10.1007/s10661-021-09738-z.
- [69] B. Li *et al.*, “A self-designed versatile and portable sensing device based on smart phone for colorimetric detection,” *Anal Bioanal Chem*, vol. 413, no. 2, pp. 533–541, Jan. 2021, doi: 10.1007/s00216-020-03024-6.
- [70] Z. Cheng *et al.*, “An Optofluidic Monitor with On-Chip Calibration for Online Analyzing Surface Water Quality,” *Arab J Sci Eng*, vol. 48, no. 7, pp. 8629–8639, Jul. 2023, doi: 10.1007/s13369-022-07205-6.
- [71] P. K. (Sandy) D. K. A. S. Gary D. Christian., *Analytical Chemistry, 7th Edition*.

- [72] “UNIT 19 OPTICAL METHODS .” Accessed: Jul. 31, 2024. [Online]. Available: <https://www.egyankosh.ac.in/bitstream/123456789/13555/1/Unit-19.pdf>
- [73] P. R. G. S. Napoleone Fabbri, “Quaderni di Analisi Chimica Strumentale: Spettrofotometria (v.06-VII).” Accessed: Jul. 31, 2024. [Online]. Available: https://www.e-santoni.edu.it/wp-content/uploads/2019/10/qacs_spettrofotometria.pdf
- [74] Davide Di Stasio, “SPETTROSCOPIA UV-VIS.” Accessed: Jul. 31, 2024. [Online]. Available: <https://www.makers-itis-forli.it/chimicaelettronica-e-riciclo/spettroscopia-uv-vis/>
- [75] R. Aryal, R. Nirola, S. Beecham, and B. Sarkar, “Influence of heavy metals in root chemistry of *Cyperus vaginatus* R.Br: A study through optical spectroscopy,” *Int Biodeterior Biodegradation*, vol. 113, pp. 201–207, Sep. 2016, doi: 10.1016/j.ibiod.2016.04.008.
- [76] PSIBERG Team, “d-d Transitions: The Reason Behind Colored Complexes.” Accessed: Jul. 31, 2024. [Online]. Available: <https://psiberg.com/d-d-transitions/>
- [77] Edinburgh Instruments Ltd., “The Beer-Lambert Law.” Accessed: Jul. 31, 2024. [Online]. Available: <https://www.edinst.com/blog/the-beer-lambert-law/>
- [78] Y. Kumari Shrestha and S. Krishna Shrestha, “Fundamentals of Colorimetry,” in *Advances in Colorimetry*, IntechOpen, 2024. doi: 10.5772/intechopen.112344.
- [79] IMPLLEN, “What is a UV-Vis Spectrophotometer?” Accessed: Jul. 31, 2024. [Online]. Available: <https://www.implen.de/uv-vis-spectrophotometer/>
- [80] M. T. Fernández Abedul, “Dynamic electroanalysis,” in *Laboratory Methods in Dynamic Electroanalysis*, Elsevier, 2020, pp. 1–10. doi: 10.1016/B978-0-12-815932-3.00001-2.
- [81] U. D. 2012 Jasmine Briones, “Electrolytic Cells.” Accessed: Sep. 03, 2024. [Online]. Available: https://chem.libretexts.org/Bookshelves/Analytical_Chemistry/Supplemental_Modules_%28Analytical_Chemistry%29/Electrochemistry/Electrolytic_Cells
- [82] B. Bansod, T. Kumar, R. Thakur, S. Rana, and I. Singh, “A review on various electrochemical techniques for heavy metal ions detection with different sensing platforms,” *Biosens Bioelectron*, vol. 94, pp. 443–455, Aug. 2017, doi: 10.1016/j.bios.2017.03.031.
- [83] B. Baś, R. Piech, M. Ziemnicka, W. Reczyński, and M. Robótka, “Renewable Ceramic (TiN) Ring Electrode in Stripping Voltammetry. Determination of Pb(II) Without Removal of Oxygen,” *Electroanalysis*, vol. 21, no. 16, pp. 1773–1780, Aug. 2009, doi: 10.1002/elan.200804598.
- [84] A. Bobrowski, A. Królicka, and R. Bobrowski, “Renewable silver amalgam film electrodes in electrochemical stripping analysis—a review,” *Journal of*

- Solid State Electrochemistry*, vol. 20, no. 12, pp. 3217–3228, Dec. 2016, doi: 10.1007/s10008-016-3275-7.
- [85] J. A., E. Barrado, M. Vega, Y. Castrillejo, and J. L.F.C., “Sequential Injection Anodic Stripping Voltammetry at Tubular Gold Electrodes for Inorganic Arsenic Speciation,” in *Electrochemical Cells - New Advances in Fundamental Researches and Applications*, InTech, 2012. doi: 10.5772/35159.
- [86] Thomas Forrister, “Analyzing Cyclic Voltammetry at a Microdisk Electrode with Simulation.” Accessed: Sep. 12, 2024. [Online]. Available: <https://www.comsol.com/blogs/analyzing-cyclic-voltammetry-at-a-microdisk-electrode-with-simulation>
- [87] R. Porada, K. Jedlińska, J. Lipińska, and B. Baś, “Review—Voltammetric Sensors with Laterally Placed Working Electrodes: A Review,” *J Electrochem Soc*, vol. 167, no. 3, p. 037536, Jan. 2020, doi: 10.1149/1945-7111/ab64d6.
- [88] Pierpaolo Protti, “Introduction to Modern Voltammetric and Polarographic Analysis Techniques,” in *AMEL ELECTROCHEMISTRY*, Iv., 2001.
- [89] J. Liu, Y. Xu, S. Liu, S. Yu, Z. Yu, and S. S. Low, “Application and Progress of Chemometrics in Voltammetric Biosensing,” *Biosensors (Basel)*, vol. 12, no. 7, p. 494, Jul. 2022, doi: 10.3390/bios12070494.
- [90] R. Haley, “Evaluation of a colorimetric assay for the detection of arsenic in water.” [Online]. Available: <https://www.researchgate.net/publication/323525844>
- [91] G. Mossotti, M. Periolatto, F. Catania, F. Perrucci, L. Scaltrito, and S. Ferrero, “Spectrophotometric Detection of Copper in Water by Lab-on-a-chip Technology: Application to Electroplating,” *Chem Eng Trans*, vol. 96, pp. 481–486, 2022, doi: 10.3303/CET2296081.
- [92] C. E. Säbel, J. M. Neureuther, and S. Siemann, “A spectrophotometric method for the determination of zinc, copper, and cobalt ions in metalloproteins using Zincon,” *Anal Biochem*, vol. 397, no. 2, pp. 218–226, Feb. 2010, doi: 10.1016/j.ab.2009.10.037.
- [93] A. V. Rossi and M. Tubino, “The Kinetics and Mechanism of the Reaction of ZINCON, o -[1-(2-hydroxy-5-sulfophenyl)-3-phenyl-5-formazane] Benzoic Acid, with Zn^{2+} , Cu^{2+} and $[Zn^{2+} + Cu^{2+}]$ Equimolar Mixtures,” *J Braz Chem Soc*, vol. 7, no. 3, pp. 161–168, 1996, doi: 10.5935/0103-5053.19960025.
- [94] D. Schrenk *et al.*, “Update of the risk assessment of nickel in food and drinking water,” *EFSA Journal*, vol. 18, no. 11, Nov. 2020, doi: 10.2903/j.efsa.2020.6268.
- [95] G. A. Di Bari, “Electrodeposition of Nickel,” in *Modern Electroplating*, Wiley, 2010, pp. 79–114. doi: 10.1002/9780470602638.ch3.
- [96] G. Mossotti, F. Catania, F. Perrucci, L. Scaltrito, M. Periolatto, and S. Ferrero, “Spectrophotometric Detection of Nickel in Water by Lab-on-a-chip Technology: Application to Electroplating,” *Chem Eng Trans*, vol. 99, pp. 127–132, 2023, doi: 10.3303/CET2399022.

- [97] G. Mossotti *et al.*, “Advances in Water Resource Management: An In Situ Sensor Solution for Monitoring High Concentrations of Chromium in the Electroplating Industry,” *Water (Basel)*, vol. 16, no. 8, p. 1167, Apr. 2024, doi: 10.3390/w16081167.
- [98] A. PISCITELLI *et al.*, “Cr VI in Water Continuous on Site Spectrophotometric Determination Laboratory test preliminary to microfluidic device prototyping,” Institute of Research Engineers and Doctors, LLC, Apr. 2018, pp. 1–6. doi: 10.15224/978-1-63248-148-1-01.